FLOW OF GAS MIXTURES THROUGH MICROPOROUS MEDIA

by

RICHARD THOMAS LOWSON

A thesis submitted for the degree of

Doctor of Philosophy in the

University of London

November 1968

Chemistry Department
Imperial College,
London, S.W.7.

ABSTRACT

This thesis is a report on an experimental study of the flow of the gas mixtures ammonia-helium, ammonia-hydrogen, ammonia-nitrogen, and nitrogen-hydrogen through a microporous membrane prepared by compacting a carbon powder commercially known as Carbolac I. The work required an ancillary study to be made of the flow through the same membrane of the individual components of the gas mixture together with the necessary data of gas adsorption on the membrane material. Using this same membrane a comparison was made between the hydrogen adsorption and flow results and those of its isotope deuterium. In addition a study was made of the helium flow over the wide temperature range 300 to - 200 ^{o}C through a membrane prepared from the more thermally stable microporous carbon commercially known as Graphon. Gaseous fluid flow through microporous media may be accompanied by an additional flow of material adsorbed onto the surface of the membrane. Of all the gases investigated only helium proved to have no surface component. Significant differences were found between the hydrogen and deuterium results. Evidence was obtained that ammonia gas would tend to form a capillary condensate well below the saturation vapour pressure point of ammonia for the temperature of the experiment; this was attributed to heavy adsorption on to the surface of the membrane. This condensate was capable of significantly reducing the flow of material through the membrane. Due to the excessive surface flux of ammonia large separation factors were obtained with the ammonia systems, but the method could not be recommended as a purification technique for the nitrogen-hydrogen system. Novel gas analysis techniques are described in the experimental section, and finally suggestions are made for possible applications of the unusual results.

ACKNOWLEDGEMENTS

I would like to take this opportunity to thank Professor R. M. Barrer for his friendly advice and encouragement throughout the course of the work, and to Mr R. Ash for his part in the project supervision. I am also indebted to Professor Barrer for providing a three year maintenance grant as a bursary from the Physical Chemistry department of Imperial College.

The construction of the apparatus would have been well-nigh impossible but for the experience and craftsmanship of the technical staff of the departmental metal, glass and electrical workshops.

For some of the ancillary studies I took advantage of the special skills of my colleagues. I am particularly grateful to Miss C. E. Souter who prepared and ran the infra-red spectra experiments, Dr. I. S. Kerr for the electron microscope photographs, and Dr. T. R. Singh who wrote several of the computer programs reported here and showed remarkable patience in 'de-bugging' my own attempts.

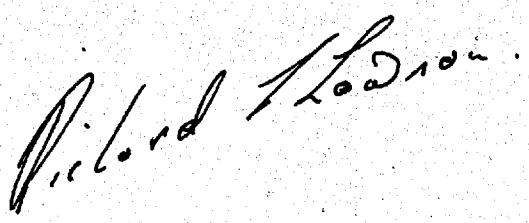

DEDICATION

This thesis is dedicated with affection to my parents in recognition of the many personal sacrifices they willingly made for my school and university education.

CONTENTS

CHAPTER 1 INTRODUCTION

The discovery that the individual components of a gas mixture had specific rates of flow when diffusing through a porous membrane formed the basis of several patents taken out in the early part of the nineteenth century for the separation of air (Mitchell, 1831). In commercial terms the process has never successfully competed with conventional means of separation in conventional applications, for as Benedict (1947) pointed out "Gaseous diffusion requires so much more energy than distillation or adsorption, that it is not likely to replace them except when gaseous diffusion has a much larger separation factor. This, of course, is the case in isotope separation, which will be the principal field of application of this process."

However more recent experiment has brought to light the existence of surface flow accompanying the diffusive flow of many gases and vapours. Under suitable conditions this additional surface flow may be very much larger than the gaseous flow, and for certain systems form the basis of an economical separation process.

The work reported here was designed to gain further insight into the nature of this surface flow, and its possible utilisation in the separation of gas mixtures.

The phenomenon of diffusion was first placed on a quantitative basis by Graham (1846), who from experiments with several gases derived the empirical law "that the velocity of diffusion of a gas is inversely proportional to the square root of its density relative to air".

Further experiments by Knudsen (1909) indicated that

Graham's law is limited to the region where the mean free path of the gas molecules is much greater than the capillary radius of the pore through which they are flowing. In this region Knudsen argued that the molecule-wall collisions controlled the rate of transport, and was able to develop a theoretical equation which was equivalent to Graham's law. Diffusive gas flow which obeys the Knudsen equation is known as Knudsen or free-molecular flow.

Further development arose from the Manhattan project. This utilised the diffusion process for the enrichment of uranium 235 by the gaseous diffusion of uranium hexafluoride in a multistage cascade arrangement. In the theoretical background to this project Present and deBethune (1949) re-examined the Knudsen equation for the separation of a gas mixture flowing through a single capillary. Their final working equation included a term for the non-separative flow of the mixture due to molecule-molecule collisions.

However models based on cylindrical capillaries are a far cry from the real geometry of the porous membrane, and fail to explain why separation factors higher than the ideal value of $(M_A/M_B)^{\frac{1}{2}}$ have been observed. As an alternative approach Mason et al (1961, 1962, 1963, 1964, 1967) developed a 'dusty gas' theory in which the porous medium was described as a uniform suspension of spherical particles (or macromolecules considered as a third component of the mixture) in the binary gas mixture. This approach was refined by Breton and Massigon (1963) so that actual properties of the media such as the radius of the particles, the surface area, the porosity, and the mean pore radius could be included in the working equation.

These theoretical equations were derived principally

for uranium isotope separation by gaseous diffusion, where diffusive flow is solely in the gas phase. The separate addition of a surface flow contributing to the total flow was derived from the work of Clausing (1930), Damköhler (1935) and Volmer et al (1921, 1925, 1926), to be used later by Wicke et al (1941, 1947) to account for abnormally high flow rates in the Knudsen region. Since then many papers describing surface diffusion have been published mainly from the schools of Barrer, Carman, Flood, and Kammermeyer.

The mechanism of surface flow is still open to debate. The two extreme views are that surface flow occurs by a viscous, hydrodynamic mechanism only; or that this transport takes place by a diffusive, random walk mechanism only (Aylmore and Barrer, 1966). The diffusive mechanism has been considered to be dominant for dilute adsorbed films. This allowed Hill (1956) to develop a theoretical equation for surface flow. This equation formed the basis of a correction term applied by Ishida, Shimokawa, and Yamamoto (1961) to the Present and deBethune equation, and by Fiocchi (1966, 1967) to the Breton and Massigon equation.

The hydrodynamic mechanism was proposed by Gilliland et al (1958, 1962) based on the ideas of Babbit (1950, 1951 a and b, 1955, 1958). They assumed that the adsorbed layer acts as a two dimensional fluid with two-dimensional properties analogous to the properties of three-dimensional fluids. In a review by Field, Watts and Weller (1963) it was considered that this mechanism was dominant even for the dilute adsorbed films.

Irrespective of mechanism, the flow of gases through porous membranes may be formulated in terms of Fick's law "the flux is proportional to the concentration gradient" (Fick, 1855). Providing the boundary conditions are

carefully defined for the mathematical manipulations of this law, then considerable information can be derived from flow experiments without recourse to rather restrictive models. This procedure has been mainly developed by Barrer and Carman, and is reviewed in the following chapter.

CHAPTER 2 REVIEW AND THEORETICAL

2.1 FLOW OF GASES IN MICROPOROUS MEDIA

2.1.1 The region of flow

Fluid flow is divided into the regions of turbulent flow; orifice flow; streamline (viscous or Poiseuille) flow; slip flow; and molecular streaming (free-molecular or Knudsen flow) which may also have an associated surface flow.

In the present work the membrane was prepared by compacting a fine carbon powder. This produced a membrane with a mean pore radius of 1.0×10^{-7} cm (see section 5.1.8). Since the mean free path for any of the gases investigated was of the order of 1×10^{-5} cm at the in-going side of the membrane, only molecule-wall collisions will be significant in controlling the gas phase transport, and the gas phase flow may be considered as pure molecular streaming.

From experimental studies in this region, Knudsen (1909), Gaede (1913), Clausing (1932), and later Adzumi (1937) showed that for single capillaries in the absence of surface flow the rate of flow is proportional to the pressure gradient but independent of the gas pressure. Knudsen, arguing that the molecule-wall collisions were the predominating factor, derived an expression for the flux of a gas in a single capillary. It was necessary to assume that all the molecules striking the surface were reflected randomly. The expression for the flux was then obtained by considering the number of molecules passing through a given cross-section from an element of surface on the tube wall, and integrating over the entire tube wall. From the equation for the flux the following expression for the

Knudsen permeability, K_K, of a gas flowing through a single capillary is obtained

$$K_K = \frac{4}{3}.r.\left(\frac{2.R.T}{\pi.M}\right)^{\frac{1}{2}} = \frac{J^o.l}{\pi.r^2.\Delta C} \qquad 2.1$$

where r is the capillary radius in cm, J^o is the steady state flux in molecules per second, l is the capillary length in cm, and ΔC is the concentration drop between the ends of the capillary in molecules per cm^3. The other symbols have the conventional meanings.

Smoluchowski (1910) corrected this equation for the case where only a fraction f of the molecules is reflected randomly, leading to

$$K_K = \frac{4}{3}.r.\left(\frac{2.R.T}{\pi.M}\right)^{\frac{1}{2}}.\frac{(2-f)}{f} \qquad 2.2$$

Huggill (1952) and Berman and Lund (1958) reported that this factor $(1-f)$ can be as high as 5% in certain cases.

The permeability equation for molecular streaming in porous media is very similar to the ideal model of a single capillary. This is despite the random pore structure, the tortuous and interconnected channels, and the existence of blind pores. However there are some differences, and the following terms should be included into the equation for the Knudsen permeability of gases in porous media.

(i) The porosity, ε.

In the unit area of the cross-section of the porous medium the area of actual pores intersected is ε, the porosity in $cm^3\ cm^{-3}$ of porous media.

(ii) The hydraulic radius, r_h.

To generalise the equation for various cross-sectional shapes of the pores, the capillary radius, r, is replaced by twice the hydraulic radius r_h given by

$$r = 2.r_h = 2.\frac{\text{area of cross-section}}{\text{circumference of cross-section}} = \frac{2.\varepsilon}{A} \quad 2.3$$

where A is the surface area of the porous medium in $cm^2\ cm^{-3}$.

(iii) The tortuosity and structure factor, χ.

Because in a porous medium there are frequent changes in direction of the flow paths then the long axial flights of molecules are no longer possible. Hiby and Pahl (1956) considered the case for pure molecular streaming in a series of repeatedly bent tubes, by an extension of the molecular path tracing analysis of Pollard and Present (1948). If the straight sections of each tube are 2h and the radius r. Then the ratio of the Knudsen permeabilities in the repeatedly bent tubes, K_h, to that of an infinitely long tube of the same radius is given in table 2.1

Table 2.1

Ratios of Knudsen permeabilities in repeatedly bent tubes, K_h, to that in an infinitely long straight tube, K_K.

h/r	2	3	4	5	10
$\frac{K_h}{K_K}$	0.672	0.766	0.820	0.855	0.925

The table shows that as the porous medium becomes more tortuous then the permeability is reduced. Because the actual degree of tortuosity is unknown for porous media the value for the structure factor factor is somewhat empirical, and it covers the following contingencies:

(a) Channels having irregular cross-sections.

(b) Variation in the shape of the channels along their lengths.

(c) The tortuosity of the channels.

(d) The presence of bottlenecks,

(e) The presence of blind pores.

(f) A range of values for the hydraulic radius amongst the channels.

(g) Non-random reflection for molecule wall collisions. (Barrer, 1963 b, 1967).

When these additional factors are included in the equation, the Knudsen permeability for gases flowing through porous media, K_k, is

$$K_k = \frac{\varepsilon . K_K}{\mathcal{K}} = \frac{8}{3} . \frac{\varepsilon^2}{\mathcal{K} . A} . \left(\frac{2 . R . T}{\pi . M} \right)^{1/2} = \frac{J^o . l}{A_c . \varepsilon . \Delta C} \qquad 2.4$$

where A_c is the cross-sectional area of the porous medium in the direction normal to flow. As capillary size, or gas pressure is increased, then the terms for slip, and viscous flow become significant. Clint (1966) who was using a similar membrane and operating conditions to those reported in this work, calculated from Weber's formulae (Weber, 1954) that there is an increase of about 1.3% in K_k at an average pressure of 1 atmosphere when these extra terms are included.

The permeability coefficient is a quantity defined to suit the mathematical formulation of the problem. For formulation of flow in terms of Fick's law the permeability coefficient defined by equation 2.4 is sometimes inconvenient. For this work a better definition which allows direct application in equations derived from Fick's law is the definition used by Ash, Baker and Barrer (1967):

$$K = \frac{J . l}{\Delta C} \qquad 2.5$$

where J is the flux per unit area of porous media normal to the x direction of flow, and the units of flux and concentration are chosen so that the permeability, K, is in $cm^2\ sec^{-1}$. This

definition will be used from here on. Other specific definitions of the permeability coefficient are discussed in section 2.1.8.

2.1.2 Formulation of flow in terms of Fick's laws.

One of the properties of molecular streaming is that it may be formulated in terms of Fick's laws (1855), that is "for steady state flow the flux J is proportional to the concentration gradient dC/dx".

$$J \equiv - D.\frac{dC}{dx} \qquad 2.6$$

where D is the coefficient of proportionality known as the diffusion coefficient. Barrer (1963 a) emphasised that Fick's law was formally equivalent to Darcy's law (1856) "the flux is proportional to the pressure gradient", and that both laws were specific examples of the more general phenomenological identity derived from irreversible thermodynamics, "that for isothermal diffusion the flux is proportional to the gradient of chemical potential $\partial\mu/\partial x$".

$$J \equiv - L.\frac{\partial\mu}{\partial x} \qquad 2.7$$

where L is the phenomenological coefficient.

For steady state flow with a diffusion coefficient independent of concentration and distance, and with the boundary conditions $C = C_o$ at $x = 0$ for all time, and $C = C_l$ at $x = l$ for all time, the flux may be written as

$$J = D.\frac{(C_o - C_l)}{l} \qquad 2.8$$

When equation 2.8 is compared with the revised definition of the permeability coefficient, equation 2.5, it can be seen

that under these conditions of flow the permeability and diffusion coefficients are identical. If the permeability is written in terms of equation 2.4 we obtain, for $C_A = C_B$, that other property of molecular streaming

$$J_A(M_A)^{\frac{1}{2}} = J_B(M_B)^{\frac{1}{2}} = \ldots \qquad 2.9$$

originally discovered by Graham.

In the work reported here the concentration at the out-going side of the membrane (subscript l), although measurable, is effectively zero when compared with the concentration at the in-going side (subscript o). For steady state flow, and using these boundary conditions, equation 2.6 may be integrated to

$$[J]_0^{C_o}.l = \int_0^{C_o} D.dC \qquad \begin{matrix} x = 0,\ C = C_o \\ x = l,\ C = 0 \end{matrix} \qquad 2.10$$

This is assuming D is a constant or a function of C only. Under these experimental conditions the flux will only vary with the in-going side concentration. Consequently differentiating the flux in equation 2.10 with respect to the concentration at the in-going side yields:

$$\left[\frac{dJ}{dC}\right]_{C_o}.l = [D]_{C_o} \qquad 2.11$$

Thus a plot of the observed flux through the membrane $[J]_{C_o}$ against the concentration at the in-going side C_o, as in figure 2.1 will either be linear (case b), or if the diffusion coefficient varies with the in-going side concentration the plot will be curved (cases a and c). The slope for a particular value of C_o will be, from equation 2.11, $[D]_{C_o}/l$.

Equation 2.10 may be rearranged to

$$K = \frac{[J]_{C_o}.l}{C_o} = \frac{1}{C_o}\int_0^{C_o} D.dC \qquad 2.12$$

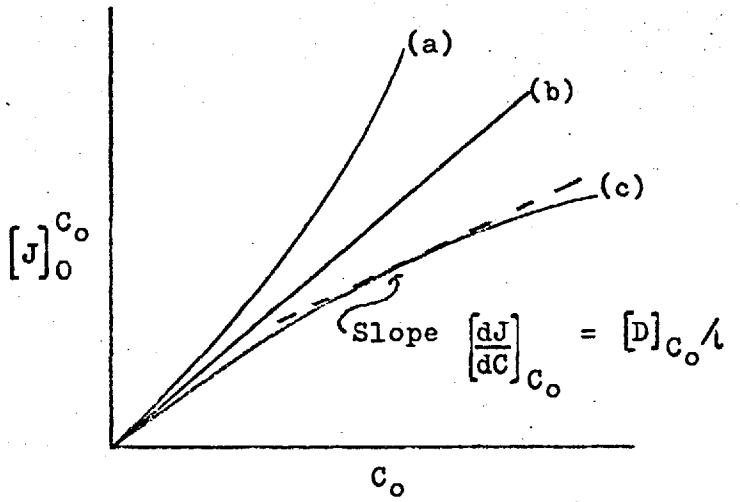

Figure 2.1 Evaluation of $[D]_{C_o}$

from which it may be seen that the permeability is the integrated form of the diffusion coefficient. Substituting for the diffusion coefficient from equation 2.11

$$K = \frac{[J]_{C_o}.l}{C_o} = \frac{1}{C_o}\int_0^{C_o}\left[\frac{dJ}{dC}\right]_{C_o}.dC \qquad 2.13$$

it may be seen that the condition for the permeability to remain constant is that (dJ/dC_o) is a constant.

It is important that the concentration limits are clearly defined. When the diffusion coefficient is independent of the concentration at the in-going side then the diffusion coefficient and permeability are equivalent as in case b of figure 2.1. If however the diffusion coefficient becomes dependent on the in-going side concentration then it is no longer equal to the permeability, and the quotient $[D]_{C_o}/l$ is now the tangent to the curve at $C_o = C_1$ as shown in figure 2.2, if in addition the concentration at the out-going side is not effectively zero then the permeability becomes a function of both the in-going and out-going side concentrations. The

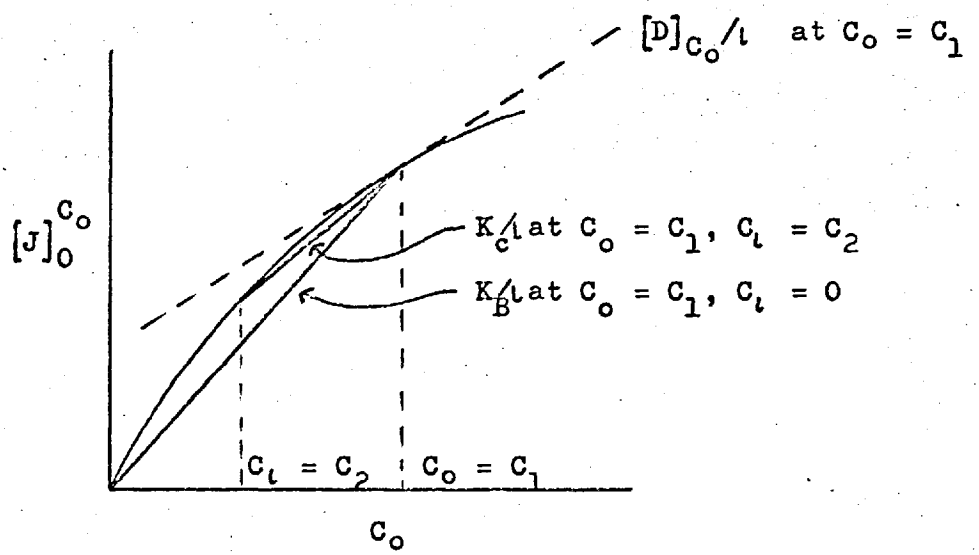

Figure 2.2 Illustration of difference between alternative definitions of permeability

permeabilities reported here are as defined by Barrer, that is with the out-going side concentration effectively zero. This is shown as K_B in figure 2.2. Other workers such as Carman (1956), and McIntosh (1966) choose a real value for the out-going side concentration and so report the term K_c as the permeability. This will only be equal to the diffusion coefficient or K_B for the linear case of figure 2.1, that is to say when the diffusion coefficient is independent of concentration. Once concentration dependency arises the Carman type permeability will take on an intermediate value between K_B and $[D]_{C_o}$, as shown in figure 2.2.

2.1.3 Surface flow

As indicated in the introduction it is now recognised that a separate surface flow can accompany molecular streaming. The flow arises from transport of molecules that have adsorbed onto the surface of the porous media, and, like the gas phase flow, this surface flow may be formulated in

terms of the Fick laws. This enables us to evaluate the respective diffusion coefficients and permeabilities for each component. To derive the equations the surface concentrations will be defined in terms of the surface excess, as this definition does not require an estimation of the volume of the adsorbed phase. The surface excess is illustrated below in figure 2.3

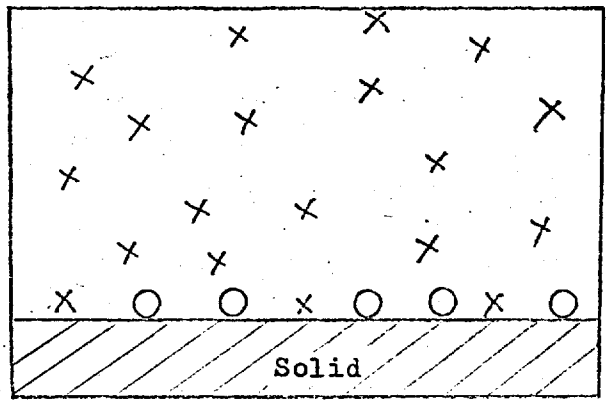

Figure 2.3 Illustrating the surface excess

× Gas phase molecules

○ Molecules at the surface in excess of the gas phase

Defining

A as the surface area of the membrane in cm^2 cm^{-3} of porous media.

ε as the pore volume in cm^3 cm^{-3} of porous medium.

C as the total quantity of adsorbable material in the gaseous and adsorbed phase in moles cm^{-3} of porous medium.

C_g as the gas phase concentration in moles cm^{-3} of porous medium. This concentration includes those molecules that will be present in the vicinity of the surface irrespective of whether adsorption takes place or not. The gas phase

molecules are represented by $\times$ in figure 2.3.

C_s as the surface excess in moles cm^{-3} of porous medium. The excess is formed by the molecules present due to adsorption and is shown as $\bigcirc$ in the diagram.

C_g^g as the gas phase concentration in moles cm^{-3} of pore space.

C_s^s as the surface excess in moles cm^{-2} of surface.

The concentrations are related to each other by the following equations

$$C_s = C - C_g \qquad 2.14$$

$$C_s = A.C_s^s \qquad 2.15$$

$$C_g = \varepsilon.C_g^g \qquad 2.16$$

$$P = R.T.C_g^g \qquad 2.17$$

An adsorption isotherm is a measure of C_s^s for a given pressure, consequently all the terms in equations 2.14 to 2.17 are directly measurable quantities. In the Henry law region of adsorption the amount adsorbed is directly proportional to the prevailing pressure (Henry, 1922)

$$C_s^s = k_s.C_g^g \qquad 2.19$$

or

$$C_s = k_s.\frac{A}{\varepsilon}.C_g \qquad 2.20$$

The degree of surface flow controls the nature and quantity of information revealed by experiment. In the Henry law region, where the flows are independent of each other, we obtain information about the mechanism of transport and the physical nature of the surface. As adsorption increases the adsorbed layer begins to block off the gas phase flux. This blockage allows one to study the range of pore diameters of the membrane, and to suggest possible gas separation systems.

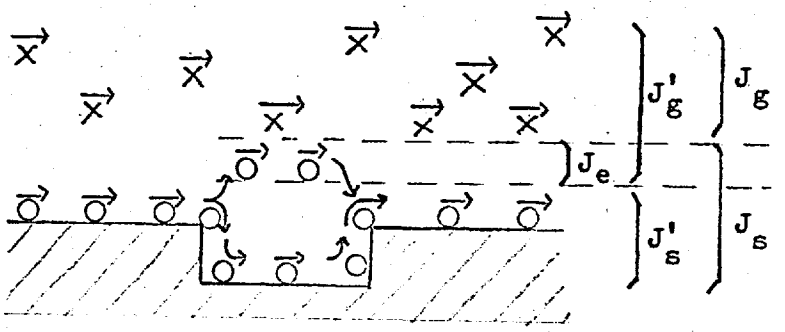

Figure 2.4 Diagram illustrating various fluxes

X Molecules of the gas phase

O Molecules present due to the surface

There are two ways of dividing up the total flux, as shown diagramatically in figure 2.4. The first method divides the total flux J into the gas phase flux J_g, and the surface flux J_s which is present due to the surface excess. As long as the adsorbed film does not block the membrane then the gas phase flux J_g can be determined using a non-sorbed calibrating gas normally helium, flowing through a sorbate free medium (Barrer and Gabor, 1960). Then from equation 2.9

$$J_g = J_g^{He} \left(\frac{M_{He}}{M}\right)^{1/2} \qquad 2.20$$

$$J_s = J - J_g \qquad 2.21$$

Blockage, which occurs at higher adsorption, may be determined by using a non-sorbed indicator gas in the presence of the adsorbing gas (Ash, Barrer and Pope, 1963). However this does not necessarily measure J_g, for the pore system may become sealed to the indicator gas by capillary condensate at the bottle-necks. This results in an under-estimation of J_g, for gas transport will still occur across the unfilled pore space before and after the restriction.

The surface flux J_s is the whole flux called into existence by the presence of mobile adsorbed films with a concentration gradient. However the surface of many porous membranes is broken up by blind pores, cracks, and crevices. At these points it is necessary for part of the surface flow to evaporate into the gas phase and condense back on to the surface beyond the point of interruption. Consequently the gas phase flux is enhanced to the detriment of the surface flux. So there is an alternative division of the total flux J into the flux J'_g through any cross-section for all the molecules in the gas phase including those molecules making evaporative flights from the surface: and J'_s, the flux through any cross-section for the molecules moving only along the surface,

$$J = J'_g + J'_s \qquad 2.22$$

From what has been said, and as shown in the diagram $J'_g > J_g$ and $J_s > J'_s$. This latter formulation is of greater interest for proposing theoretical models of surface flow and was in effect used by Hill (1956) and Higashi et al (1963, 1964, 1966) for deriving model surface diffusion coefficients. However while J_g and J_s are readily obtainable by the use of helium as a calibrating gas, no general method for measuring J'_g and J'_s has so far been developed, and direct comparison between models formulated in terms of J'_g and J'_s and experiments formulated in terms of J_g and J_s is inadmissible. Ash, Barrer and Pope (1963) calculated values for J'_g and J'_s from the experimental values of J_g and J_s for the particular case of a partially blocked medium; also Barrer and Gabor (1960) obtained an equation relating the respective diffusion coefficients D'_s and D_s for the Henry law region of adsorption.

2.1.4 Relationship between J_s and J'_s.

Both J_s and J'_s may be formulated in terms of Fick's laws

$$J_s = - D_{ss} \cdot \frac{dC_s}{dx} \qquad 2.23$$

$$J'_s = - D'_{ss} \cdot \frac{dC_s}{dx} \qquad 2.24$$

where D_{ss} and D'_{ss} are the respective steady state diffusion coefficients. For an ideally smooth surface J'_s will equal J_s, and a decrease in J'_s is a measure of the surface roughness. To evaluate J'_s an expression must be found for its diffusion coefficient D'_{ss} in terms of D_{ss}, since only D_{ss} can be measured by experiment. Barrer and Gabor (1960) applied the following argument to surface films in the Henry law region of adsorption.

In the Henry law region of adsorption any progressive flux interconversion down the length of the membrane of the surface phase into the gas phase is absent. Consequently for any cross-section the number of evaporative flights is constant. However the summation of all the evaporative flights is equivalent to a fraction X of the length l of the membrane for which J_s has joined the gas phase. This allows us to rewrite the flux for the evaporative flights J_e in terms of J_g and J_s.

$$J_e = D_e \cdot \frac{(J_g + J_s)}{J_g} \cdot \frac{\Delta C_g}{l} \qquad 2.25$$

Re-arranging the expressions for the total flux from

$$J_g + J_s = J'_g + J'_s \qquad 2.26$$

to

$$J_g + J_s = (1 - X)(J'_g + J'_s) + X.J_e \qquad 2.27$$

and with the simplifying assumption that

$$D_{gs} = D'_{gs} = D_e \qquad 2.28$$

one obtains

$$D'_{gs} = \frac{D_{ss}}{(1 - X) - (J_s/J_g).X} \qquad 2.29$$

The value of X is unknown, but is limited to a certain range of values by the following conditions.

(a) It must lead to positive values of D'_{ss}.

(b) In this region of adsorption the diffusion coefficients obey an Arrhenius equation ($D'_{ss} = D_o.\exp(-E^*/RT)$, (Barrer 1963 b, Clint 1966), so the value of E^* must be positive and according to Glasstone (1941) should lie between ¼ and ½ the sorption energy "ΔE".

(c) X should lie in the range in which the decrease of $-E^*/$"ΔE" becomes abrupt. (Barrer 1963 b).

This analysis has been applied to the surface diffusion coefficients of methane, ethane, and propane flowing through cracking catalyst (Barrer 1963 b). Fairly high values for X were found suggesting that for cracking catalysts the surface flow is mainly governed by evaporative flights across the cracks, crevices, and blind pores, the surface being very broken.

In the above derivation the fraction X, of the length of the membrane l, for which the surface flux has passed into the gas phase, is a summation for all the evaporative flights across microscopic lengths of the membrane. The majority of the flights end in condensation back onto the surface, and the actual macroscopic length X does not exist as a single length. This is because the following conditions are operative:

(1) Only steady state fluxes are measured, and the rate of

flow for each phase is the same for any point along the membrane.

(2) Both the gas phase and surface phase concentration gradients are linear

$$\frac{dC_g}{dx} = \frac{\Delta C_g}{l} \quad ; \quad \frac{dC_s}{dx} = \frac{\Delta C_s}{l}$$

(3) There is local equilibrium between the surface and gas phase at all points along the membrane.

These conditions only apply in the Henry law region of adsorption. Once the adsorption isotherm becomes curved the diffusion coefficient becomes a function of concentration and equation 2.29 is no longer valid.

When there is very heavy adsorption the membrane becomes partially blocked to the gas phase flux, and in order to retain local equilibrium the surface phase will convert into the gas phase past the point of blockage. This results in progressive flux interconversion along the length of the membrane.

2.1.5 Flux interconversion

Evidence for flux interconversion was found by Ash, Barrer and Pope (1963) in their studies of the flow of hydrogen-sulphur dioxide mixtures through a similar membrane to the one reported here. The hydrogen flux was limited to the gas phase and the sulphur dioxide flux was completely dominated by the transport of the densely adsorbed film (only 0.3% was in the gas phase). For these experiments it was possible to calculate the concentration profiles for each phase by the method to be out-lined in section 2.1.7. Assuming local equilibrium existed for all points along the length of the membrane, the gas phase concentration profile for

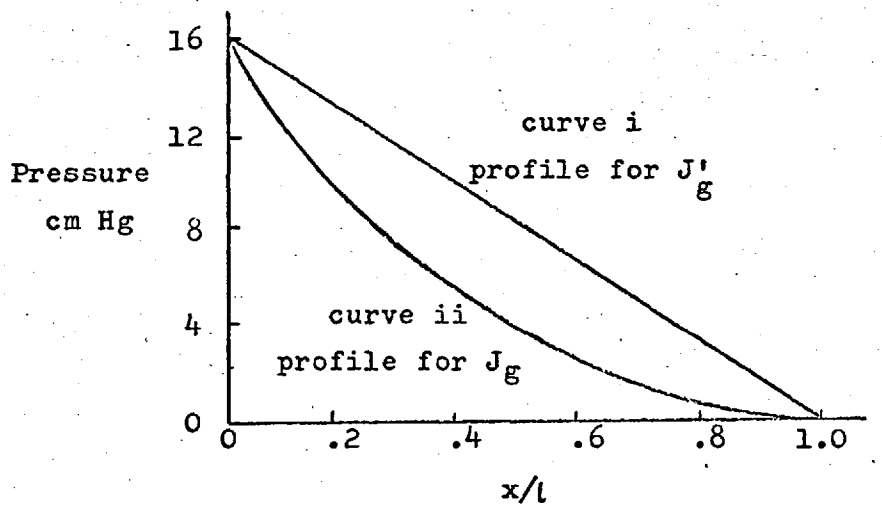

Figure 2.5 Gas phase concentration profiles after Ash, Barrer and Pope (1963).

sulphur dioxide (curve i in figure 2.5) was calculated from the sorbed phase concentration profile and the adsorption isotherm. This profile was associated with the flux J'_g (SO_2). The flux $J_g(SO_2)$ may be evaluated from the hydrogen flux by

$$J_g(SO_2) = J_g(H_2)\left(\frac{M_{H_2}}{M_{SO_2}}\right)^{\frac{1}{2}} \qquad 2.30$$

so we may calculate the profile associated with the flux $J_g(SO_2)$ since it will be identical with that for hydrogen at the same in-going side pressure. This is shown as curve ii, which shows that there is progressive interconversion of the fluxes along the length of the plug.

2.1.6 Relationship between J_s and J_g.

J_s is the flux called into existence by the presence of a surface, but it is immaterial as to whether it is actually on the surface or in the gas phase. Assuming that the membrane is isotropic and that anomalies due to blockage are absent, then J_s is independent of x since $J_s = J - J_g$

and both J and J_g are independent of x. Barrer and co-workers in a series of papers (Barrer 1954, 1963 a, Ash, Barrer and Nicholson 1963, Ash, Barrer and Pope 1963, Ash, Baker and Barrer 1967) showed that under these conditions the ratio of the surface to gas phase diffusion coefficients D_{ss}/D_{gs} varies with the inverse slope of the isotherm $1/\sigma$.

Formulating the steady state fluxes J_s and J_g per unit area normal to the x direction of flow in terms of the Fick law:

$$J_s = -D_{ss}.\frac{dC_s}{dx} = -D_{ss}.A.\frac{dC_s^s}{dx} \qquad 2.31$$

$$J_g = -D_{gs}.\frac{dC_g}{dx} = -D_{gs}.\varepsilon.\frac{dC_g^g}{dx} \qquad 2.32$$

The ratio J_s/J_g is necessarily a constant independent of x. So combining equations 2.31 and 2.32

$$\frac{J_s}{J_g} = \frac{D_{ss}}{D_{gs}}.\frac{A}{\varepsilon}.\frac{dC_s^s}{dC_g^g} = \text{constant} \qquad 2.33$$

When the out-going side concentrations are effectively zero, then at the out-going side $dC_s^s/dC_g^g = k_s$, the Henry's law adsorption constant, and D_{gs} and D_{ss} assume their limiting values D_{gs}^o and D_{ss}^o. The constant may then be expressed as

$$\frac{D_{ss}^o}{D_{gs}^o}.\frac{A}{\varepsilon}.k_s = \text{constant}$$

and the ratio of the diffusion coefficients becomes

$$\frac{D_{ss}}{D_{gs}} = k.\frac{1}{\sigma} \quad \text{where } k = \frac{D_{ss}^o}{D_{gs}^o}.k_s \qquad 2.34$$

In the Henry law region of adsorption dC_s^s/dC_g^g is also a constant and so the ratio of the diffusion coefficients is independent of surface concentration. This is in agreement with the experiments of Barrer and Strachan (1955), and Aylmore and Barrer (1966). Outside the Henry law region the ratio of the diffusion coefficients will vary as the inverse

slope of the isotherm, and this has recently been demonstrated by Ash, Baker and Barrer (1967).

2.1.7 Concentration gradients along the membrane

It is possible to calculate the total, gas phase, and surface phase concentration profiles within the membrane from the respective steady state fluxes. This is assuming that the membrane is isotropic and is not blocked by adsorbed phase, the diffusion coefficients being a function only of concentration. There is also the additional assumption that there is local adsorption equilibrium so that surface concentrations may be determined from static adsorption experiments.

Only the equation for the total concentration profile will be derived, the procedure being identical for either the gas phase or surface phase concentration. The boundary conditions will be those used in the present work, that is to say the concentration at the out-going side is effectively zero, although this limitation is not necessary for the general result as long as the boundary conditions are clearly defined. For steady state flow, the total flux J per unit cross-section is formulated by Fick's law as

$$J = - D.\frac{dC}{dx} \qquad 2.35$$

where $J = J_s + J_g$, and $C = C_s + C_g$, and D is the overall diffusion coefficient defined by equation 2.35.

For a series of experiments the in-going side total concentration C_o is

$$C_o = C_o^1 , C_o^2 , C_o^3 , C_o^n , \ldots , \text{etc} \qquad 2.36$$

and the corresponding fluxes are

$$J = J^1 , J^2 , J^3 , J^n , \ldots , \text{etc} \qquad 2.37$$

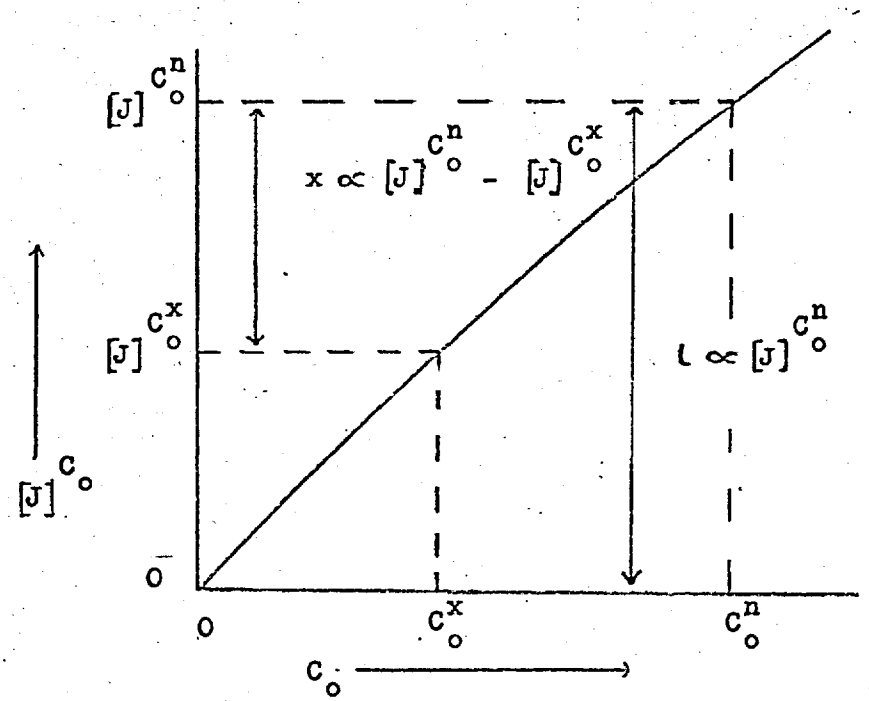

Figure 2.6 Illustrating calculation of concentration profiles

Now for the n^{th} experiment the integral of equation 2.35 between the limits $x = 0$, $C = C_o^n$, and $x = l$, $C = 0$, is

$$[J]^{C_o^n}.l = \int_0^{C_o^n} D.dC \qquad 2.38$$

At point x along the membrane the total concentration is C^x, and the corresponding integral of equation 2.35 up to this point x will be between the limits $x = 0$, $C = C_o^n$, and $x = x$, $C = C^x$. However the flux will still be flowing under the same concentration gradient C_o^n to 0, so

$$[J]^{C_o^n}.x = \int_{C^x}^{C_o^n} D.dC \qquad 2.39$$

$$= \int_0^{C_o^n} D.dC - \int_0^{C^x} D.dC \qquad 2.40$$

$$= \left[[J]^{C_o^n} - [J]^{C^x} \right].l \qquad 2.41$$

$$\frac{x}{l} = \frac{\left[[J]^{C_o^n} - [J]^{C^x} \right]}{[J]^{C_o^n}} \qquad 2.42$$

Now we may plot J versus C_o for a series of experiments (figure 2.6). Then for the n^{th} experiment

$$[J]^{C_o^n} \propto l$$

and for any concentration C_o^x which is less than C_o^n

$$[J]^{C_o^n} - [J]^{C_o^x} \propto x$$

and this concentration C_o^x wil also be equivalent to the concentration C^x for the point x along the membrane when the in-going side concentration is C_o^n. Proceeding in this way we may evaluate C against x/l for the length of the membrane for each experiment.

2.1.8 The permeability

The physical properties of the membrane exercise a large degree of control over the flow of material through it. This degree of control may be compared for different membranes by evaluating the flux for a given gas that would occur through a standard membrane under standard conditions. This standardised flux is known as the permeability and is defined as: 'the quantity of material flowing per unit time through unit length of porous medium of unit cross-sectional area under a unit concentration gradient'. This rather general description allows a number of different permeabilities to be defined according to one's choice of units. The range covers any combination of the following:

(1) The quantity of material may either be the total flux J, or the gas phase fluxes J_g or J'_g, or the surface fluxes J_s or J'_s.

(2) If the membrane swells on adsorption the unit length may either be the original length, or the swollen length.

(3) The unit area may either be the cross-sectional area of the membrane A_c, or the cross-sectional area of the pore space εA_c, or a swollen area.

(4) The concentration gradient may be for the total concentration C, or for the gas phase concentration C_g or C_g^g or P, or for the concentration on the surface C_s or C_s^s.

Irrespective of one's choice of units the general equation for permeability in terms of the above definition is

$$K = \frac{J.l}{\Delta C} \qquad 2.43$$

and as shown in section 2.1.2 it is the integral of the gradient (dJ/dC_o). It is when this gradient departs from linearity that the permeability becomes concentration dependent. However, the variation of permeability with concentration is very susceptible to the choice of units, as is demonstrated with the following examples.

The flux is the total flux J per unit area A_c normal to the x direction of flow, and we assume the membrane does not swell.

Case 1 For concentration gradient ΔC

Permeability $K_T = J.l./\Delta C$

Following the procedure out-lined in section 2.1.2

$$J = -D.\frac{dC}{dx} \qquad \text{and} \qquad \left[\frac{dJ}{dC}\right]_{C_o} = [D]_{C_o}/l$$

Then the gradient at the point x along the membrane is given by

$$\left[\frac{dJ}{dC}\right]_{C_o} = -\frac{[J]^{C_o}}{l}.\left(\frac{dx}{dC}\right) \qquad 2.44$$

and so the total permeability K_T will remain constant so long as the inverse of the total concentration gradient (dx/dC) is constant.

Case 2 For the gas phase concentration gradient ΔC_g

Permeability $K_T^g = J.l./\Delta C_g$

$$J = - D_a . \frac{dC_g}{dx} \quad \text{and} \quad \left[\frac{dJ}{dC_g}\right]_{C_{g,o}} = \left[D_a\right]_{C_{g,o}} / l$$

and for the point x along the membrane

$$\left[\frac{dJ}{dC_g}\right]_{C_{g,o}} = - \frac{[J]^{C^{*}_{g,o}}}{l} . \left(\frac{dx}{dC_g}\right) \qquad 2.45$$

Here the permeability is a function of the reciprocal gas phase concentration gradient (dx/dC_g). As long as this gradient is linear then the permeability K_T^g remains a constant. When the permeability becomes a function of the gas phase concentration, then referring back to section 2.1.5, it is to be expected that flux interconversion is occuring along the length of the membrane.

Case 3 For the surface phase gradient ΔC_s

Permeability $K_T^s = J.l./\Delta C_s$

$$J = - D_b . \frac{dC_s}{dx} \quad \text{and} \quad \left[\frac{dJ}{dC_s}\right]_{C_{s,o}} = \left[D_b\right]_{C_{s,o}} / l$$

and for the point x along the membrane

$$\left[\frac{dJ}{dC_s}\right]_{x} = - \frac{[J]^{C^{*}_{s,o}}}{l} . \left(\frac{dx}{dC_s}\right)_{x} \qquad 2.46$$

or

$$\left[\frac{dJ}{dC_s}\right]_{x} = - \frac{[J]^{C^{*}_{s,o}}}{l} . \left(\frac{dx}{dC_g}\right)_{x} . \left(\frac{dC_g}{dC_s}\right)_{x} \qquad 2.47$$

Equation 2.47 shows that the permeability K_T^s will only remain constant while the slope of the isotherm is linear. So it is to be expected that K_T^s will take a functional form with the in-going side surface concentration as soon as adsorption is outside the Henry law region. Consequently K_T^s is much more sensitive to its concentration term C_s than

K_T^g since K_T^g only takes on a functional form when there is very heavy adsorption causing blockage and flux interconversion. Similar conclusions would be reached for the permeabilities of the gas phase flux and surface phase flux defined as:

$$J_g = -D_{gs} \cdot \frac{dC_g}{dx} \quad \ldots\ldots \quad K_g^g = \frac{J_g \cdot l}{\Delta C_g} \qquad 2.48$$

$$J_s = -D_{ss} \cdot \frac{dC_s}{dx} \quad \ldots\ldots \quad K_s^s = \frac{J_s \cdot l}{\Delta C_s} \qquad 2.49$$

2.1.9 The diffusion coefficient

The diffusion coefficient is defined by Fick's equation and may be regarded as the coefficient of the identity

$$J \equiv -D \frac{\partial C}{\partial x}$$

In the general case D may be a function of concentration C, distance x, and time t. The present work is limited to steady state flow through a uniform membrane (for a discussion on the isotropy of the membrane see section 5.1.9), so we may consider the diffusion coefficient to be independent of time, and in the absence of blockage, membrane swelling and flux interconversion D is also independent of distance. Each flux has its own individual diffusion coefficient, and evaluation of these separate quantities is outlined below.

(1) No surface flow

In the absence of surface flow the total flux and gas phase flux are one and the same. The concentration gradient is linear, and as indicated in section 2.1.2 the diffusion coefficient is equal to the permeability K.

$$K = D = \frac{J \cdot l}{\Delta C} \qquad 2.50$$

Clint (1966) showed that for a similar membrane to the one reported here, only helium has no measurable surface flow.

(2) Independent surface and gas phase flow

(a) Total diffusion coefficient D

The total diffusion coefficient D is readily evaluated from equation 2.11, the quotient D/l at $C = C_o$ being the slope at C_o of the plot of total flux versus total in-going side concentration, C_o.

(b) Gas phase diffusion coefficient D_{gs}

While the fluxes are independent of each other the gas phase diffusion coefficient may be evaluated by the helium calibration method:

$$D_{gs} = D_{gs}^{He} \cdot (M_{He}/M)^{\frac{1}{2}} \qquad 2.51$$

(c) Surface phase diffusion coefficient D_{ss}

Having measured the total flux, and evaluating the gas phase flux by helium calibration, the surface flux will be

$$J_s = J - J_g$$

The surface concentration at the in-going side may be found from the adsorption isotherm and hence D_{ss} may be similarly evaluated as for case (a) where D_{ss}/l at $C_{s,o}$ is the slope of the plot of surface flux versus in-going side concentration, $C_{s,o}$, for a series of experiments:

$$\left[D_{ss}\right]_{C_{s,o}}/l = \left[\frac{dJ_s}{dC_s}\right]_{C_{s,o}} \qquad 2.52$$

The total diffusion coefficient D may be related to the surface diffusion coefficient D_{ss} in the following manner. If the total concentration is split up into its individual parts C_g and C_s, then the total concentration gradient may be expressed as

$$\frac{dC}{dx} = A \cdot \frac{dC_s^s}{dx} \cdot \left(1 + \frac{\varepsilon\sigma}{A}\right) \quad \text{where} \quad \frac{dC_g^g}{dC_s^s} = \sigma \qquad 2.53$$

Since $J = -D.(dC/dx) = J_s + J_g$, we may write, using equations 2.33 and 2.53

$$D.A.\frac{dC_s^s}{dx}.(1 + \frac{\varepsilon\sigma}{A}) = D_{ss}.A.\frac{dC_s^s}{dx} + D_{ss}.A.\frac{dC_s^s}{dx}.\frac{D_{gs}}{D_{ss}}.\frac{\varepsilon\sigma}{A} \qquad 2.54$$

$$\text{so} \qquad D = \frac{D_{ss}.(A\sigma + \varepsilon D_{gs}/D_{ss})}{(A\sigma + \varepsilon)} \qquad 2.55$$

$$\text{or} \qquad D_{ss} = \frac{D.(A\sigma + \varepsilon) - \varepsilon D_{gs}}{A\sigma} \qquad 2.56$$

(3) Predominating surface flux

When the surface flux is very much larger that the gas phase flux then blockage may start to occur. The evaluation of D_{gs} by the helium calibration method is no longer valid, but if a non-sorbed gas is mixed with the sorbing gas as indicated in section 2.1.5, then both D_{gs} and D'_{gs} may be determined along with D_{ss} and D'_{ss}. In these conditions the total diffusion coefficient is effectively the surface diffusion coefficient. From equation 2.56 the condition for D to approach D_{ss} is $A\sigma \gg \varepsilon$ and $\varepsilon(D_{gs}/D_{ss})$.

2.1.10 Flow of gas mixtures

The equations derived in the previous sections for single gas flow equally apply to the diffusion of gas mixtures through a microporous membrane. Consequently from the flow data for single components of the mixture we may predict the separation efficiency of the membrane.

The separation factor is defined as

$$\eta = \left(\frac{x_A}{x_B}\right)_o.\left(\frac{x_B}{x_A}\right)_l \qquad 2.57$$

where the x's denote mole fractions of the gases A and B, and the subscripts o and l denote the values at the in-going

and out-going sides respectively. This may be rewritten as

$$\eta = \left(\frac{C_A}{C_B}\right)_o \cdot \left(\frac{J_B}{J_A}\right)_\ell \qquad 2.58$$

where C is the respective concentration at the in-going side, and J the respective flux through the membrane.

Gas mixtures from the view point of diffusion fall into three groups, although the dividing line is not sharp.

Group 1 This group comprises mixtures made up of weakly or non-sorbed components. Providing the flow is in the Knudsen region, both components will flow independently of one another in the gas phase. If the components also flow independently of one another in the surface phase we may conclude that the transport is by a diffusive mechanism (Aylmore and Barrer 1966, Ash and Barrer 1967).

Group 2 This group comprises mixtures made up of one strongly sorbed and one weakly sorbed or non-sorbed component. For strongly sorbed gases the surface flux in high area, microporous media is very much larger than the gas phase flux, and very large separations can be achieved. In addition the sorbed phase can block off the gas phase flux by capillary condensation at bottle-necks and the medium effectively becomes a semi-permeable membrane for the sorbed species. As pointed out in section 2.1.5 this group also yields valuable information on flux interconversion (Ash, Barrer and Pope 1963).

Group 3 This group comprises two strongly sorbed gases. In this case it is difficult to predict the degree of separation. However work in this region would give valuable information on the transport mechanism for strongly sorbed films.

2.2 ADSORPTION

2.2.1 The adsorption isotherm

An adsorption isotherm is a plot of the amount adsorbed, C_s^s, as a function of the prevailing pressure, P, or C_g^g,

$$C_s^s = f(C_g^g)$$

and it is to be intuitively expected that the nature and quantity of adsorption will have some bearing on the surface flux. The various regimes of adsorption are controlled by the surface concentration, the energetic heterogeneity of the surface, mobility of the adsorbed species, and interactions between the adsorbed species, thus forming the following groups.

(i) Henry law adsorption

This is the simplest type of adsorption in which the amount adsorbed is proportional to the equilibrium pressure. The regime is limited to the region of very high dilution in the adsorbed phase, but the other variables have no controlling influence.

(ii) Localised adsorption below monolayer coverage

Fowler (1936) laid down the conditions for localised adsorption as: "the atoms (or molecules) of the gas are adsorbed as wholes on to definite points of attachment on the surface of the adsorber, that each point of attachment can accommodate one and only one adsorbed atom, and that the energies of the states of any adsorbed atom are independent of the presence or absence of other adsorbed atoms on neighbouring points of attachment". Adsorption in zeolites is probably the closest approach to these rather stringent conditions, but several model isotherms have been developed, notably the Langmuir isotherm, and modifications of it to take into account possible surface heterogeneity and sorbate-sorbate interactions (Young and Crowell 1962, pp. 106).

(iii) Mobile adsorption below monolayer coverage

In localised adsorption migration across the surface is restricted (but not prevented) by the potential energy barrier separating neighbouring sites. If this restriction is removed then the adsorbed molecules will be able to enjoy an unrestricted two-dimensional mobility. Thus the area occupied by each molecule is determined by the size, concentration and orientation of the adsorbed species, whereas in the localised model the site area is fixed by the lattice parameters of the solid. Once again a number of model isotherms have been derived according to the various conditions of adsorption (Young and Crowell 1962, pp. 110).

(iv) Multilayer adsorption

The isotherms for multilayer adsorption vary from the 'monotonous to the fantastic', although Brunauer et al (1940) have classified them into five types. Brunauer et al (1938) also derived the B.E.T. equation for multilayer adsorption from which the surface area can be derived. However there is no heuristic equation describing mutilayer adsorption, and it would be defeating the purpose to substitute a model equation into equation 2.34 which relates, entirely on heuristic arguments, the ratio of the diffusion coefficients to the reciprocal slope of the isotherm. The only practical test of equation 2.34 is to fit the experimental isotherm to a polynomial equation by computer, and compute the slope for particular values of pressure.

In addition to providing the surface concentration data for the flow experiments, adsorption isotherms also provide information about surface forces and surface heterogeneity. Such information is derived from the thermodynamics of adsorption. Since there are now a number of reviews on the subject (e.g. Hill, 1949, 1950, 1952; Everett, 1950a, b, c,

1952; Young and Crowell, 1962; Ross and Olivier, 1964), only the results, definitions and limitations in the context of the present work need be mentioned in the following section.

2.2.2 The thermodynamics of adsorption

There are three approaches to the thermodynamics of adsorption. The first 'Solution Thermodynamics' considers the system as a solution of adsorbate and adsorbent, and the solution is in equilibrium with the gaseous phase. Application of the Clausius-Clapeyron method leads to a heat of adsorption being defined by the following equation

$$\left(\frac{\partial P}{\partial T}\right)_{x_s} = \frac{\Delta\bar{H}}{T(\bar{V}_s - \tilde{V}_g)} \qquad 2.59$$

$\Delta\bar{H}$ = The partial molar heat of adsorption
$\bar{V}_s$ = The partial molar volume of the adsorbate in solution
$\tilde{V}_g$ = The molar volume of the gas phase
x_s = The mole fraction of adsorbate in solution
P = The prevailing pressure in the gas phase
T = The absolute temperature

At very low coverages we must decide how to apply the restriction in equation 2.59 of constant mole fraction of adsorbate, x_s, and how to interpret the partial molar volume of the adsorbate in solution, $\bar{V}_s$. This was discussed in detail by Clint (1966) who showed that if the adsorbed phase is considered as a solution of gas dissolved inside the adsorbent as in clathration, then equation 2.59 reduces to

$$\left(\frac{\partial P}{\partial T}\right)_{x_s} = \left(\frac{\partial P}{\partial T}\right)_{\Gamma} = -\frac{\Delta\bar{H}}{T.\tilde{V}_g} \qquad 2.60$$

where Γ is the surface excess. On the other hand the sorbed phase may be defined as occupying a specific volume above the surface as this represents a more valid picture of physical

adsorption. However, this sorption volume will include those molecules of the gas phase that would be present whether adsorption takes place or not. Only above 0.1 of a monolayer will this gaseous term become insignificant enough to allow the aproximation

$$\left(\frac{\partial P}{\partial T}\right)_{x_s} = \left(\frac{\partial P}{\partial T}\right)_{\Gamma} = \left(\frac{\partial P}{\partial T}\right)_{n_s} = -\frac{\Delta\bar{H}}{T.\tilde{V}_g} \qquad 2.61$$

n_s = Moles of adsorbate

So above 0.1 of a monolayer the models become equivalent which allows equation 2.61 to be re-arranged to

$$-\left(\frac{d\ \ln\ P}{dT}\right)_{\Gamma} \cong -\frac{\Delta\bar{H}}{R.T^2} \qquad 2.62$$

where the approximate equality $\cong$ is used to indicate the application of the perfect gas law. Equation 2.62 serves as a definition for the isosteric heat q_{st}; that is the isosteric heat is the negative partial molar heat of adsorption at constant surface excess

$$\left(\frac{d\ \ln\ P}{dT}\right)_{\Gamma} = \frac{q_{st}}{R.T^2} \qquad 2.63$$

so $$q_{st} = -\Delta\bar{H} \qquad 2.64$$

or more generally

$$q_{st} = -\frac{\Delta\bar{H}}{\left(1 - \frac{\bar{V}_s}{\tilde{V}_g}\right)} \qquad 2.65$$

We may also define an integral heat of adsorption $\Delta\mathcal{H}$ as

$$\Delta\mathcal{H} = \frac{1}{n_s}\int_0^{n_s} \Delta\bar{H}.dn_s \qquad 2.66$$

this heat may be found from calorimetry after correcting for any expansion or compression work done on the gas phase.

The second approach 'Adsorption Thermodynamics' regards the adsorbate as forming a pure one component sorbed phase on a completely inert surface of adsorbent. All the thermodynamic quantities are molar quantities which allows another heat of adsorption to be defined as

$$\left(\frac{\partial P}{\partial T}\right)_{\phi} = \frac{\Delta\tilde{H}}{T(\tilde{V}_s - \tilde{V}_g)} \qquad 2.67$$

$\Delta\tilde{H}$ = The molar heat of adsorption at constant spreading pressure

ϕ = The two-dimensional spreading pressure of the adsorbed phase

$\tilde{V}_s$ = The molar volume of the adsorbed phase

ϕ can be evaluated exactly from the experimental isotherm data by following equation (see Clint 1966, p. 148)

$$\phi = R.T\int_0^P \frac{\Gamma'}{P}.dP \qquad 2.68$$

so equation 2.67 reduces to

$$\left(\frac{d\ \ln P}{dT}\right)_{\phi} = -\frac{\Delta\tilde{H}}{R.T^2\left(1 - \frac{\tilde{V}_s}{\tilde{V}_g}\right)} \qquad 2.69$$

However an estimation has to be made for $\tilde{V}_s$. At high surface coverage the film density is approaching that of the liquid state and so the term $\tilde{V}_s/\tilde{V}_g$ is very small and may be neglected. At very low coverages the film density is approaching that of the gaseous state and the term $\tilde{V}_s/\tilde{V}_g$ can become significant. An example of this situation will be shown in section 5.2.2.

Clint (1966) discussed the special relationships that apply in the Henry law region of adsorption, and showed that the heat of adsorption "ΔH" and energy of adsorption "ΔE" of Henry law adsorption is given by

$$\text{"}\Delta H\text{"} = -R.T^2.\frac{d\ \ln(v/P)}{dT} = \frac{\Delta\bar{H}}{(1 - \bar{V}_s/\bar{V}_g)} \qquad 2.70$$

$$\text{"}\Delta E\text{"} = -R.T^2.\frac{d\ \ln k_s}{dT} = \frac{\Delta\tilde{H}}{(1 - \tilde{V}_s/\tilde{V}_g)} \qquad 2.71$$

v = The up-take in cc at NTP per g

and within this region the heat and energy are related by

$$\text{"}\Delta E\text{"} = \text{"}\Delta H\text{"} + R.T \qquad 2.72$$

The third approach is by 'Total System Thermodynamics' which was discussed in some detail by Tykodi (1954). The system is considered in total as a two component system gas and solid which form a surface excess. The thermodynamic properties of the excess are evaluated as the difference between the properties of the system in the adsorbed state and the properties of the system prior to adsorption, this is called the calibrated state. The chemical potential of the adsorbent in the adsorbed state is defined as

$$\mu_a \equiv \mu_a^o + \mu_f \qquad 2.73$$

μ_a = Chemical potential of the adsorbent in the adsorbed state

μ_a^o = Chemical potential of the adsorbent in the calibrated state

μ_f = Chemical potential of the surface excess

A result of this definition is that for any process which takes place at constant μ_f, the differential coefficients of the solid are the same under adsorption conditions as under calibration

conditions. Thus the resulting thermodynamic properties of the excess are a function purely of the adsorbed species, and are the properties for the ideal adsorption process:

$$i \text{ (gas)} \longrightarrow i \text{ (adsorbed)} \quad \left[\begin{matrix}\text{constant} \\ \text{environment}\end{matrix}\right]$$

The differences between the thermodynamic properties evaluated at constant μ_f and the experimentally evaluated thermodynamic properties at constant surface excess, represent the degree of departure from ideality for the process.

Tykodi derived a molar heat of adsorption at constant chemical potential of the surface excess as

$$\Delta\bar{\mathcal{H}} \cong -R.T^2\left(\frac{\partial \ln P}{\partial T}\right)_{\mu_f} \qquad 2.74$$

(The nomenclature used here is that of Barrer, and Clint, in Tykodi's derivations superscript bars were used to designate molar quantities.)

This heat was related to the isosteric heat by

$$q_{st} = -\Delta\bar{\mathcal{H}} + \frac{T}{\Gamma'}\cdot\left(\frac{\partial \mu_f}{\partial T}\right)_{\Gamma'} \qquad 2.75$$

This extra term was considered to represent the work for swelling the solid and is to be considered in more detail in section 5.2.4.

2.2.3 Evaluation of the Heats of Adsorption

To determine the isosteric heat, q_{st}, we have to assume

(1) The gaseous phase is ideal.

(2) There is equilibrium between the adsorbed and gaseous phase, thus the calculations will not be valid in the hysteresis region.

(3) The coverage is high enough to neglect the $\bar{V}_s/\bar{V}_g$ term.

(4) The isosteric heat is independent of temperature.

Integration of equation 2.63 leads to

$$(\ln P)_{\Gamma} = -\frac{q_{st}}{R.T} + C' \qquad 2.76$$

which in application is

$$\left(\log_{10}\frac{P_1}{P_2}\right)_{\Gamma} = \frac{q_{st}}{2.303\ R}\left(\frac{1}{T_2} - \frac{1}{T_1}\right) \qquad 2.77$$

q_{st} may either be determined from the values of the pressure at the same up-take from the adsorption isotherms at different temperatures, or if several isotherms are available a plot of log P versus 1/T at constant coverage will be linear with a slope of $q_{st}/2.303\ R$.

As a first step in determining the molar heat of adsorption, $\Delta\tilde{H}$, the spreading pressure is evaluated from equation 2.68

$$\phi = R.T\int_0^P \frac{\Gamma}{P}.dP \qquad 2.68$$

This integral may be determined from the experimental isotherm data, ϕ being the area underneath the graph for a plot of v/P versus P. The disadvantage with this method is that large errors occur in the low pressure region. To avoid this difficulty the experimental isotherm v versus P was fitted to a twelve term polynomial by computer, and from this polynomial values for v/P computed in 1 cm Hg pressure increments. Then the computed v/P versus P isotherm was in turn fitted to a twelve term polynomial, this second polynomial was then integrated and values for the integrated polynomial (i.e. $\phi/R.T$) computed in 1 cm Hg steps of pressure. Using the same assumptions as in the evaluation of isosteric heat, equation 2.69 may be integrated to

$$(\ln P)_{\phi} \cong \frac{\Delta\tilde{H}}{R.T} + C' \qquad 2.78$$

$$\left(\log_{10} \frac{P_1}{P_2}\right)_{\phi} = - \frac{\Delta\tilde{H}}{2.303\ R} \left[\frac{1}{T_2} - \frac{1}{T_1}\right] \qquad 2.79$$

$\Delta\tilde{H}$ may then be determined either from values for the pressure at the same ϕ from graphs of ϕ versus P at different temperatures, or if several graphs are available a plot of log P versus 1/T at constant ϕ will be linear with a slope of $-\Delta\tilde{H}/2.303\ R$.

CHAPTER 3 EXPERIMENTAL

3.1 GENERAL DESCRIPTION

The final apparatus was the result of evolution according to the needs of the experiments over a period of three years. It ultimately consisted of two high vacuum pumping units and a separate low vacuum line serving a volumetric adsorption system, a gas mixture diffusion unit, a single gas diffusion unit, a gas analysis system and a set of gas lines. Pyrex glass was used throughout. The complete apparatus was mounted on a 6 ft by 2½ ft table and supported with Chemiframe rod.

3.1.1 The pumping system

The pumping system is shown in figure 3.1. An old rotary pump provided the rough vacuum needed for adjusting manometer levels and lowering mercury levels in McLeod gauges. A triple stage mercury diffusion pump backed by an Edwards two-stage rotary oil pump (type 25 C 20 A capable of pumping down to 1×10^{-3} cm Hg) was used to provide a high vacuum of 1×10^{-6} cm Hg. Each oil pump was provided with a non-return valve, a one litre oil trap, and an air vent. A line by-passing the mercury diffusion pump system was included so that large quantities of gas need not be drawn through the diffusion pump. By providing isolating taps and a 5 litre buffer volume, the oil pump could be serviced while the diffusion pump discharged into the buffer volume. The liquid nitrogen traps either side of the diffusion pump collected vagrant mercury and prevented the high vacuum line from

Figure 3.1 PUMPING SYSTEM

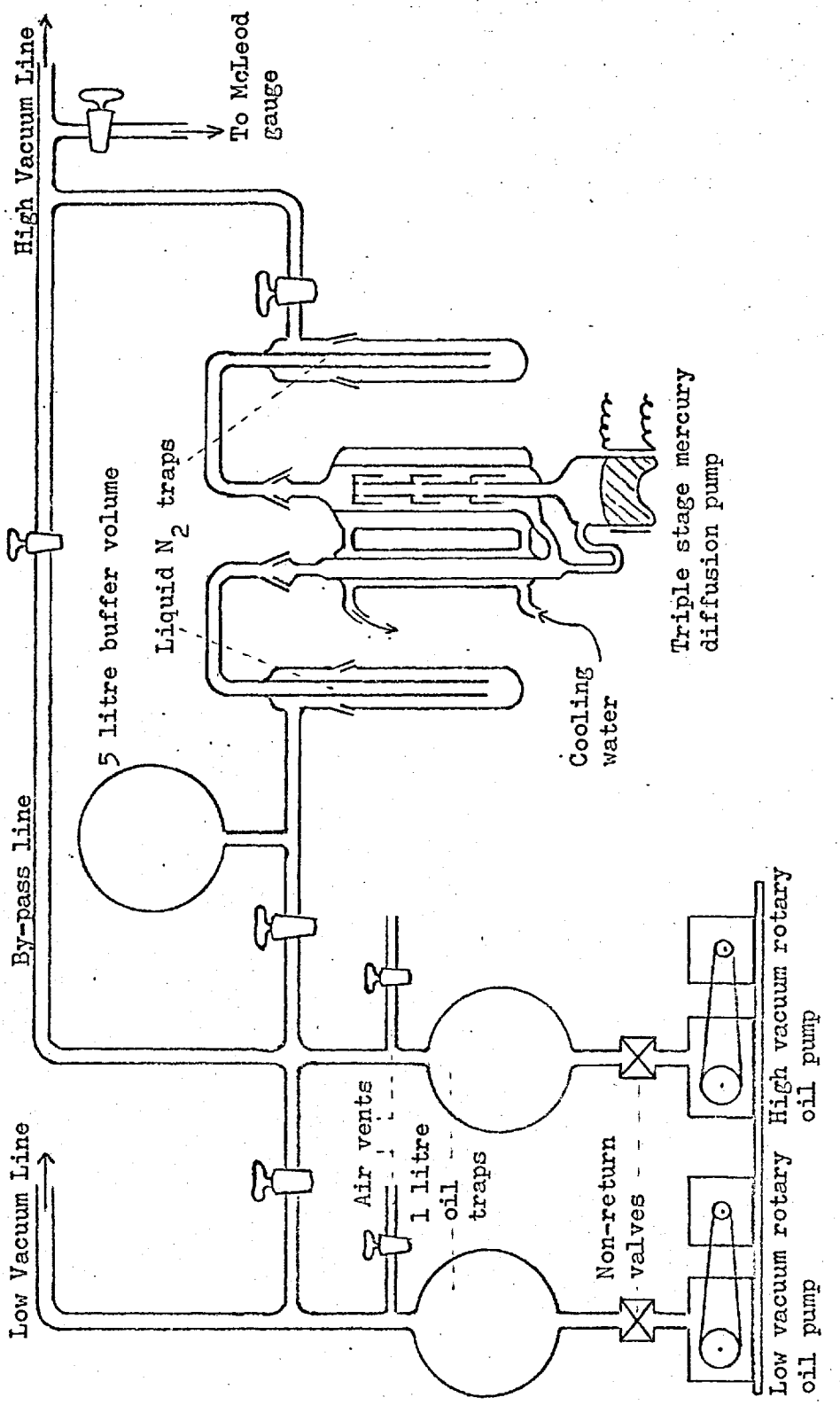

becoming contaminated with low vapour pressure residues from the pump oil and tap grease. A connection between the low and high vacuum lines enabled the rough pump initially to evacuate the whole apparatus. A separate high vacuum system was made for the single gas diffusion apparatus. Experience indicated that the most efficient assembly would be for the high vacuum lines of each individual unit to be separately connected to a parallel pair of pumping units; this would allow each unit to be out-gassed independently of the other units. Efficient pumping speeds were achieved by using wide bore glass tubing (minimum 12 mm diameter) and wide bore high vacuum taps (15 mm diameter openings). 12 mm internal diameter rubber pressure tubing was used to connect the rotary pumps to the rest of the apparatus.

3.2 VOLUMETRIC ADSORPTION APPARATUS

A conventional volumetric adsorption apparatus was built to operate independently of the other units and is shown in figure 3.2. The manometer limbs were made from 1 cm bore Veridia tubing to avoid capillary depression effects. The volume of each burette bulb was chosen so that a change from one bulb to another doubled the total volume. The burette was thermostatted to 25 ^{o}C by circulating water through the surrounding jacket from a large thermostat tank. The lead from the adsorption bulb was lightly packed with glass wool to prevent loss of adsorbent during any sudden pressure fluctuations and the bulb made detachable with a B 7 Quickfit joint so that the sample could be out-gassed to constant weight. In order to eliminate unnecessary dead space 1 mm internal bore high vacuum capillary taps were used in conjunction with 2 mm internal bore capillary tubing. At

Figure 3.2 ADSORPTION APPARATUS

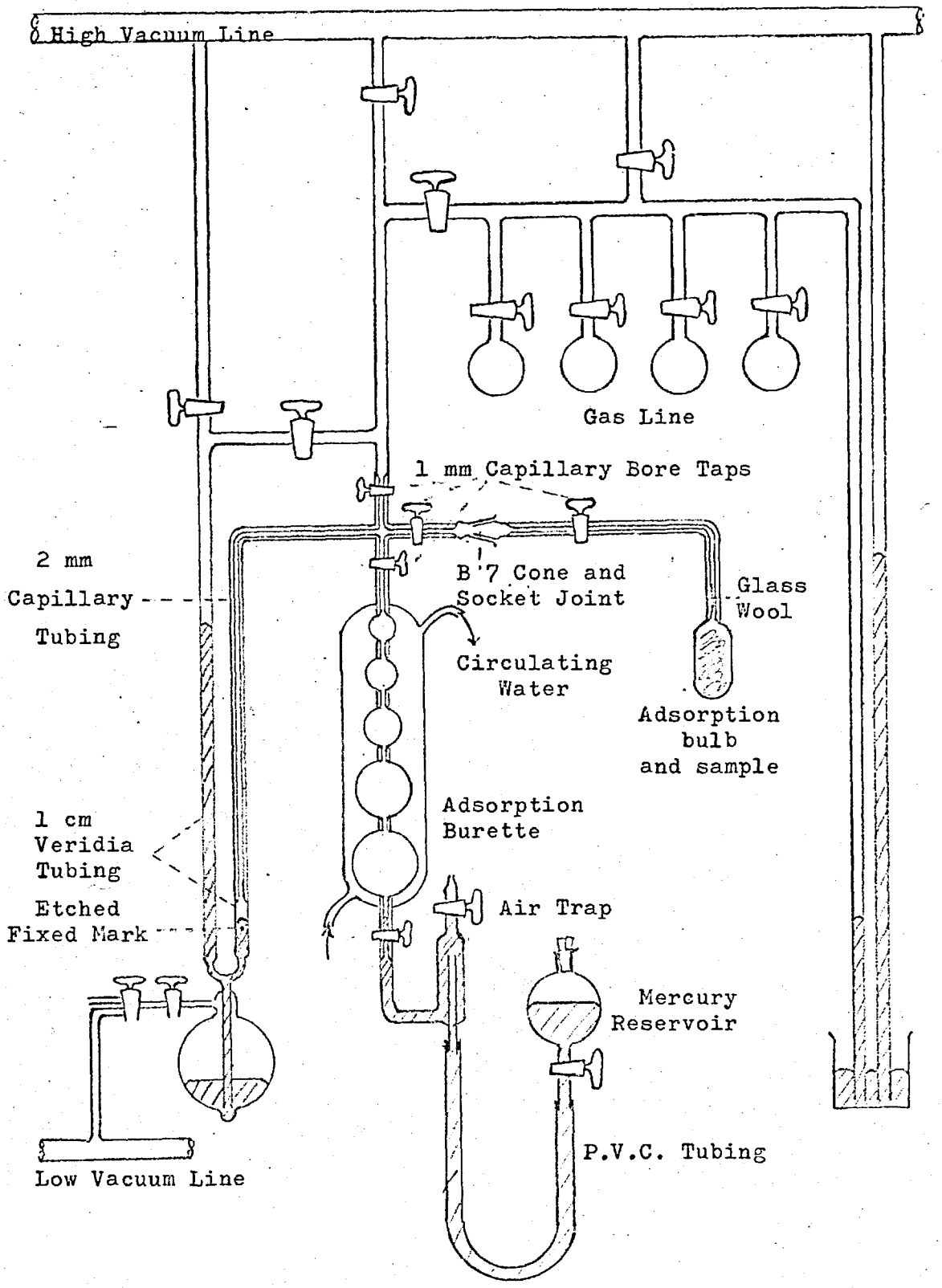

the pressures used any thermal transpiration effects could be neglected (Bennett and Tompkins, 1957). The experimental method followed closely the descriptions of Young and Crowell (1962), p. 284, and Ross and Olivier (1964), pp. 29 and 66. The burette bulb volumes were determined by mercury weighings and the dead space volumes by helium expansion. There are three temperature regions (1) the burette at 25 °C (2) the dead space at ambient (3) the adsorption bulb, together with a temperature gradient between each region. With the tap to the adsorption bulb closed the dead space at ambient temperature was first evaluated. Since in the calibration the amount of gas is constant we may sum for each region at different temperatures when changing from one burette volume to the next. Initially

$$\frac{P^{o}V_{d}}{T_{d}} = \frac{P'V_{d}}{T_{d}} + \frac{P'V_{b}}{T_{b}} + P'\sigma_{s}$$

where $\sigma_{s} = \sum_{1}^{1} \frac{\delta}{T}$ is the summation of the volume elements divided by the respective temperature of the element in the temperature gradient. This quantity we may consider to be constant and be included in the experimental value obtained for the dead space. The mean value for the dead space for a series of burette readings was obtained by the method of least squares. The calibration was then repeated with the tap to the adsorption bulb open. σ_{s} for the adsorption bulb is dependent on the temperature of the adsorption bulb and so a calibration was carried out for each isotherm temperature.

The total quantity of gas present is the sum of the volumes for each region corrected to N.T.P.; the amount adsorbed is the total volume before adsorption minus those gaseous volumes remaining after adsorption and is expressed as cc at N.T.P. per g of adsorbent. Errors for the adsorption

experiments are discussed in section 3.9. In practice where there was no hysteresis the adsorption and desorption branches were co-incident. Pellets for the adsorption sample of similar porosity to the diffusion membrane were prepared by compressing the powder in a steel cylinder split length-ways, during the compression the two halves being retained in an outer casing (Clint 1966, Gabor 1957).

3.3 DIFFUSION UNITS

3.3.1 Single gas diffusion unit

This unit, figure 3.3, is a modified form of similar units used within these laboratories (Baker, 1966, Pope, 1961 Gabor, 1957). The membrane was a plug of compressed carbon powder. The plug assembly was of the same form as that used in the gas mixture diffusion unit thus allowing the plugs to be interchanged. A description of this will be given in section 3.3.3. Pressure at the in-going side was measured with a mercury-in-glass manometer with limbs of 1 cm bore Veridia tubing. A balance line across the limbs also served as the out-gassing line for the in-going side of the plug. A tap isolating the plug from the rest of the in-going side was incorporated so that 'time-lags' could be measured. The in-going side pressure was kept reasonably constant ($\pm$ 1%) by the 300 cc Toepler pump used in conjunction with a 500 cc buffer volume. The gases were stored in 1 litre gas bulbs on the gas line. The out-going side pressure was measured with a McLeod gauge of range 1×10^{-5} to 5×10^{-2} cm Hg. By using four 5 litre buffer volumes which could be separately out-gassed a series of experiments could be run using each buffer volume in turn while out-gassing the idle or previously used volumes, this allowed continuous use of the unit.

Figure 3.3 SINGLE GAS DIFFUSION UNIT

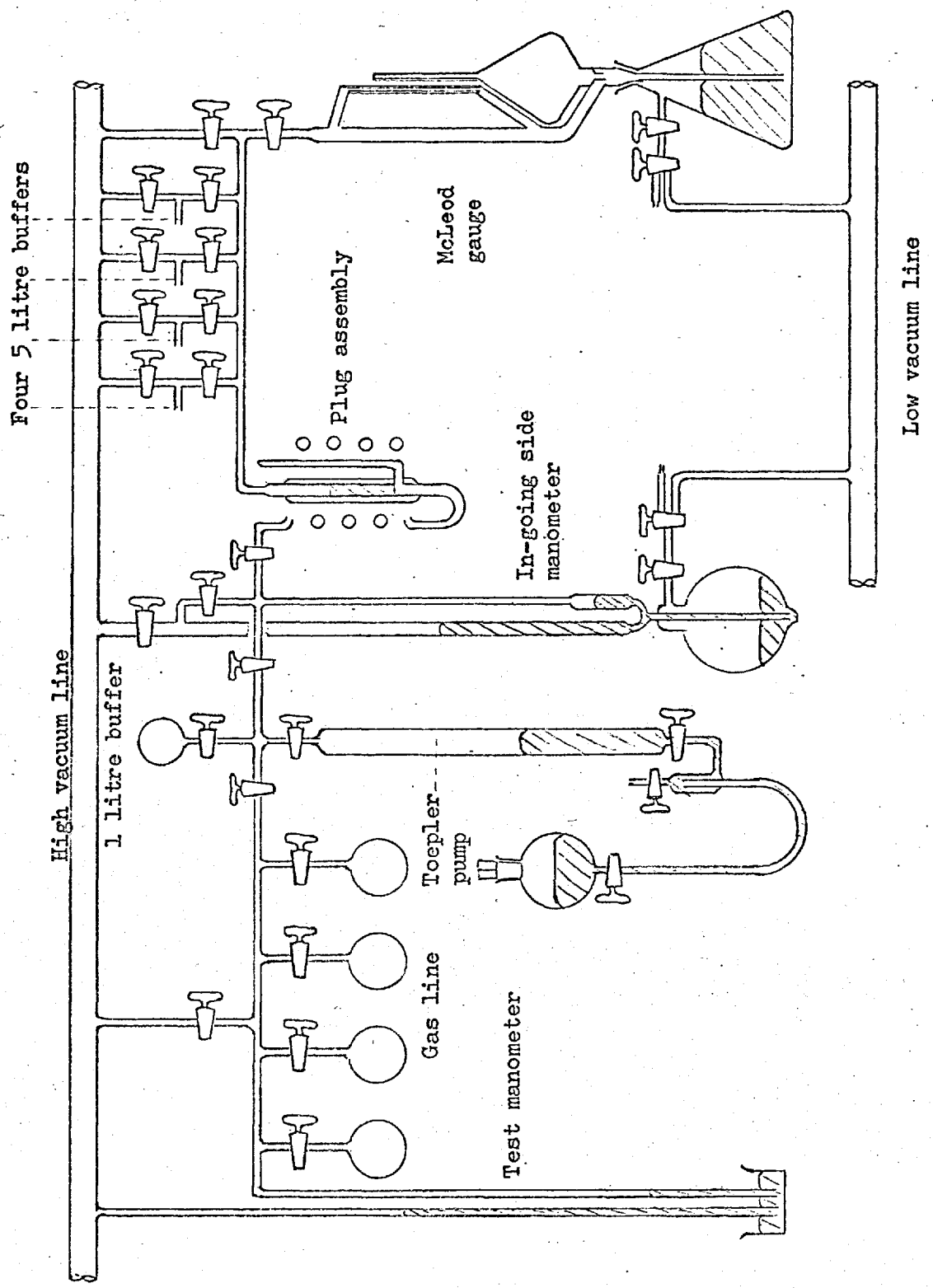

Figure 3.4 GAS MIXTURE DIFFUSION UNIT

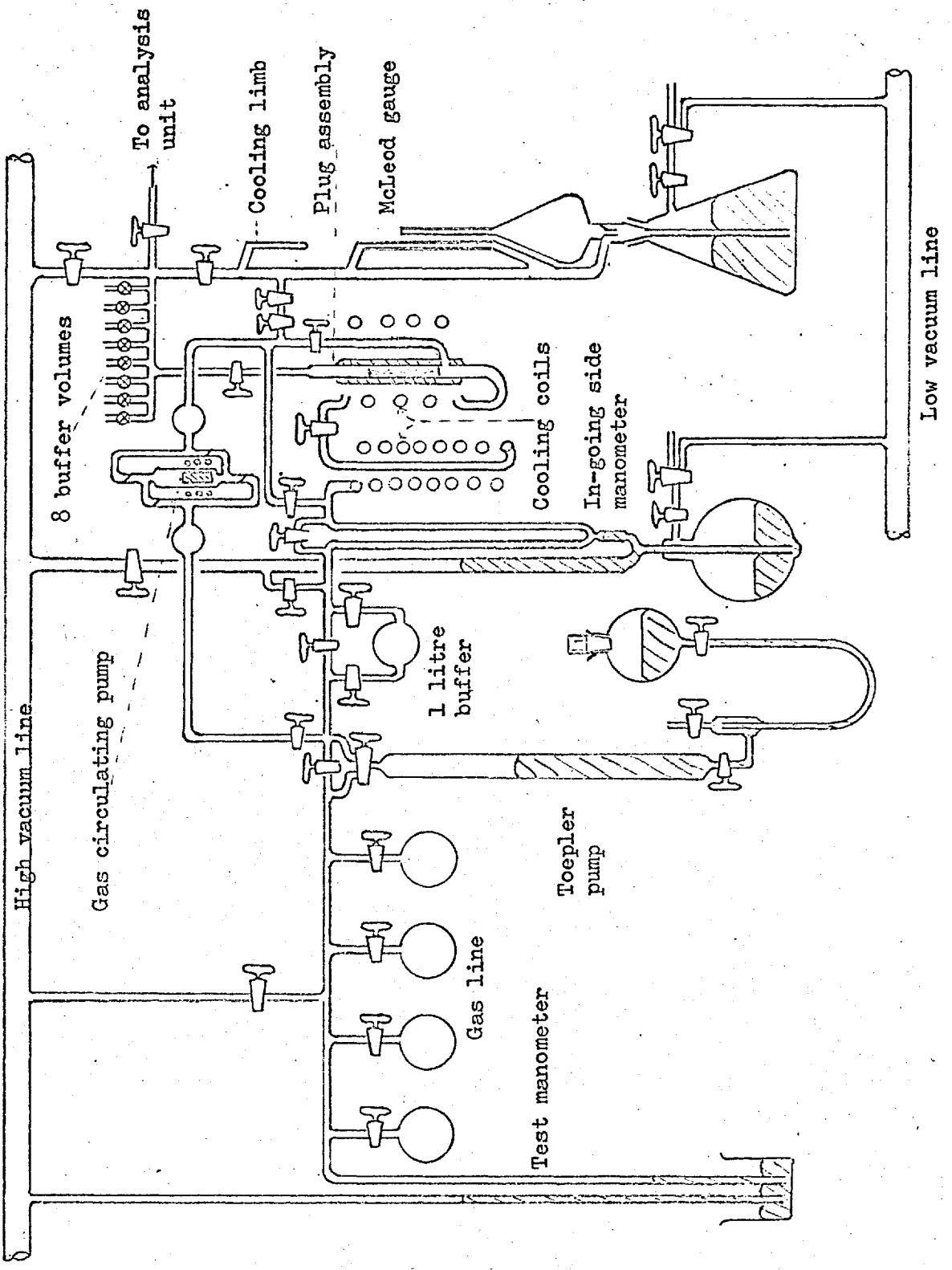

3.3.2 The gas mixture diffusion unit

This unit (figure 3.4) is similar to the single gas diffusion unit but has to include a means of circulating the gas mixture past the in-going face of the plug. The design was based on Pope's apparatus (Pope, 1961) but with special consideration being given to eliminating stagnant pockets of gas mixture.

3.3.3 The plug assembly

This is shown in detail in figure 3.5 and plate 3.1. The plug holder was a stainless steel tube of overall length 9 cm and outside diameter 1½ cm. It was manufactured in the departmental workshops. The ends had an internally tapped thread and a heat flange. The internal diameter of the centre section (0.303 cm) was measured accurately by resting the plug holder on a compression plunger and adding weighed amounts of mercury into the holder. The length of the mercury column was then measured by lowering a needle attached to the telescope of a cathetometer until it touched the mercury, the point of contact being found by making the needle, plug holder and consequently the mercury, part of an electric light circuit, the bulb lighting up on making contact. Corrections for the error due to the mercury meniscus were taken from the table given by Vogel (1951), p. 783.

The side port for the in-going side was then drilled out and a 0.24 cm internal diameter copper tube joined on with silver solder. The plug was made by compressing the carbon into the plug holder using hardened steel compression plungers and a 1½ ton Dennison press. Because it was necessary to locate the face of the in-going side just above the side port the plug holder was seated on a compression plunger whose shaft extended just beyond the port. Then three accurately weighed

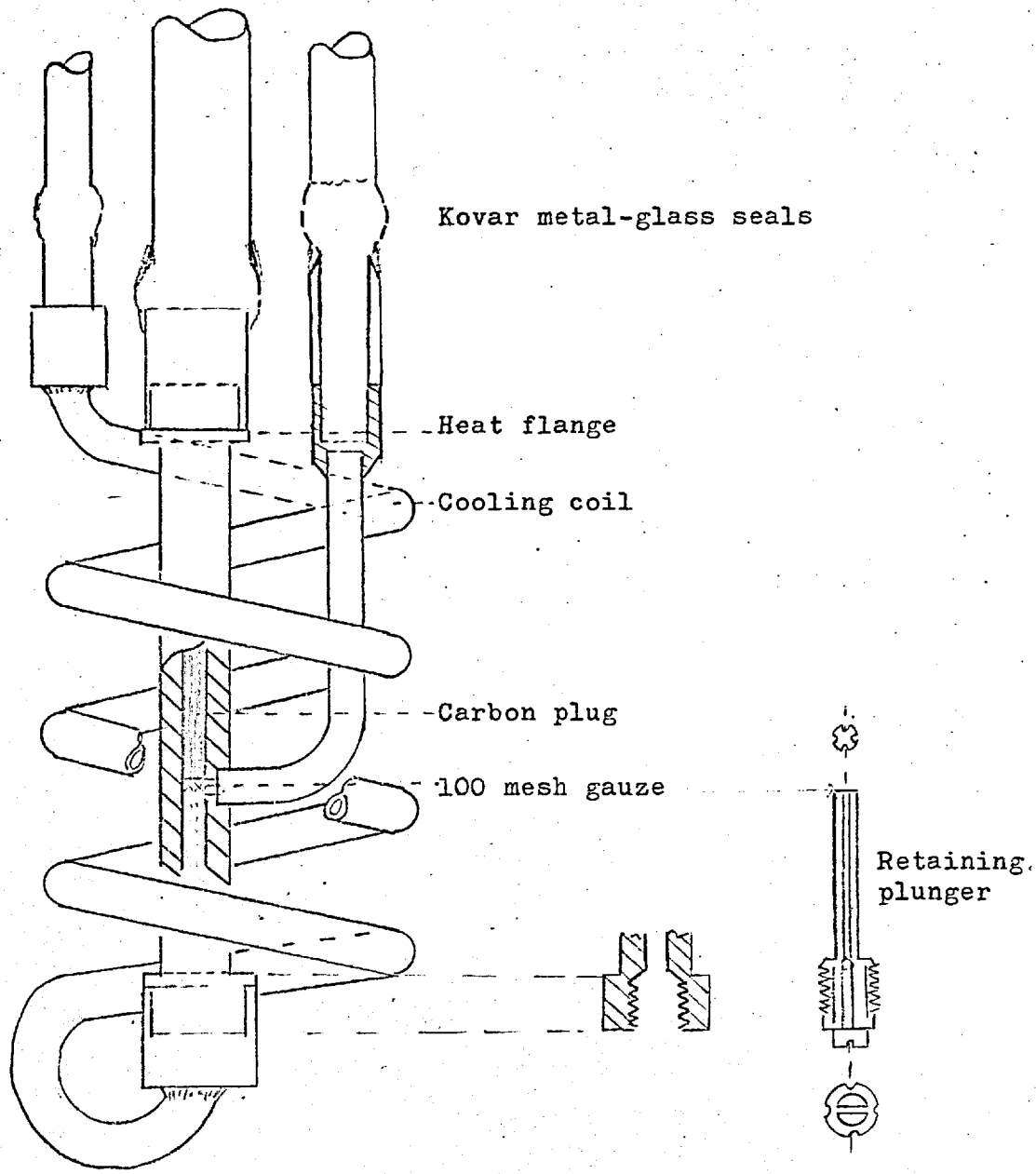
Kovar metal-glass seals
Heat flange
Cooling coil
Carbon plug
100 mesh gauze
Retaining plunger

Plate 3.1

Component parts of plug assembly

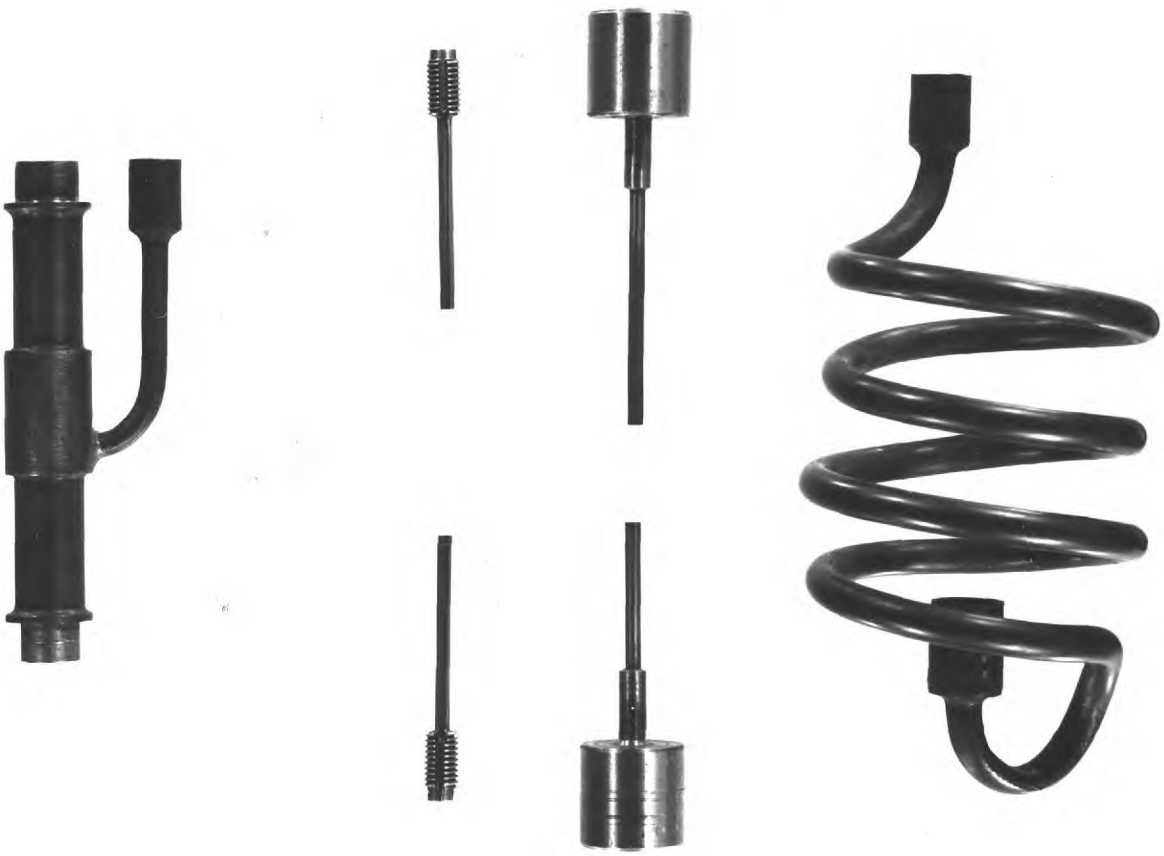

From left to right :- plug holder with side tube attached, sample of 100 mesh packing gauze, threaded and grooved retaining plungers, compression plungers and cooling coil.

approximately 0.02 g quantities of powder were added and compressed in turn to the required porosity. The length of each increment was found by measuring the distance between the ends of the compression plungers with vernier calipers. By building the plug in increments from the in-going face in this way it was possible to obtain a reasonably uniform membrane. Three layers of stainless steel 100 mesh gauze (kindly given with the compliments of R. Cadish and Sons) were packed against both plug faces. Finally the stainless steel, length-wise grooved retaining plungers were inserted and screwed home against the mesh to prevent the plug from swelling. A 5 cm wide coil made from 0.3 cm internal diameter copper tubing was then silver soldered on to the bottom of the plug holder and Kovar metal-glass seals silver soldered on to the three assembly outlets. During the soldering operations the outlets were stoppered and the assembly immersed in water in order to prevent excessive heating of the plug. The heat flanges also provided additional protection.

3.3.4 The circulating pump

To counteract variable composition occuring in the region of the in-going side due to preferential adsorption and differing flow rates, the gas mixture had to be streamed past the face of the in-going side with the aid of a circulating pump. The general specifications required for the pump were :-

(1) At N.T.P. it should pump 500 cc/min of gas across the plug face; this was 1×10^5 times the largest flux through the membrane.

(2) It should be vacuum tight, and capable of being out-gassed.

(3) In operation the pump should cause the minimum of pressure fluctuations.

Figure 3.6 THE CIRCULATING PUMP

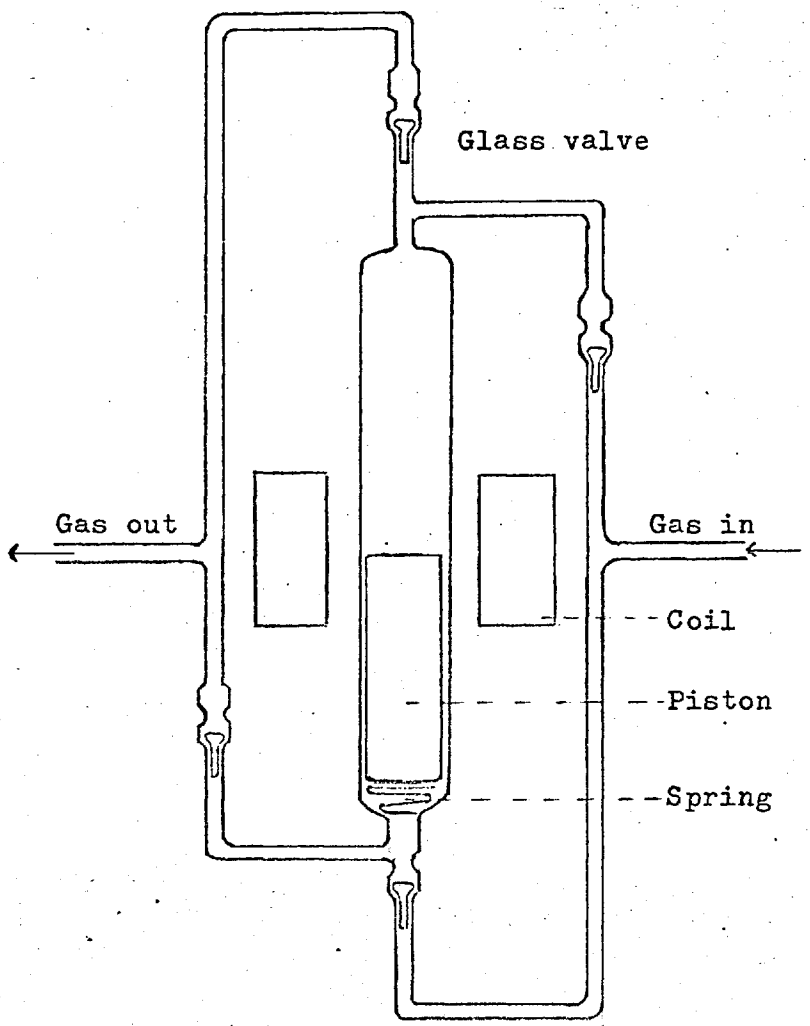

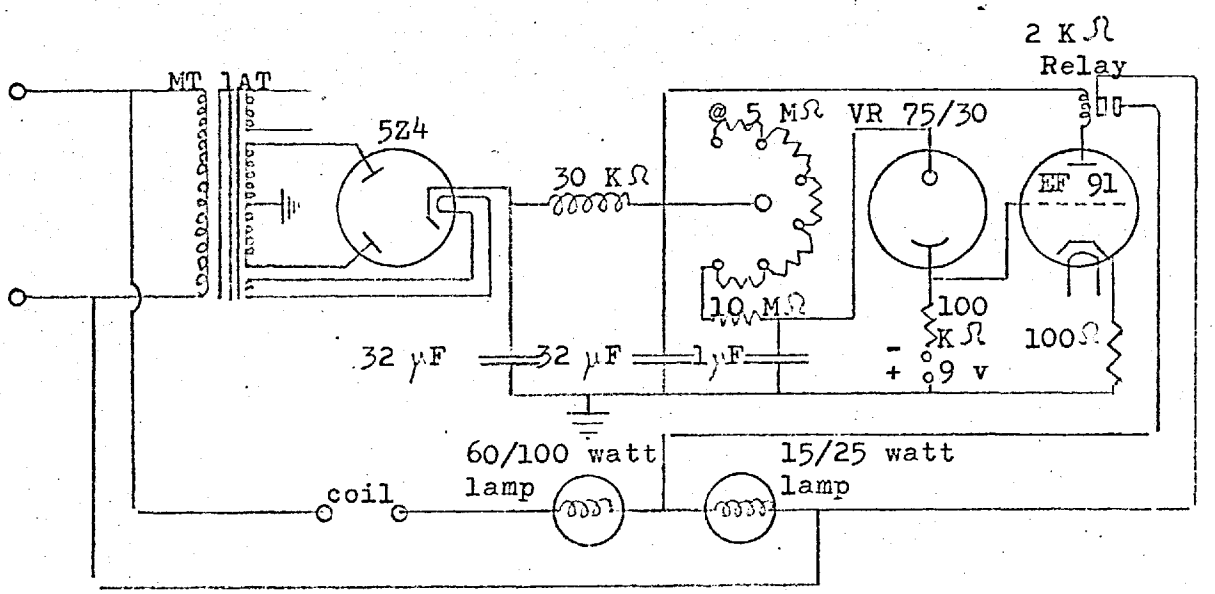

Pumps using copper or P.T.F.E. bellows, or turbines proved to be inadequate, and finally the all-glass reciprocating pump recommended by Pope (1961) was used. It is illustrated in figure 3.6. The piston was a 2 cm diameter glass tube filled with lengths of soft iron rod, packed tightly with asbestos wool, and sealed at both ends. The cylinder was surrounded by a 2,300 turns coil made from 30 s.w.g. enamelled copper wire, and the piston reciprocated in the cylinder under the action of the magnetic flux associated with an intermittent current of 0.2 A supplied to the coil from the power unit shown in the diagram. Damage to the cylinder was prevented by breaking the fall of the piston with a spring, and gas-tight valve seals were achieved by grinding in the glass shanked valves into the valve seatings. Pressure fluctuations were reduced to a minimum by adding a 250 cc buffer volume to each side of the pump.

3.3.5 Remaining units of the in-going side.

Constant pressure and, to within 1%, effectively constant composition at the in-going side, was maintained with a 200 cc Toepler pump used in conjunction with a 1 litre buffer. The lines were arranged so that the gas mixture flowed through the buffer instead of past it. For small fluxes through the plug the buffer was isolated out and the flow diverted through the by-pass line. The stagnant volume of the manometer limb was eliminated by making the pressure limb in the shape of a 'U' attached to a short tail so that the gas would flow around the 'U' and across the top of the mercury in the tail. 1 cm diameter Veridia glass tubing was used for the tail and the vacuum limb. The mercury level was adjusted into the tail by varying the pressure in the mercury reservoir. A by-pass line across the top of the 'U' was included so that the limbs of

the 'U' could be balanced to equal pressure when the mercury level was above the tail. A by-pass line to the vacuum limb also served as an out-gassing line.

The gas was pre-cooled in a glass spiral before entering the plug assembly. Taps were provided either side of the pump system so that it could be isolated during single gas experiments and like-wise the plug assembly could also be isolated for 'time-lag' measurements and while making up the gas mixtures. A by-pass line across the plug assembly allowed the gas mixture to be thoroughly mixed before the start of each experiment. The in-going side composition was analysed by taking a 0.4 cc sample between two straight-through 2 mm bore taps and expanding this dose into the out-going side for analysis.

3.3.6 The out-going side

The out-going side consisted of a set of eight buffer volumes, a McLeod gauge with a small condensing limb attached and an analysis system. The McLeod gauge was designed to operate between 5.0×10^{-2} and 1.0×10^{-5} cm Hg. The pressure was maintained in this region by switching in the series of buffers allowing the total volume of the out-going side to be varied from 500 to 25,00 cc.

3.3.7 Gas analysis

In the pressure region of 1×10^{-3} cm Hg there is no instrument capable of acting as an accurate continuous monitor of the gas composition and batch techniques had to be used. The ammonia systems (NH_3/He, NH_3/H_2, NH_3/N_2) were conveniently analysed by measuring the total pressure, isolating the McLeod, freezing out the ammonia into the condensing limb with liquid nitrogen and measuring the residual

pressure of the non-condensable gas. A check run with pure ammonia showed that in this pressure region all the ammonia was removed within five minutes. A small correction for the different temperature of the non-condensable gas in the condensing limb was applied from a calibration run for each non-condensable gas.

For the non-condensable gas pair (N_2/H_2) a modified version of Pope's thermistor unit was used (Pope, 1961). The thermistor bead is a thermally sensitive resistor made from semi-conductor material. In the present application the resistance change is due to the heat generated internally because of the change in the rate at which it may dissipate power to the surrounding atmosphere. Between 2 and 10 cm Hg pressure the rate of working is fairly insensitive to pressure fluctuations but is very sensitive to composition, producing a not quite linear, large variation of resistance with gas composition. Although it was operated at constant voltage and constant ambient temperature, fluctuations due to these variables could be reduced to a minimum by comparing the resistance of the analysing thermistor via a wheatstone bridge with the resistance of a matched standard thermistor enveloped in one of the pure components of the mixture under the same conditions of pressure, ambient temperature and at constant voltage. The unit is shown in figure 3.7 together with an insert diagram of the thermistor mountings.

The P23/MP thermistors were supplied by Stantel, Ltd., as beads mounted between copper leads which in turn were sealed through a glass tube. They were bought as a matched pair and table 3.1 lists some of their properties. To increase their stability they were aged for three weeks at 100 ^{o}C prior to use.

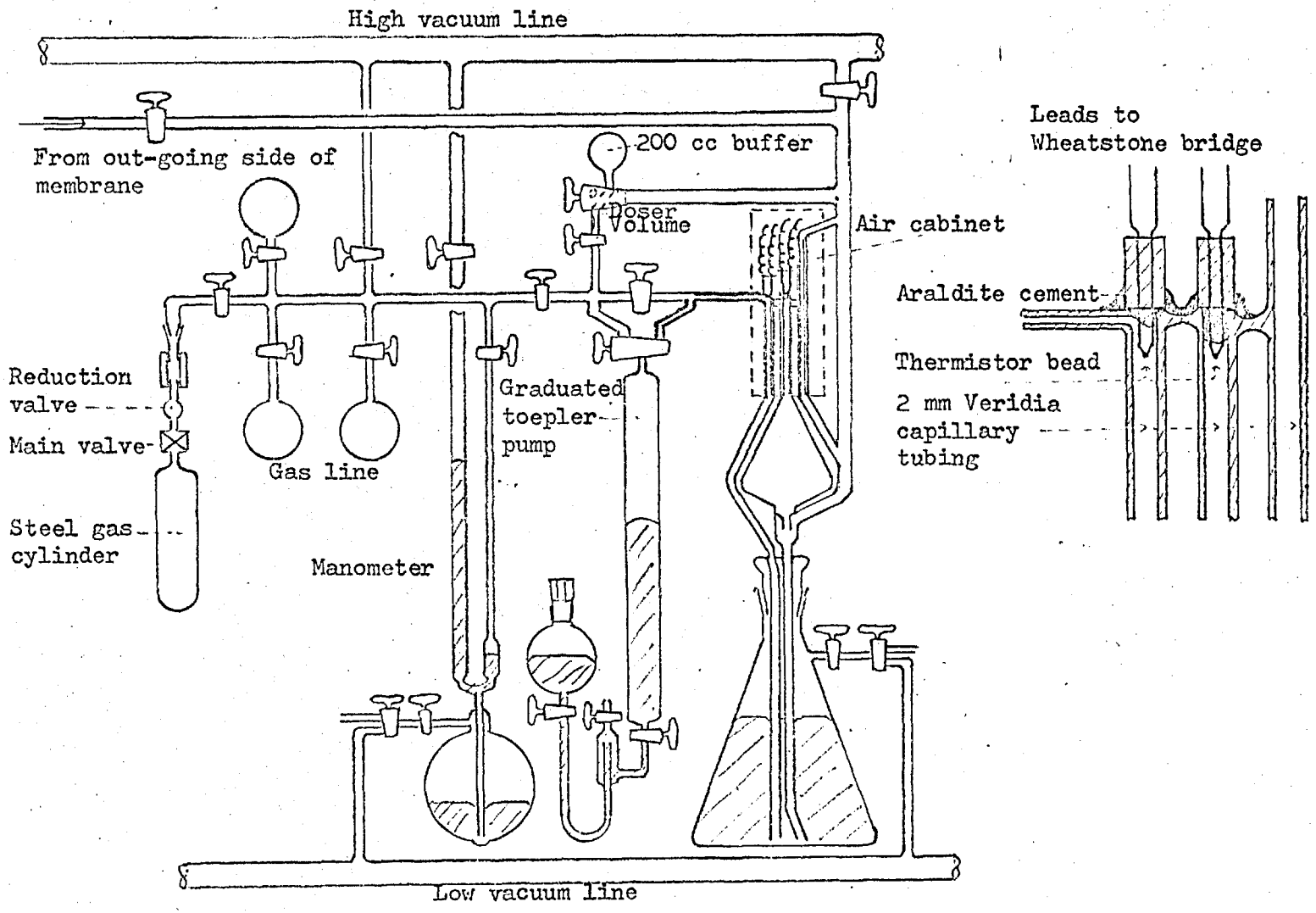

Figure 3.7 GAS ANALYSIS UNIT

Figure 3.8 BRIDGE CIRCUIT FOR GAS ANALYSIS UNIT

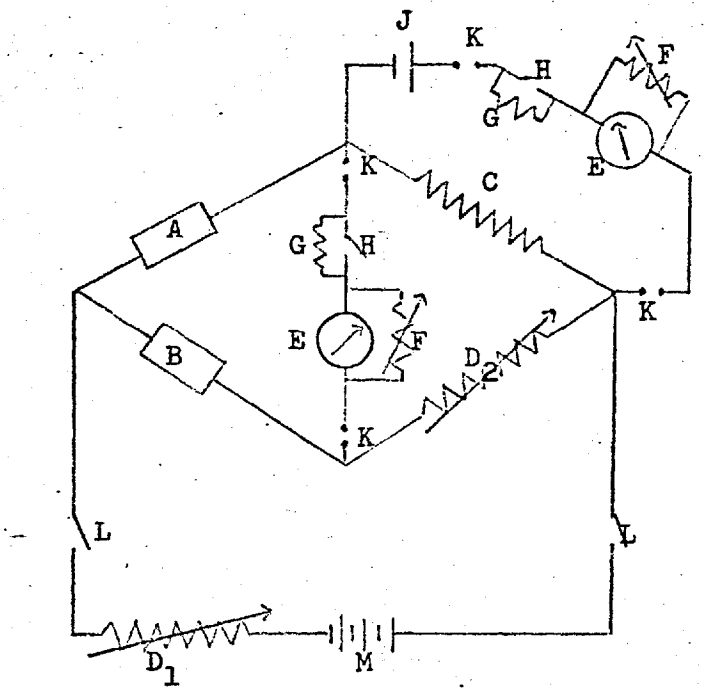

A	Standard thermistor
B	Test thermistor
C	1.5 KΩ Temperature constant resistor. 1 watt 1% tolerance
D	0.1 to 10,000 Ω Decade box
E	Spot deflection galvanometer
F	500 Ω Variable resistance
G	5 MΩ Resistance
H	Tap key
J	Weston normal cell
K	Two-way two-pole switch
L	Two-way two-pole switch
M	6 volt heavy duty accumulator

Table 3.1

Properties of the P23/MP thermistor

Manufacturers code No.	Type P23/MP
Resistance at 20 °C	2000 Ω
Matching to	± 1% at 20 °C
Maximum power dissipation	20 mW
Sensitivity	11.5 °C per mW
Activation energy for conduction	5.6 Kcal

The gauge was similar in design to a McLeod gauge with the analysing thermistor mounted in 'Araldite' cement to the top of the closed limb. The standard thermistor was similarly mounted in a separate capillary alongside the McLeod capillaries and the top end of this capillary led off with the minimum of volume to a 100 cc graduated Toepler pump and thence to a gas line. The lower end of the capillary was led by a wider tube into the mercury reservoir of the McLeod gauge. The three capillaries were of 2 mm bore Veridia tubing and were joined together by a glass tie bar at the top of the gauge for added strength. The ends of the reservoir leads were separated to prevent the mercury meniscus allowing air to creep around the bottom of the leads. To calibrate the analysing thermistor an accurate mercury manometer was included on the gas line together with a 200 cc calibrated volume on the gas line side of the Toepler pump. Mixtures of known composition could then be prepared and admitted to a 0.5 cc doser volume that could be expanded into the analysing side of the gauge. The gauge capillaries were enclosed in a small perspex cabinet which was thermostatted to 25 ± 0.05 °C.

To obtain maximum sensitivity for change in resistance

with thermal conductivity of the surroundings, the gauge was operated at a constant voltage of 1.55 v across the standard thermistor. This is just below the maximum value of 1.6 v in the voltage/current characteristics curve supplied by the manufacturers for a P23 thermistor dissipating heat at a steady rate. The necessary bridge circuit is shown in figure 3.8. The bridge could be balanced to $\pm$ 0.1Ω, the maximum sensitivity required of the galvanometer being 1.0μA.

The gauge was calibrated by making up gas mixtures of known composition with the aid of the Toepler pump and the calibrated volume and expanding a dose of this mixture into the analysing side of the gauge.

To analyse the mixture the mercury was raised until there was a pressure difference of 5 cm Hg between the open and closed limbs. One of the pure components of the mixture was admitted to the standard thermistor limb and the mercury level adjusted to the same level as in the analysing limb with the aid of the Toepler pump (the pressure between each limb would then be equal). To operate the standard thermistor at constant voltage the standard cell was switched in and D_1 adjusted to balance. The mixture was then analysed by switching the galvanometer to bridge circuit and adjusting D_2 to balance. The composition was interpolated from the calibration curve of D_2 versus percentage composition.

3.4 FURNACES AND THERMOSTAT BATHS

300 to 200 °C

This range of temperature was covered with electric furnaces made by winding resistance wire around an asbestos former. The various temperatures within the region were obtained by adjusting the voltage to the furnace with a Variac transformer. Once the steady rate of working was achieved

the temperature would remain constant to within ± 1.0 °C (± 0.2% °K) without any further adjustment being required. These furnaces were also used for out-gassing at 300 and 200 °C.

200 to 75 °C

This range was covered using an oil bath made from a 2 litre beaker wrapped in asbestos cloth for insulation and contained in a tin can for safety. As a check, experiments at 200 °C were performed with both the oil bath and furnace as the thermostat. The temperature was controlled to within ± 0.5 °C with a 'Sunvic Bi-metallic Strip' regulator which switched in via a 'Hot Wire Vacuum Switch' relay a 300 watt 'Red-rod' heating element. When the regulator and relay was operated in conjunction with the heater at mains voltage the regulator contacts were rapidly corroded by the high voltage sparks. The useful life and stability of the regulator was improved by running the regulator and relay from a separate 30 v ac supply. The most suitable oil for this temperature range was the Hopkins and Williams silicone fluid 'MS 550' which has a low viscosity at room temperature and does not degrade until well above 200 °C. A uniform temperature across the bath was maintained with a paddle stirrer.

50 °C

A similar bath to the one described above was used for this temperature but with the 300 watt heater replaced by a 50 watt heater.

25 °C

For this temperature an uninsulated beaker of water was used in conjunction with a 25 watt heater, regulator, relay, and stirrer.

0 °C

The apparatus was thermostatted to this temperature with

melting ice contained within a dewar vessel.

- 10 to - 50 °C

Accurately controlled temperatures were obtained using the 'leaky-dewar' system. The leaky-dewar was wrapped with a sheet of copper foil to reduce temperature gradients and was contained within a sound outer dewar. For this temperature range the intervening space between the two dewars was filled with crushed 'Cardice' and, providing this space was large enough, the bath could be held at the desired temperature for up to 15 hours with one charge of Cardice. Well-stirred methanol was used as the thermostatting fluid and the temperature controlled to $\pm$ 0.2 °C with the previously described regulator/relay system and a 25 watt heating lamp. The leaky-dewar was operated at atmospheric pressure.

- 75 to - 110 °C

The same system was used as described in the previous paragraph but with the Cardice refrigerant replaced by liquid nitrogen and an evacuated inner dewar. Below - 80 °C methanol becomes highly viscous and so was replaced by 40/60 petroleum ether containing a small amount of methanol to dissolve any ice crystals that formed around the inside of the dewar.

90 and 77 °K

The apparatus was thermostatted to these temperatures with boiling liquid oxygen and boiling liquid nitrogen respectively.

3.5 THERMOMETERS

Once again the range of temperature demanded a range of instruments. For out-gassing a 0 to 300 °C mercury-in-glass thermometer was quite adequate, but for the experiments between 100 and 300 °C an iron/constantin thermocouple was

used. The thermocouple was made and calibrated at the international temperature points of 100, 232, and 327 °C by Spembly Technical Products Ltd., and the thermocouple emf measured on a calibrated Doran Thermocouple Potentiometer. The emf could be measured to 0.01 mv corresponding to a temperature difference of 0.2 °C.

Temperatures between 100 and 0 °C were measured to ± 0.05 °C with a calibrated NPL mercury-in-glass thermometer.

To cover the range 0 to - 110 °C three vapour pressure thermometers were made following the general method outlined by Dodd and Robinson (1954). The regions covered by the appropriate vapours were: 0 to - 40 °C, n-butane; - 30 to - 80 °C, ammonia; - 70 to - 115 °C, carbon dioxide. Vapour pressure data were taken from the Chemical Engineers Handbook, 2nd ed. (1941), the Handbook of Chemical and Physical Constants, 48th ed. (1967), Physico-Chemical Constants of Pure Organic Compounds (1950). The purest gases available were used in preparing the gauges and no difference could be detected for the value of the temperature when measured by the different thermometers.

The liquid oxygen and liquid nitrogen boiling points were assumed to be those quoted in the above references.

3.6 VOLUME CALIBRATIONS

McLeod gauges

The radius of the Veridia capillary tubing was checked by adding small weighed quantities of mercury into the capillary and measuring the length of the mercury thread with a cathetometer. The volume of the bulb was measured by weighing the bulb empty and when filled with water.

Buffer volumes

The leads to the buffer volumes were constructed as a

sub-assembly prior to joining to the rest of the apparatus and this allowed the volume of the leads to be measured by filling them with water. There was also the additional advantage that the sub-assembly could be completely annealed in an annealing oven. The buffer volumes were also calibrated by filling with water.

The remaining volumes of the out-going side were calibrated by helium expansion from the known volumes.

3.7 GASES

Ammonia 99.99% pure and anhydrous, and deuterium 99.5% pure was supplied by Cambrian Chemicals Co. Ltd. as compressed gas in small steel cylinders. 1 litre samples of the gases were stored on the gas line by attaching the steel cylinders to the gas line via a reduction valve, rubber pressure tubing, a B 10 cone and socket 'Quick-fit' joint and a 4 mm high-vacuum glass tap. A typical assembly is included in figure 3.7. The assembly down to the main cylinder valve would hold a vacuum of 1×10^{-3} cm Hg for at least 10 minutes which was quite adequate for transferring the gas. Ammonia could be drawn back into the 1 litre storage bulb at the end of the experiment by surrounding with liquid nitrogen a small condensing limb attached to the bulb. Any suspect impurities were then removed by pumping out the system while the ammonia was frozen.

Helium, nitrogen, carbon dioxide and hydrogen were obtained as 'spectrally pure' from the British Oxygen Co. Ltd. in 1 litre glass bulbs. Similarly n-butane was obtained from the National Physical Laboratory as 99.9% pure by mass-spectrometric analysis.

3.8 SUNDARY EXPERIMENTAL DETAILS

The individually ground high vacuum taps manufactured by Springham Co. Ltd. were used throughout the apparatus. In general 4 mm internal bore taps were preferred, although smaller taps had to be used in confined spaces. Before working, the glass tubing and taps were washed with water and detergent to remove surface dirt and glass dust. Where possible the apparatus was constructed in sub-assemblies so that they could be annealed in the departmental glass-blower's annealing oven. This eliminated many potentially dangerous strain zones which always occur in blown glass.

Permanent cone and socket joints were sealed with Picein wax. At room temperature this wax provides a vacuum tight seal while its own vapour pressure is below 1×10^{-9} cm Hg.

Two greases were available for the taps: Apeizon N and Silicone. The Apeizon N grease has a vapour pressure of 1×10^{-9} cm Hg at 25 ^{o}C, but while providing a good vacuum seal it is slightly too viscous at room temperature, and the tap has to be gently heated with a hot air-blower before it may be safely turned. The Silicone grease has a vapour pressure of 1×10^{-9} cm Hg at room temperature and is a good sealent. It has the added advantage of non-Newtonian viscosity which allows the tap to be easily turned at room temperature, but experience showed that this property also allowed the grease to either slowly flow out of the cylinder leaving a dry, unturnable tap, or to streak across the barrel of the tap and break the vacuum seal. Eventually after several disasters caused by the use of Silicone grease only Apeizon grease was used.

To a large extent many of the errors associated with manometers and McLeod gauges can be eliminated using ultra-pure mercury; such purity was obtained by the following method of chemical cleaning. About 500 cc of the dirty

mercury was filtered through a pin-holed filter paper into a 2 litre Buckner flask. This initial filtration removed any large particles. Then two spatular ends of sodium peroxide were added together with 500 cc of water, and the mixture agitated over-night. This alkaline wash removed all acid impurities. The aqueous liquor was decanted off and the mercury washed by decantation until free of alkali. Metal impurities were then removed by agitating the mercury over-night with 500 cc of acidified potassium permanganate solution. This treatment formed an oxide scum which was dissolved in a 2 N Nitric acid wash leaving a mirror-bright mercury surface. The mercury was then washed with distilled water by decantation until the washings had no detectable trace of nitrate radicals or oxidising agents when tested with diphenylamine reagent (limit 1 part in 10,000 Vogel 1954, p. 365). The remaining water was mopped-up with clean tissue paper, and the pure mercury dried by heating to 110 ^{o}C for half an hour. It was finally filtered into a clean storage bottle.

3.9 ERRORS

Errors may be considered in two forms:-

(i) The absolute error. This is the sum of the errors between the observed and the true values of all the measured quantities, and it is the error to be considered when comparing the results for different samples, plugs, and operators.

(ii) The relative error. This is the sum of the errors between the observed and true values for only those quantities which change when repeating the experiment. It is a measure of the reproducibility of an experiment.

3.9.1 Errors in the adsorption isotherm

A difficulty in discussing adsorption isotherm errors is that they are constantly changing, but in general the lower the pressure and the less adsorbed then the greater is the percentage error. The main errors may be listed as:

(i) Calibrated Volumes. These only affect the absolute error. The burette volumes were calibrated by mercury weighing to an error of better than $\pm$ 0.1%, but the dead space volume which was calibrated by helium expansion would have an error of at least $\pm$ 1.0%.

(ii) Pressure. The cathetometer could be read to $\pm$ 0.001 mm, so at 0.1 cm Hg the error was at least $\pm$ 2% of pressure, but at 60 cm Hg the percentage error would have dropped to $\pm$ 0.01%.

(iii) Error in dose. Ross and Olivier (1954) show that this can be reduced to a minimum by arranging the dosing volume at N.T.P. to be equivalent to the remaining volume at N.T.P. after adsorption, under these conditions the error becomes very small.

(iv) Temperature. This random error has two effects. The first is the error involved in calculating the volume of gas in the adsorption space corrected to N.T.P.; this is only a small effect since the temperature is measured to $\pm$ 0.5 ^{o}C, or $\pm$ 0.2% ^{o}K. The second effect is that the amount adsorbed depends on the temperature of the adsorbent which can cause an error in reproducibility of up to $\pm$ 2%.

(v) Adsorbent. The adsorbent could be weighed to $\pm$ 0.0001 g with a corresponding absolute error of $\pm$ 0.1%, but there are other causes for error that can only be estimated in a qualitative manner. These relate to the actual nature of the adsorbing surface and whether it undergoes any permanent change on being heated or on adsorbing an acidic or basic adsorbate for the first time. There was some evidence found that ammonia

altered the surface of Carbolac I, this will be discussed in chapter 5.

In the circumstances it is clearly difficult to quote a figure that has any meaning for the absolute error of an adsorption isotherm. As far as the relative error is concerned, in practice it was observed to be around $\pm$ 2% for ammonia isotherms and less than $\pm$ 1% for the other gases investigated.

3.9.2 Errors in flow experiments

These may be listed as follows:

(i) In-going side manometer. The pressure at the in-going side was measured between the range 5 to 60 cm Hg, so the percentage error varied over the range $\pm$ 0.1 to $\pm$ 0.01%. An additional error however was the pressure drift due to material diffusing through the membrane. This was reduced to a minimum by buffering the in-going side volume and adjusting the volume to constant pressure with a Toepler pump. Even so this drift would cause an error of up to $\pm$ 1%.

(ii) Temperature. The error in temperature in the worst case was $\pm$ 0.2% ^{o}K. Once again there were two effects: the first caused an error in the calculation of the flux and permeabilities and the second effect was to alter the true value of the flux and permeability.

(iii) Calibrated Volumes. The out-going side calibrated volumes were measured to an accuracy of $\pm$ 0.5%.

(iv) McLeod Gauge. By taking suitable precautions the many reported errors that occur in a McLeod gauge were reduced to manageable proportions. Sticking of the mercury thread was prevented by using the carefully cleaned mercury, and 2 mm bore capillary tubing. Electrostatic and surface tension effects were eliminated by tapping the limbs with one's fingers. Pressures were measured at room temperature with gases that

showed very little deviation from ideality at these temperatures. By restricting the out-going side volume it was not necessary to perform the experiments at pressures of lower than 1×10^{-5} cm Hg at the out-going side, so the large errors that start to occur in this pressure region were avoided. Taking all these factors into account the total error for the McLeod gauge was around $\pm$ 1%.

(v) Composition. Errors in composition for both the in-going and out-going side were the same because a common method of measuring composition was used. Analysis by freezing out a condensible component will have the same accuracy as the McLeod gauge for each component, the sum being $\pm$ 2%. The thermistor gauge had a similar overall percentage error.

Summing for all these errors produces a relative error of $\pm$ 2% for the single gas experiments and $\pm$ 5% for the mixture experiments. The absolute error is much larger because errors for the membrane dimensions have to be included; this requires an estimate of the out-gassed weight causing the absolute error to rise to the region of $\pm$ 10%. In practice the experimental errors proved to be less than $\pm$ 2%. This value was for the experimental measurements and did not include irreversible changes occuring within the membrane which were considered to be a separate phenomenon.

CHAPTER 4 RESULTS

4.1 THE POROUS MEDIA

4.1.1 Adsorption samples

One sample of compressed Carbolac I was prepared, the powder being compressed in 0.145 g increments into the split cylinder to a porosity of just below 0.5. After breaking open the cylinder and transferring the chippings to the adsorption bulb, the sample was out-gassed at 200 °C at a vacuum of better than 1×10^{-5} cm Hg to a final weight of 0.5719 g. The out-gassed porosity was 0.5. This was calculated using the value of 2.12 g cm^{-3} for the absolute density of Carbolac I (Barrer and Strachan, 1955). Out-gassing lasted 48 hours with a weight loss of 8.1%. This sample was too small for measuring hydrogen and deuterium isotherms satisfactorily over the range - 40 to + 25 °C. For these particular isotherms the 9.432 g sample of Carbolac I chippings prepared by Clint (1966) was used.

4.1.2 Diffusion membranes

Three diffusion membranes were prepared. The major part of the work reported here refers to the membrane made from Carbolac I. A membrane made from Graphon powder was prepared for examining the permeability of helium over the temperature range 300 to - 200 °C. A similar membrane was prepared from graphitised Black Pearls 2 for future work and is reported here to act as a source reference for the membrane data. The data for the three membranes is listed in tables 4.1, 4.2, and 4.3. While Carbolac I loses around 10% weight on out-gassing, neither Graphon nor graphitised Black Pearls 2 has a measurable weight loss on heating at 1000 °C in vacuum.

Table 4.1 Carbolac I Diffusion Membrane

	Weight g	Length cm	Unoutgassed porosity	Gauge pressure lb/sq in
Ingoing face section	0.0253	0.306	0.452	600
Middle section	0.0265	0.330	0.468	700
Outgoing face section	0.0244	0.340	0.525	1100

Final Properties of Membrane

Cross-sectional area	0.07119	cm^2
Length	0.976	cm
Weight of Carbolac I	0.0762	g
Estimated out-gassed weight	0.0694	g
Estimated out-gassed porosity	0.528	
(Estimated weight loss (Clint 1966)	9%)	

Table 4.2 Graphon Diffusion Membrane

	Weight g	Length cm	Porosity	Gauge pressure lb/sq in
Ingoing face section	0.0235	0.332	0.497	80
Middle section	0.0265	0.340	0.503	100
Outgoing face section	0.0244	0.299	0.456	100

Final Properties of Membrane

Cross-sectional area	0.07146	cm^2
Length	0.971	cm
Weight of Graphon	0.0692	g
Porosity	0.494	

The graphitised Black Pearls 2 diffusion membrane was designed for single gas flow experiments in either direction. It was built up in ten compression increments starting from the centre, each section being added from a particular end in the order shown in the accompanying sketch.

Bottom	10	9	8	7	1	2	3	4	5	6	Top

Table 4.3 Graphitised Black Pearls 2 Diffusion Membrane

	Weight g	Length cm	Porosity	Gauge pressure lb/sq in
1	0.1371	0.510	0.505	460
2	0.1360	0.501	0.500	460
3	0.1380	0.499	0.491	460
4	0.1343	0.449	0.449	460
5	0.1356	0.500	0.501	200
6	0.1403	0.546	0.529	200
7	0.1371	0.524	0.519	300
8	0.1364	0.496	0.493	350
9	0.1365	0.502	0.500	350
10	0.1346	0.498	0.503	350

Final Properties of Membrane

Cross-sectional area	0.3177	cm^2
Length	5.054	cm
Weight of membrane	1.3637	g
Porosity	0.503	

The 'Carbons' were manufactured by Cabot Corporation, 125 High Street, Boston, Mass., U.S.A., and the following information is taken from the company's technical data sheets.

Carbolac I is a fluffy High Colour Channel Black. Graphon is a graphitised form of the pelletised Regular Colour Channel Black known as Spheron 6; the code number of the graphitised form is S6-D4. The other Carbon Black used was a graphitised form of the pelletised High Colour Channel Black known as Black Pearls 2; the code number of the graphitised form is BP-D4. Both graphitised blacks were prepared by the manufacturers by heating the parent black to between 2800 - 3000 °C in vacuum. Table 4.4 lists the properties of the blacks mentioned.

Table 4.4 Properties of several Carbon Blacks

	Carbolac I	Spheron 6	S6-D4 (Graphon)	Black Pearls 2	BP-D4	units
Surface area (N_2)	950	110	90	850	212	m^2/g
" by electron microscope	264	-	117	-	295	"
Particle size (N_2)	3.5	30.0	36.0	3.9	15.3	mμ
" by electron microscope	9	25	28	12	11	"
Volatile content	16.0	5.0	0.06	13.0	0.0	%
Ash	0.05	0.05	0.08	0.05	0.06	%
pH	3.0	4.5	10.6	3.0	10.0	
Helium density	2.12	-	1.97	-	1.71	g/cm^3

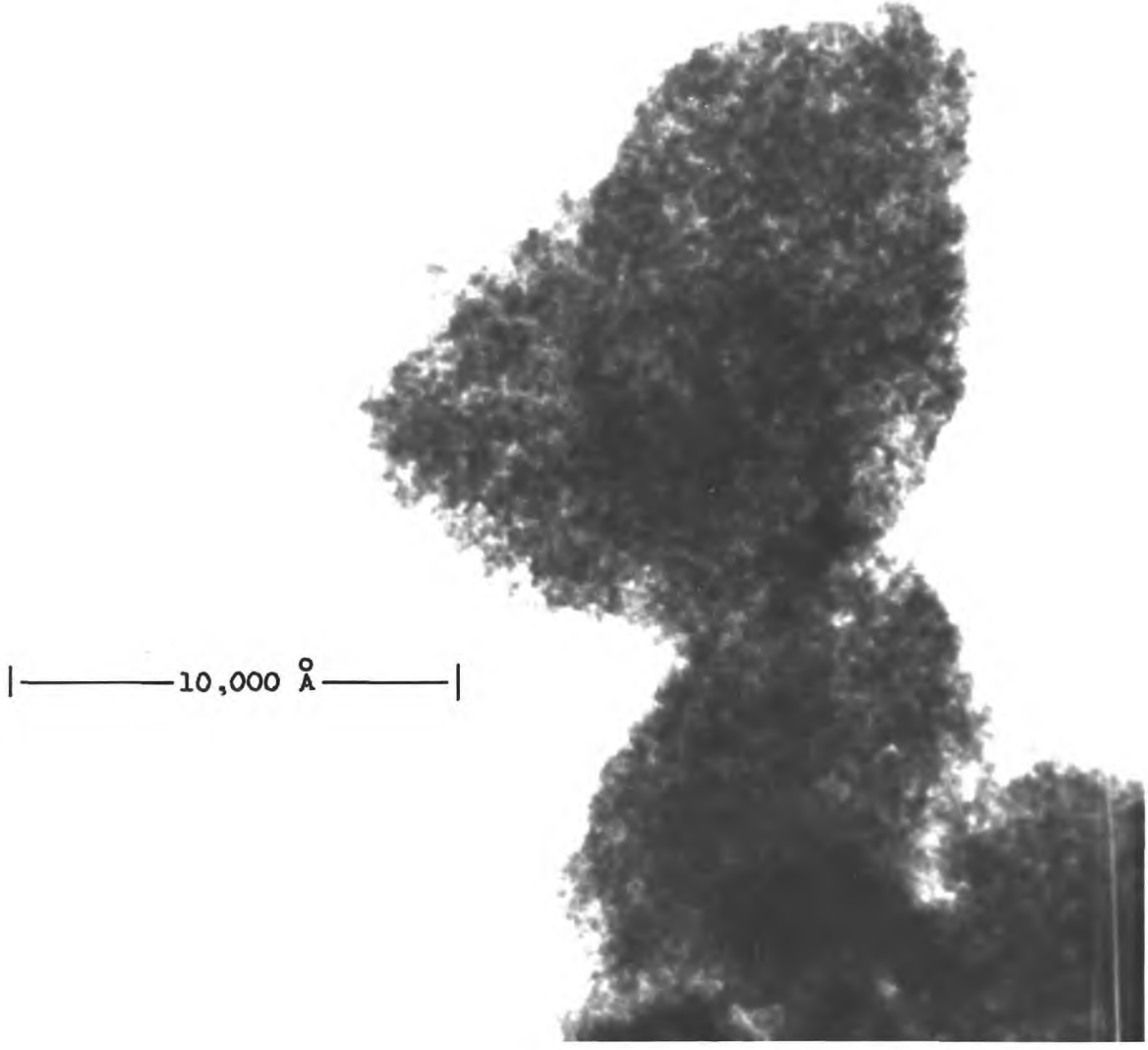

Plate 4.1

Electron microscope photograph of Carbolac I

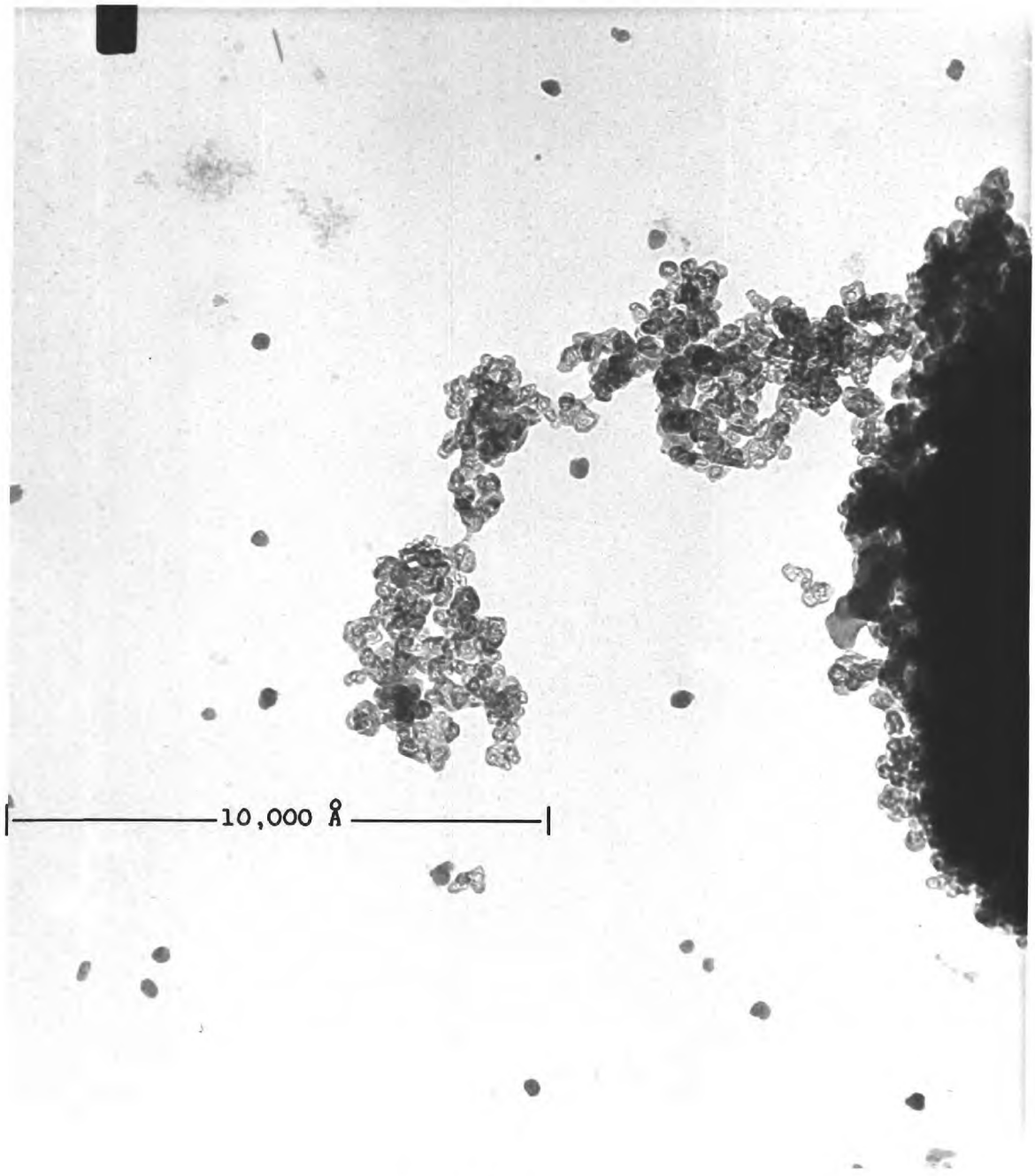

Plate 4.2

Electron microscope photograph of Graphon

4.1.3 Electron microscope photographs

A series of electron microscope photographs of the Carbolac I and Graphon powder were taken and the clearest examples obtained are shown in plates 4.1 and 4.2. The structures will be discussed in section 5.1.2.

4.1.4 Infra-red spectra of Carbon Blacks

Infra-red spectra of Carbolac I and of the graphitised form of Black Pearls 2 were run on a Grubb Parson's Spectromaster Infra-red spectrometer, the samples being smears held between potassium bromide windows. Direct tracings of the relevant parts of the spectra are shown grouped together in figure 4.1, and the frequencies of the observed peaks are listed in table 4.5.

Table 4.5 Infra-red spectra of Carbon Blacks

	Spec.	f cm^{-1}		f cm^{-1}	
Carbolac I in Nujol	1	1766	w	1597	s
Graphitised Black Pearls in Nujol	2	-		-	
Carbolac I free powder	3	1703	w	1579	s
Carbolac I in Fluorolube	4	?		1579	s
Shift in wavenumbers cm^{-1}		63		18	
Carbolac I in Nujol Garten 1957		1760	w	1600	s
Ukhta Channel Black in petrolatum Lygin et al 1960		1750	w	1585	s
Carbonised coal in Nujol Brown 1955		-		1600	s

The spectrum of Carbolac I mulled in Nujol (a straight chain paraffin oil) shows a strong peak at 1597 cm^{-1} and a weak peak at 1766 cm^{-1}, but these peaks are absent in the spectrum of graphitised Black Pearls 2. The intensity of

Figure 4.1 Infra-red Spectra of Channel Blacks

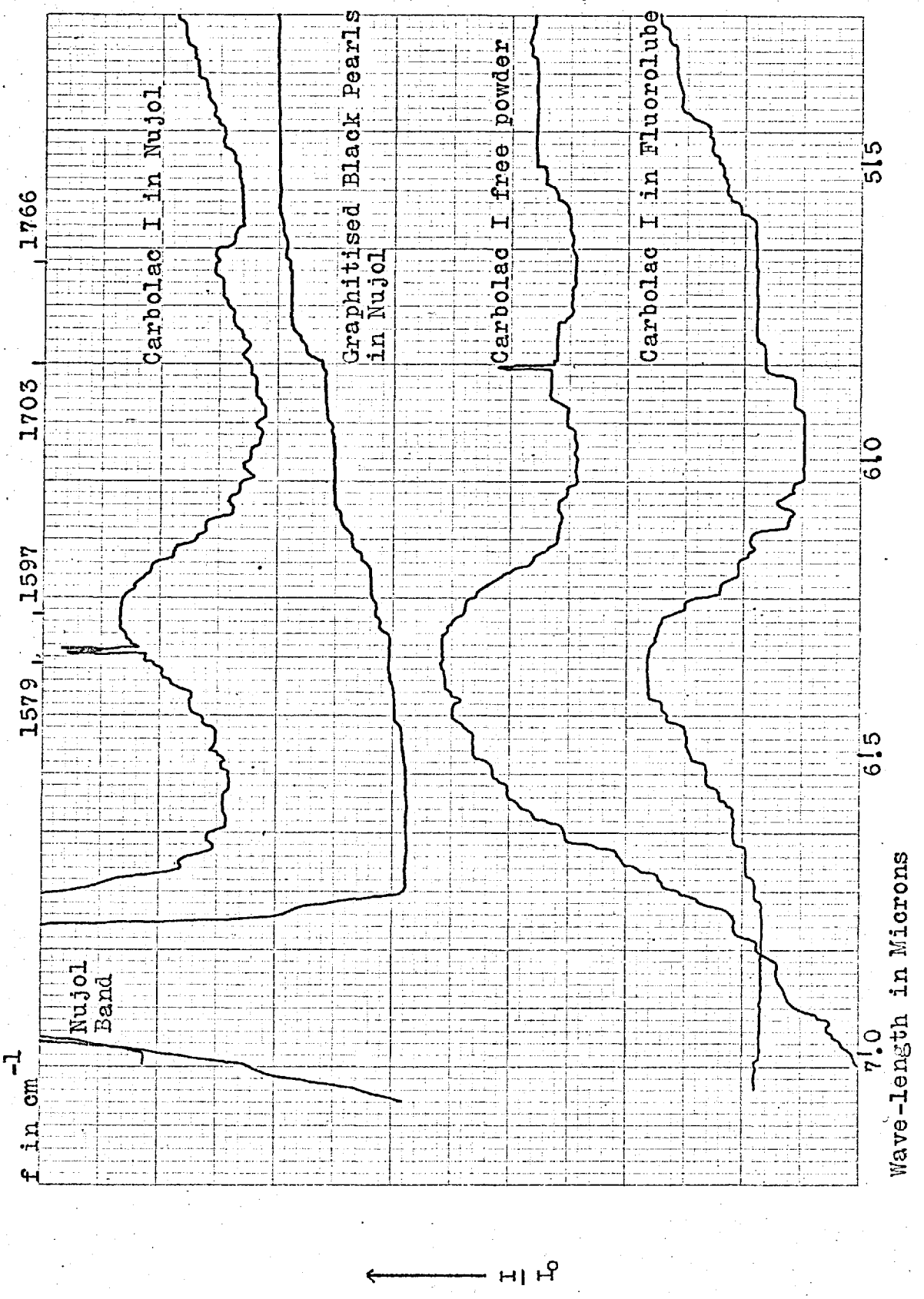

the peaks is limited by the massive Nujol signal, but because Carbolac I is a very fine powder, it was found to be unnecessary to disperse the powder in Nujol, an adequate spectrum being obtained with just the free powder smeared between the potassium bromide windows. In this free powder spectrum the two peaks found with the mulled sample again occurred but with a shift in frequency. This shift proved to be genuine on repeating the spectra with fresh samples. To see if this effect was specific for a Nujol mull a further sample was mulled in Fluorolube (Nujol that has been completely fluorinated) and no shifts were observed, the spectrum comparing well with that for the free powder.

4.2 Adsorption isotherms

4.2.1 Nitrogen isotherms on Carbolac I

Figure 4.2 shows the nitrogen adsorption isotherm at 77.4 ^{o}K (liquid nitrogen boiling point) after out-gassing the 0.5 g Carbolac I chippings sample to constant weight (run 1). The isotherm was repeated (run 2) after the ammonia adsorption experiments to see if any change had occurred. The slight difference in up-take was probably due to temperature fluctuations. B.E.T. plots using the ∞ form of the B.E.T. equation (see Young and Crowell (1962), pp 190 and 231) are shown in figure 4.3. Both isotherms formed identical B.E.T. plots and the surface area A, and the monolayer capacity v_m, was calculated from the initial linear portion of the graphs. Values obtained were

$$A = 960\ m^2\ g^{-1} \qquad v_m = 220\ cc\ at\ N.T.P.\ g^{-1}$$

A thickness, or 't', plot using de Boer 't' values (de Boer et al 1964) is shown in figure 4.4 and is similar to the curve obtained by de Boer (1965). The surface area

Figure 4.2

Nitrogen on Carbolac I Isotherm at 77.4 ^{o}K

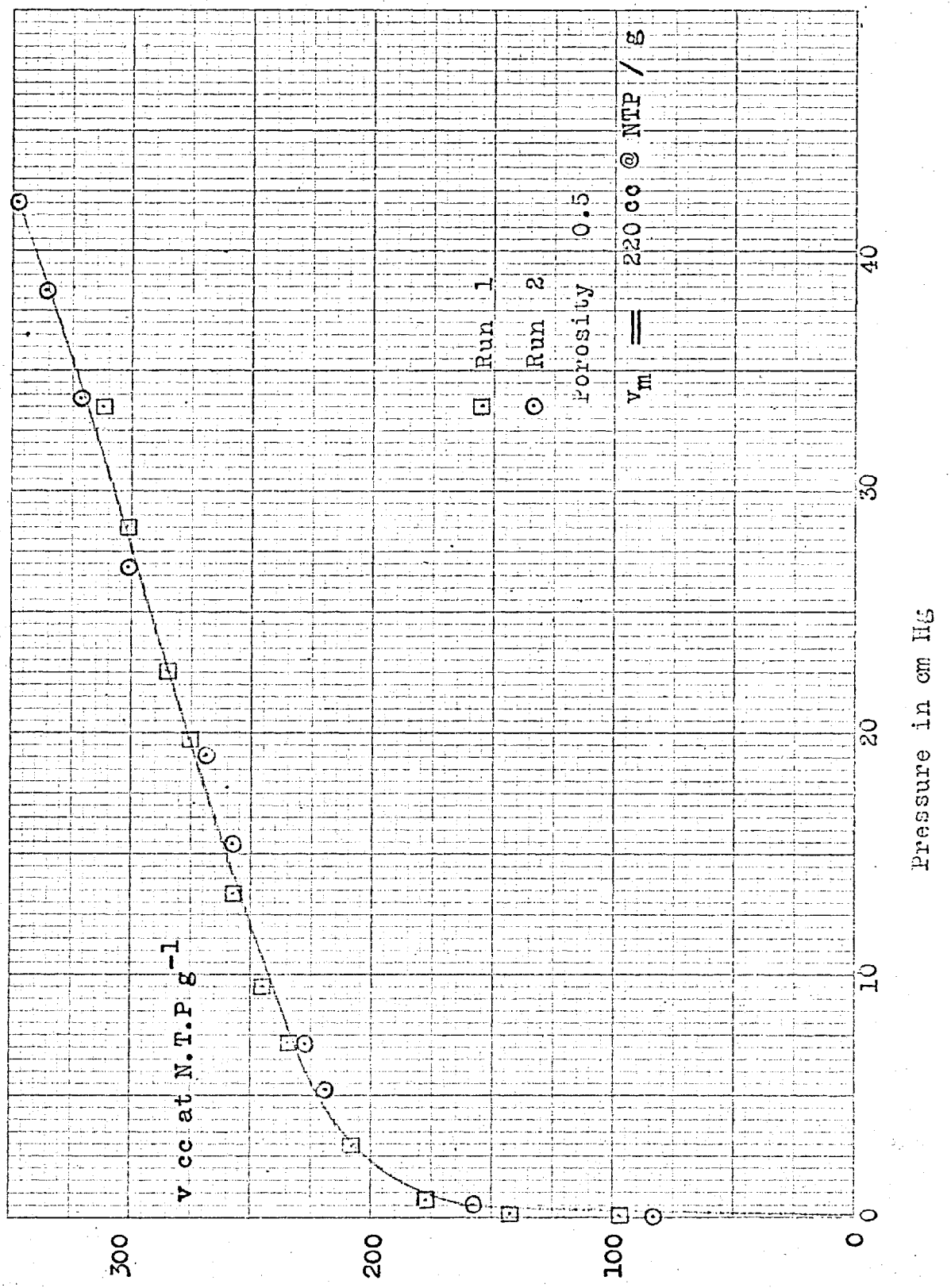

B.E.T. Plot Nitrogen on Carbolac I at 77.4 ^{o}K

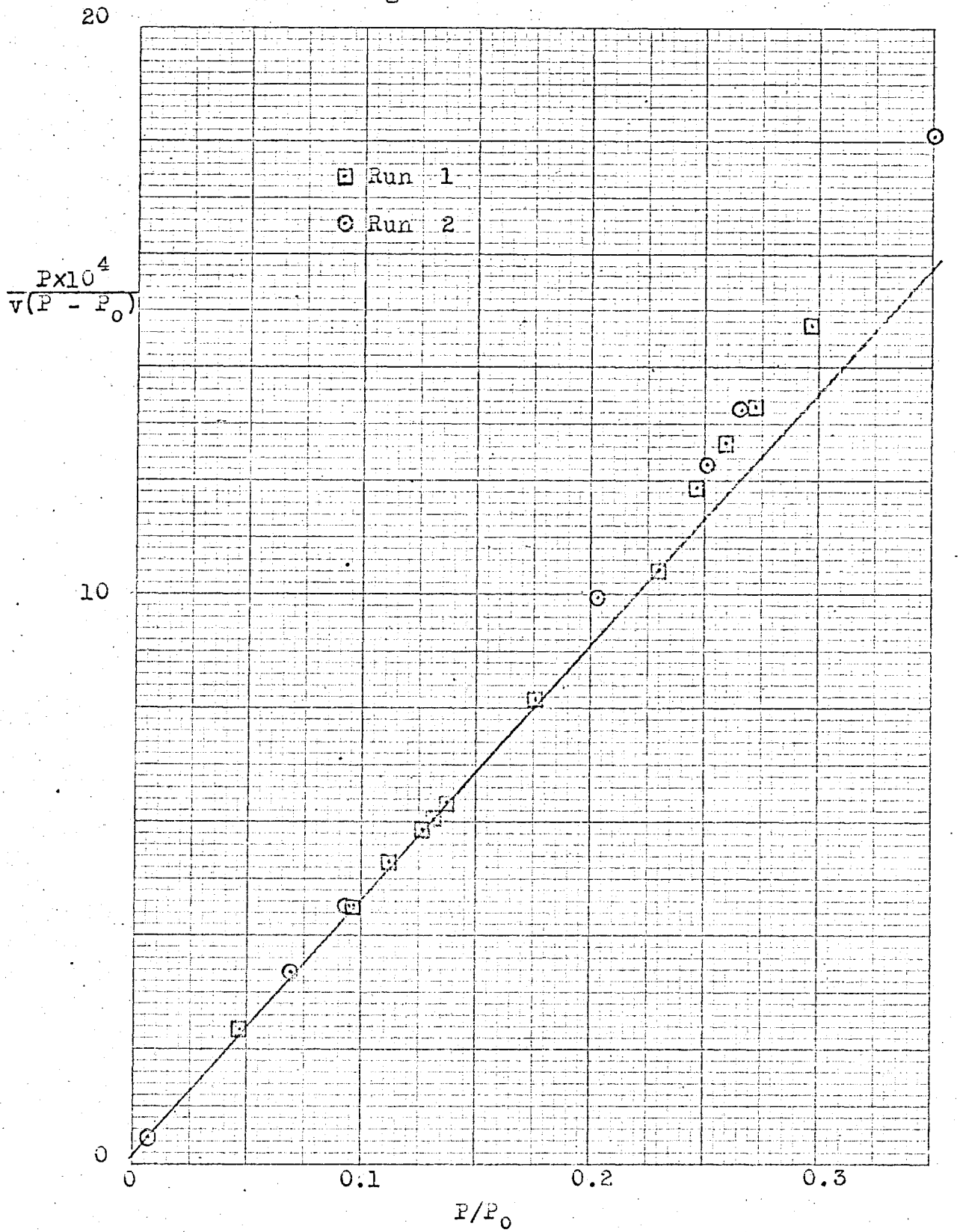

Figure 4.4

't' plot Nitrogen on Carbolac I at 77.4 ^{o}K

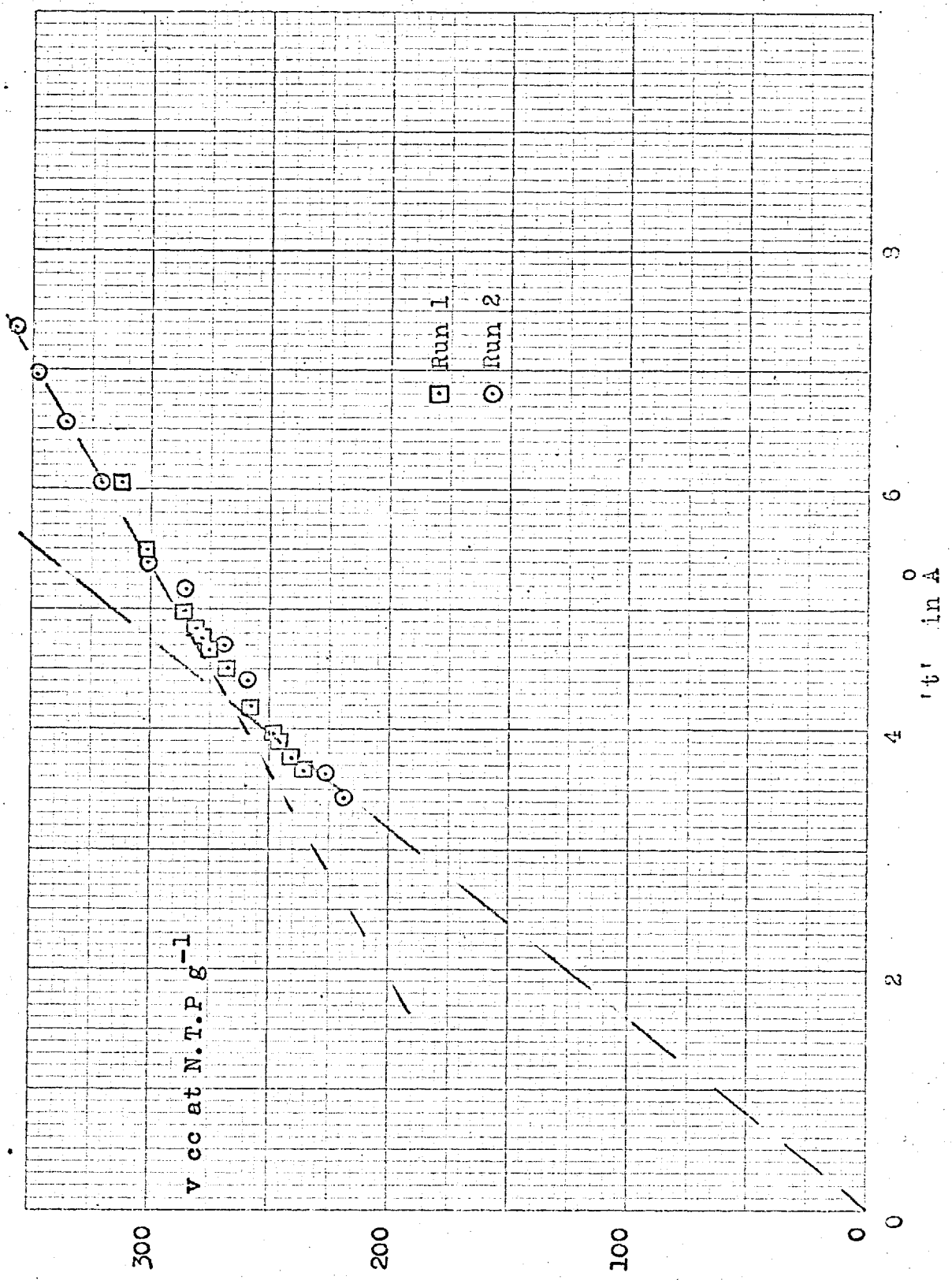

Figure 4.5

Nitrogen on Carbolac I Isotherms

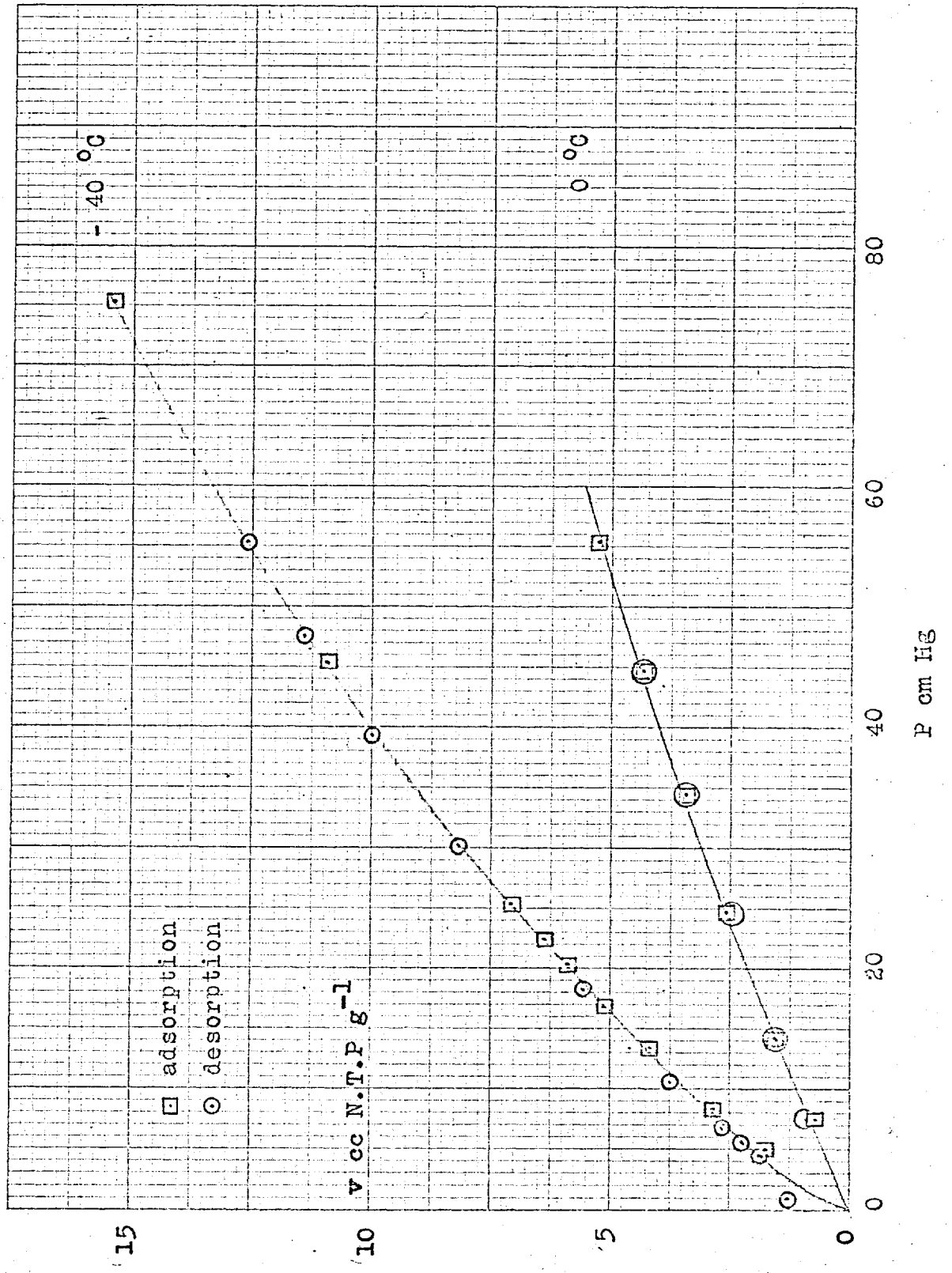

was calculated from the initial slope according to de Boer's method

$$A = 15.47(dv/dt) = 975 \quad m^2 g^{-1} \qquad 4.1$$

Isotherms for nitrogen at - 40 °C and 0 °C are shown in figure 4.5. Even at 0 °C the isotherm is slightly curved.

4.2.2 Hydrogen and Deuterium Isotherms on Carbolac I

The isotherms for hydrogen and deuterium adsorbed on to Carbolac I at 25, 0.0, - 20, - 40 °C are shown in figures 4.6 and 4.7. For these isotherms Clint's ~ 9 g sample of chippings was used. An additional isotherm for hydrogen which was run at - 27 °C by mistake is also included. The isotherms for the two gases at liquid oxygen (90.2 °K) and liquid nitrogen (77.4 °K) boiling point using the ~ 0.5 g sample of chippings prepared by the author is shown in figure 4.8. Between - 40 and 25 °C both gases obeyed Henry's law of adsorption and within the limits of the experiment had identical uptakes. The Henry law constant k_s is defined as

$$k_s = \frac{\text{excess No. of molecules per cm}^2 \text{ of surface}}{\text{No. of molecules per cm}^3 \text{ of gas phase}} = \frac{v}{P} \cdot \frac{76\ T}{273.2\ A} \qquad 4.2$$

where P is the pressure in cm Hg, v the uptake in cc at N.T.P. per g, T is the temperature in °K, and A is the surface area of the adsorbent in $cm^2\ g^{-1}$. The values obtained for k_s over the temperature range studied for the two gases are listed in table 4.6.

Plots of $\log_{10}(v/P)$ and $\log_{10} k_s$ against 1/T for both gases are shown in figures 4.9 and 4.10 together with the

Figure 4.6

Hydrogen on Carbolac I Isotherms

(Clint adsorption sample)

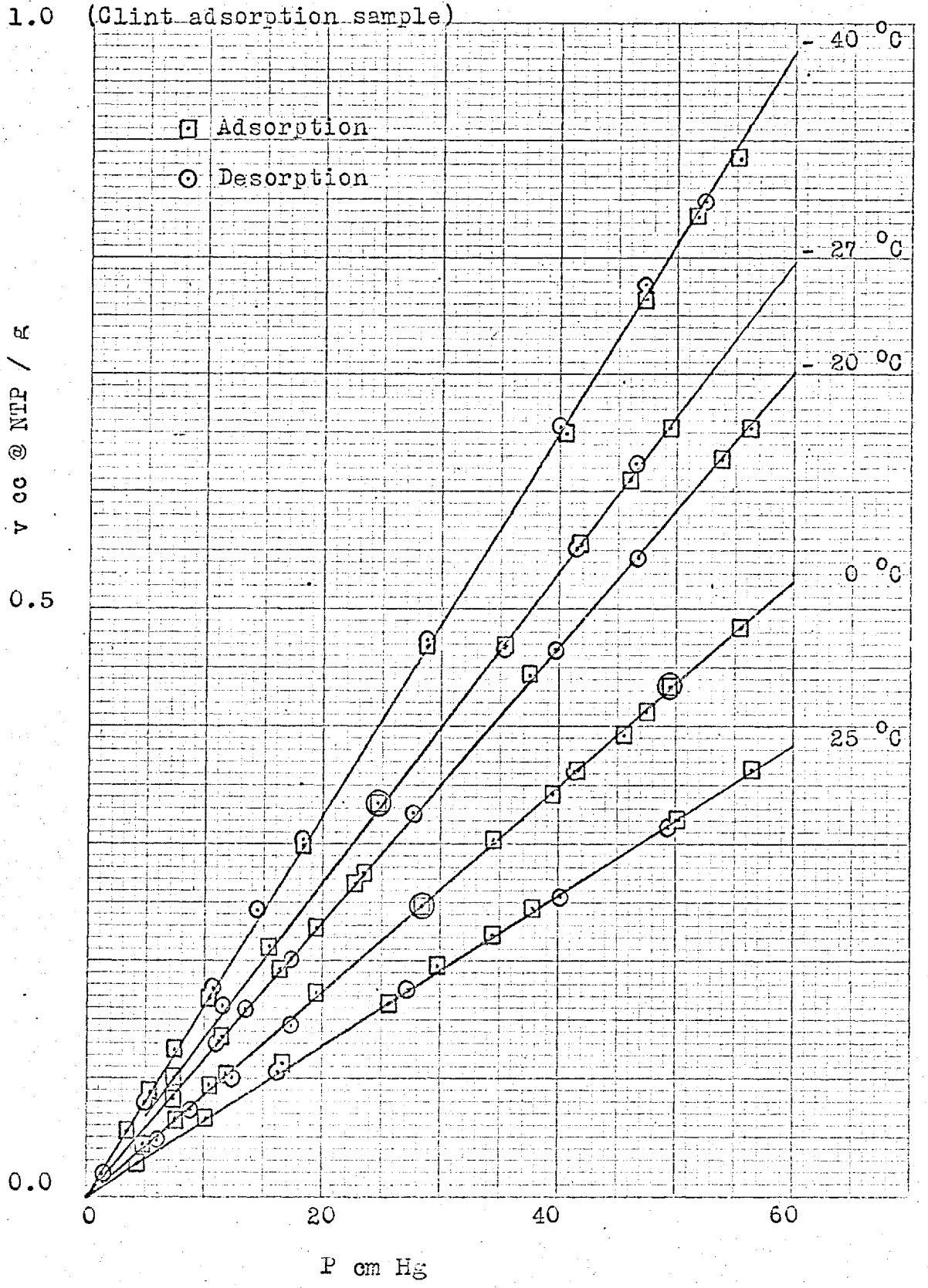

Deuterium on Carbolac I Isotherms

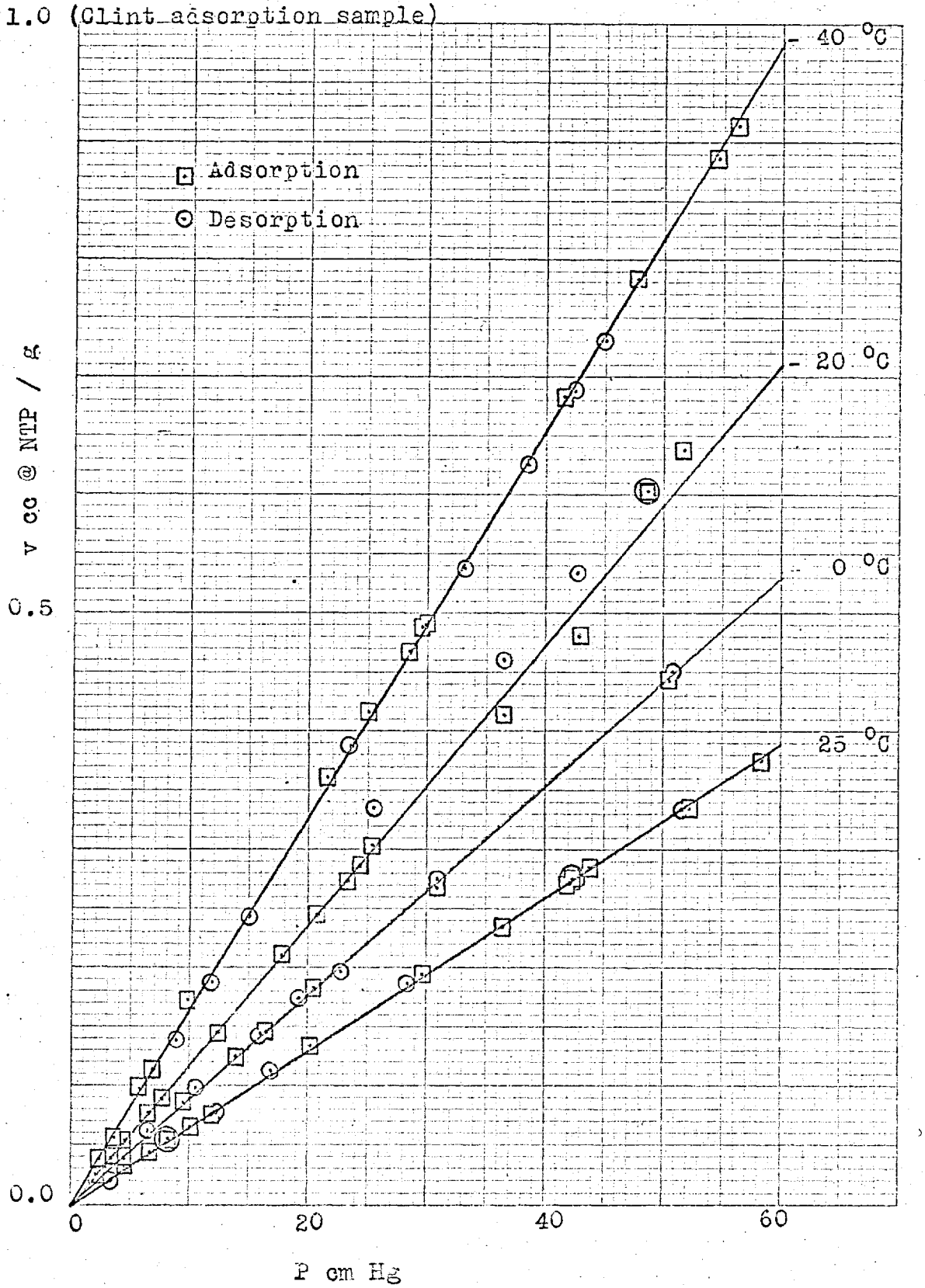

Hydrogen & Deuterium on Carbolac I Isotherms

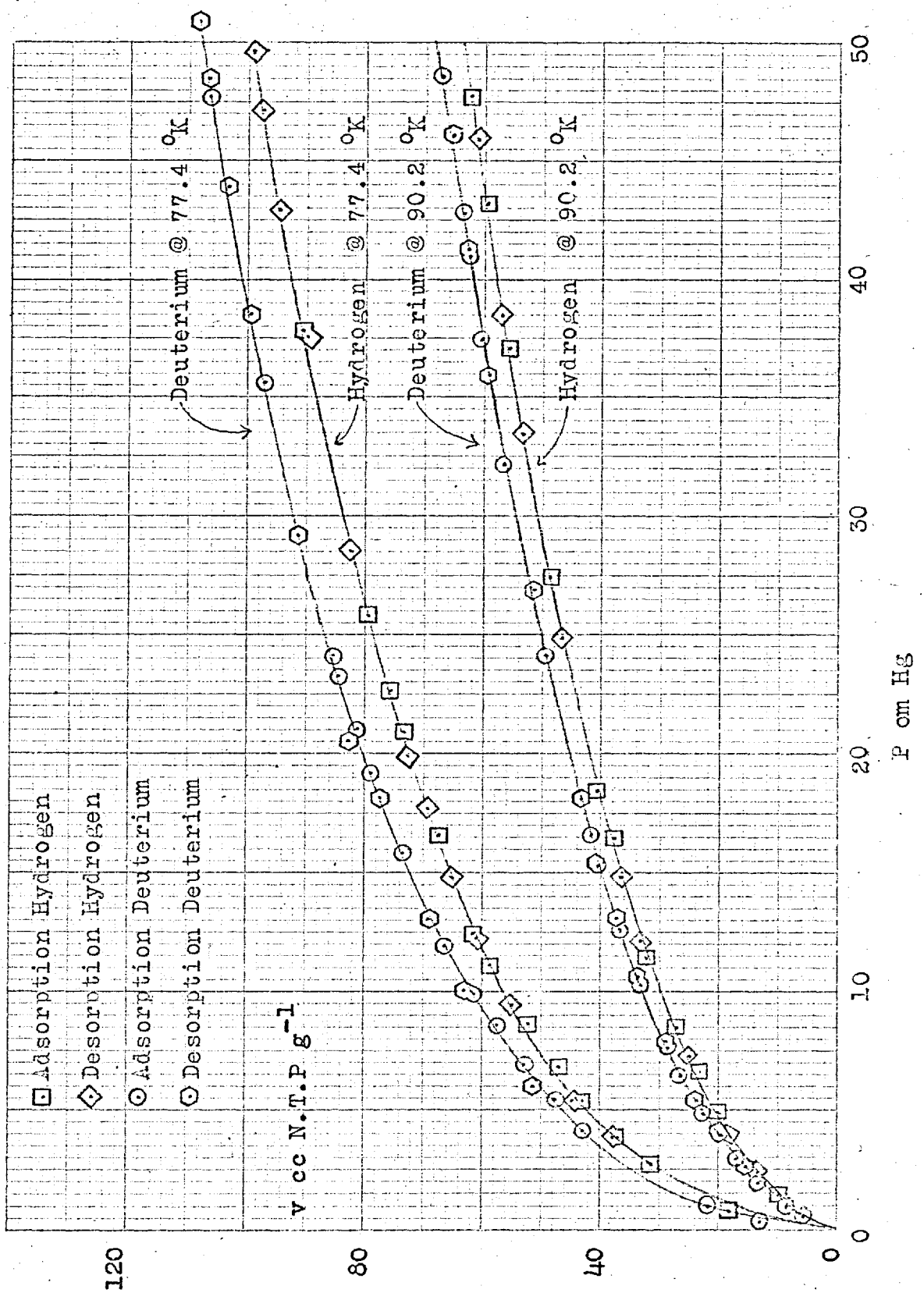

Figure 4.9

$Log_{10}(v/P)$ v 1/T for Hydrogen and Deuterium on Carbolac I Isotherms

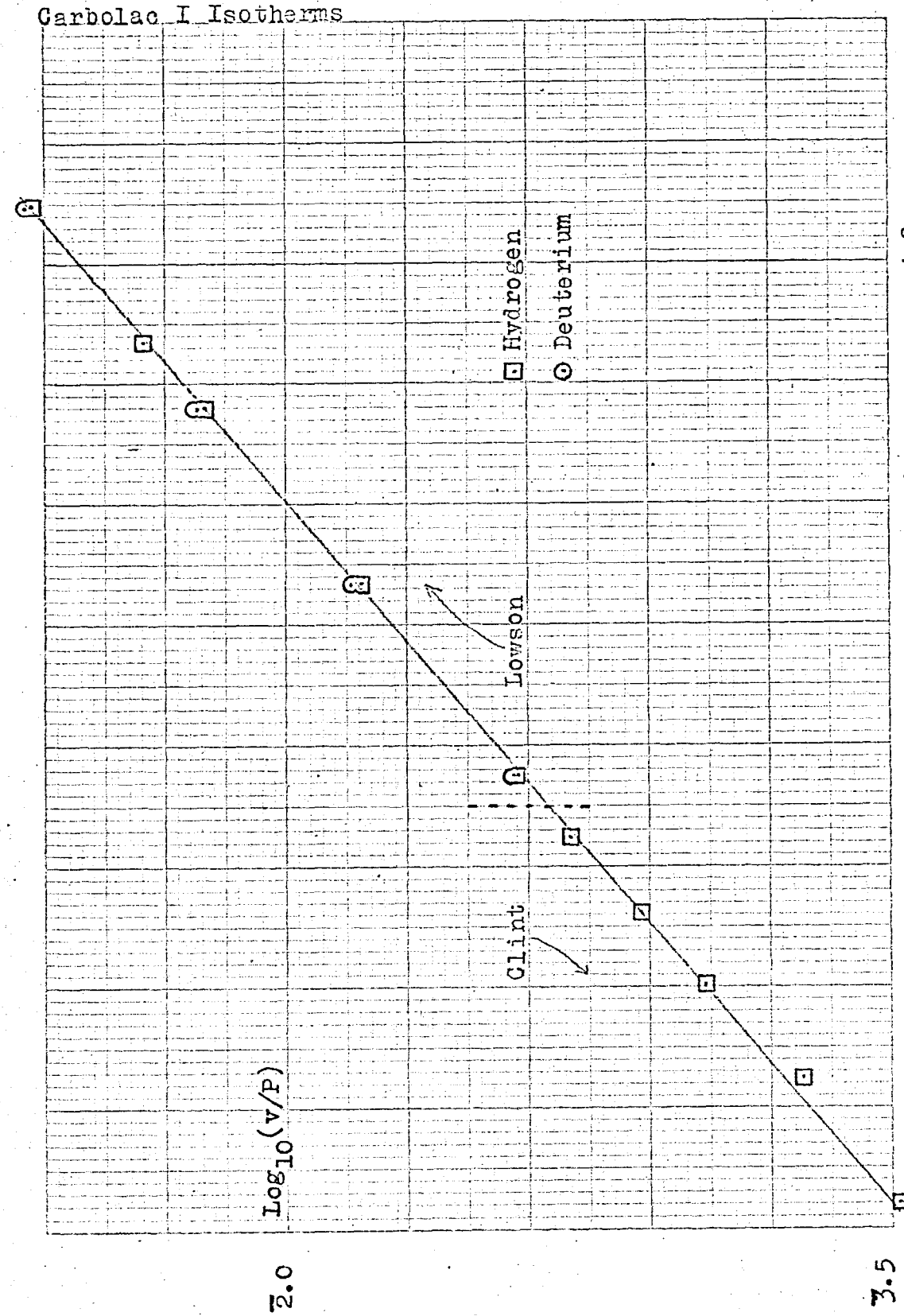

Figure 4.10

$Log_{10}(k_s)$ v 1/T for Hydrogen and Deuterium on Carbolac I Isotherms

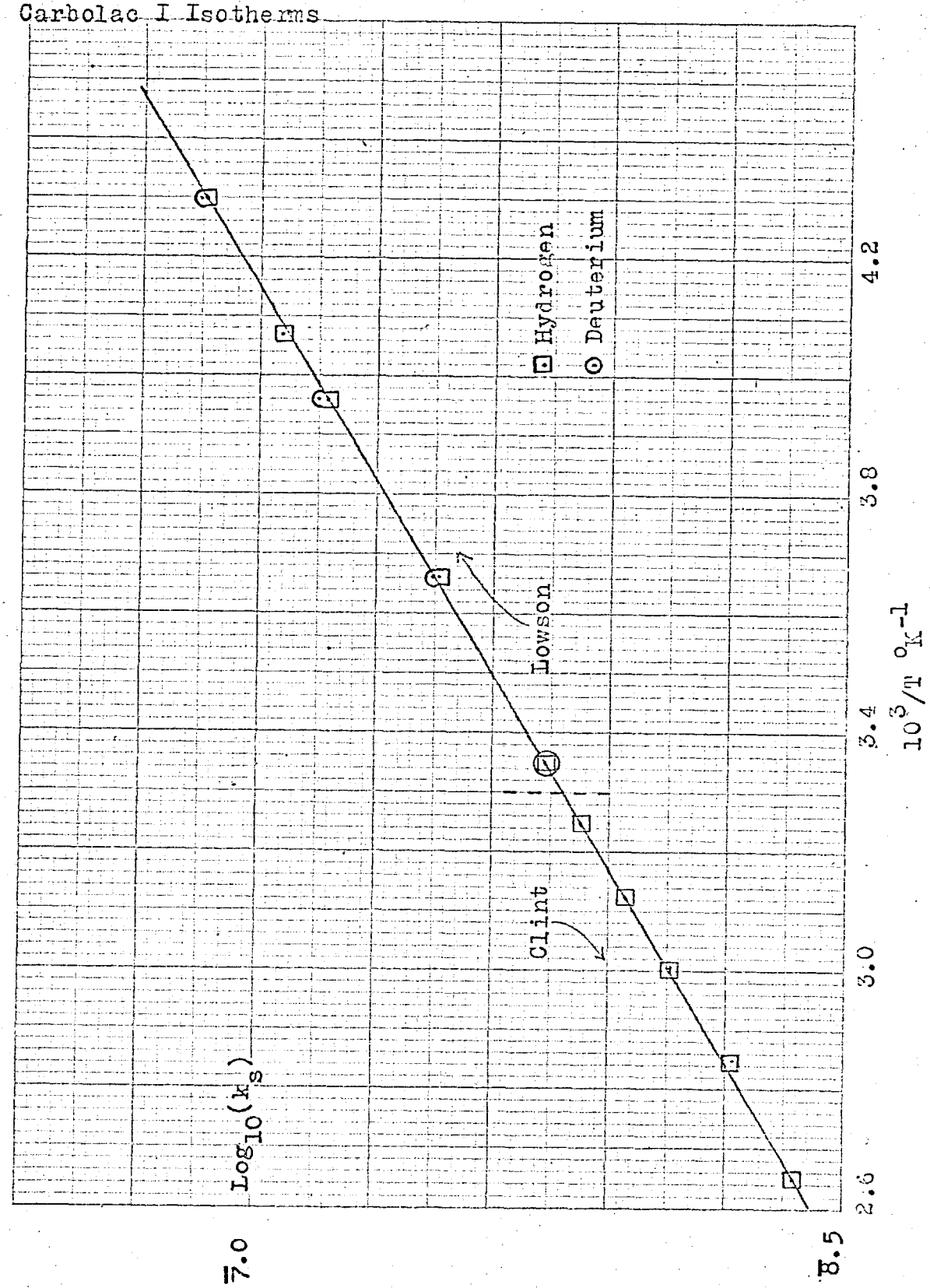

Figure 4.11

Isosteric Heats for Hydrogen and Deuterium Isotherms on Carbolac I between 77.4 & 90.2 °K

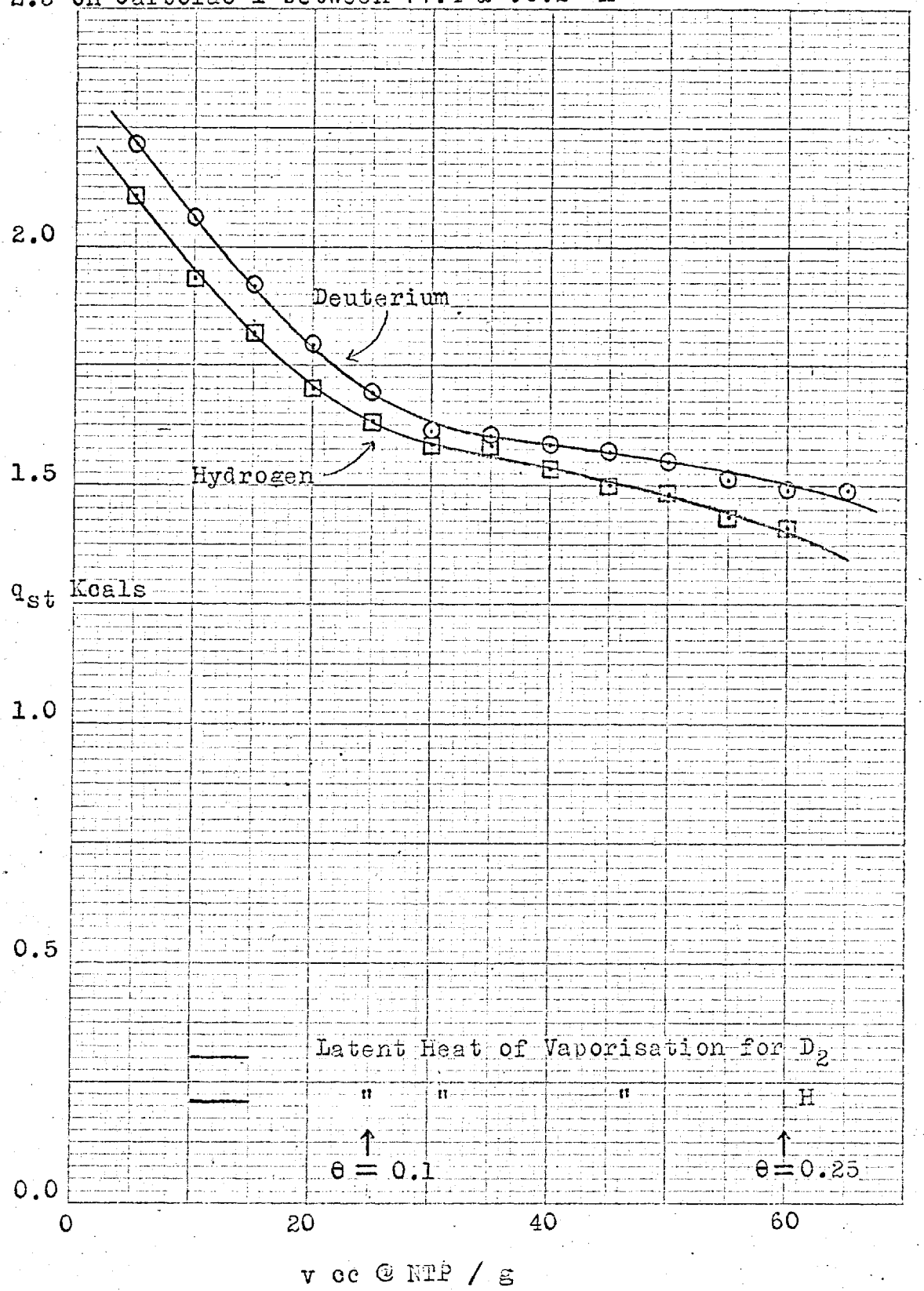

Table 4.6 k_s values for Hydrogen and Deuterium

T in °C	k_s H_2 x 10^8	k_s D_2 x 10^8
25	5.69	5.68
0	7.03	7.11
- 20	8.74	8.92
- 27.4	9.57	-
- 40	11.17	11.26

values obtained by Clint for hydrogen on the same sample at higher temperatures. Applying equations 2.70 and 2.71 from section 2.2.2, the following values for the heat and energy of adsorption were obtained.

"ΔH"	H_2 (Author)	1950	cal. $mole^{-1}$
	H_2 (Clint)	2100	cal. $mole^{-1}$
	D_2 (Author)	1950	cal. $mole^{-1}$
"ΔE"	H_2 (Author)	1430	cal. $mole^{-1}$
	H_2 (Clint)	1430	cal. $mole^{-1}$
	D_2 (Author)	1430	cal. $mole^{-1}$

The small difference between the values for "ΔH" obtained by Clint and those reported here is propably due to experimental error in the choice of slope.

The isosteric heats at higher coverages were calculated for both gases from the isotherms at liquid nitrogen and liquid oxygen temperatures using equation 2.77 and are shown plotted against coverage in figure 4.11.

4.2.3 Ammonia Isotherms on Carbolac I

Adsorption isotherms for ammonia on the 0.5 g sample of Carbolac I chips were measured in the following order:-

Run Number	1	2	3	4	5	6	7	
Temperature	0.0	-40	-30	-20	-10	0.0	-50	°C

The graphs of numbers 2 to 7 are shown in figure 4.12. In order to retain clarity in the diagram only the adsorption branches are shown except for the - 50 °C isotherm, where there was a large hysteresis loop. At high relative pressures the system was very sensitive to small temperature fluctuations with a corresponding large variation in pressure; at - 40 °C the high relative pressure region was just within the limit of the manometer, but due to the temperature fluctuations ammonia gas was lost to the vacuum limb, and so no desorption branch was measured at this temperature.

Figure 4.13 illustrates the sorption-desorption branches of the isotherm at - 10 °C and the difference between the initial adsorption isotherm at 0 °C (run 1) and the adsorption isotherm at 0 °C (run 6) after adsorbing at lower temperatures and out-gassing at 200 °C between each run.

The hysteresis loop did not close for any of the isotherms, and a re-adsorption re-desorption run at - 10 °C scanned across the loop back onto the adsorption and desorption branches.

Linear plots of $\log_{10} P$ versus 1/T at constant coverage were obtained using the values for runs 2, 3, 4, 5, and 6. Using these graphs together with equation 2.76 the isosteric heats were calculated for different coverages and are shown in figure 4.14.

From the adsorption isotherms the integral $I = \int_0^P (v/P).dP$ was computed and is shown plotted against pressure in figure 4.15. These graphs were used to calculate the spreading pressure ($\phi = \frac{R.T}{A}.I$), and hence the molar heat of adsorption at constant spreading pressure $\Delta\tilde{H}$. The graph of $\Delta\tilde{H}$ versus ϕ is shown in figure 4.16.

Figure 4.12

Ammonia on Carbolac I Isotherms

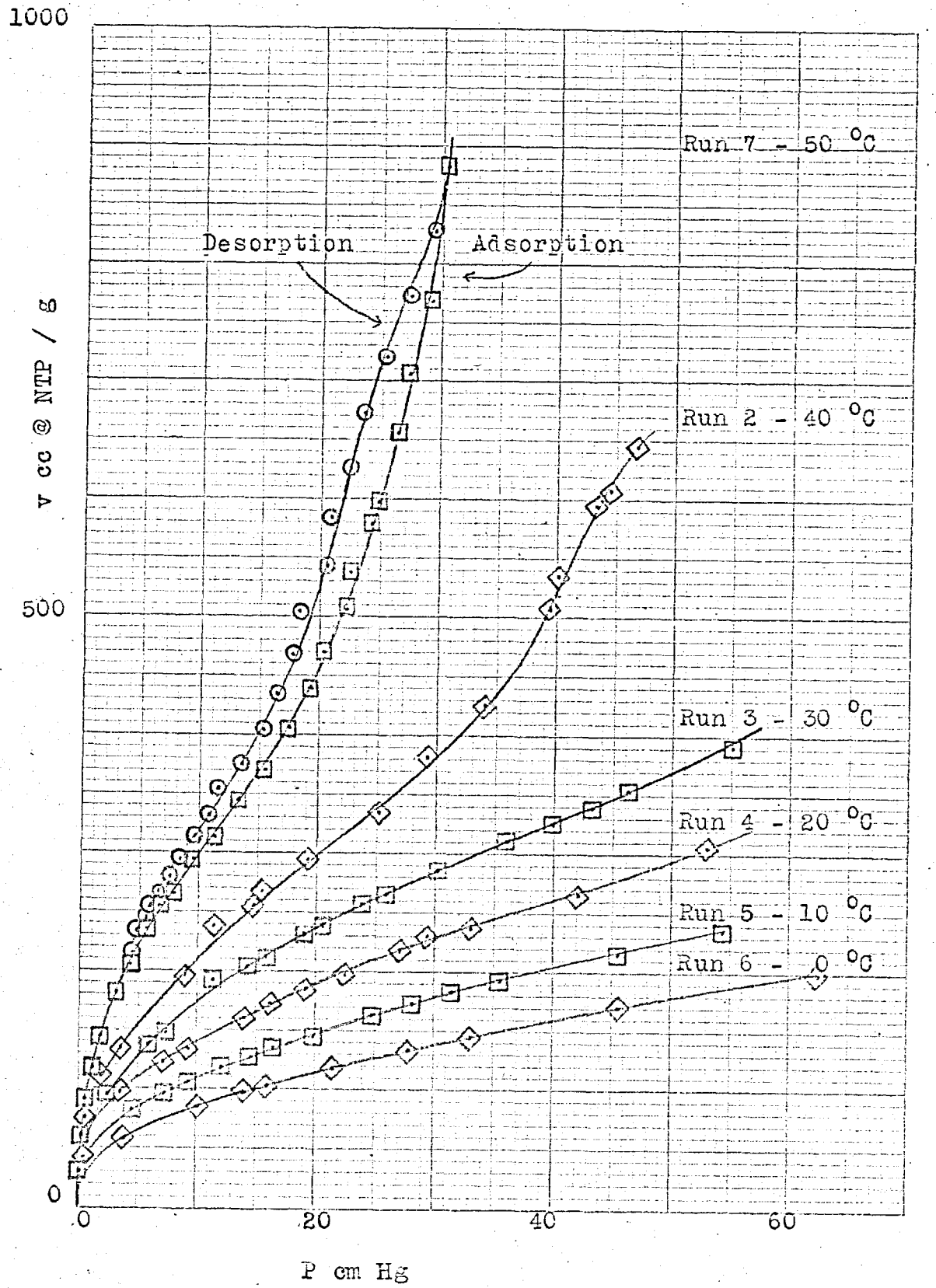

Figure 4.13

Ammonia on Carbolac I Isotherms

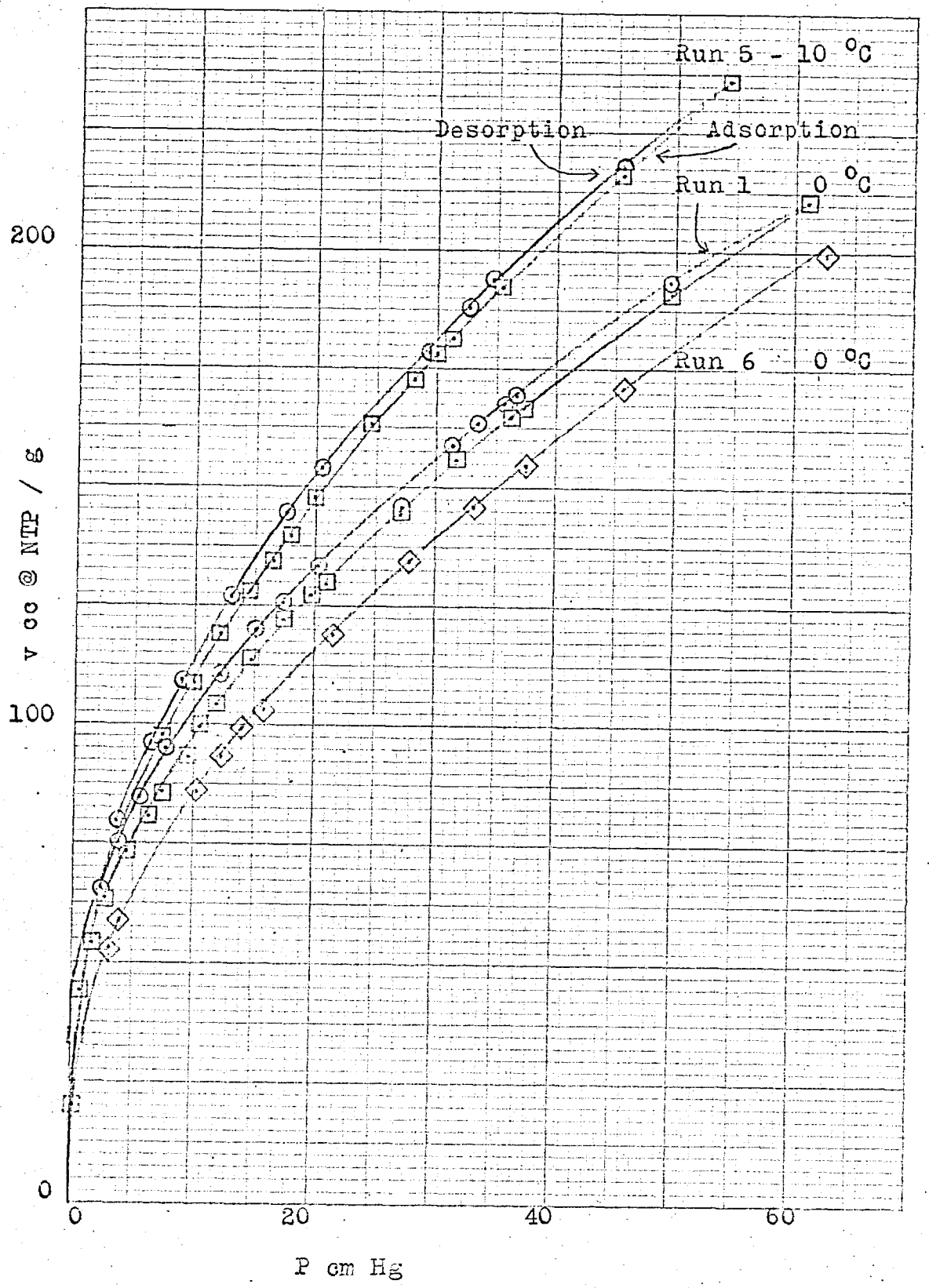

Figure 4.14

Isosteric Heats for Ammonia on Carbolac I for temperature range 0 to - 40 °C

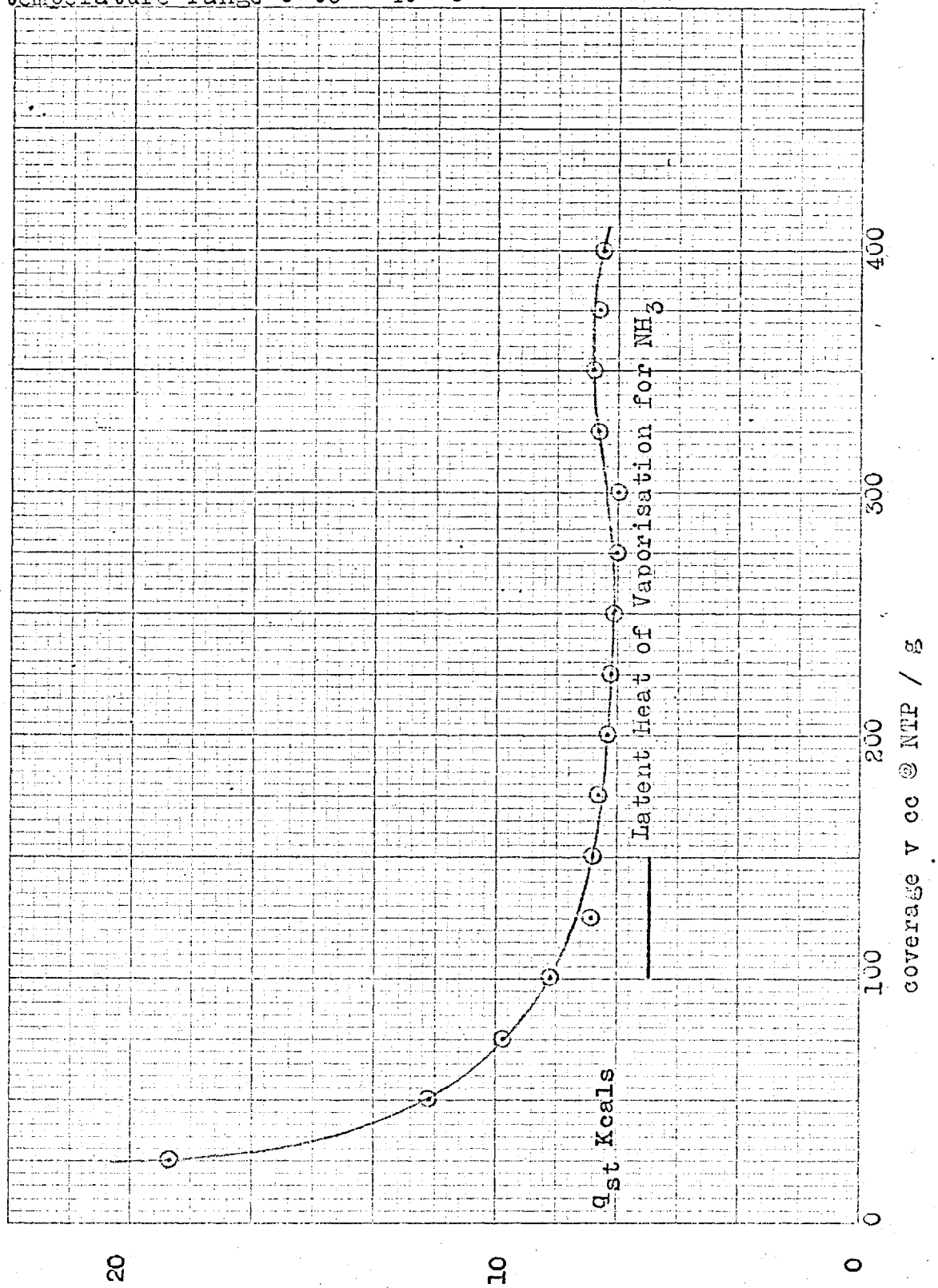

Figure 4.15

The computed integral $\int_0^P \frac{v}{P}.dP$ for Ammonia Isotherms on Carbolac I

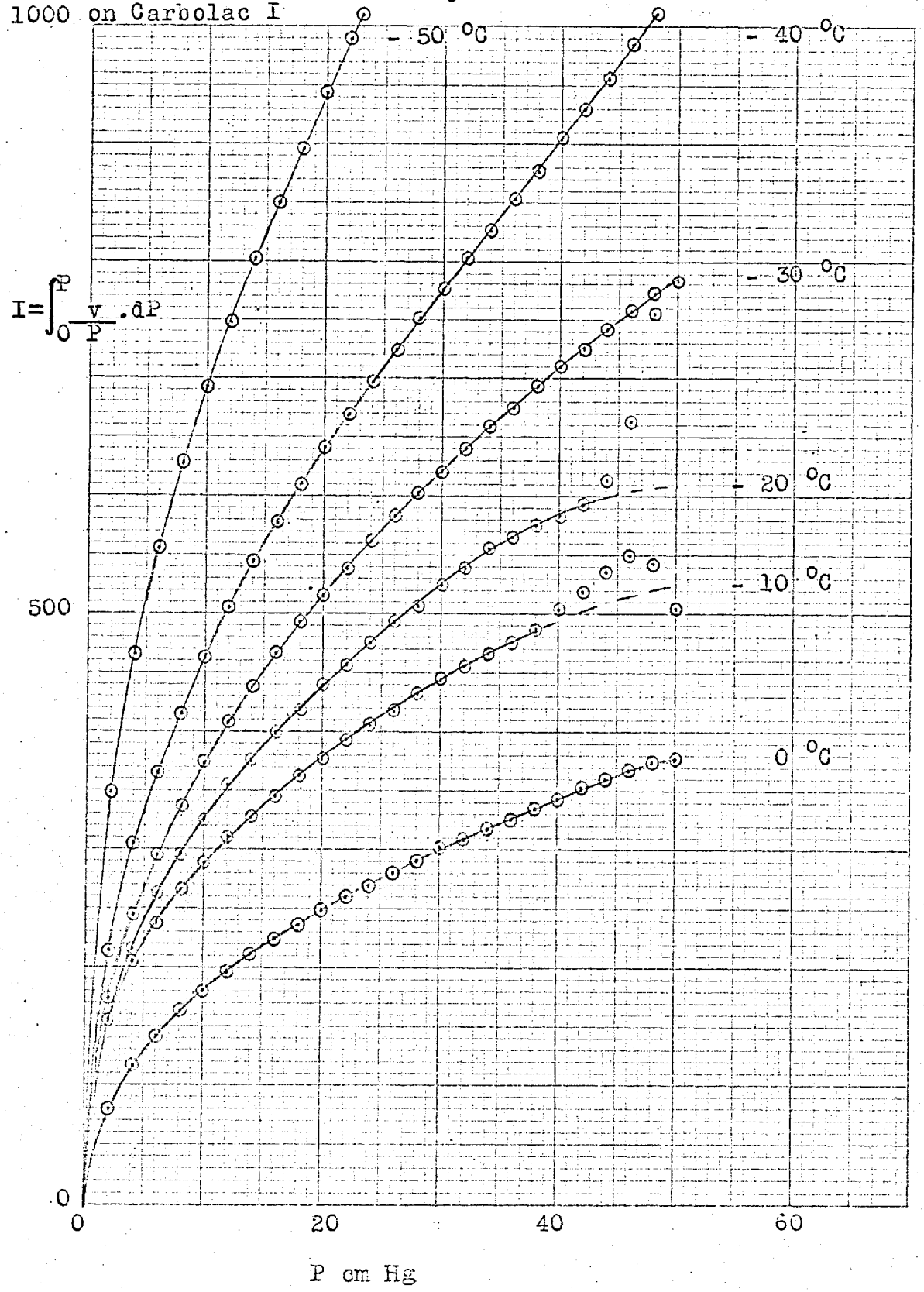

Figure 4.16

Molar Heats of Adsorption for Ammonia on Carbolac I

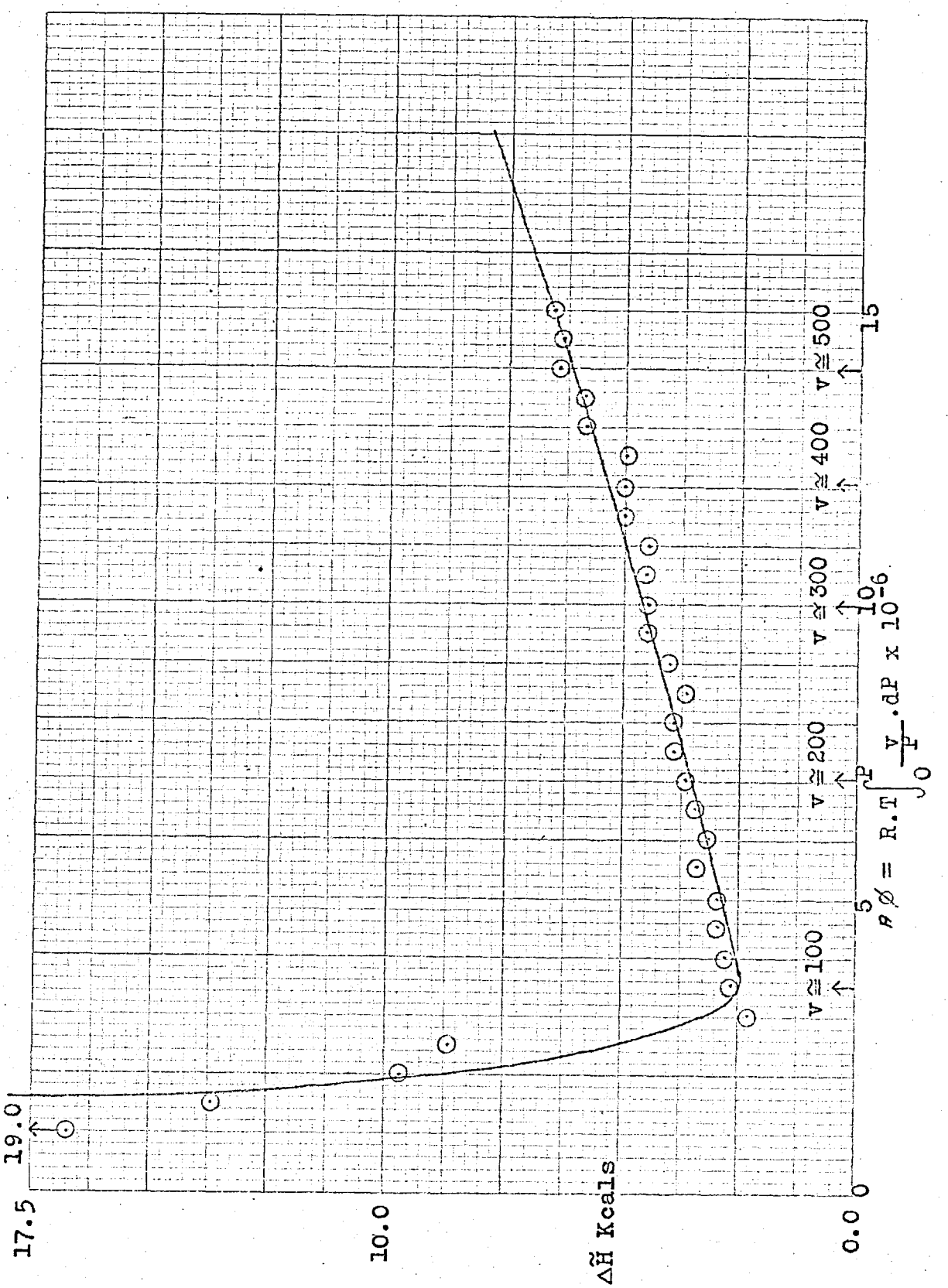

4.3 SINGLE GAS FLOW

4.3.1 Helium flow through Graphon

Helium permeation through Graphon was investigated over the temperature range 300 to - 196 °C. The time-lag was less than a minute and so only the steady state flow was measured. In order to differentiate between small significant variations of permeability with temperature and experimental random error, a set of five experiments were run per temperature covering a pressure range at the in-going side of 5 to 60 cm Hg. So as not to be overwhelmed by excessive computation the measurements were standardised to ten readings per run, and processed by computer.

The Graphon plug was initially out-gassed at 200 °C for 24 hours once the pressure had been reduced to 1×10^{-6} cm Hg. Prior to each set of experiments the plug was out-gassed overnight at the temperature of the experiments to be performed.

For a given temperature the first experiment of the set was run at an in-going side pressure of around 5 cm Hg, and the change of out-going side pressure followed with time. At the end of the run the in-going side pressure was increased and the out-going side quickly out-gassed by opening it to the high vacuum pumps and switching over to a new buffer volume. On closing the tap to the vacuum pumps the apparatus was ready for the next experiment at the new in-going side pressure. The values for the in-going side pressure, temperature, flux, permeability, and the permeability constant $K.(M/T_p)^{\frac{1}{2}}$, are listed in appendix 4. The flux was defined as

$$J = V_{ogs} \cdot \frac{\Delta P}{\Delta t} \cdot \frac{1}{R.T_r.A_c} \quad \text{moles/cm}^2\text{/sec} \qquad 4.3$$

J = The total flux in moles cm^{-2} sec^{-1}.

V_{ogs} = The volume of the out-going side in cc.

Figure 4.17

Permeability of Helium through Graphon

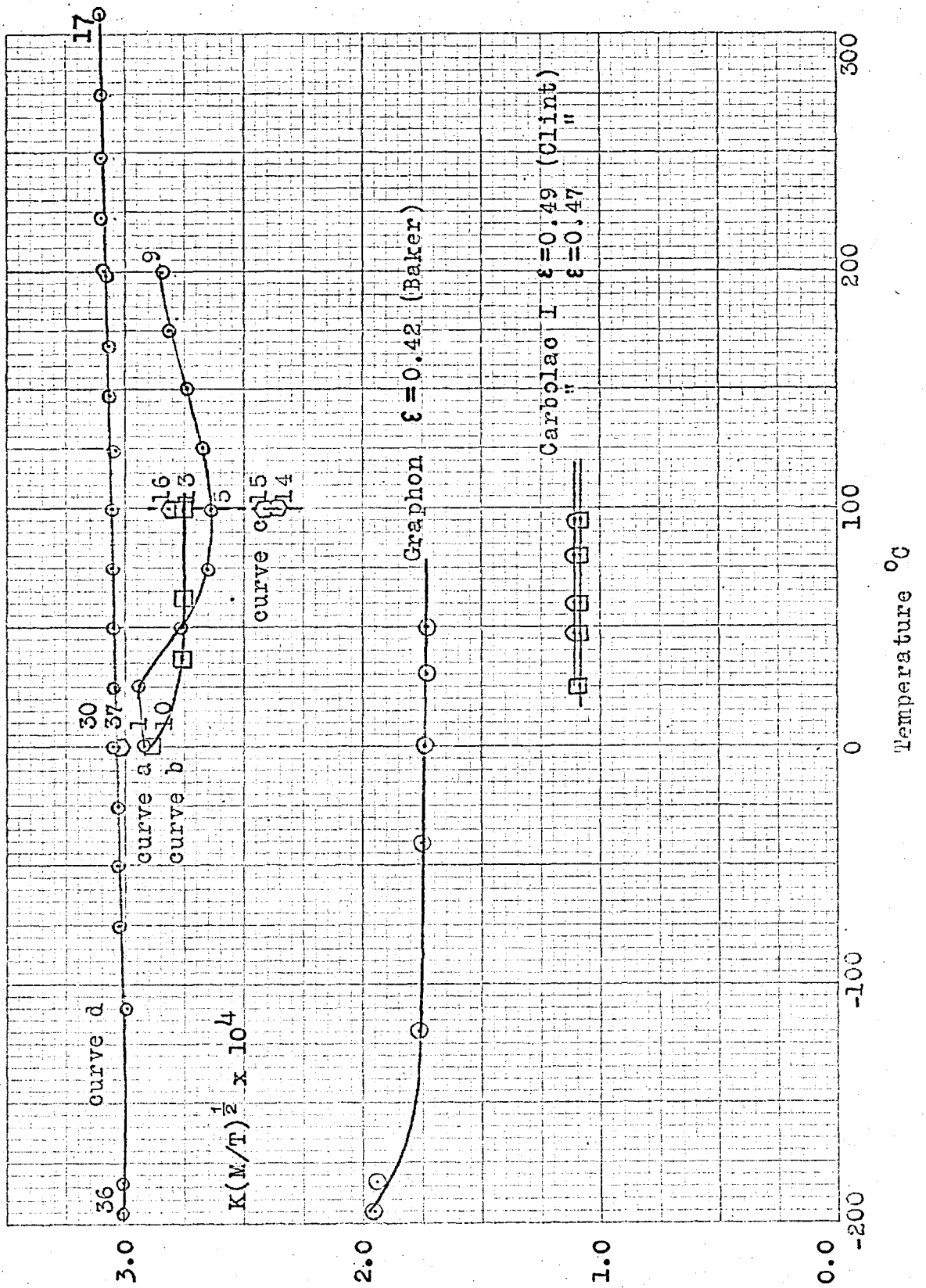

$\Delta P/\Delta t$ = The slope of the graph of out-going side pressure versus time in cm Hg sec^{-1}.

T_r = The ambient temperature in ^oK.

A_c = The cross-sectional area of the membrane in cm^2.

R = The gas constant in the appropiate units.

The permeability was defined as

$$K = \frac{J.l}{\Delta C_g^g} = V_{ogs}.\frac{\Delta P}{\Delta t}.\frac{T_p.l}{T_r.A_c}.\frac{1}{P} \quad cm\ sec^{-1} \qquad 4.4$$

l = The length of the membrane in cm.

T_p = The temperature of the membrane in ^oK.

P = The pressure at the in-going side in cm Hg.

For all the experiments the permeability was invariant with in-going side pressure, but for the first group of experiments (sets 1. to 9.) the permeability constant was found to vary with temperature, this is shown in figure 4.17 as curve (a) which is a graph of $K.(M/T_p)^{\frac{1}{2}}$ versus T_p. Each point represents the mean value for the set of experiments for the given temperature. Although each set of experiments was performed within a day, a period of anything between 1 to 7 days would lapse between each set. To see if curve (a) was reproducible a further group of experiments were performed (sets 10. to 13.), selecting the intermediate temperatures of curve (a). The results formed curve (b) which while starting at curve (a), flattens off much sooner with rising temperature. A period of two months then lapsed during which time the plug was stored under vacuum, open to the mercury gauges, but isolated from the vacuum pumps. The experiments at 100 ^oC were then repeated having out-gassed the plug at room temperature to a pressure of less than 1×10^{-6} cm Hg. The result (set 14.) fell well below curves (a) and (b). The experiment was repeated using a new sample of helium (set 15.), but only marginal improvement was obtained. The plug was then

out-gassed at 200 °C for 72 hours at a pressure of less than 1×10^{-6} cm Hg, and the experiments at 100 °C repeated. The result (set 16.) brought the value for $K.(M/T_p)^{\frac{1}{2}}$ to within 3% of the value at 0 °C and 0.5% of the value at 200 °C. So results 5., 13. to 16. form a vertical line, curve (c). It was now noticeable that small droplets of mercury had collected on the glass surface just above the plug assembly. This mercury had probably travelled from the gauges and condensed onto the plug at temperatures below 100 °C over a period of months, and it only evaporated away from the plug when the plug was heated to 200 °C. Consequently curves (a), (b) and (c) may be due to the following causes.

(i) The effect is real and due to surface flow.

(ii) The effect is due to slow sorption of mercury below 100 °C causing a drop in permeability, above 100 °C the mercury slowly desorbs causing a rise in permeability.

(iii) The effect is due to a characteristic baked into the plug at 200 °C which increases the value for the permeability. The characteristic gradually falls away with time causing a drop in permeability, but starts to be rejuvenated when the plug is heated above 100 °C.

The discovery of curve (c), where at constant temperature $K.(M/T_p)^{\frac{1}{2}}$ has a greater degree of variation than curve (a), suggests that the variation of $K.(M/T_p)^{\frac{1}{2}}$ with temperature found with curve (a) is not real, but is due to either mercury sorption or variations in the geometry of the plug. Accordingly a further group of experiments were performed (sets 17. to 36.) in which much greater attention was paid to the out-gassing conditions, storage, and run order of the experiments. The plug was heated to 300 °C and out-gassed for 24 hours once the pressure had fallen to 1×10^{-6} cm Hg. Then starting at 300 °C sets of five experiments per temperature were run day after day

without break, dropping the temperature in 25 °C steps and out-gassing the plug overnight at the new temperature until 200 °C was reached (sets 17. to 21.). A period of one month then lapsed during which time the plug was isolated from the rest of the apparatus. The plug was then reheated to 200 °C and the experiments continued as before with temperature steps of 25 °C as far as 0 °C (sets 22. to 30.). The experiments at - 25 and - 50 °C were run the next day (sets 31. and 32.), and the following day the experiments at - 75 and - 110 °C (sets 33. and 34.). The plug was then heated to 100 °C and out-gassed over-night to remove any sorbed mercury, and the following day the experiments at liquid oxygen and liquid nitrogen temperatures were performed (sets 35. and 36.). The results form curve (d) in figure 4.17. Within each set the permeabilities are remarkably consistant to ± 0.5%, while each drop in temperature of 25 °C causes a change in permeability of - 3%. Over the temperature range 300 to - 196 °C the permeability constant $K.(M/T_p)^{\frac{1}{2}}$ only changes by 3%, decreasing with temperature. The result at - 110 °C may have a slight error either due to sorbed mercury or incorrect measurement of temperature. The temperature in this region was measured with a carbon dioxide vapour pressure thermometer which tends to become inaccurate at - 110 °C. A difference of only 3 °C is needed to bring the point back into line with the other results. A final set of experiments was performed (set 37.) at 0 °C after surrounding the plug assembly with liquid nitrogen for ten days. This treatment does not appear to have caused any change in the permeability.

4.3.2 Helium flow through Carbolac I

The helium permeability at 0 °C through the Carbolac I membrane was regularly measured through-out the course of

Figure 4.18

Schematic comparison of Helium permeability through Carbolac I at 0°C

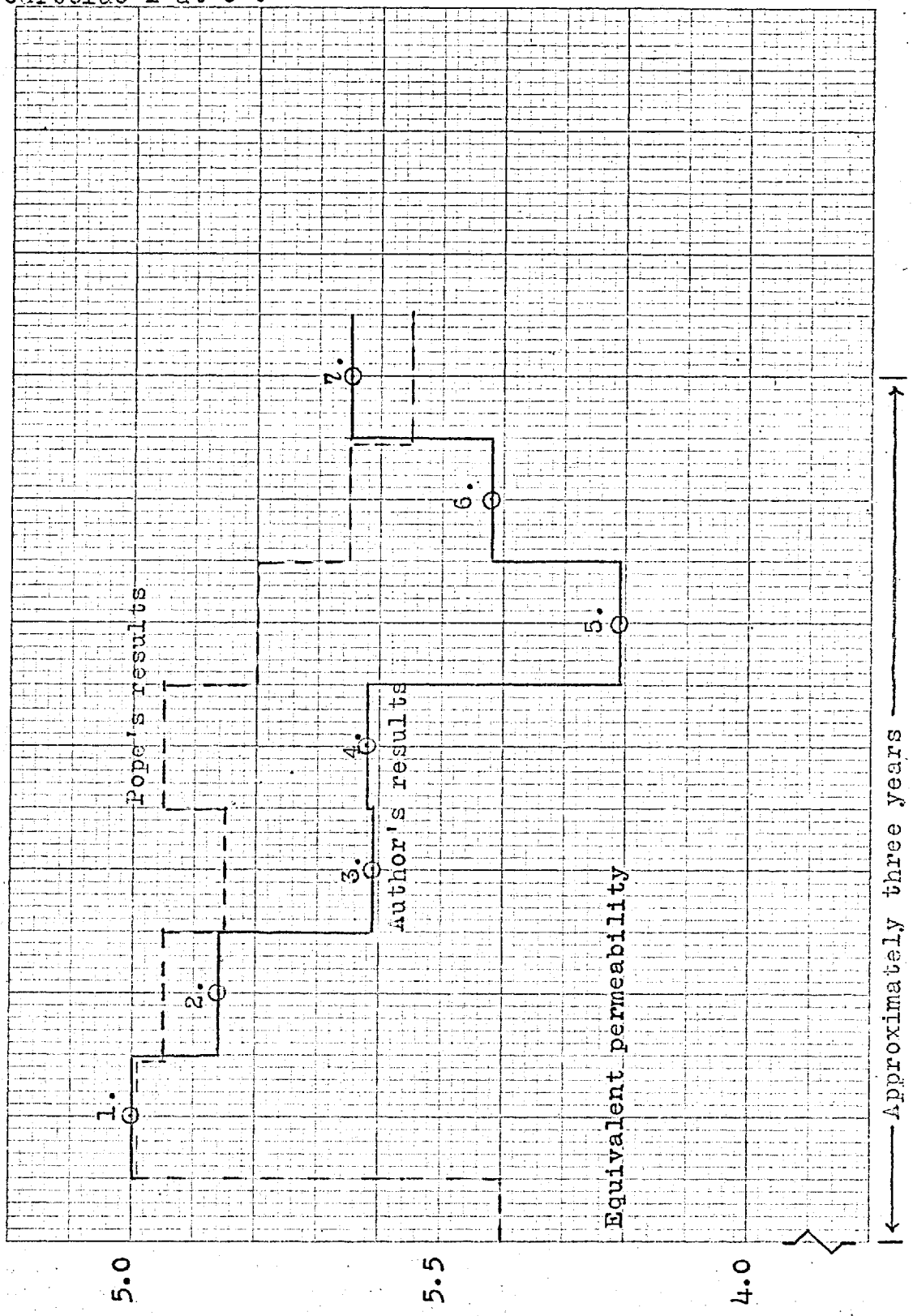

the research. The results (see appendix 5) suggest that a number of irreversible changes occurred within the membrane over a period of three years causing a slow, irregular drop of about 10% in the permeability. Pope (1961), who used a similar membrane, observed an analogous variation. As a comparison the initial permeability for the present membrane has been multiplied by a factor of 3.312 to make it equivalent to Pope's initial value; then the rest of the results were similarly multiplied by the same factor and plotted schematically with Pope's results in figure 4.18. The fluctuations are similar to Pope's and are most marked after very heavy adsorption at the in-going face of the membrane.

A set of helium experiments were also run at - 40 °C, and the permeability constant $K.(M/T_p)^{\frac{1}{2}}$ compares well with the value for the 0 °C runs.

4.3.3 Single gas flow of Hydrogen, Deuterium and Nitrogen through Carbolac I at - 40 °C

The results for the steady state flow experiments for these gases are listed in appendix 5. The boundary conditions for all the experiments were

$C = C_o$ $\quad x = 0$ for all time

$C = 0$ $\quad x = l$ for all time

The total flux J was calculated from equation 4.3. All three gases possessed a small element of surface flow, so the gas phase flux was calculated from the corresponding helium flux for the given temperature and pressure by equation 4.5:

$$J_g = J^{He}.(M_{He}/M)^{\frac{1}{2}} \qquad 4.5$$

and the surface flux by subtraction

$$J_s = J - J_g \qquad 4.6$$

Two permeabilities were defined, the first

$$K = \frac{J.l}{\Delta C_g^g} \qquad 4.7$$

expressed the standard flux for a standard gas phase concentration drop, and follows the previous definitions of Ash, Baker and Barrer (1967), and equation 4.4. The second definition was

$$K_C = \frac{J.l}{\Delta C} \qquad 4.8$$

This definition expresses the standard flux for the total concentration drop across the membrane, and from the discussion in section 2.1.8 would be expected to become a function of total concentration at the in-going side once the adsorption isotherm was outside the Henry law region. The results are presented in graphical form in figures 4.19 to 4.24. These graphs show the variation of

J	v	C_g	for He, H_2, D_2, N_2.	Figure 4.19
J	v	C	for H_2, D_2, .	Figure 4.20
J	v	C	for N_2.	Figure 4.21
K	v	C_g	for He, H_2, D_2, N_2.	Figure 4.22
K_C	v	C	for H_2, D_2, .	Figure 4.23
K_C	v	C	for N_2.	Figure 4.24

A period of six months lapsed between the first and second set of hydrogen experiments. The difference between the values for the fluxes and permeabilities is similar to the fluctuations found for helium. Set 1. was obtained just before the ammonia-hydrogen mixture experiments and lies between sets 4. and 5. for helium. Set 2. was obtained just before the deuterium experiments and follows the helium run set 7. . Set 2. of the hydrogen runs was used in graphs 4.19 to 4.24.

The time-lag to achieve the steady state was less than a minute for hydrogen and deuterium, so ten readings were

J v C_g for Helium, Hydrogen, Deuterium, and Nitrogen through Carbolac I at - 40 °C

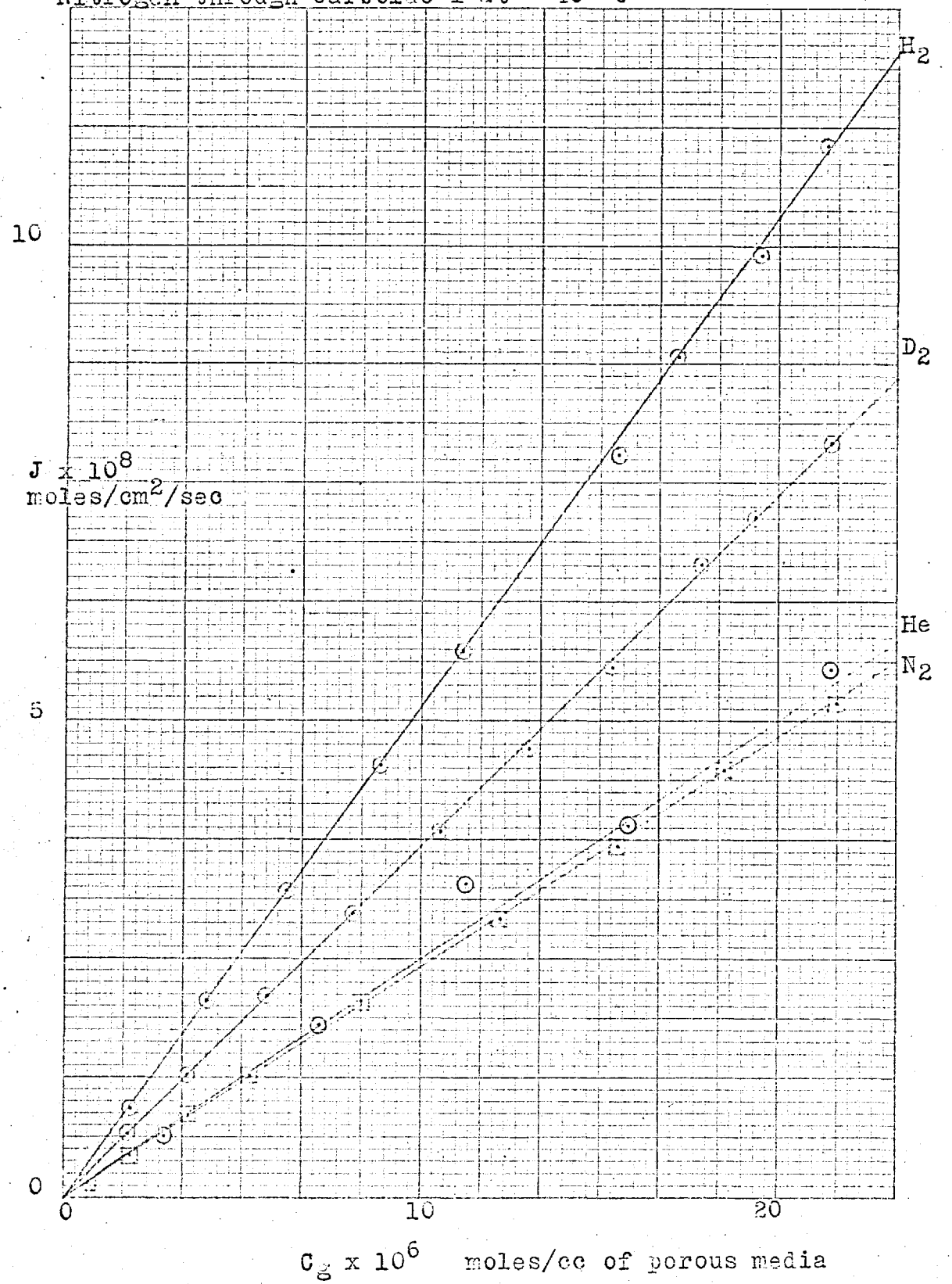

Figure 4.20

J v C for Hydrogen and Deuterium through Carbolac I at - 40 °C

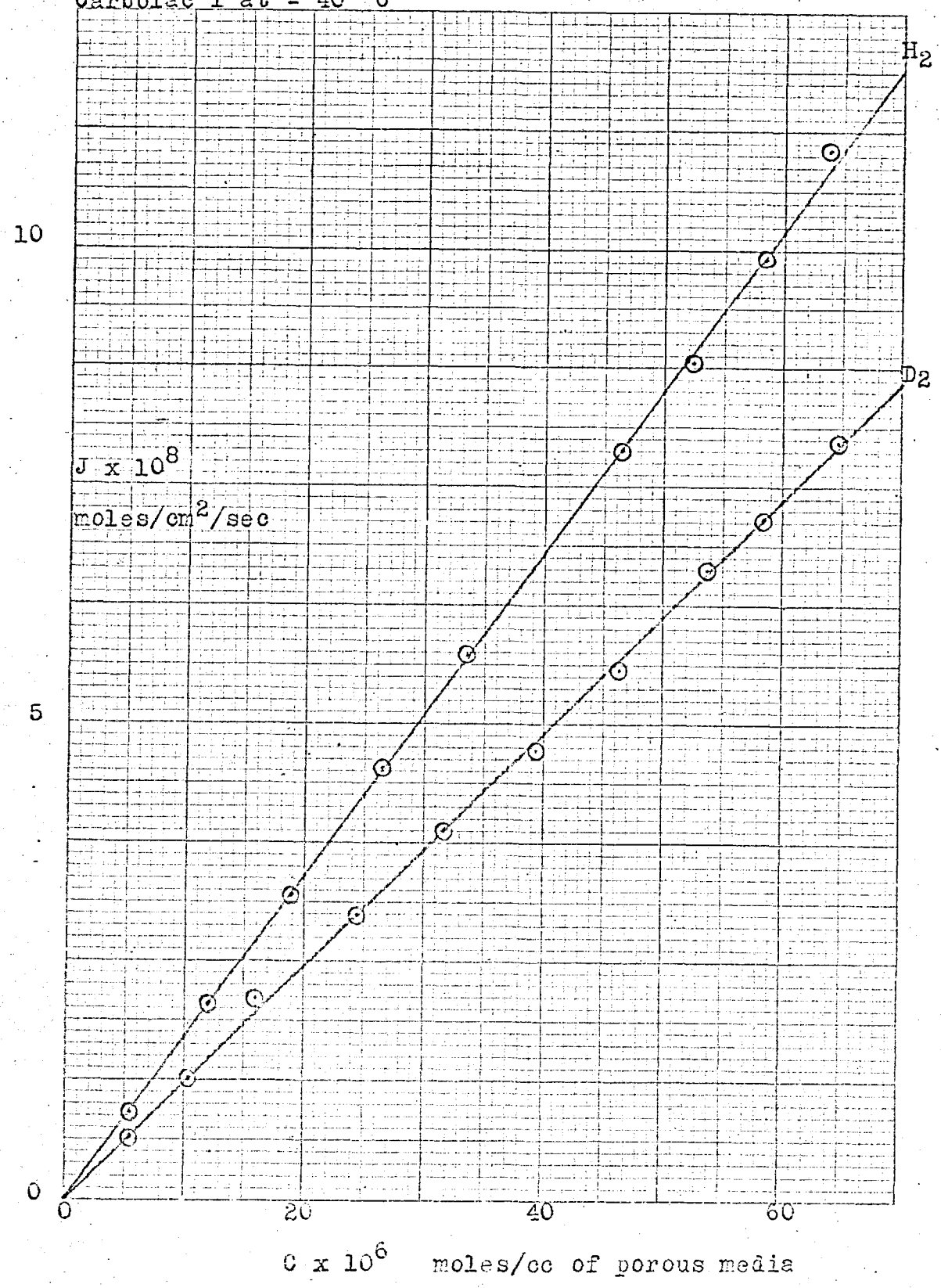

Figure 4.21

J v C for Nitrogen through Carbolac I at - 40 °C

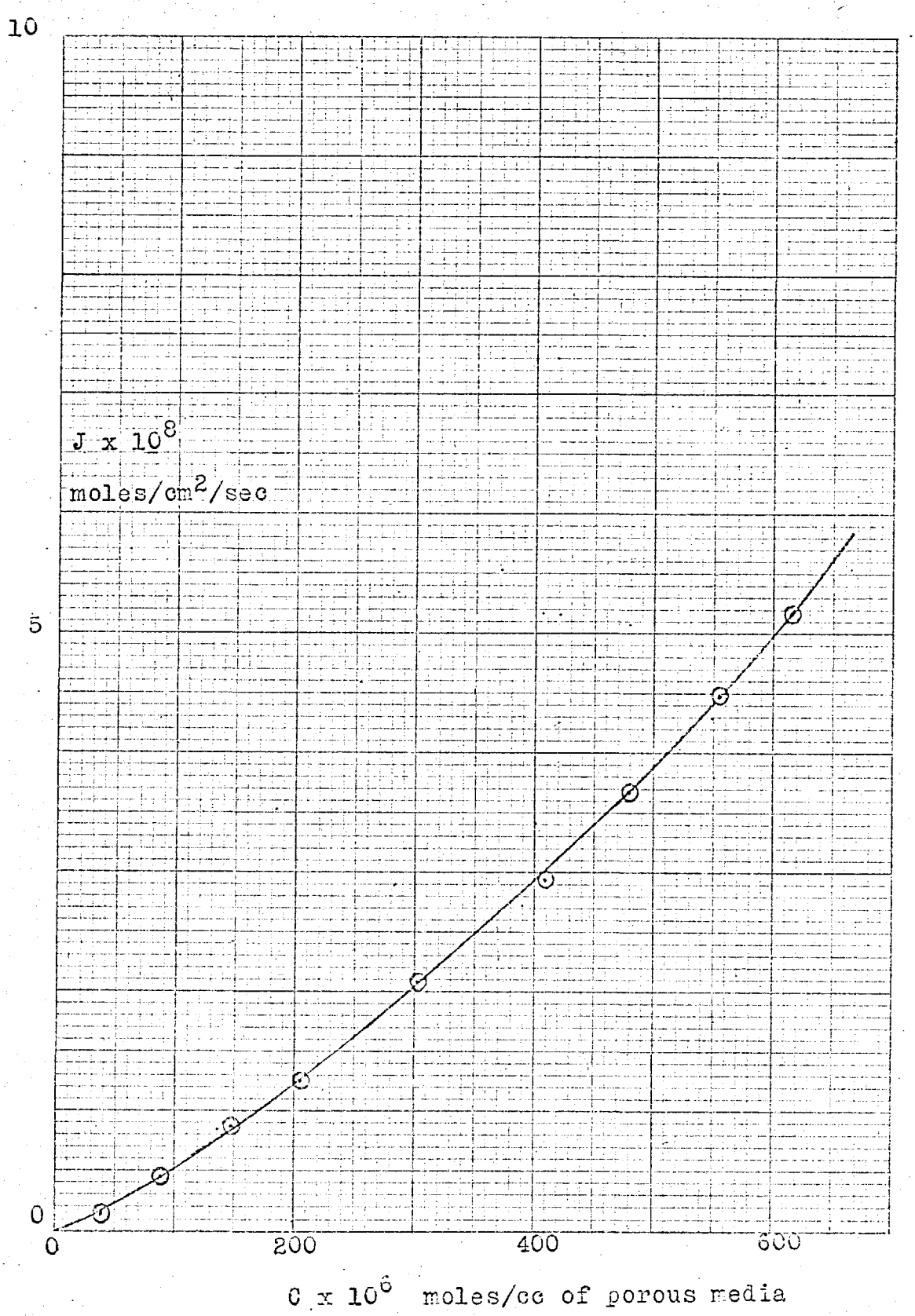

K v C_g for Helium, Hydrogen, Deuterium, and Nitrogen through Carbolac I at - 40 °C

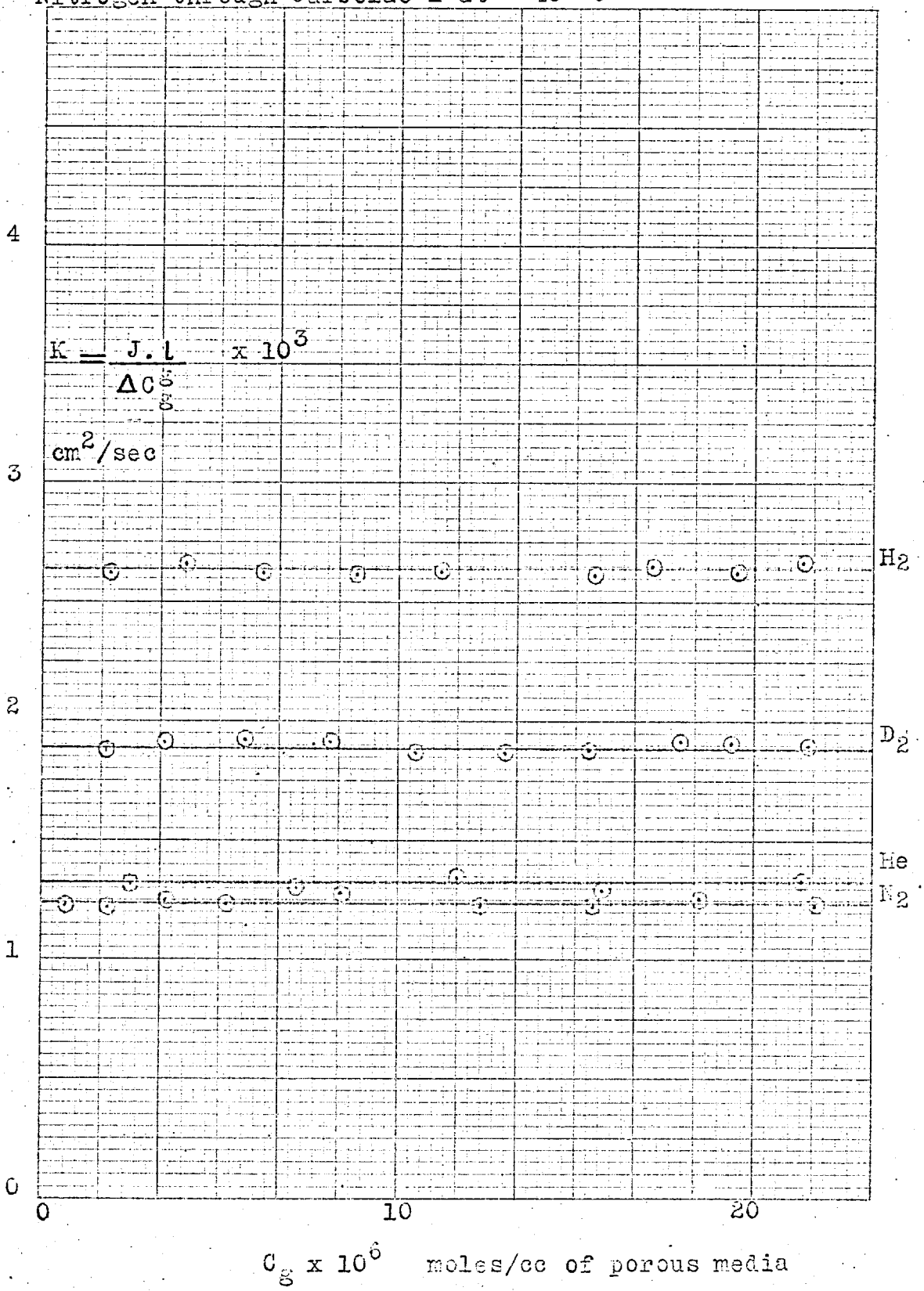

K_C v C for Hydrogen and Deuterium through Carbolac I at - 40 °C

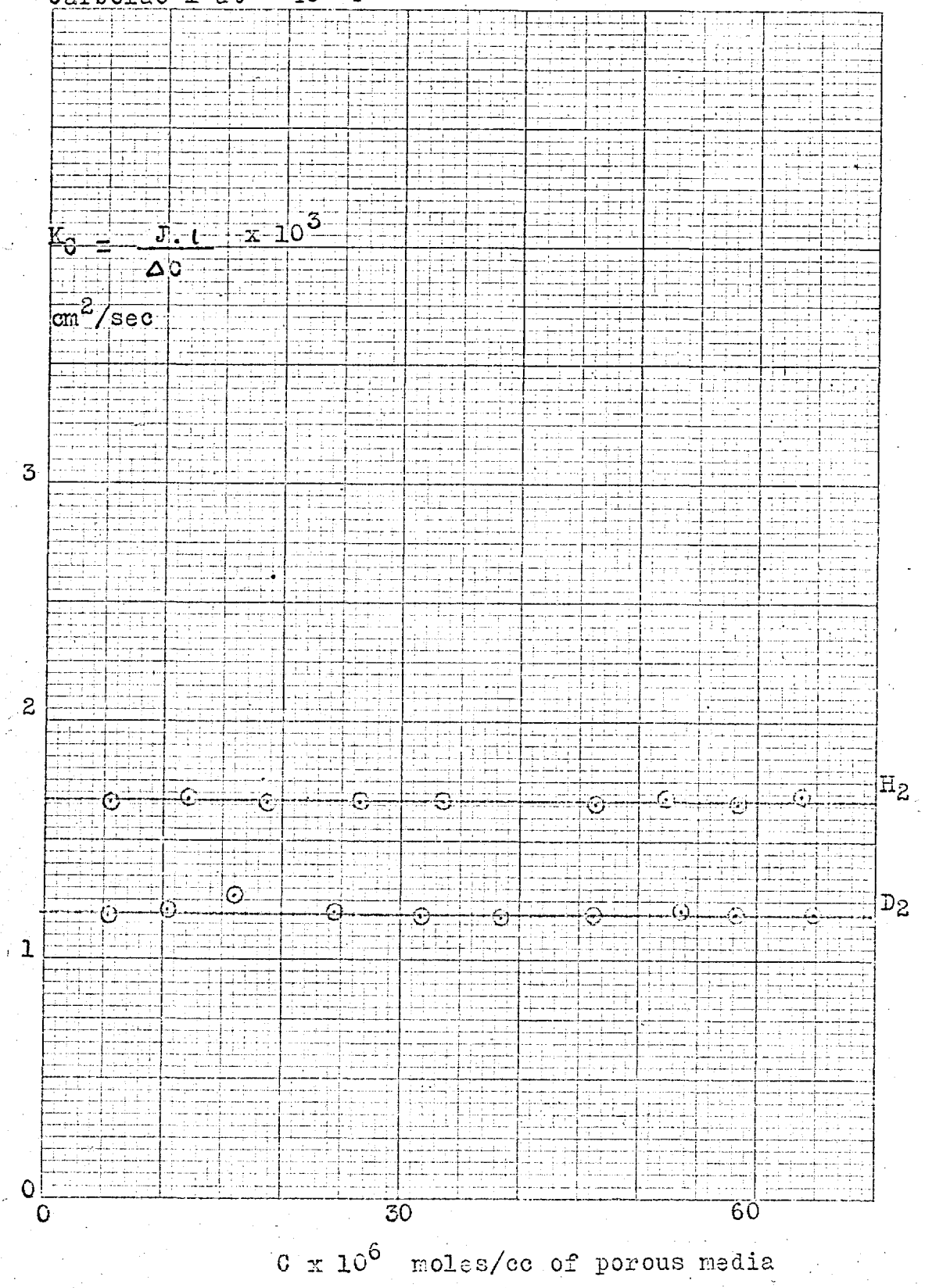

Figure 4.24

K_C v C for Nitrogen through Carbolac I at - 40 °C

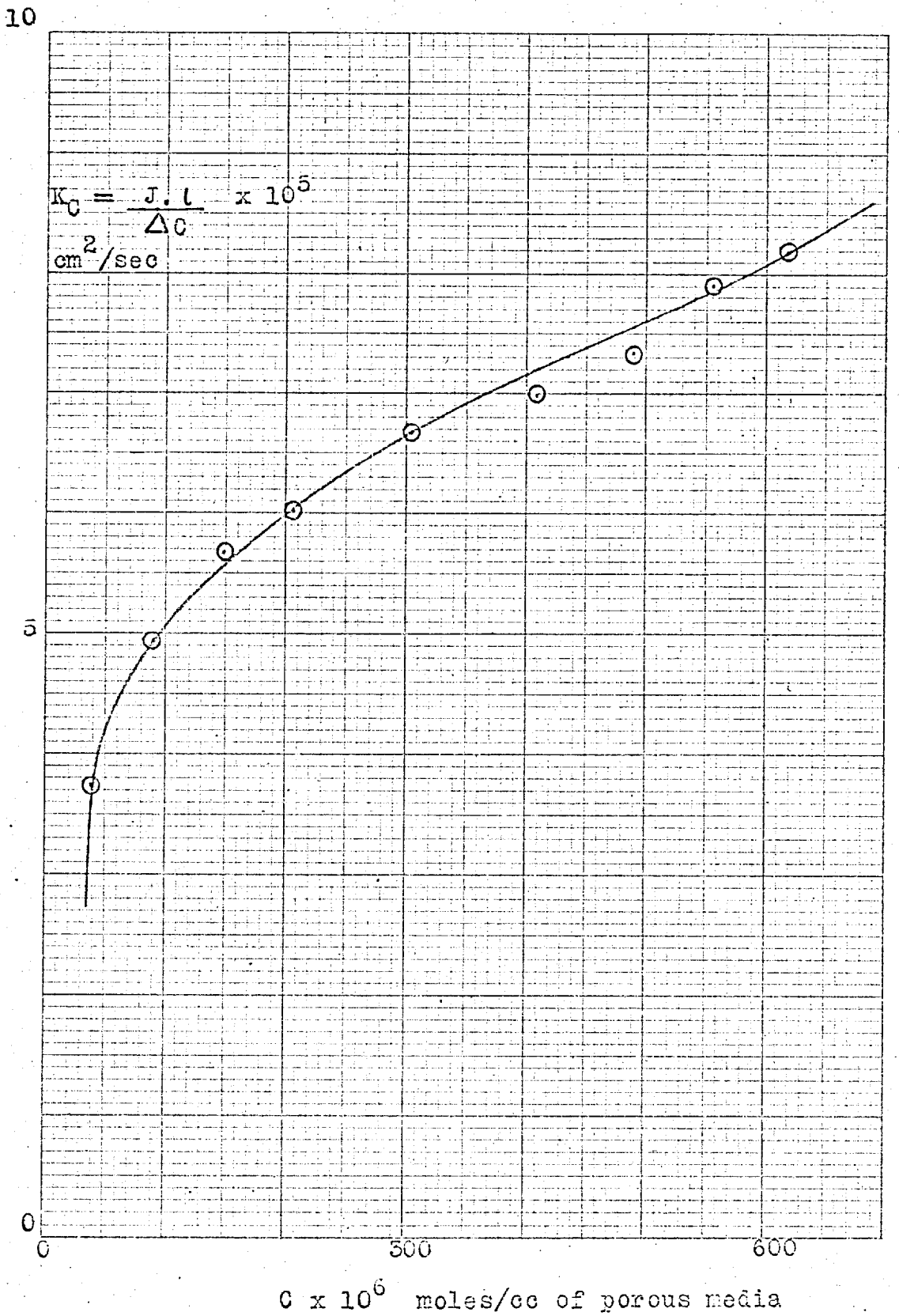

taken at five minute intervals for each experiment. The time-lag for nitrogen was about half an hour in the low pressure region, so initially the time interval between readings was lengthened to half an hour.

4.3.4 Single gas flow of Ammonia through Carbolac I

Permeation experiments for ammonia were performed at 0, - 20, - 30, - 40, and - 50 °C; the results are listed in appendix 6. The time-lags were measured for the 0 °C experiments using the boundary conditions

$$C = 0 \text{ at } x = 0 \text{ for } t = 0$$
$$C = C_o \text{ at } x = 0 \text{ for } t > 0$$
$$C = 0 \text{ at } x = l \text{ for all } t$$

However because the time-lag was so large and tends to increase at lower temperatures, only steady state fluxes were measured for the other temperatures. Even so since each flux should be measured for six to eight times the time-lag each set of experiments would last two to three weeks.

The flux was dominated by the surface flux, and although the gas phase flux J_g could be calculated from the helium experiments the actual gas phase flux was probably much reduced by partial blockage of the membrane by the adsorbed phase. Figures 4.25 to 4.28 illustrate the following variations of flux and permeability with concentration:

$J \cong J_s$	v C_g $(= \varepsilon C_g^g = P.\varepsilon./R.T)$	Figure 4.25
$J \cong J_s$	v $C \cong C_s$	Figure 4.26
K	v C_g	Figure 4.27
K_C	v C	Figure 4.28

The most remarkable feature of these graphs is the drop in flux above an in-going side surface concentration of 2.0×10^{-2} moles per cc of porous media. This drop has not been observed before.

Figure 4.25

J v C_g for Ammonia through Carbolac I at

0, - 20, - 30, - 40, - 50 °C

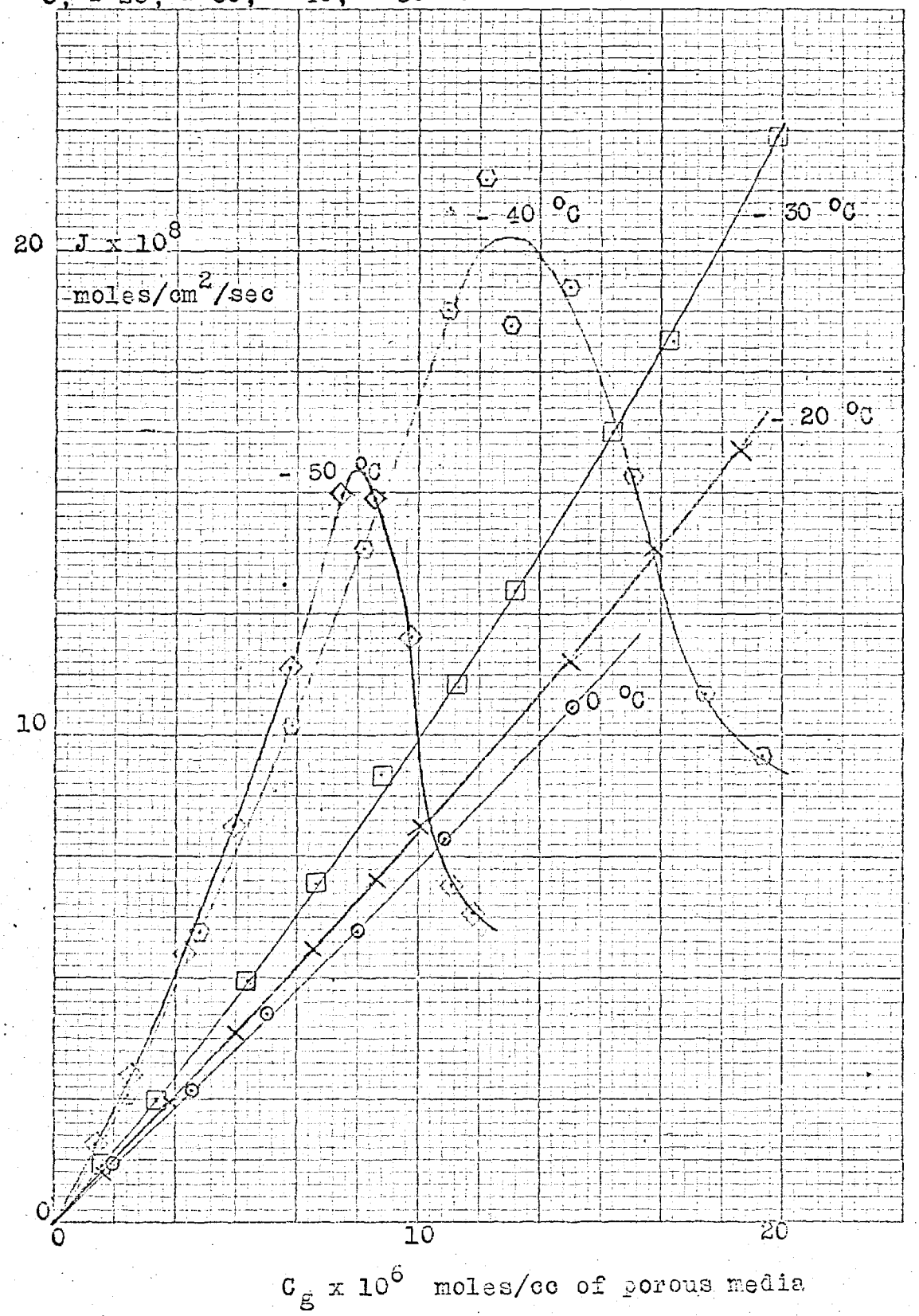

J v C for Ammonia through Carbolac I at

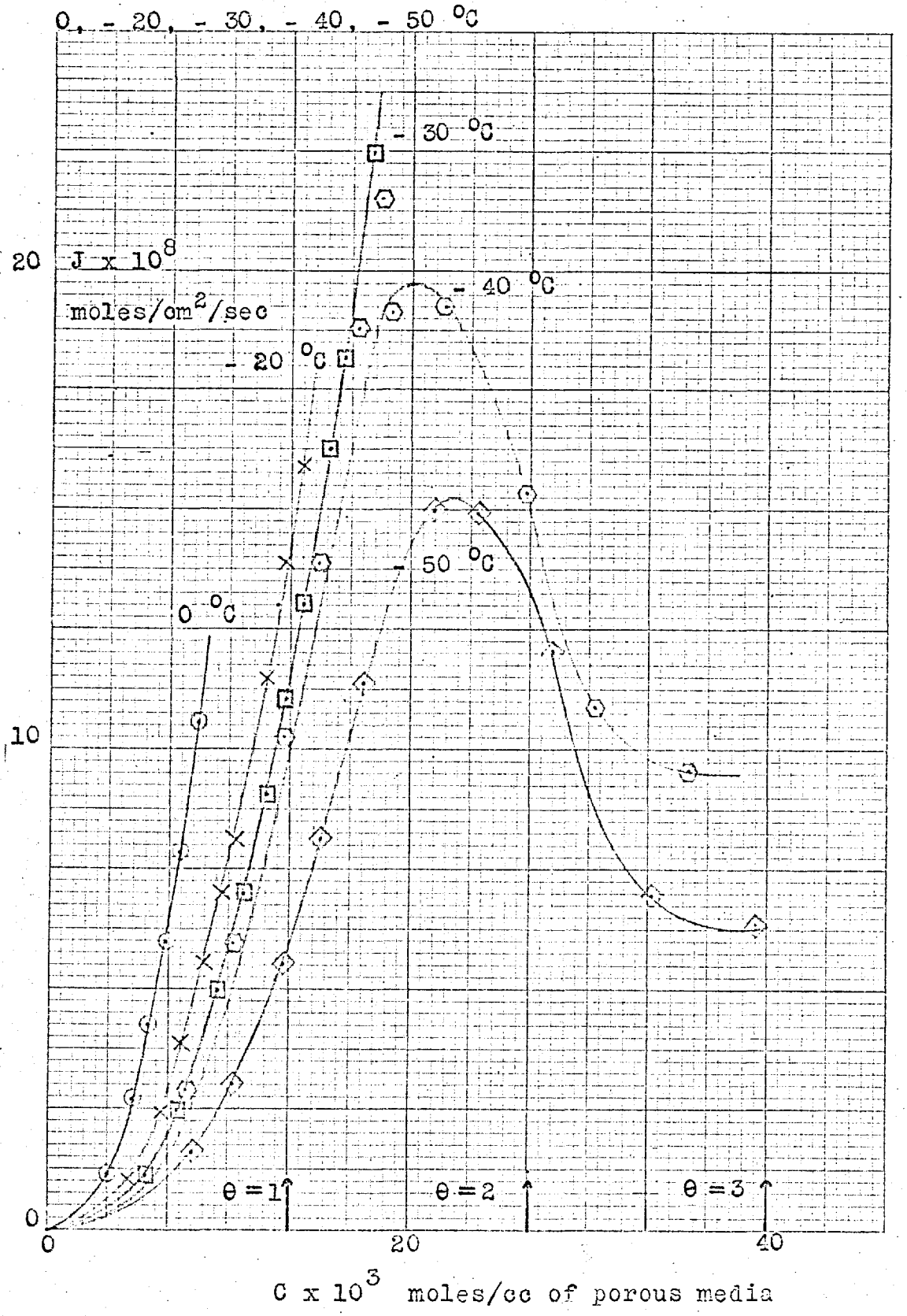

Figure 4.27

K v C_g for Ammonia through Carbolac I at 0, - 20, - 30, - 40, - 50 °C

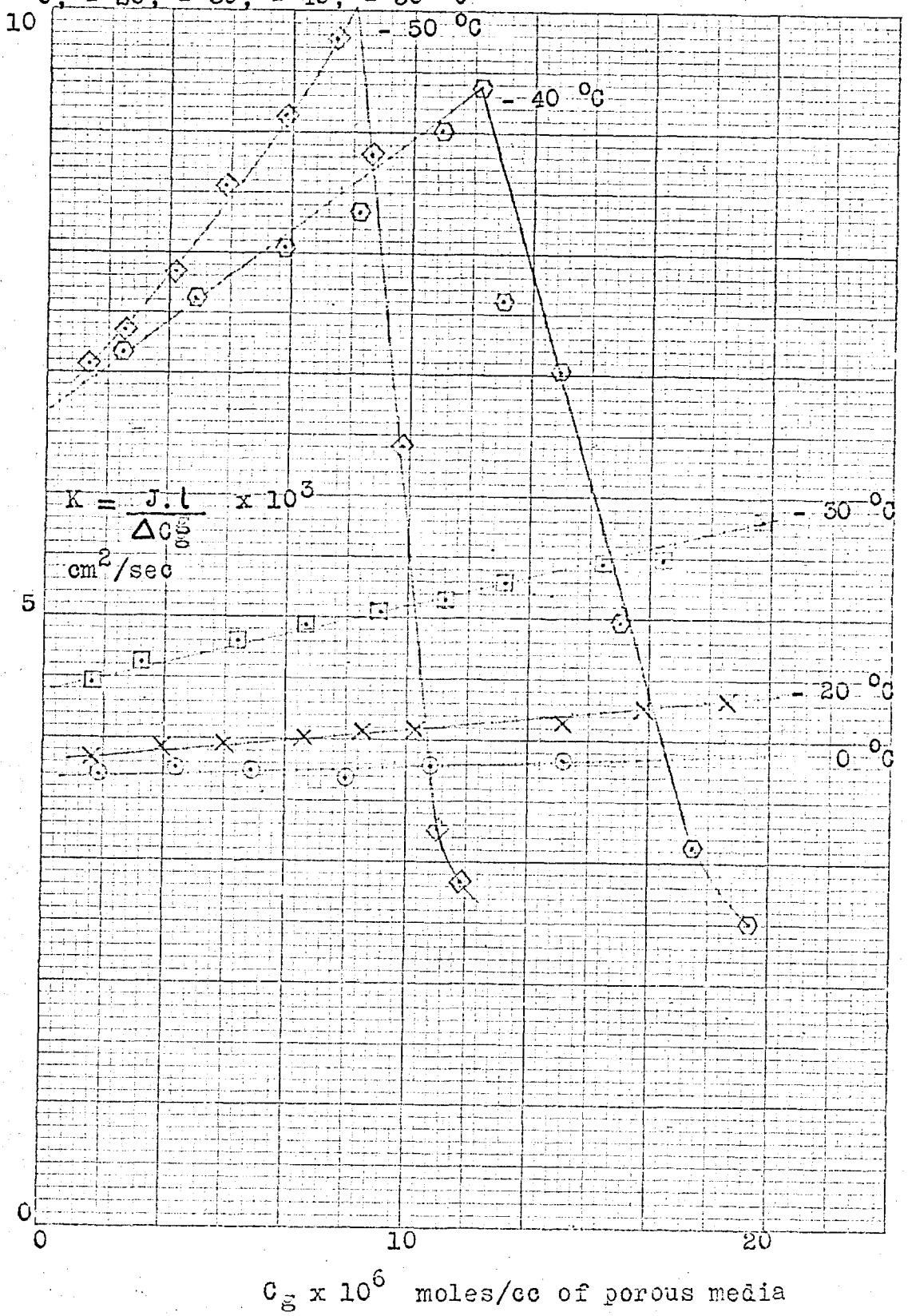

K_C v C for Ammonia through Carbolac I at 0, - 20, - 30, - 40, - 50 °C

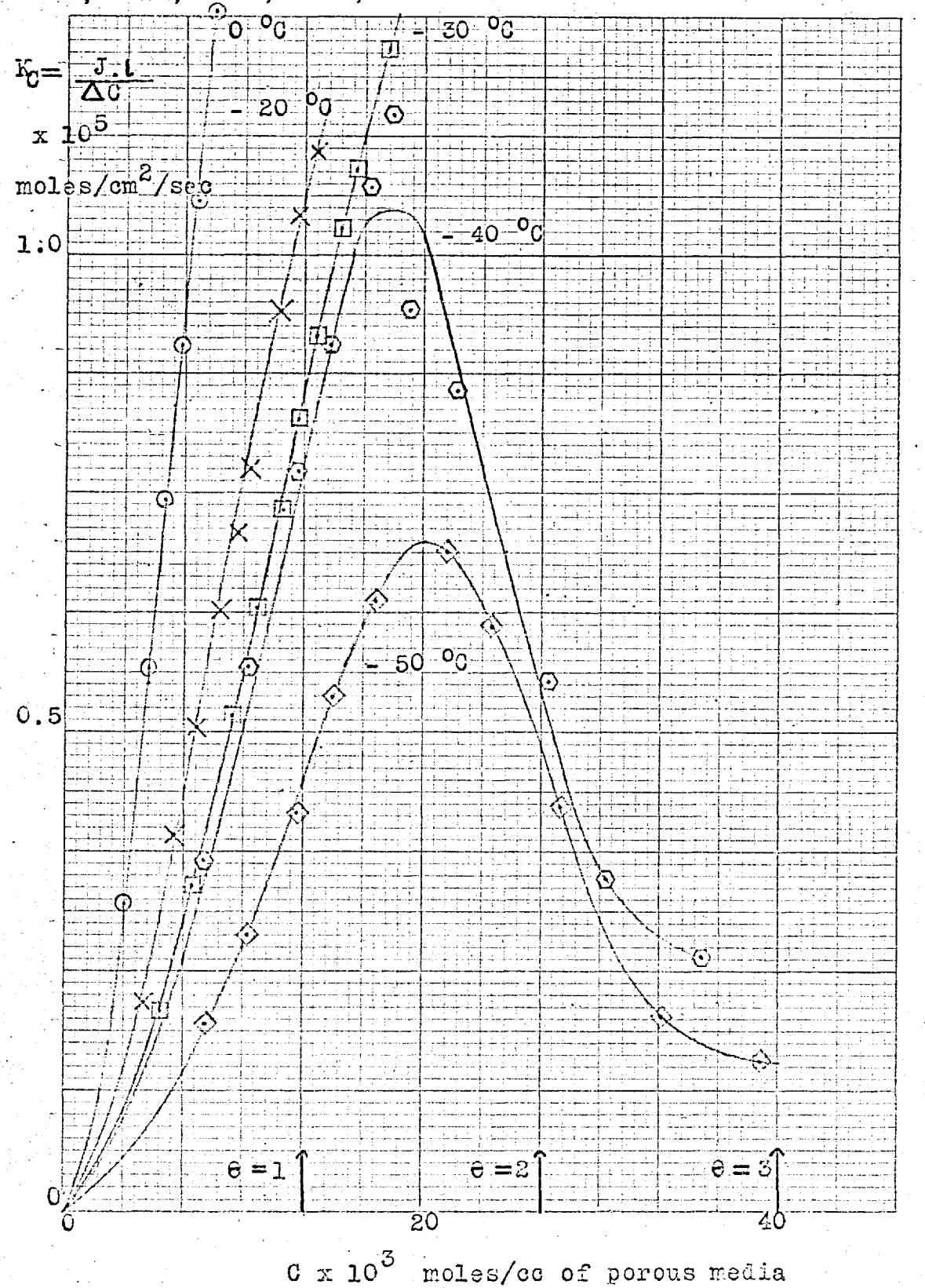

4.4 BINARY GAS FLOW

4.4.1 Flow of Ammonia-Helium, Ammonia-Hydrogen and Ammonia-Nitrogen gas mixtures through Carbolac I

The pressures, fluxes, concentrations, and permeabilities for the total mixture and for each gas in the mixture are listed in appendix 7 for the three mixtures. Two sets of fluxes were calculated for the ammonia mixtures: (a) J_g and J_s where J_g was calculated from the single gas helium results. This would over-estimate the gas phase flux if blockage occurred. (b) $\mathscr{J}_g$ and $\mathscr{J}_s$ where $\mathscr{J}_g$ was calculated from the ammonia-helium results. This would automatically compensate for blockage at the in-going face of the membrane, but would not include any contribution to the gas phase from flux interconversion along the length of the plug. The definitions of section 4.3.3 were used in calculating the permeabilities K and K_c.

In general for each set of experiments the pressure at the in-going face for the non- or weakly sorbing gas was held constant while the pressure of the ammonia, initially at a low value, was increased from run to run by dosing the in-going side with ammonia from the Toepler pump. In the first run of each set it was possible to measure the transient state fluxes. The ammonia time-lag was usually over 30 hours, and initially only helium which had a time-lag of less than a minute would permeate through the plug at a rate only slightly less than that of the single gas value. This initial helium flux is recorded as the .0 run of each set. After about two hours the helium flux would begin to drop, although no ammonia would be detected until the limit of the ammonia time-lag was almost reached. This behaviour of the ammonia is similar to the break-through time, t_1, discussed by Barrer (1954). Apart from this initial flux of each set no other transient state measurements were taken.

J v $P_{i.g.s.}$ for Ammonia through Carbolac I @ 0°C

Comparison between single gas and Helium mixture runs

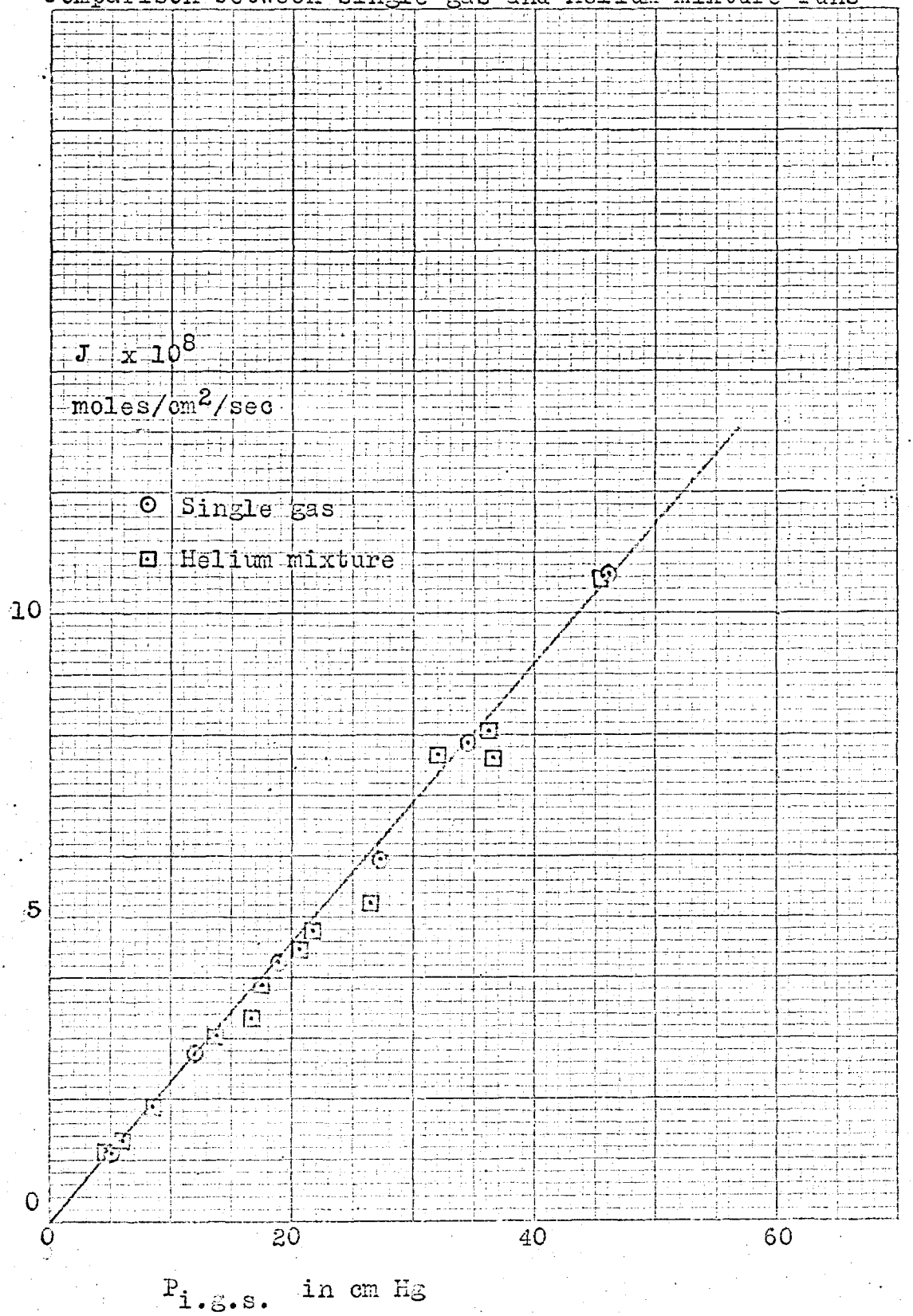

Figure 4.30

J v $P_{i.g.s.}$ for Ammonia through Carbolac I @ - 40 °C

Comparison between single gas and gas mixture runs

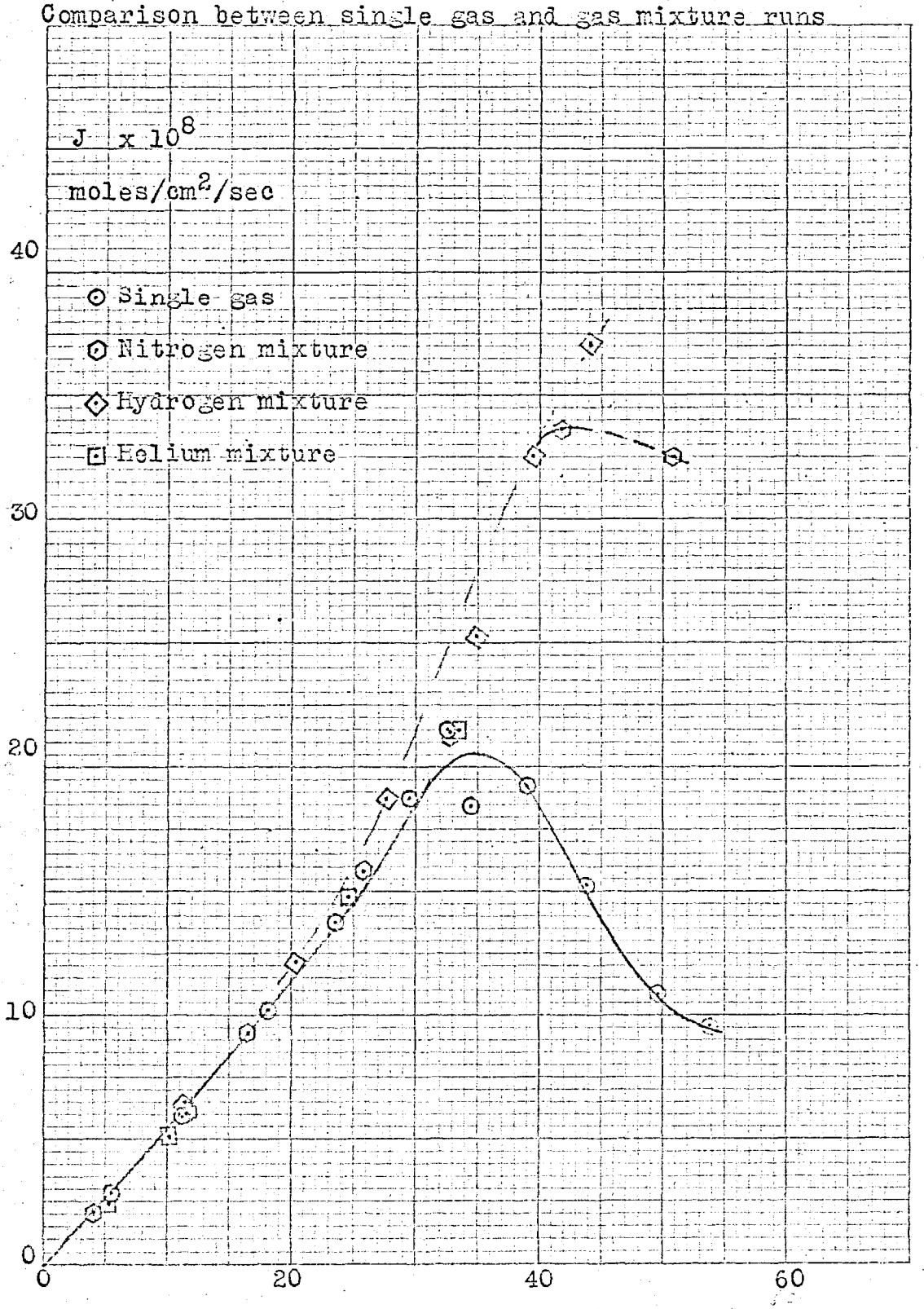

Each set of experiments would require continuous running of the apparatus for several weeks, and so there was a correspondingly high probability of premature curtailment of each set due to thermal strain relief cracks in the glass, leaking taps, or failure of the electricity or water services, before the run using the highest possible ammonia pressure was reached. Consequently the ammonia-helium set at - 40 °C only proceeded as far as the point of maximum flux in the single gas ammonia experiments. However, it was possible to extend the ammonia-hydrogen and ammonia-nitrogen sets past this point.

The ammonia fluxes for the three mixtures and the single gas are recorded in figures 4.29 and 4.30 as functions of the pressure of ammonia at the in-going side. The most significant feature was the monotonic increase in ammonia flux past the point of maximum flux observed in the single gas experiments.

4.4.2 Flow of Nitrogen-Hydrogen gas mixtures through Carbolac I

The nitrogen-hydrogen mixture experiments yielded a very satisfactory set of results considering the novelty of the method. The complete set of experiments was split into two parts. In the first (Nos. 1.1 to 1.7) the nitrogen pressure at the in-going side was kept constant while the in-going side hydrogen pressure was varied from run to run. In the second part (Nos. 1.8 to 1.14) the roles of the two gases were reversed. The analysis gauge was operated with pure nitrogen surrounding the standard thermistor at 5 cm Hg pressure and 25 °C temperature. Since the gauge had a non-linear response with gas composition a calibration graph was drawn up so that percentage composition could be read directly from the

J v C_g at i.g.s for Hydrogen through Carbolac I @ -40 °C

Comparison between single gas and N_2/H_2 mixture runs

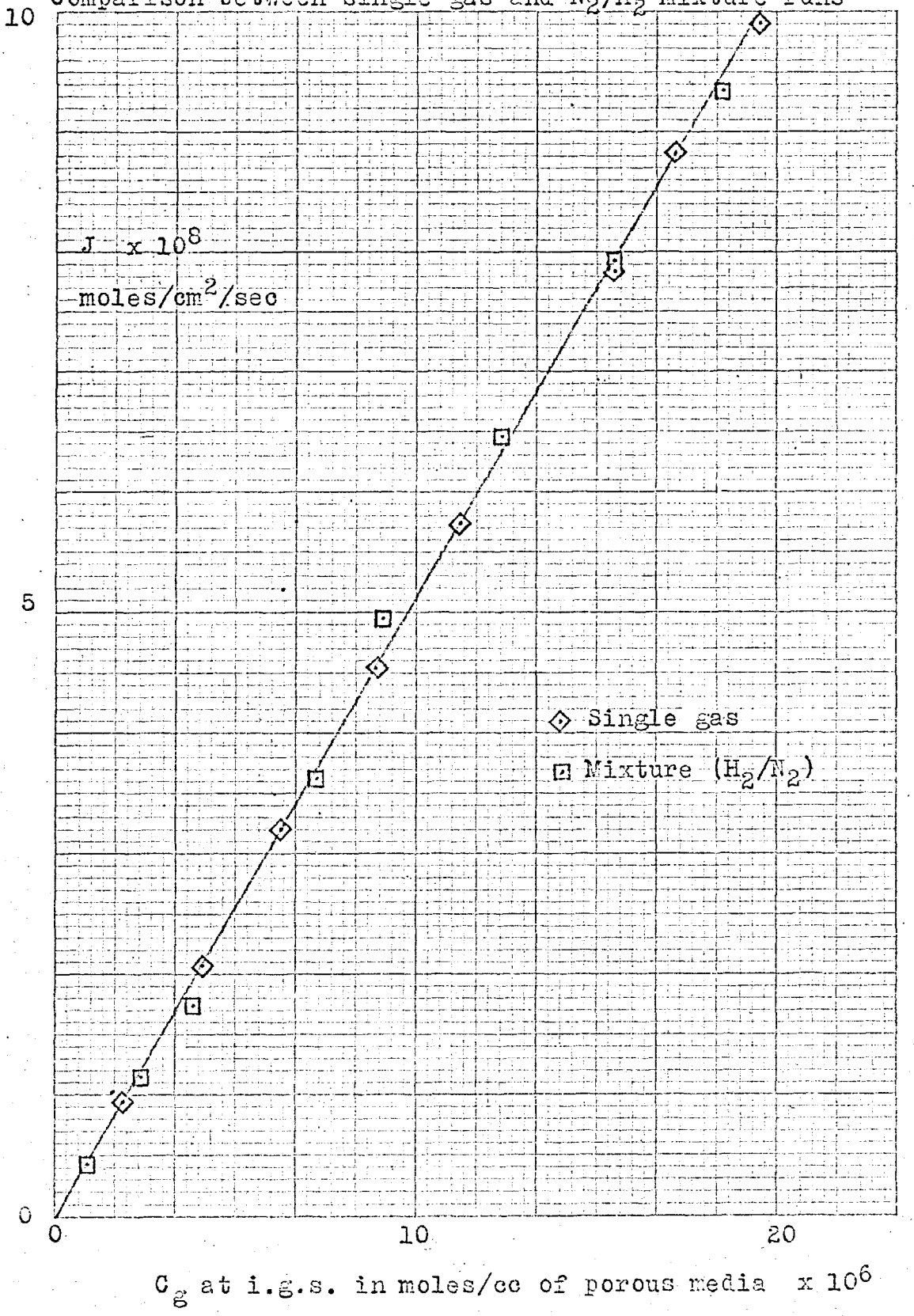

J v C_g at i.g.s for Nitrogen through Carbolac I @ -40 °C

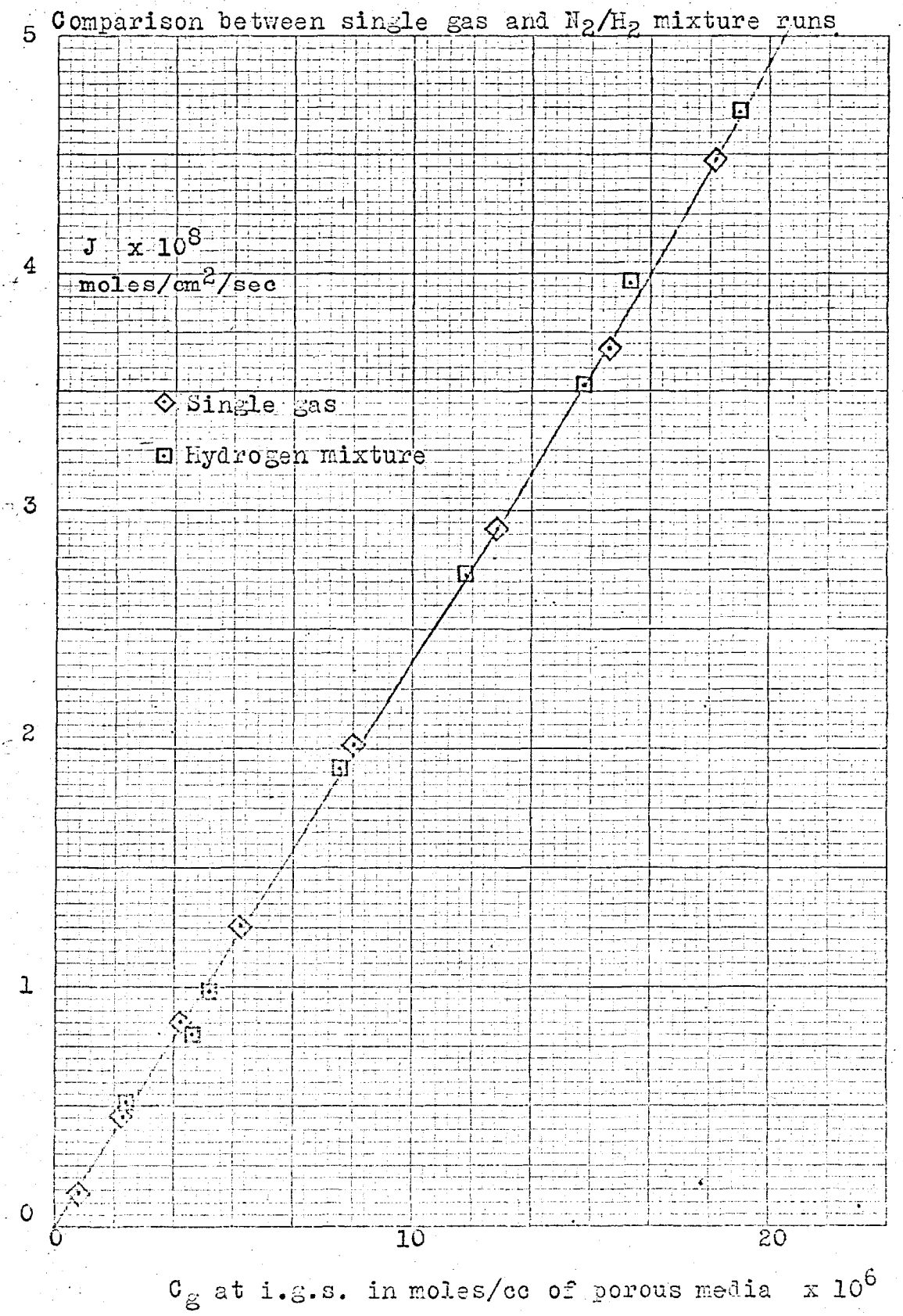

calibration curve. The gauge resistance varied from 1700 Ω for pure nitrogen to 1450 Ω for pure hydrogen. The time-lag for hydrogen was less than a minute but for nitrogen could be as long as 30 minutes, so the period of the experiments was accordingly lengthened in order to measure only steady state flow. It was possible to standardise the method thus allowing the rather excessive computations to be carried out by computer. The program is given in appendix 7 and could serve as the master program for future single or mixed flow work. The computer will process the results regardless of the correctness of the in-put data, and to guard against mis-read or mis-punched data being used in the flux and permeability calculations the out-put was programmed to include the out-going side pressure and time values which could be plotted as a check on the condition of steady state flow and the correctness of the in-put data. The major error lay in analysing the in-going side only once per run, and it would seem preferable in future to include a continuous analysis unit such as a thermal conductivity gauge in the in-going side circulation system.

CHAPTER 5 DISCUSSION OF RESULTS

5.1 THE POROUS MEDIA

5.1.1 Manufacture

Although the basic material used for the porous media was carbon, the diffusion experiments of section 4.2 indicated that the physical structure of the powder and the chemical nature of the surface exercised a certain degree of control over the flow of fluids through the membrane. Therefore it seems important to have as full an understanding as possible about the nature of the material used for preparing the membrane.

The 'Channel' blacks used in this present work were manufactured by burning under-ventilated natural gas from a lava tip burner and allowing the flame to impinge onto a slowly reciprocating steel channel, the deposited carbon being removed by steel scrappers. The initial chemical and physical properties of this type of black depend on the composition of the natural gas, the amount of air admitted, the size and shape of the flame, and the speed of the moving channel. By suitable control of these variables the surface area may be altered from 100 to 500 sq m per g, and the particle size from 10 to 30 mμ. At this stage of production the oxygen content is in the region of 5%. Carbolac I is then further treated by partial burning in air between 400 to 500 °C to increase the oxygen content to approximately 13%. This after-treatment also increases the surface area to 950 sq m per g, (as measured by nitrogen adsorption) producing a very fine pigment of intense jetness and particle size of 9 mμ by electron-microscopy (Smith 1954, and Cabot Technical Data Sheet for Carbon Blacks).

5.1.2 Structure of the Carbon Particle

For oxidised Channel Blacks there is always a discrepancy

Figure 5.1 a

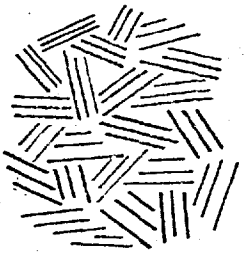

Particle of a small particle size carbon black illustrating random orientation of the crystallites.

Figure 5.1 b

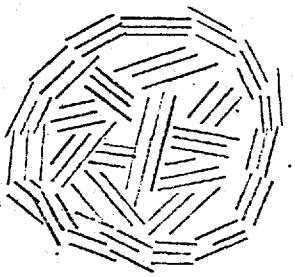

Particle of a large particle size carbon black illustrating regularly orientated outer shell of crystallites with a ramdomly orientated centre.

Figure 5.1 c

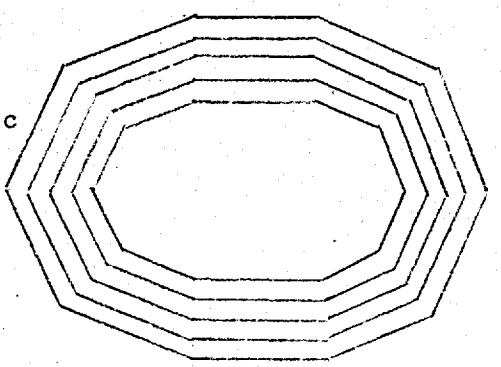

Particle of a completely graphitised black illustrating complete orientation of crystallites.

between the value obtained by electron-microscopy and that obtained by nitrogen adsorption for the surface area and particle size, see table 4.4. This is due to the nitrogen penetrating the internal micro-pores within the individual particles.

X-ray and electron diffraction shows that the basic building block for all Carbon Blacks is a randomly ordered stack of 3 to 5 layer planes made up of hexagonal nets of carbon atoms. These layer planes are roughly parallel and about 20 Å wide and 15 Å high. The crystallite is termed 'turbostatic' because although the layer planes have no specific order of stacking the structure is closer to the crystalline state than the amorphous or glassy state. The crystallites in turn cluster together to form the particles observed under the electron microscope. With the smaller size particle Carbon Blacks such as the Channel Blacks before oxidation, the crystallites are randomly orientated within the particle, as shown diagramatically in figure 5.1 a, but the larger size particle Carbon Blacks which are produced by the Furnace or Thermal processes have a shell of ordered crystallites encapsulating a disordered centre (as shown in figure 5.1 b). Graphitisation of the particles by heating under vacuum up to 3000 °C causes the inner crystallites to migrate to the surface forming a completely ordered shell (Biscoe and Warren 1942), and if the process is allowed to go to completion an empty space is left at the centre, see figure 5.1 c (Hall 1948 and Heckman 1964).

5.1.3 After-treatment Oxidation

The after-treatment oxidation of a Carbon Black is controlled by several variables. It is now known that the ash acts as a catalyst (Snow et al 1959). The nature of

the ash depends on the feed stock and method of manufacture. It could contain a mixture of iron, calcium, magnesium, sodium, silica, or sulphur in different proportions (Smith 1964). In general the higher the ash content the lower the fraction of carbon monoxide formed during burn-off, and the lower the ash content the higher the fraction of combined oxygen and the higher the surface area of the product. The rate of oxidation has also been found to be proportional to the hydrogen content (Snow et al 1960).

Progressive oxidation studies have revealed that the Carbon Black particles do not oxidise from the outside to the inside, but that the point of attack is at a randomly orientated site. For Carbolac I this results in a spongy mass riddled with micro-pores of approximately 10 Å diameter. For the Furnace and Thermal Blacks the oxygen will penetrate the outer ordered shell and burn off the disordered interior leaving behind a hollow sphere (Kollensky and Walker 1960). The graphitised blacks, however, have no disorder at the centre and Harling and Heckman (see Heckman 1964) have shown that in this case the oxidation takes place exclusively from the outside inwards.

5.1.4 Chemical nature of the carbon substrate

The chemical nature of the carbon substrate also influences the quantity and type of surface oxide. The substrate is formed by a continuing process of dehydrogenation,

$$CH_3\text{-}CH_3 \longrightarrow HC\equiv CH + 2H_2$$

aromatisation

$$3C_2H_2 \longrightarrow C_6H_6$$

and polycondensation

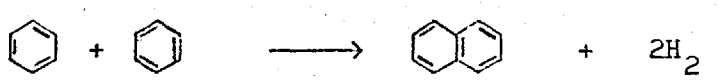

although the neatness of the above reactions is not expected to occur in practice (Thorpe et al 1955, Smith et al 1956).

Continuing pyrolysis will remove the edge hydrogens probably leaving incomplete valence bonds. These polycondensed aromatic rings are Lewis bases and are considered to account for the high pH of oxide free Carbon Blacks rather than possible alkaline ash impurities, for if an oxidised Channel Black, which has an acidic ash and in the oxidised form has a pH of 3, is heated under vacuum to remove all the surface oxide then the pH will rise to $\sim$10 irrespective of the acidic ash (Studebaker 1957, Wiegand 1937, and this is also demonstrated in table 4.4).

The electron donor properties of the Lewis base will be most pronounced in the small ring Carbon Blacks i.e. the Channel Blacks, because increased polycondensation tends to change the aromatic bonds into olefinic bonds and addition reactions will then become predominant (Badger 1954).

Differences in ring size between various Carbon Blacks are clearly demonstrated by Electron Spin Resonance Spectroscopy. In general the g value (which is a measure of the break down of the coupling of the orbital and electronic spin momenta of the electrons within the solid) remains near the value for a localised free electron with Channel Blacks. This is particularly true for Carbolac I, indicating that the crystallites in Channel Blacks are composed of small polycondensed layers turbostatically stacked. Increased polycondensation and crystallinity due to variations in the method of manufacture or by graphitisation, will allow the free electron to delocalise causing a rise in the g value up to the limiting value for an ideal fine grained polycrystalline graphite. This rise was reported by Arnold (1967).

5.1.5 The surface oxide

Because the radical nature and quantity of the surface oxide is so dependent on the method of production, the following discussion will be limited to the surface oxide on Carbolac I. Even here our knowledge is far from complete and interpretation open to debate.

Reported percentage ultimate analyses for Carbolac I vary as may be seen from table 5.1

Table 5.1 Ultimate analysis of Carbolac I

	(a)	(b)
Carbon %	85.81	-
Hydrogen %	1.46	0.56
Oxygen direct %	9.84	-
Oxygen by subtraction % (Excluding water)	12.58	11.63

(a) de Bruin et al (1964), (b) Studebaker (1956), (1957) and (1963).

Due to the method of manufacture we may consider that most of the oxygen and hydrogen is at the surface. Anderson et al (1952) examined this surface complex of the very similar Channel Black known as Black Pearls I, by decomposition under vacuum, the results are listed in table 5.2

From the table we may conclude that the complex is chemically bonded to the surface, and that only water and the physically adsorbed gases are removed under normal out-gassing conditions (200 ^{o}C).

To estimate the stoichiometry of the complex we may consider the carbon to lie on the surface of a cubic box the outside total surface area being 950 sq m g^{-1}. The carbon layer is made up from carbon atoms each of which occupies

Table 5.2 Products from the thermal decomposition of Black Pearls I

Temperature range °C	cc of gas at N.T.P. evolved per g			
	H_2	CO	CO_2	H_2O
25 - 300	0.0	0.2	1.32	2.3
300 - 600	0.32	25.9	4.88	3.35
600 - 900	5.42	78.40	3.60	0.15
900 - 1200	30.6	1.95	0.05	0.05

Total volatile content is $\sim$ 16% (Cabot data sheet)

a cube of side 'd' and solid density 2.12 g cc^{-1} since this is the absolute density of Carbolac I (Barrer and Strachan 1955).

Therefore

Volume of each atomic cube is $d^3 = \frac{12}{2.12 \times N}$ cc

Side of each atomic cube is $d = \sqrt[3]{\frac{12}{2.12 \times N}}$ cm

$= 2.13 \times 10^{-8}$ cm

Side of box is $= \sqrt{\frac{950 \times 12}{6}}$ m/mole

$= 4359.0$ cm/mole

No. of atoms per side of box covered with a mole of carbon $= \frac{4359.0}{2.13 \times 10^{-8}}$

$= 2.045 \times 10^{11}$

No. of atoms per area of box covered with a mole of carbon $= (2.045 \times 10^{11})^2 \times 6$

$= 2.5 \times 10^{23}$

so the atomic ratio of surface carbon to internal carbon is

2.5 : 3.5

Consequently the percentage surface carbon in Carbolac I is 35.7% and the atomic ratio of surface carbon to hydrogen to oxygen is

4 : 1½ : 1

C : H : O

Although only a qualitative calculation, it does indicate that most of the surface may be considered as a surface oxide complex.

The chemical nature of the surface oxide is uncertain; it probably contains a high proportion of acidic groups since a water slurry of Carbolac I has a pH of 3 (Cabot data sheet). Several workers, Studebaker (1956) (1957) (1963) Anderson (1952) Rivin (1962) Puri (1964 a b c) (1966 a b) Donnet (1964) Boehm et al (1964), reported a range of functional groups on the surface from experiments using specific organic analytical techniques. In interpreting their results they had to assume that there was no interference from other functional groups and that the surface does not adsorb the reagents irrespective of the surface oxide. An alternative method is to use infra-red spectroscopy. The disadvantages with this method are the low concentration of functional groups producing a poor signal to noise ratio, extensive scattering by the solid, unknown group interactions occuring, and the presence of several functional groups in different environments causing peak broadening. It is thus difficult to assign any band to a specific type of compound, although a quantitative estimation of the main type of group present is possible. The following conclusions were drawn from the infra-red spectra reported in section 4.1.4.

5.1.6 Infra-red spectra of Carbolac I

An unexpected result was the shift in frequency of the absorption peaks on changing from the Nujol mulled to the Fluorolube mulled and free powder sample. The energy involved for each shift will be

$$\Delta E = h.c.(v_1 - v_2)$$

where ΔE is the energy in calories, h is Planck's constant, c the velocity of light, and v the wave number. So applying the relevant conversion factors

ΔE = 2.86 x (v_1 - v_2) cals per mole.
= 51 cals per mole for the 1600 cm^{-1} band
= 180 cals per mole for the 1700 cm^{-1} band

These shifts are energetically small, and assuming that the bands are associated with surface groups, they are probably due to a change of environment at the surface by adsorption of the mulling oil. Such adsorption could interfere with the bond stretching modes resulting in an increase in the required energy and hence observed frequency. Similar shifts have been observed in the spectra for resorcinol using crystalline, melt and slurry samples but the shifts appear to be specific to certain peaks (Price and Tetlow 1948). The effect is also a recognised hazard when comparing the infra-red spectra of materials adsorbed on a surface using free powder, mulled or potassium bromide pressed disc samples (Hair 1967). On this basis assignment of the bands should be made from the spectra of the free powder rather than the spectra of the mulled powder.

The weak absorption peak at 1703 cm^{-1} (free powder) is in the accepted region for the carbonyl group $-C\overset{O-}{=O}$ of carboxylic acids (Bellamy page 162), and this would account for Carbolac I having a pH of 3. Fujii (1967) reached a similar conclusion for air oxidised coals whose oxygen content varied directly with the intensity of the absorption peak at 1705 cm^{-1} and with the amount of potassium hydroxide required for neutralisation. The equivalent band for the Nujol mulled sample, 1766 cm^{-1}, is in a similar position to that found by Lygin et al (1960) for oxidised Ukta Channel Black mulled in light petrolatum, 1750 cm^{-1}, and by Garten et al (1957) for Carbolac I mulled in Nujol, 1760 cm^{-1}. Since these bands lie in the accepted region for lactones (Bellamy page 179) the above workers have suggested that the band was due to γ or δ lactones.

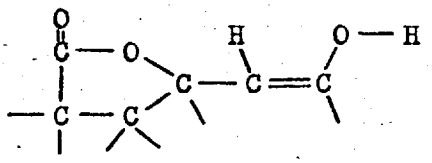

γ lactone

However the position of the free powder band is well outside the lactone region and so the acid carbonyl grouping is to be preferred.

Again taking into account the shift when using mulled samples, the strong band found at 1579 cm^{-1} (free powder) is similar to that found by Garten et al (1957) Lygin et al (1960) Brown (1955). It has been variously described as being due to either a γ diketone or a conjugated aromatic bond.

Conjugate chelation of γ diketones is known to lower the carbonyl stretching frequency to 1600 cm^{-1} (Bellamy 1958, Fujii 1966).

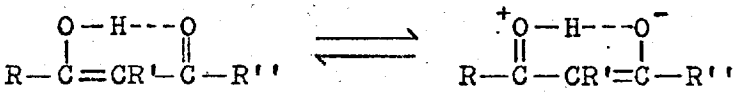

and if the conjugation is destroyed by removing the hydrogen bond with either alkali or diazomethane:

$$XOH + CH_2N_2 \longrightarrow XOCH_3 + N_2$$

then the peak will shift to the normal carbonyl stretching frequency. This shift has been found using mulled samples for the spectra and cited as proof of structure, Garten et al (1957) Lygin et al (1960) Hallum et al (1958). However the peak for the free powder is well below the experimental and theoretically expected frequency for γ diketones. In addition diazomethane reacts with any active hydrogen such as phenolic, carboxylic, aldehydic, and in some cases alcoholic (Elucidation of Structures by physical and chemical Means, part i, volume XI, page 456), and so almost any conjugation associated with the group responsible for the absorption peak at 1579 cm^{-1} could be destroyed by diazomethane. The frequency of the free

powder sample is in the middle of the aromatic $-C=C-$ stretching band region, Colthrup (1950). This band is normally of only medium intensity but conjugation with a carbonyl or unsaturated group attached directly to the aromatic ring turns it into a very prominent band (Bellamy, page 72). Destruction of the conjugation by diazomethane would cause the observed reduction in peak intensity and the appearance of a new band. Garten et al (1957) found that on heating samples of Carbolac I the band at ~ 1750 cm^{-1} disappeared at 600 °C but that the intensity of the band at 1600 cm^{-1} had not yet appreciably diminished. This may be due to the 1750 cm^{-1} band being associated with a removable surface complex, while the 1600 cm^{-1} band is connected with the carbon substrate. This argument is further supported from the values for the frequency shifts. The 1700 cm^{-1} band shift is energetically the larger of the two possibly because the band is for a surface group capable of interaction with the mulling oil, whereas the group responsible for the 1600 cm^{-1} is on the carbon substrate and not so readily accessible for interactions which cause frequency shifts. The weight of the evidence suggests that the 1600 cm^{-1} band is from an aromatic $-C=C-$ bond.

5.1.7 Physical nature of the surface

In section 2.1.3 and 4 it was pointed out that the surface of many porous membranes is broken up by blind pores, cracks, and crevices, and that the surface flux negotiates these obstacles by evaporative flights across the interruptions. An expression was obtained for the fraction X of the length of the membrane for which the flux J_s (as measured by the helium method) had joined the gas phase.

$$D'_{ss} = \frac{D_{ss}}{(1 - X) - (J_s/J_g)X} \qquad 2.29$$

The value of X is a measure of the degree of discontinuity of the surface. Equation 2.29 is limited to the Henry law region of adsorption, and there is not enough data from the present work available for determining X. However Clint (1966) studied the flow of hydrogen, neon, and argon in the Henry law region of adsorption for a membrane very similar to the one reported here, the membranes are compared below

Table 5.3 Comparison of Carbolac I membranes

	Lowson	Clint
Material	Carbolac I	Carbolac I
Out-gassing temp. ^{o}C	200	200
Porosity	0.528	0.484
He permeability as $K.(M/T)^{\frac{1}{2}}$	1.69×10^{-4}	1.11×10^{-4}

Using Clint's results equation 2.29 was solved for trial values of X. The results are listed in table 5.4

Table 5.4 Analysis of surface roughness

	Hydrogen			Neon			Argon		
X	D'_{ss}	E^*	$E^*/\Delta E''$	D'_{ss}	E^*	$E^*/\Delta E''$	D'_{ss}	E^*	$E^*/\Delta E''$
0.0	+	+790	0.55	+	+770	0.52	+	+1880	0.66
0.1	+	+910	0.64	+	+755	0.51	+	+1450	0.51
0.2	+	+700	0.49	+	+710	0.48	+	+1040	0.36
0.3	+	+730	0.51	+	+680	0.46	+	+ 0	0.0
0.4	+	+365	0.25	+	+655	0.45	-	-	-
0.5	+	+256	0.18	+	+520	0.35	-	-	-
0.6	+	-	-	+	+340	0.23	-	-	-
0.7	+	-	-	+	+164	0.11	-	-	-
0.8	-	-	-	+	-	-	-	-	-
0.9	-	-	-	-	-	-	-	-	-

The best fit for X fulfilling the conditions attached to equation 2.29 is $X \cong 0.4$. This suggests that the surface is fairly broken in character.

5.1.8 Pore size distribution

An accurate description of the size and distribution of the capillaries within the plug is almost impossible. As a qualitative guide we may estimate the average radius from the value for the hydraulic radius to be 11.5 Å using equation 2.3 (Emmett and de Witt 1943), but this yields no information about the pore size distribution. Initially we may say that the plug was made from 90 Å diameter particles. The smallest capillary will be the entrance to a close packed interstice.

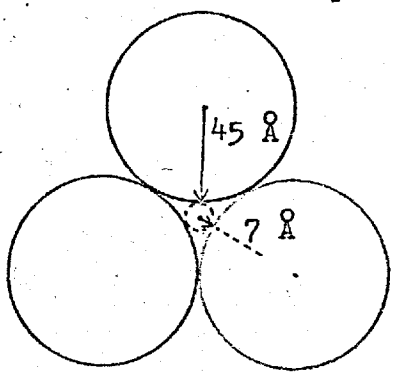

Figure 5.1

This will allow up to 14 Å wide particles to pass through the port (the diameter of a nitrogen molecule in the adsorbed state is 4.3 Å, Barret et al 1951). However if fine powder particles are packed into the interstitial spaces then there will be a number of much smaller capillaries (Wise 1952). Thus from particle packing considerations alone we can say that there will be capillaries of radii much greater than the mean of 11.5 Å and also much less than the mean value. This has not taken into account the internal micro-pores within the particles that were formed by the after-treatment oxidation. From plots of thickness or 't' of the adsorbed film against the amount adsorbed, as in figure 4.4, de Boer

(1964, 1965) concluded from the nitrogen adsorption isotherm at liquid nitrogen temperature on the free powder of Carbolac I, that the width of these internal micro-pores varies from 7 to 15 Å. 't' plots require the assumption that the adsorbate has the properties of the bulk liquid, but there is now evidence to suggest that for the pores below 18 Å wide the bulk liquid properties of the adsorbate cease to apply (Harris 1967). This seems particularly pertinent to a 7 Å wide hole into which only one nitrogen molecule can possibly fit. Estimations for the capillary radius have been made using the desorption branch of an isotherm showing hysteresis and the Kelvin equation

$$\ln \frac{P}{P_o} = - \frac{2.\gamma.V.\cos \theta_w}{r.R.T} \qquad 5.1$$

where γ is the surface tension and θ_w the angle of wetting (Gregg and Sing 1967). However when one considers a meniscus of molecular dimensions the meaning of surface tension and angle of wetting, which are macro-scale phenomena, tends to disappear (Pierce et al 1948). Finally the particles may be crushed during the preparation of the membrane resulting in the formation of smaller internal micro-pores in the membrane than occur in the free powder. When all these possible effects are taken into account it is clear that no exact description of the membrane capillaries is possible.

5.1.9 Heterogeneity of the membrane

Any heterogeneity along the length of the membrane introduces an x dependency into the diffusion coefficient D. This may be evidenced by differences between the experimental time-lag, L, and the calculated time-lag, L_1, which is calculated from the steady state flow results assuming D is a constant or a function of C only. Ash, Baker and Barrer (1968)

considered the case where the heterogeneity is introduced by the compaction process, the surfaces of each increment being compressed more than the centre. They showed that for a membrane fabricated in only one increment there was a considerable difference between the time-lag L_1 calculated for D independent of x and the calculated time-lag L_1' which assumed that D had the functional form with x of

$$D = D_o/[1 - (\alpha'.x/l)(1 - x/l)]$$

α' being a coefficient. This function is in accord with the compaction process in that D is less near x = 0 and x = l than in the middle of the increment. However when the membrane is prepared by compacting the powder in a series of increments, then the diffusion coefficient should vary in a periodic manner with x, and it was demonstrated that this tended to minimise the value $(L_1' - L)/L_1'$ as the number of increments was increased. It was concluded that the macroscopic heterogeneity brought about by compaction was effectively smoothed out when at least three similar increments were used to prepare the membrane.

5.1.10 Summary of the discussion on the porous media

The porous medium is basically an alkaline carbon the surface of which is almost completely covered by an acidic oxide. The surface is thermally stable up to 200 °C, but may be susceptible to chemical attack resulting in changes in the surface flow properties of the membrane. There is a wide range of pores, the pore radii varying from molecular dimensions to 50 Å but the mean being around 12 Å radius. Since the plug was fabricated in three increments we may consider that on the macro-scale the membrane is effectively homogeneous along its length.

5.2 THE ADSORPTION ISOTHERMS

The 'raison d'etre' for the adsorption isotherm measurements was to allow the total concentrations to be determined for the flow experiments, rather than forming a complete study within themselves. However the measurements do provide additional information about the porous media, and as discussed in section 2.1.6 provide an independent check for the correctness for the formulation of the flow equations.

5.2.1 The low temperature Nitrogen isotherm

For a material such as Carbolac I the use of the B.E.T. equation for calculating the surface area from the nitrogen adsorption isotherm at liquid nitrogen temperatures has only limited validity. The B.E.T. equation was developed for a geometrically smooth, and energetically homogeneous surface, and from the previous discussion of section 5.1 this is clearly not the case here. Young and Crowell (1962) discussed the extension of the B.E.T. theory to multilayer adsorption on heterogeneous surfaces and concluded that since the model was already inadequate for the homogeneous surface, any flexibility of the isotherm equation brought about by such extensions to the heterogeneous surface must be thought of as being chiefly due to the use of extra parameters. The exceptionally high surface area of Carbolac I is probably due to adsorption in the micropores, which will tend to make the material selective to different sized molecules. The contribution of the micropore surface area to the total surface area may be estimated from a 'de Boer thickness' plot. The thickness of an adsorbed layer of nitrogen at liquid nitrogen temperature is obtained from equation 5.2

$$'t' = 3.54\ (v/v_m) \qquad 5.2$$

where 't' is the thickness of the adsorbed layer in $\mathring{A}$, v the

amount adsorbed in cc at N.T.P. g^{-1}, v_m the monolayer capacity also in cc at N.T.P. g^{-1} and 3.45 is a numerical constant which includes the value for the effective adsorbing area of the nitrogen molecule. In a series of papers de Boer et al (1964 a b, 1965 a b c, 1966) showed that for several well-selected samples of aluminium hydroxides and oxides, and graphitised carbons, which had no micropore characteristics, the multi-molecular layer of adsorbed nitrogen was freely formed on all parts of the surface and the statistical thickness was practically independent of the nature of the sample. This resulted in the plot of 't' versus P/P_o forming a universal curve for all the adsorbents which contained no micropores. However for the microporous adsorbents the nitrogen would adsorb on to the adsorbent according to equation 5.2 and in the process fill up the micropores. Once the micropores were full the effective adsorbing area was reduced to that of the external surface of the adsorbent with a corresponding drop in the monolayer capacity v_m. If the thickness 't' is determined from the universal curve, then a plot of v versus 't' will show a break and change of slope at the point at which the micropores become saturated with adsorbate. Sharp breaks in the graph have been found for samples of boehmite which have clearly defined narrow distributions of micropore dimensions. The slope of the 't' plot will be $v_m/3.54$, and this allows us to calculate the surface area before and after filling the micropores. The 't' plot for Carbolac I, figure 4.4, was curved. This indicates that there is a fairly wide distribution of micropore sizes. The total surface area A_t was calculated from the initial slope, and it compares very favourably with the value, A, found from the B.E.T. equation, see table 5.5. The final slope yielded a value, A_f, for the surface area of 440 sq m g^{-1}. de Boer measured the nitrogen isotherm on free

Table 5.5 Surface areas of Carbolac I in sq m g^{-1}

A	A_t	A_f	A_w	A_{em}	A_n
960	975	440	280	264	680

powder Carbolac I up to much higher relative pressures and obtained a value for the final surface area, A_w, of 280 sq m g^{-1}. This value compares favourably with the geometrical surface area calculated from the measurement of particle diameters with the electron microscope, A_{em}, and it appears that the remaining surface area represents only the external surface of the carbon particles. From table 5.5, and using de Boer's value for the external surface area, the surface area of the micropores is given by

$$A_n = A - A_w = 680 \text{ sq m } g^{-1} \qquad 5.3$$

so the micropores make the greater contribution to the total surface area.

de Boer calculated the volume V_n' of a micropore of surface area A_n' that is ~~is~~ filled at the statistical thickness t' as

$$V_n' = A_n'.t' \qquad 5.4$$

To calculate the volume of the micropores of Carbolac I the range of micropore radii was divided into 1 Å steps. The surface area was then obtained from the slope of the 't' plot for each value of the radius, and the corresponding micropore volume calculated using equation 5.4. The total volume was obtained by summing over the complete range of radii. Since the calculation was not considered to be exact and the 't' plot was a fairly smooth curve, ~~so~~ the surface area for each radius step was simply taken as the corresponding step for the change in surface area from total surface to external surface. The results are listed in table 5.6

Table 5.6 Micropore volume of Carbolac I

t' in Å	A_t sq m g^{-1}	A'_n sq m g^{-1}	V'_n cc g^{-1} x 10^2
0 - 3	960	0	0
3	860	100	3
4	760	100	4
5	660	100	5
6	560	100	6
7	460	100	7
8	360	100	8
9	260	100	9

$$\sum V'_n = 0.42 \text{ cc } g^{-1}$$

The density of the membrane is 1.0 g cc^{-1} so the void volume is 0.528 cc g^{-1} of porous media, comparing this value with the value for the volume of the micropores it appears that most of the void volume is associated with the internal micropores. The value for $\sum V_n$ is probably higher than the true value for two reasons. The first is concerned with the geometry of a micropore. Equation 5.4 is effectively treating the micropore as a rolled up sheet of thickness 't'. The volume of the sheet is calulated with the sheet laid out flat since 't' is a statistical thickness calculated for a flat surface. Now it is assumed that when the sheet is rolled up no deformation occurs to the inside surface. This is certainly not true for pores of radii below ~ 3 times the thickness of the sheet, the circumference of the inner surface being very much smaller than the circumference of the outer surface. This is diagramatically illustrated in figure 5.2.

Figure 5.2

A filled micropore of molecular dimensions comparing the inner and outer circumferences

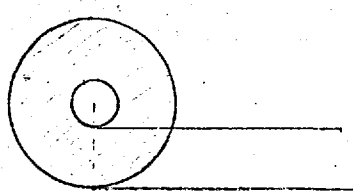

The second source of error is in the choice of the value for the adsorbing area of the nitrogen molecule. de Boer assumed that the adsorbate had a closed packed structure on the surface, this leads to a value of 16.27 $\AA^2$ for the adsorbing area of nitrogen. However this figure was arrived at from macroscopic measurements divided by the Avogadro number. The result is perfectly acceptable for nitrogen adsorbing on to a smooth flat surface where it will act as a liquid with macroscopic liquid properties. But macroscopic measurements do not necessarily apply to microscopic dimensions. This is particularly true for molecular packing in micropores because while factors due to bad packing at the walls of a macroscopic box are negligibly small when calculating the volume of a close packed system in a macroscopic box, distorted packing may be the predominant form in a microscopic box. Under these conditions the physical value of a statistical thickness is lost.

A more detailed analysis of the packing within micropores produced some surprising results which do not apply to flat surfaces. The problem was simplified to the two dimensional case of packing spherical molecules into circular capillaries as shown in figure 5.3. The adsorbing molecule of radius a lies against the wall of a micropore capillary of radius r. However the molecule effectively occupies the truncated segment w,x,y,z which forms part of a ring of outer radius r and inner radius (r - 2a). This ring represents the monolayer so the number of molecules in the monolayer is

$$\frac{\text{Area of ring}}{\text{Area of truncated segment}}$$

The area of the ring is $= \pi.r^2 - \pi.(r - 2.a)^2$

$$\pi.(4.r.a - 4.a^2) \qquad 5.5$$

Area of truncated segment $= 2.\pi.r^2.\frac{\alpha}{360} - 2.\pi.(r - 2.a)^2.\frac{\alpha}{360}$

Figure 5.3

Molecular packing in circular micro-pore capillaries

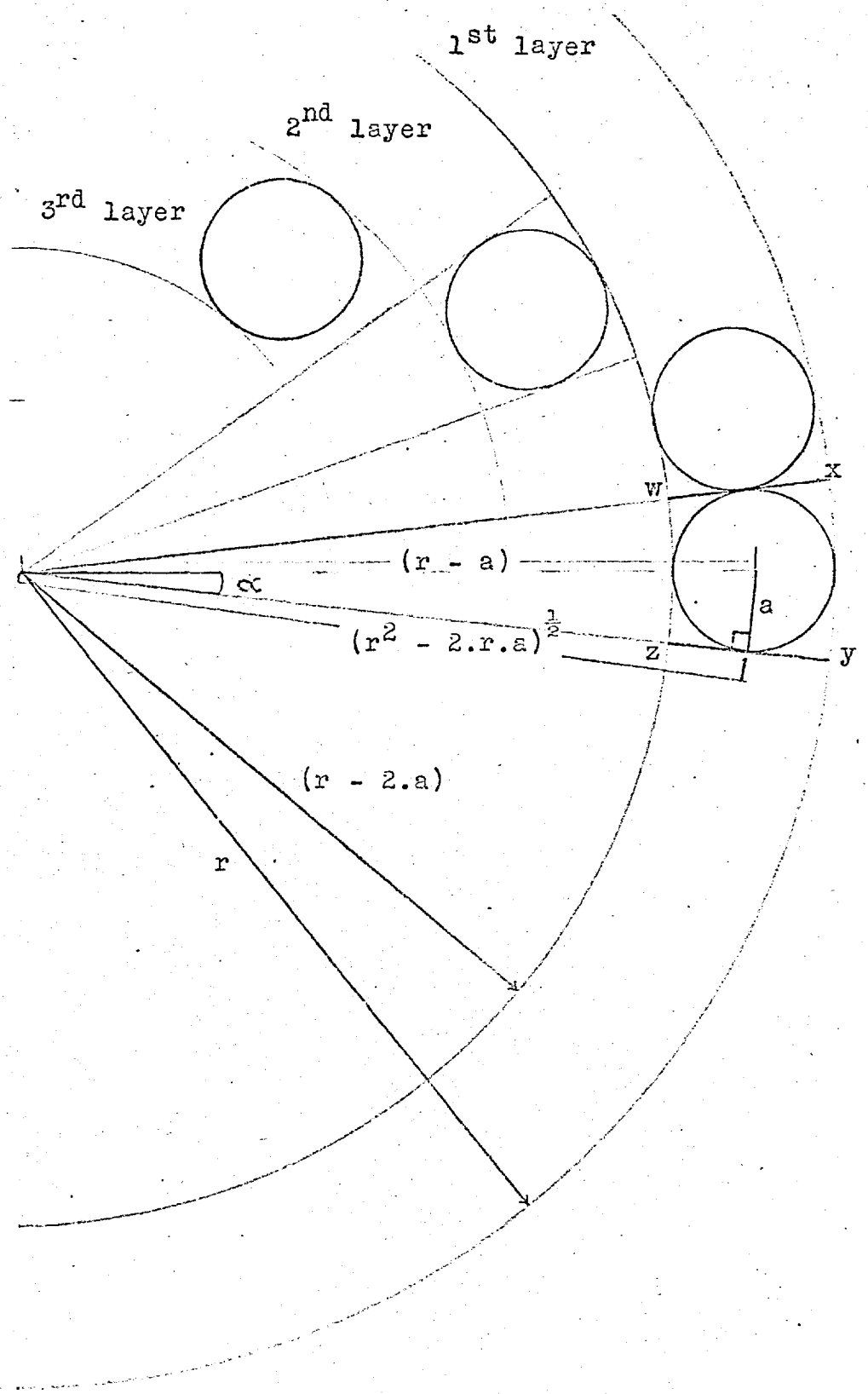

Figure 5.4

Variation of monolayer capacity of a filled micropore with capillary diameter for a 3.4 Å diameter molecule

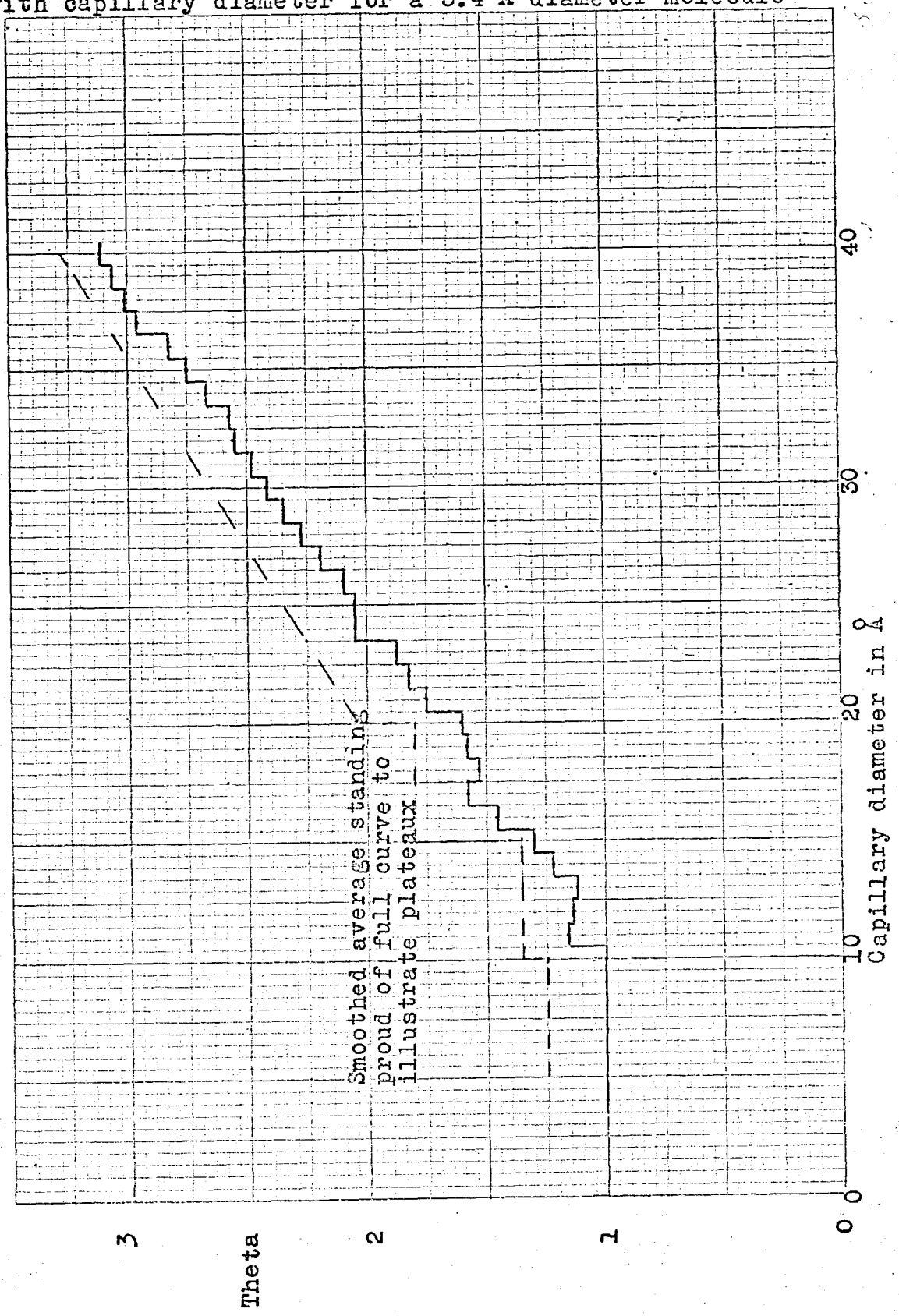

$$\text{Area of truncated segment} = 2.\pi.\frac{\alpha}{360}.(4.r.a - 4.a)^2 \qquad 5.6$$

$$\text{Tan } \alpha = \frac{a}{\sqrt{(r^2 - 2.r.a)}} \qquad 5.7$$

$$\text{Number of molecules in layer} = \frac{180}{\text{Tan}^{-1}\left[\frac{a}{\sqrt{(r^2 - 2.r.a)}}\right]} \qquad 5.8$$

α was expressed in terms of tangent because $\text{Tan}^{-1}\alpha$ is the only inverse angle function readily available in computer processing.

The number of molecules in the second layer will be found by replacing r by (r - 2.a) in equation 5.8, and so on for each successive layer until (r - n.a) < 0 . Using equation 5.8 a computer program was written to calculate the number of molecules in each layer, the degree of filling in terms of the fractional monolayer capacity θ, and the total number of molecules in the full micropore. The micropore diameter was ranged from 4 to 50 Å in 1 Å steps, and the molecular diameter from 2 to 5 Å in 0.2 Å steps. The program is given in appendix 1, together with the results for a molecular diameter of 3.4 Å. This is the diameter of an ammonia molecule, Pauling (1960) page 134. Figure 5.4 is a graph taken from these results for θ versus the diameter of the micropore. The broken curve standing proud of the full curve by 0.25θ is the smoothed out average of the results. The computer program is not a complete analysis of all possible situations, for instance it does not consider the example of figure 5.5, however it does indicate that there are sudden jumps in the range of filled micropores as the fraction of the monolayer capacity is increased. The position of the plateaux was surprisingly insensitive to the size of the molecule, the shifts to higher micropore diameters being fairly small as the molecular size was increased. The results do show the marked difference between the capacity of the first

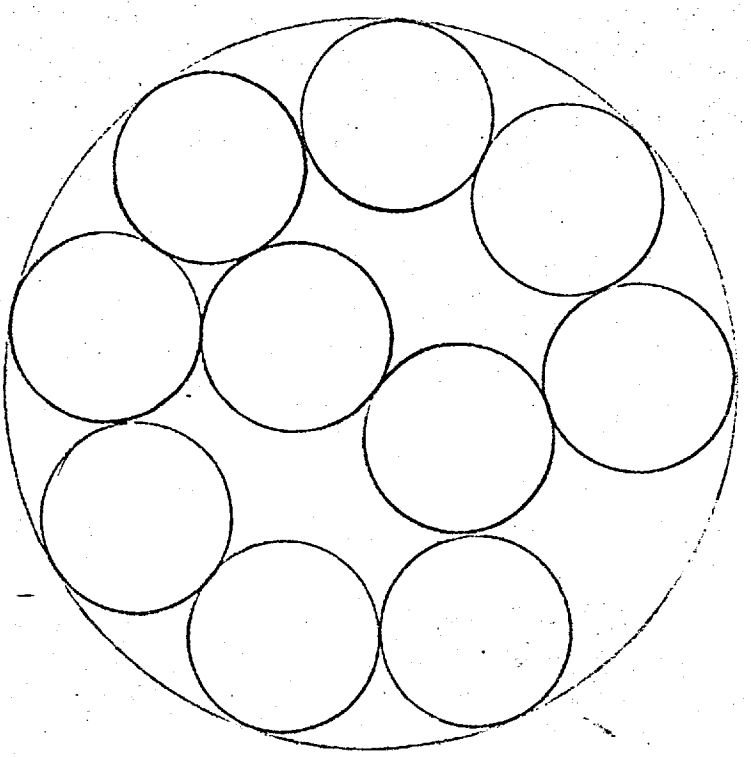

Figure 5.5
Example of packing in a micropore capillary

and second layer of a filled micropore, and it can be readily verified from a small number of test drawings that a similar situation arises if the circular micropore is replaced by a square or triangular sectioned micropore. Figure 5.5 is also an example of the lose packing that is more likely to occur in micropore capillaries. Such packing may appreciably affect the average value for the adsorbing area of the adsorbate molecule.

5.2.2 Room temperature Nitrogen, Hydrogen and Deuterium adsorption isotherms on Carbolac I

Both the hydrogen and deuterium adsorption isotherms were in the Henry law range of adsorption. From section 2.2.2 the limiting heat of adsorption in the Henry law region was defined as

$$\text{"}\Delta H\text{"} = R.T^2.\frac{d\ \ln(v/P)}{dT} = \frac{\Delta\bar{H}}{\left[1 - \bar{V}_s/\bar{V}_g\right]} = -q_{st} \qquad 2.70$$

To evaluate this limiting heat of adsorption for the slightly curved nitrogen adsorption isotherms, the isosteric heat was calculated for a range of surface coverage as out-lined in section 2.2.3 and extrapolated back to zero coverage. The graph of q_{st} versus coverage is shown in figure 5.6 together with the limiting value of q_{st} for hydrogen and deuterium. The slight decrease in q_{st} for nitrogen towards lower coverages is most likely experimental error and the average value of 5.5 Kcals/mole was taken as the value for "ΔH" of nitrogen at zero coverage. Dacey (1961) studied the adsorption of hydrogen and deuterium over the temperature range 0 to - 100 °C on Saran charcoal (prepared by sintering polyvinylidene chloride up to 750 °C in vacuo; it has a surface area of $\sim$600 sq m g^{-1}). As in the present work he found that the adsorption isotherms were linear, and the uptakes for the two gases practically identical. Dacey's values for the heat of adsorption are compared with the author's and Clint's in table 5.7

Table 5.7 Heats of adsorption as Kcals per mole

	Author Carbolac I	Clint Carbolac I	Dacey Saran
Ne	-	2.08	1.65
H_2	1.95	2.10	2.35
D_2	1.95	-	2.40
Ar	-	3.49	4.90
CH_4	-	3.48	5.90
N_2	5.50	-	-

The energy for adsorption in the Henry law region was defined as

$$\text{"}\Delta E\text{"} = -R.T^2.\frac{d \ln k_s}{dT} = \frac{\Delta\tilde{H}}{\left[1 - \tilde{V}_s/\tilde{V}_g\right]} \qquad 2.71$$

Isosteric Heats for Nitrogen on Carbolac I between 0 and - 40 °C

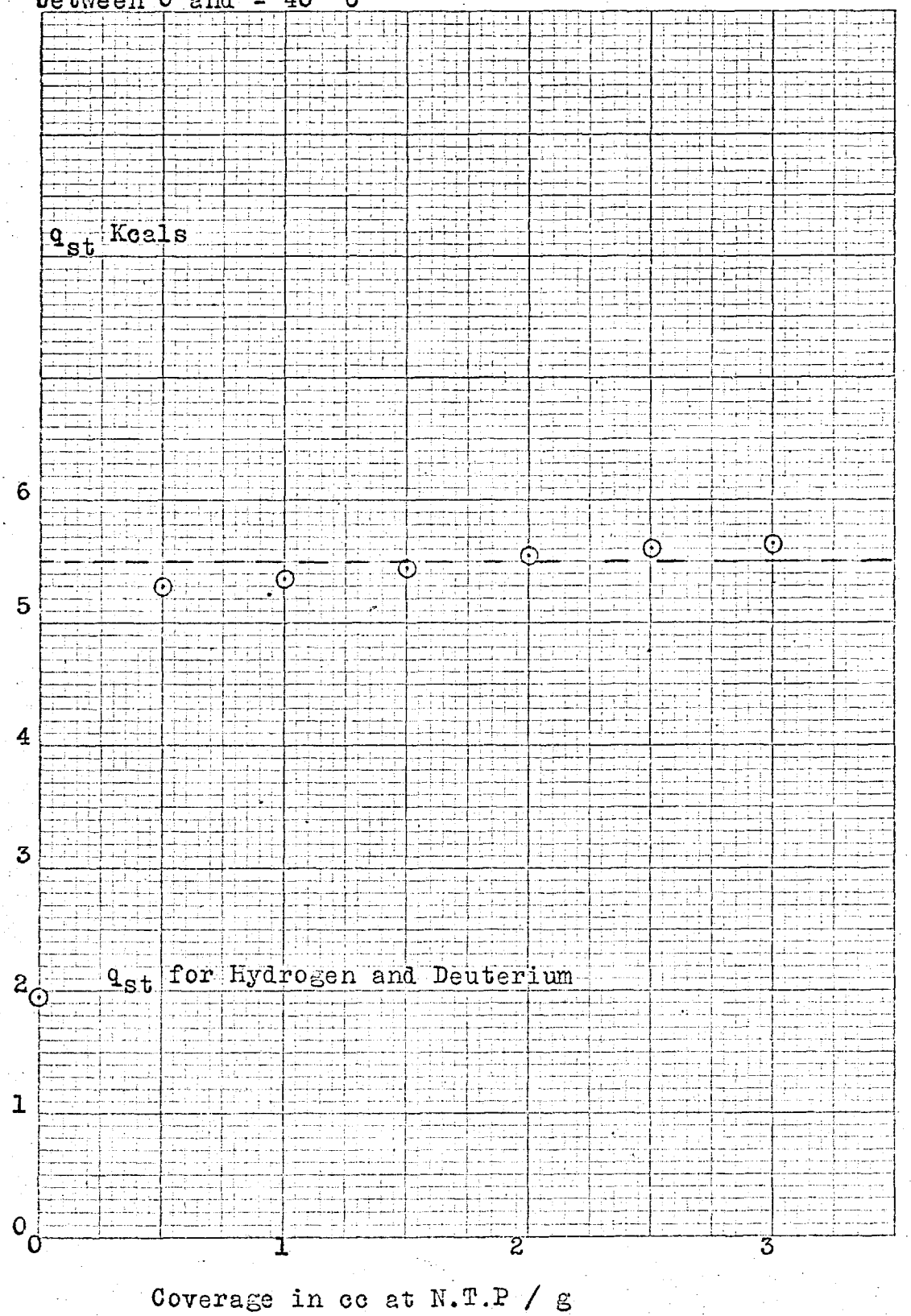

For nitrogen "ΔE" was evaluated from equation 2.72

$$\text{"}\Delta E\text{"} = -(q_{st})_{v=0} + RT \qquad 2.72$$

The justification of the use of this equation was out-lined by Clint (1966). Using a mean value of temperature for the nitrogen and Dacey's results, the values of "ΔE" are listed in table 5.8 together with the values calculated by Kiselev (1965 a b) for adsorption at an exterior basal plane of graphite.

Table 5.6 Energies of adsorption as Kcals per mole

	Author Carbolac I	Clint Carbolac I	Dacey Saran	Kiselev Theoretical
H_2	1.43	1.43	1.91	1.11
D_2	1.43	-	1.96	1.18
N_2	4.97	-	-	2.01

Agreement is not really expected between the experimental and theoretical results for the following reasons.

(i) The quantity experimentally determined is $\Delta\tilde{H}/(1 - \tilde{V}_s/\tilde{V}_g)$. If we define the volume of the adsorbed phase as the volume within one molecular diameter σ_m of the surface, then after some algebraic manipulation the ratio of the molar volumes is given by equation 5.9 (Clint 1966)

$$\frac{\tilde{V}_s}{\tilde{V}_g} = \frac{\sigma_m}{k_s + \sigma_m} \qquad 5.9$$

For hydrogen at - 40 °C this term is quite significant , the value for $\tilde{V}_s/\tilde{V}_g$ being 0.118 ($\sigma_m = 1.5 \times 10^{-8}$ cm). This corrects the author's and Clint's value of "ΔE" to 1.27 Kcals per mole.

(ii) The surfaces of both Carbolac I and Saran charcoal are energetically heterogeneous, so in this region adsorption

will be predominantly at the high energy sites rather than at the low energy graphite basal face.

(iii) Much of the adsorption will be in the micropores. de Boer and Custers (1934) showed that as a molecule becomes more encapsulated by the surrounding walls of the adsorbent then the energy of interaction increases. In the limiting case a sorbed molecule in a spherical shell of adsorbent has 8 times the energy of interaction for a sorbed molecule on a plane surface. Although this extreme example would not occur in the present work, a small contribution from enhanced capillary wall interaction is to be expected.

Since Kiselev's theoretical results compare well with the experimental results of Constabaris et al (1961) who used a graphitised carbon black P33 (2700°) which is considered to have a homogeneous surface, we may conclude that Carbolac I has an enhanced heat of adsorption at low coverage due to the molar volume of the adsorbate having a significant value, the surface being energetically heterogeneous, and the microporous character of the solid.

5.2.3 Low temperature Hydrogen and Deuterium adsorption isotherms on Carbolac I

The most significant difference between the room temperature and low temperature adsorption isotherms for these two gases was the marked increase of deuterium sorption to hydrogen at 77 and 90 °K. This effect was first reported by Barrer and Rideal (1935) who used a sugar charcoal, and more recently by Pace and Siebert (1959) for Graphon, Freeman (1960) for sugar charcoal SU-60, and Constabaris et al (1961) for the graphitised carbon black P33 (2700°). There is also a corresponding higher value for the isosteric heat of deuterium. The difference in q_{st} is independent of coverage and lies about the mean value of

80 cals per mole. This change in q_{st} with isotopic species is hard to detect from the room temperature adsorption isotherms because of the limited number of experiments. A slight difference in choice of slope for the graph $\log_{10}(v/P)$ versus 1/T would easily account for the 80 cals per mole as exampled by the discrepancy between the author's and Clint's values for q_{st} of hydrogen using the same sample of adsorbent. A difference of 50 cals per mole was also predicted from Kiselev's theoretical calculations. The difference in uptake may be explained from several points of view.

(i) Zero point energy

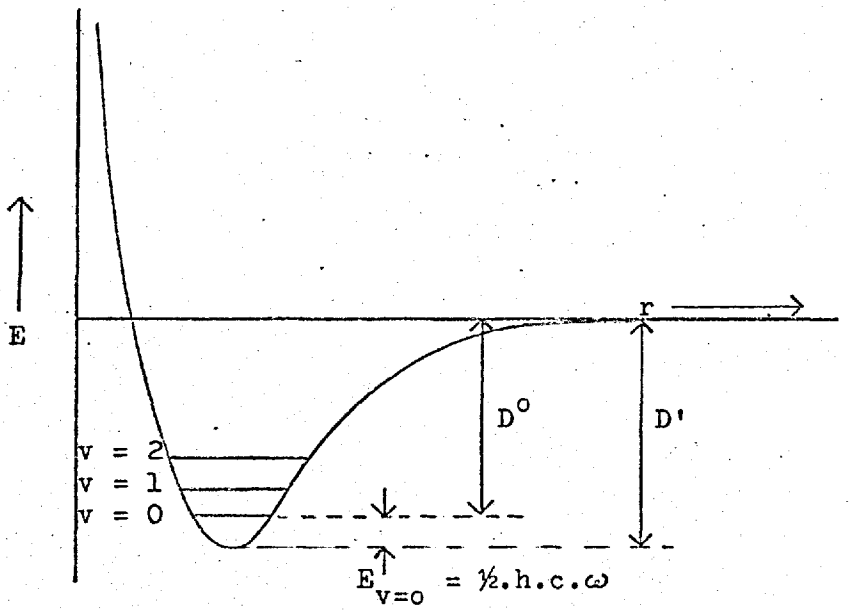

Figure 5.7 Potential energy curve for a gas approaching and adsorbing on to a solid

Figure 5.7 illustrates the common potential energy curve for hydrogen and deuterium approaching and adsorbing on to a surface. As the molecule approaches the adsorbed state it will redistribute its energy according to its new degrees of freedom, and this will include a quantised vibrational state

between the molecule and the surface. The zero point energy for this vibrational mode is expressed by the usual equation

$$E_{v=o} = \tfrac{1}{2}.h.c.\omega = \tfrac{1}{2}.h.(k/\mu)^{\frac{1}{2}} \qquad 5.10$$

where $E_{v=o}$ is the zero point energy, h is Planck's constant, c the velocity of light, ω is the fundamental vibration frequency in wave numbers, k the force constant for the vibrational mode and is constant between isotopic species, and μ is the reduced mass of the nuclei associated with the vibrational mode. Assuming that the gases are adsorbing on to the basal face of graphite then

$$\mu_{H-C} = \frac{12 \times 1}{12 + 1} = \frac{12}{13}$$

$$\mu_{D-C} = \frac{12 \times 2}{12 + 2} = \frac{12}{7}$$

and the marked increase of the reduced mass of the D-C bond will cause a decrease in vibrational zero point energy of that bond. There is then of necessity an increase in the corresponding thermal dissociation energy D^o since

$$D^o = D' - E_{v=o} \qquad 5.11$$

where D' is the spectroscopic dissociation energy. Pace and Siebert (1959) evaluated the potential energy curve for hydrogen and deuterium adsorbing on to a graphite surface basing their calculations on Barrer's original approach (1937). They obtained the following values,

$$D' = 1020 \text{ cal per mole}$$

for H_2 $E_{v=o}$ = 200 cal per mole D^o = 820 cal per mole

for D_2 $E_{v=o}$ = 140 cal per mole D^o = 880 cal per mole

so as found in practice less energy is required to desorb hydrogen than deuterium. The assumption that adsorption is occurring on the basal face of graphite is only required for the quantitative calculations, it does not affect the qualitative argument. Irrespective of the depth of the

potential energy curve which will vary according to adsorption site, there will be a mass effect between isotopic species. An interesting consequence of this approach is that for an adsorbent containing two or more elements it may be possible to detect preferential adsorption on a particular element; for by the mass effect there will be a change in $(q_{st(H_2)} - q_{st(D_2)})$ when sorption saturation of a particular element causes the adsorption to shift to a new element of the adsorbent. Although such an effect may be occurring on the oxide surface of Carbolac I, the surface is unfortunately too heterogeneous to make any firm conclusions.

(ii) ortho-para isomers

An alternative explanation may be found in the preferential adsorption of either the ortho or para isomers of the two isotopes. These isomers arise from the nuclear spin of hydrogen and deuterium. On theoretical grounds only certain combinations of molecular rotation and nuclear spin are allowed (Herzberg, Spectra of diatomic Molecules, p 133). This results in each molecular rotation having the specific nuclear spin listed in table 5.7

Table 5.7 Nuclear spin states of Hydrogen and Deuterium

Hydrogen						
Rotational quantum number J	0	1	2	3	4	5
Allowed nuclear spin	para	ortho	para	ortho	para	ortho
Orientation	↑↓	↑↑	↑↓	↑↑	↑↓	↑↑
Deuterium						
Allowed nuclear spin	ortho	para	ortho	para	ortho	para
Orientation	↑↑	↑↓	↑↑	↑↓	↑↑	↑↓

In addition a selection rule forbids the transition $J \pm 1$.

So transitions from ortho to para spin states cannot occur resulting in the formation of isomers of different nuclear spin. These isomers may be identified by their different thermal and optical properties. Providing conversion can take place by chemical means, only para hydrogen and ortho deuterium will exist at the absolute zero of temperature. At higher temperatures and once again providing conversion by chemical means can take place there will be a Boltzman distribution between the rotational states, each level having a statistical weighting according to the degeneracy of the rotational and nuclear spin quantum numbers.

Table 5.8 Ortho-para ratios of hydrogen and deuterium

	H_2		D_2	
Temperature ^{o}K	%ortho	%para	%ortho	%para
0	-	100	100	-
77.4	50	50	70.3	29.7
90.2	57.5	42.5	68.6	31.4
room temp.	75	25	66.7	33.3

Data taken from Farkas, Light and Heavy Hydrogen (1935)

Conversion by other than chemical means though not impossible is statistically improbable. The combined effects of the nuclear magnetic moment interacting with the magnetic moment of the rotating molecule, and nuclear interchange by gas collision have a half-lifetime of 3 years for an ortho-para transition (Farkas, page 13). Consequently if an equilibrium mixture is cooled or heated to a new temperature the mixture will retain its original isomer composition. Conversion of a non-equilibrium mixture to its equilibrium composition is possible by several means (Farkas, page 60), and the method of

heterogeneous catalysis is very pertinent to the present work. Bonhoeffer and Harteck (1929), and Rummel (1933), showed that charcoal was an efficient catalyst for ortho-para conversion at low temperatures but not at room temperature, whilst the converse is found for platinum black. For conversion on charcoals at low temperatures the half-lifetime becomes independent of pressure above 1 cm Hg and the absolute amount of gas converted is proportional to the isomer concentration in the adsorbed layer

$$\frac{dc_t}{dt} = k.c_t \qquad 5.12$$

where (dc_t/dt) is the rate of reaction, k the rate constant and c_t the ~~initial~~ concentration, so the reaction is first order. At pressures below 1 cm Hg the half-lifetime decreases indicating that initial adsorption occurs on those parts of the surface that have high catalytic activity. Because the reaction is first order the conversion involves isolated hydrogen molecules, and rules out such reactions as that between atomic and molecular hydrogen

$$H + p\text{-}H_2 \longrightarrow o\text{-}H_2 + H \quad \text{order } \frac{3}{2}$$

or molecular collision in the liquid or solid phase

$$o\text{-}H_2 + o\text{-}H_2 \longrightarrow p\text{-}H_2 + p\text{-}H_2 \quad \text{order } 2$$

The conversion most likely occurs under the influence of the intermolecular forces of the surface, in particular from the para-magnetic forces of unsaturated and free valent carbon atoms. These could perturb the inter-atomic forces enough to waive the prohibition on the $J \pm 1$ transitions. If this is the case the adsorbed state would not be selective to a particular isomer and so fails to explain the difference in uptake between the two hydrogen isotopes which have differing isomer concentrations. However the adsorbed state may be

considered as a stable intermediate for the conversion process. Now although the isomers for a particular isotope will have the same intermediate, they do not necessarily have the same rate of reaction in forming the intermediate i.e. sorbed state. At equilibrium the rate of adsorption is equal to the rate of desorption for both isomers

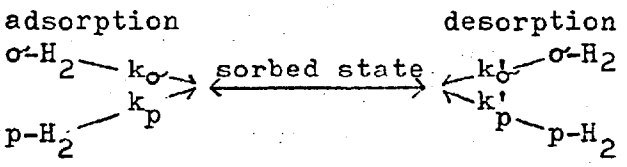

and the total system

rate of adsorption = rate of desorption

$$k_\sigma . C_{e,\sigma} + k_p . C_{e,p} \longleftrightarrow k'_\sigma . C_{s,\sigma} + k'_p . C_{s,p} \qquad 5.13$$

where k is the rate constant, C the concentration, subscript σ for ortho, subscript p for para, subscript e for equilibrium, C_s is the concentration of the sorbed state and the rate constants are primed (') for desorption. Equation 5.13. rearranges to

$$C_s = \frac{k_\sigma . C_{e,\sigma} + k_p . C_{e,p}}{(k'_\sigma + k'_p)} \qquad 5.14$$

So the amount adsorbed would depend on the concentrations of the isomers in the gas phase.

There seems no a priori reason for choosing one explanation in preference to the other. Particularly in the light of the experiments of Constabaris et al (1961) who examined the adsorption of the isotopic pair CH_4/CD_4. Here the effect was the exact opposite of that for the H_2/D_2 pair, CH_4 having a higher uptake than CD_4. This is contrary to the predicted result from zero point energy considerations, and CH_4 and CD_4 do not have ortho-para isomers. It seems fairly clear that much more data is required over a fairly wide temperature range before a definite conclusion can be reached as to which explanation is correct.

5.2.4 Ammonia adsorption on Carbolac I

The ammonia adsorption isotherms on Carbolac I are unusual in their exceptionally high uptake. This may be due in part to the oxide surface of the adsorbent and in part to the polar nature of the ammonia molecule. Anderson and Emmett (1952) showed that the very large ammonia uptake on the very similar oxidised channel black Black Pearls I was initially substantially reduced if the oxide surface was removed by out-gassing the adsorbent at 1200 °C. Similar results have been found by Holmes and Beebe (1957) and by Spencer, Amberg and Beebe (1958). So we may conclude that the high uptake may be attributed to the polarity and capacity of ammonia to form a type of chemi-sorbed bond with the surface complex.

However in the multilayer region the uptake appears to be independent of the nature of the surface of the adsorbent. This is probably due to the ammonia now condensing to form a hydrogen bonded liquid. There is an analogous situation found with water sorption on oxidised carbons which have been out-gassed at different temperatures (Anderson and Emmett 1952, Puri 1966 a).

The oxide complex also accounts for the first isotherm at 0 °C having a higher uptake than the second. The first dose of ammonia chemically reacting with the more acidic oxides of the surface to form either a permanent ammonia complex on the surface, or to be removed as ammonium carbonate on out-gassing. In either case there would be no change in surface area, but successive ammonia adsorptions would be reduced.

The failure of the hysteresis loop to close may be due to a certain amount of the ammonia being irreversibly fixed by chemi-sorption, the gas only being completely desorbed on out-gassing at 200 °C. A similar effect was noted by Puri

(1966 a) from his studies of water adsorption.

The above discussion indicates that there is a whole spectrum of oxides on the surface varying from those capable of chemical reaction, those involved with chemi-sorption, to those causing enhanced physical adsorption and possibly even reduced physical adsorption.

The basic explanation for hysteresis is capillary condensation in the micropores which act as exits from the macropores (Adamson, Physical Chemistry of Surfaces, page 634). The condensate in the micropore is considered to prevent the gas in the macropore from desorbing until the pressure has dropped to a low enough value for the condensate to evaporate out of the micropore. In general the greater the difference between the size of the macropores and micropores then the wider the hysteresis loop. The loops found in the present work are very narrow suggesting that there is not a very wide distribution between the macro- and micropores.

The graph of isosteric heat versus coverage follows the characteristic curve for adsorption of a polar molecule on an energetically heterogeneous adsorbent. Initially the value of q_{st} is very high for adsorption at high energy sites (i.e. ammonia adsorbing on to the acid oxides of the surface). The value of q_{st} then drops towards the latent heat of condensation as adsorption occurs on the less energetic sites.

The molar heat of adsorption at constant spreading pressure, $\Delta\tilde{H}$, followed a very similar pattern when plotted against the spreading pressure, $\emptyset$, (figure 4.16). Values for $\Delta\tilde{H}$ had a very much larger error due to the inaccuracies of computing $\emptyset$ at low coverages.

The heavy adsorption of condensable vapours can cause measurable swelling of the adsorbent (Meehan 1927, Bangham et al 1930, 1932, 1938, 1943, McIntosh et al 1947, 1952,

Wiig et al 1949, McBain et al 1933, Yates 1954, 1956, Flood et al 1954, 1955, 1957 a b c, 1963), and it has been suggested that such swelling may alter the flow characteristics of an adsorbable vapour permeating a porous membrane (Carman and Malherbe 1950, Barrer and Strachan 1955). Actual measurement of the amount of swelling of each Carbolac I particle is not practicable, but the degree of swelling may be estimated from an application of 'Total System Thermodynamics' of adsorption. Flood (1955, 1957 a) found fairly good agreement between the experimentally measured swelling of a zinc chloride activated carbon rod on adsorbing a gas and the theoretically expected degree of swelling. The following derivation is based on the nomenclature and thermodynamic definitions out-lined in section 2.2.2 as originally described by Tykodi (1954). Excepting the nomenclature, the approach is very similar to that of McIntosh and Haines (1947), Harkins and Jura (1944, 1946), and Flood and Heyding (1954, and the papers already mentioned).

That a solid has a tendency to swell on adsorption is clear when the change in chemical potential is examined using Tykodi's postulates :-

(1) The chemical potential of the system (macro or micro) is a function of its surroundings.

(2) The chemical potential of a solid can be expressed in terms of the chemical potentials of the lattice elements of the solid.

(3) The chemical potential of each species of lattice element can be defined so as to be homogeneous throughout the solid.

Now when a solid adsorbs the chemical potential of the environment will change. This will cause an accompanying change in the chemical potential of the surface lattice elements on the solid. However, by postulate (3) the

chemical potential of the solid must remain uniform throughout. So the chemical potential of the internal lattices will also change either by swelling of the lattice, or by some other unknown mechanism, in order to preserve the homogeneity. Since swelling is the only mechanism observed in practice it will be considered to be the predominating effect. Such swelling is small and therefore the chemical potential of the solid can be expressed in terms of the calibration volume as a series expansion keeping first order terms only,

$$\mu_a = \mu_a^o + \left(\frac{\partial \mu_a^o}{\partial \tilde{V}_a^o}\right)_T .(\tilde{V}_a - \tilde{V}_a^o) + \ldots \text{(constant T)} \qquad 5.15$$

$$= \mu_a^o + \tilde{V}_a^o \left(\frac{\partial P}{\partial \tilde{V}_a^o}\right)_T . \Delta\tilde{V}_a \qquad 5.16$$

$$= \mu_a^o - (\Delta\tilde{V}_a/\beta) \qquad 5.17$$

where $\beta = -(\partial \tilde{V}_a^o/\partial P)_T/\tilde{V}_a^o$ is the isothermal compressibility of the solid. Since

$$\mu_f = \mu_a - \mu_a^o \qquad 2.73$$

then

$$\mu_f = -\Delta\tilde{V}_a/\beta \qquad \text{(constant T)} \qquad 5.18$$

and in the general case

$$\mu_f\,(T,X_M) = -\Delta\tilde{V}_a\,(T,X_M)/\beta\ \ (T,P) \qquad 5.19$$

where X_M is the molar surface excess per mole of adsorbent. Consequently if the chemical potential of the excess can be determined, then a value can be obtained for the swelling of the adsorbent for a given temperature and excess. Now Tykodi showed that

$$\left(\frac{\partial \mu_f}{\partial X_M}\right)_T = -X_M.\tilde{V}_g\left(\frac{\partial P}{\partial X_M}\right)_T \qquad 5.20$$

$$\cong -X_M.R.T\left(\frac{\partial \ln P}{\partial X_M}\right)_T \qquad 5.21$$

where the approximate equality $\cong$ is used to indicate the application of the perfect gas law. At constant temperature equation 5.21 integrates to

$$\mu_f = - R.T \int_0^{X_M} X_M . \left(\frac{\partial \ln P}{\partial X_M}\right)_T . dX_M \qquad 5.22$$

This equation is the usual integral form of the Gibb's equation and allows us to evaluate the chemical potential of the surface excess by replacing the molar excess, X_M, with $(v.M_a)/V'$ where v is the volume adsorbed in cc at N.T.P. per g, V' is the molar volume, and M_a is the molecular weight of the adsorbent. The swelling of the adsorbent in cc per mole of adsorbent is then given as

$$\Delta \bar{V}_a = \frac{\beta.R.T.M_a}{V'} \int_0^P \frac{v}{P} . dP \qquad 5.23$$

Now 1 cc of porous medium will contain $w/(M_a.l.A_c)$ moles of adsorbent where w is the out-gassed weight of the membrane in g, l is the length of the membrane in cm, and A_c the cross-sectional area of the membrane in cm^2. So the swelling of the adsorbent in cc per cc of porous medium ΔV_a is

$$\Delta V_a = \frac{w.\beta.R.T}{l.A_c.V'} \int_0^P \frac{v}{P} . dP \qquad 5.24$$

Equation 5.24 requires a value for the isothermal compressibility of the solid, β, and in the absence of the necessary data we have to fall back to employing the bulk modulus for graphite, 3.0×10^{-6} atmos.$^{-1}$ (The Geological Society of America, Handbook of Physical Constants, Ed S.P.Clark 1966). This value has the correct order of magnitude when compared with derived values for β estimated from the quoted adsorption-extension experiments. So using the same computed values for the integral as determined for the evaluation of the integral molar heats, the volume changes listed in table 5.9 were calculated.

Table 5.9 Estimated swelling of Carbolac I on adsorbing Ammonia

Temp. °C	P in cm Hg	$\int_0^P (v/P).dP$	ΔV_a cc per cc
- 40	32	802.3	2.00×10^{-3}
	50	1045.7	2.59 "
- 50	22	989.1	2.67 "
	31	1217.7	2.92 "

These results have the same order of magnitude as calculated by Tykodi (1954) from the results of Harkins and Jura (1944) for the saturation adsorption of water at 25 °C on an anatase sample of area 13.8 sq m g^{-1}. However, conversion of some of Flood's adsorption-extension results into the corresponding volume extensions via

$$\frac{\partial V_a}{V_a} = \frac{3.\partial l}{l} \qquad 5.25$$

shows that increased swelling can occur when adsorbing polar molecules on to activated carbon ($\Delta V_a \sim 1 \times 10^{-2}$ cc / cc as $P/P_o \rightarrow 1$). A draw-back of equation 5.24 is in the choice of value for β. It is to be expected that the turbostatic stacking of the layer planes in Carbolac I, and the spongy nature of the particle would cause a divergence from the value for the bulk modulus of crystalline graphite.

5.3 SINGLE GAS FLOW

5.3.1 Helium flow through Graphon

One of the working assumptions for evaluating surface flow in terms of Fick's law was that the helium flux does not have a surface component. This has recently been questioned by Kammermeyer and co-workers in a series of papers reporting the flow of gases through Vycor glass (Hwang and Kammermeyer 1966 a b, 1967). It therefore seemed pertinent to include

an ancillary study of helium flow through a compacted carbon membrane.

Up to the time of Hwang and Kammermeyer's work the cited evidence for helium surface flow was somewhat slender. For there to be a surface flux there must be adsorption. Flood (1957 a) incorporated a correction term for such adsorption when quoting the helium density of his carbon rods. The degree of helium adsorption was estimated from the known surface potentials of helium and krypton and the measured krypton adsorption isotherm. Thus it only represented a computed value. From these calculations it would appear that adsorption at atmospheric pressures and room temperature is in the region of 0.03 cc at N.T.P. per g. A similar value was reported by Kini and Stacy (1963) for helium adsorption on a number of carbonaceous solids. These isotherms were calculated from the apparent change in dead space as the temperature of the adsorption bulb was lowered from 560 ^{o}K. Experiments with the sample bulb empty, or containing potassium chloride showed that the decrease could not be explained by changes in the volume of the bulb. The degree of supposed adsorption increased with increasing surface area. Unfortunately while the high area chars continued to show marked dead space volume changes as the temperature was lowered below 200 ^{o}K, the low area vitrains showed zero or even what was effectively negative adsorption. Hence the volume changes may equally well have been due to reversible thermal expansion and contraction of the sample. Adsorption of helium at liquid nitrogen temperature on carbon blacks has been studied by Steel and Halsey (1954, 1955) and Steel (1956), but even at these low temperatures the uptake is not very large.

The principal test for the absence of surface flow is that the permeability obeys equation 2.4. Consequently

the permeability constant, $K(M/T)^{\frac{1}{2}}$, should not vary with temperature. Ash, Baker and Barrer (1967) reported a rise in $K(M/T)^{\frac{1}{2}}$ at liquid oxygen and nitrogen temperatures for helium flow through Graphon and Black Pearls II compacts. This was attributed to surface flow arising from adsorption at these low temperatures. The only similar evidence for helium surface flow at room temperature is that of Hwang and Kammermeyer (1966 b) for flow through Vycor glass. Indirect evidence was suggested by Barrer and Strachan (1955) who were able to calculate a Henry law adsorption constant from their transient state flow data, but more recent work (Ash, Baker and Barrer 1968) would suggest that during the transient state the 'sorbed' gas was filling the blind pores of the membrane rather than adsorbing on to the surface. The only other evidence is that of Kammermeyer and Rutz (1959) who reported a lower hydrogen permeability through a porous glass membrane than was predicted from the helium flow. However, they admit that the difference could have been accounted for by experimental error.

Hwang and Kammermeyer (1966 a) derived a theoretical equation from an adsorption and diffusion model with which to compare their experimental results. The following section is a précis of the argument translated into the nomenclature employed in the previous sections.

The gas phase and surface phase fluxes were respectively defined by equations 5.26 and 5.27

$$J_g = - \frac{G_1}{(2.\pi.M.R.T)^{\frac{1}{2}}} . \frac{dP}{dx} \qquad 5.26$$

$$J_s = - G_2 . D_{ss} . \frac{dC_s}{dx} \qquad 5.27$$

where G_1 is a structure factor for the gas phase of the membrane, and G_2 is a structure factor for the surface phase.

Kammermeyer then combined the model isotherm for localised adsorption at low surface coverage (Glasstone, Laidler and Eyring, The Theory of Rate Processes, pp. 355 (1941)) with a random-walk model for the surface diffusion coefficient (Hill, An Introduction to Statistical Thermodynamics, pp. 198, (1960)). Thus equation 5.27, after several mathematical manipulations, rearranges to

$$J_s = - \frac{B}{(M.T)^{\frac{1}{2}}}.T.\exp(\Delta'/T).\frac{dP}{dx} \qquad 5.28$$

where B is a combined constant of the structure factors of the porous media and the molecular properties of the adsorbing gas. Δ' is the quotient of the difference between the activation energy of desorption and the minimum potential energy of an adsorbed molecule, the difference being divided by the Boltzman constant.

The total flux is the sum of the separate gas and surface fluxes, so combining equations 5.26 and 5.28

$$J = - \frac{A'}{(M.T)^{\frac{1}{2}}}.\frac{dP}{dx} - \frac{B}{(M.T)^{\frac{1}{2}}}.T.\exp(\Delta'/T).\frac{dP}{dx} \qquad 5.29$$

where $A' = G_1.(2.\pi.R)^{\frac{1}{2}}$

The permeability Q is defined by equation 5.30

$$J = - Q.\frac{dP}{dx} \qquad 5.30$$

so combining equations 5.29 and 5.30

$$Q.(M.T)^{\frac{1}{2}} = A' + B.T.\exp(\Delta'/T) \qquad 5.31$$

This is Kammermeyer's working equation. To evaluate the constants A', B and Δ' Kammermeyer argued that the constant A' was a geometry constant for a given porous medium, so the value of A' was fixed regardless of the kind of gas and temperature. On the other hand, B and Δ' were constants for a particular gas and microporous medium combination. This allowed

equation 5.31 to be re-arranged to

$$\ln\left(\frac{Q(M.T)^{\frac{1}{2}} - A'}{T}\right) = \ln B + \frac{\Delta'}{T} \qquad 5.32$$

Assuming a value for A', the values for B and Δ' were calculated from the experimental results by the method of least squares together with the sum of the squared errors for all the gases studied (He, Ne, H_2, O_2, N_2, CO_2). The value for A' was then corrected and the procedure repeated by computer until the sum of the squared errors for all the gases was minimised. However, there is a certain basic weakness in this approach that was not considered by Kammermeyer. The computation just described does not evaluate the constants A', B and Δ' of equation 5.32, but the constants for an equation of the same form of equation 5.32 which is the best fit to the experimental results. Thus it is not really surprising that the experimental and calculated points lie on the same curve since they were derived from common data. Hence the shape of the theoretical curve remains unknown, so although the data are self-consistent there is no means of knowing whether they are consistently right or consistently wrong. The fact that the equation calculated from the experimental results is similar in form to the equation derived from the theoretical model is simply due to the fortuitous choice of an equation of the same form which was to be best fitted to the experimental results by a computer program. No test was made as to whether or not it was the most suitable equation. Because the constants of equation 5.32 were not evaluated independently it is incorrect to conclude that the constants describing the experimental equation are also the constants for the theoretical model. This situation may be compared with the experimental proof of the Clausius-Clapeyron equation in which the latent heat may be evaluated from the theoretical equation and

compared with the value independently obtained from calorimetry.

Because of this limitation in the argument the following possible inconsistancies between the theoretical equation and the experimental results will remain undetected.

(i) Since no adsorption measurements were made it is not known if the adsorption isotherm is within the boundaries of the localised, low concentration adsorption isotherm model. This is particularly pertinent for the low temperature experiments, for this is not only the region where adsorption is most likely to be outside the defined regime, but also if any errors do occur they will be proportionately magnified by the reciprocal relationship with temperature.

(ii) The model describes the surface flux J'_s of section 2.1.3. It assumes that there are no evaporative flights across cracks and crevices. However, the gas phase flux was defined and evaluated as J_g, consequently the total flux is the sum of $(J_g + J_e + J'_s)$. In effect Kammermeyer assumed that J_e was zero.

(iii) Vycor glass is a microporous membrane and therefore may have a slight molecular sieving effect. Because of the pore distribution the effect would not be large, but for the smaller molecular species there may be a small additional flux from penetration through the micropores that are too small for the larger molecules. In this case the geometry constant A' is not only a function of the porous medium, but also of the molecular species.

(iv) Since A' was not measured independently of the permeability experiments, there is no means of telling whether or not it is a function of temperature, although the only evidence for changes in the pore geometry by thermal expansion is the suggested alternative explanation of the results of Kini and Stacy.

(v) Because of the nature of the argument, experimental artifacts such as sorption of mercury or tap grease residues,

or ageing of the membrane may easily be misinterpreted as genuine results. It is only by chance variation of the experimental conditions that such errors will be detected.

Any one, or all of these errors may account for the variation of $Q(M.T)^{\frac{1}{2}}$ with temperature found by Hwang and Kammermeyer (1966 b). The gas phase permeability is known to be very sensitive to pore geometry. This is illustrated by table 5.10 which lists the permeabilities for several materials compacted to different porosities. The variation due to sorbed material was also clearly demonstrated by Ash, Barrer and Pope part II (1963), in the extreme case the sorbed material completely blocking the gaseous flow.

Table 5.10 Variation of helium or air permeability with porosity

Gas and material	ε	K	Source
Helium / Carbolac I at 0 °C	0.64	34.60×10^{-3}	a
	0.37	2.65×10^{-3}	
Helium / Aluminium-Silica	0.53	36.40×10^{-3}	b
cracking catalyst	0.40	6.30×10^{-3}	
Air / Linde-Silica II	0.84	11.80×10^{-10}	c
at - 35 °C	0.50	0.57×10^{-10}	

a Barrer and Strachan (1955) K in $cm^2\ sec^{-1}$

b Barrer and Gabor (1959) K in $cm^2\ sec^{-1}$

c Carman and Malherbe (1950) K in $cm^2\ sec^{-1}$ (The high porosity compact may have some slip and viscous terms)

The permeability is also sensitive to the history of the membrane. For Carbolac I membranes a marked difference has been found between the helium permeability at 0 °C before and after flow experiments with strongly adsorbing vapours (Ash, Barrer and Pope, part I 1963, see also figure 4.18 of the present work).

It is believed that the work reported by Ash et al was mis-read by Hwang and Kammermeyer (1966 b). All the helium experiments referred to in figure 1 of Ash et al part 1 were performed at 0 °C (Pope 1961), and the ordinate of the figure is the run order of the experiments. The temperatures in the diagram referred to the flow experiments for the other gases performed in between the helium runs. Thus the 15% fluctuation in the helium permeability mentioned by Hwang and Kammermeyer was not a function of temperature, but of run order or more correctly membrane 'ageing'.

The experiments of section 4.3.1 were designed to examine critically the evidence for helium surface flow over the temperature range 300 to - 200 °C. In order to eliminate possible structural alterations of the porous membrane clouding the issue, the membrane was prepared from Graphon powder in preference to Carbolac I. In spite of these precautions the initial series of experiments (sets 1. to 16.) clearly indicated that exceptional care had to be taken to eliminate the extraneous effects of ageing and possible mercury sorption on the compact which could so easily swamp any evidence for surface flux. Once these stray effects had been eliminated the maximum difference of $K(M/T)^{\frac{1}{2}}$ between the highest and lowest temperature was only 3% (the term $Q(M.T)^{\frac{1}{2}}$ defined by Hwang and Kammermeyer is formally equivalent to $K(M/T)^{\frac{1}{2}}$ defined in the present work providing neither Q nor K is a function of C). Since the permeability constant increases towards higher temperatures it seems unlikely that the additional flux can be explained in terms of surface flow or changes in pore geometry. If it is not an experimental error then it is most likely connected with the mechanism of the molecule-wall collision. In the light of the present results it is considered that the 10% variation of

$Q(M.T)^{1/2}$ over the same temperature range for helium flow through Vycor glass reported by Hwang and Kammermeyer (1966 b) is an experimental artifact, although the increased permeability at liquid hydrogen temperatures reported by the same authors in a later paper (1967) is almost certainly due to surface flow. In consequence Kammermeyer's correlation between the experimental results and his derived theoretical equation is invalid. It is concluded that there is no surface component for helium flow through Graphon membranes between the temperature range 300 to - 200 °C. This is also believed to apply to Carbolac I membranes, although because of the very large surface area and energetic heterogeneity of the surface there may be a small degree of surface flow at the liquid nitrogen temperature. Unfortunately the experimental evidence for Carbolac I may well be masked by the instability of the surface.

5.3.2 Helium flow through Carbolac I

The repeated check measurements of the helium permeability through the Carbolac I membrane at 0 °C through-out the course of the experimental program, bears out the conclusions of the previous section that the instability of the pore geometry far out-weighs any evidence for surface flow of helium through Carbolac I. When the helium data were required to calculate the gas phase flux for experiments with other gases, the results for the helium runs immediately prior to the experiments were used.

5.3.3 Single gas flow of Hydrogen, Deuterium and Nitrogen through Carbolac I at - 40 °C

All three gases exhibited an additional flux over and above the value calculated from the helium data. This additional flux was attributed to surface flow. Comparison

of the two defined permeabilities between the gases demonstrates the sensitivity of the permeability to the in-going side concentration term in which it is defined.

K, the permeability defined in terms of the gas phase concentration at the in-going side, $C^{g}_{g,o}$, (equation 4.7) shows no variation with its concentration term whether the adsorption isotherm is linear (H_2, D_2), or curved (N_2), see figure 4.2. This is because K is independent of the in-going side surface concentration and is a function only of the in-going side gas phase concentration; thus it will remain constant until blockage occurs. However, K_C, the permeability defined in terms of the total in-going side concentration, C_o, (equation 4.8) only remains constant for those gases obeying the Henry law adsorption isotherm (H_2, D_2), and it becomes a function of the in-going side concentration as soon as the isotherm becomes curved, compare figures 4.23 and 4.24. This is because K_C is dependent on the sum of the in-going side gas phase and surface phase concentrations.

For hydrogen and deuterium, where the isotherms are in the Henry law region of adsorption, a plot of J_s versus $C_{s,o}$ would be linear, and D_{ss} would be independent of coverage. Accordingly D_{ss} was obtained as the average of $(J_s/C_{s,o})l$ for each experimental point.

For nitrogen the plot of J_s versus $C_{s,o}$ is curved, see figure 5.8. Consequently D_{ss} was calculated for different coverages from the slope $(dJ_s/dC_{s,o})l$ of the graph J_s versus $C_{s,o}$ and is shown plotted as a function of coverage in figure 5.9. The limiting value of D_{ss} in the Henry law region was found by extrapolating back to zero coverage. Table 5.11 lists these limiting values for the three gases.

Unfortunately there are not enough data to establish whether or not there is any relationship between D_{ss} at zero

Figure 5.8

J_s v C_s for Nitrogen through Carbolac I at - 40 ^{o}C

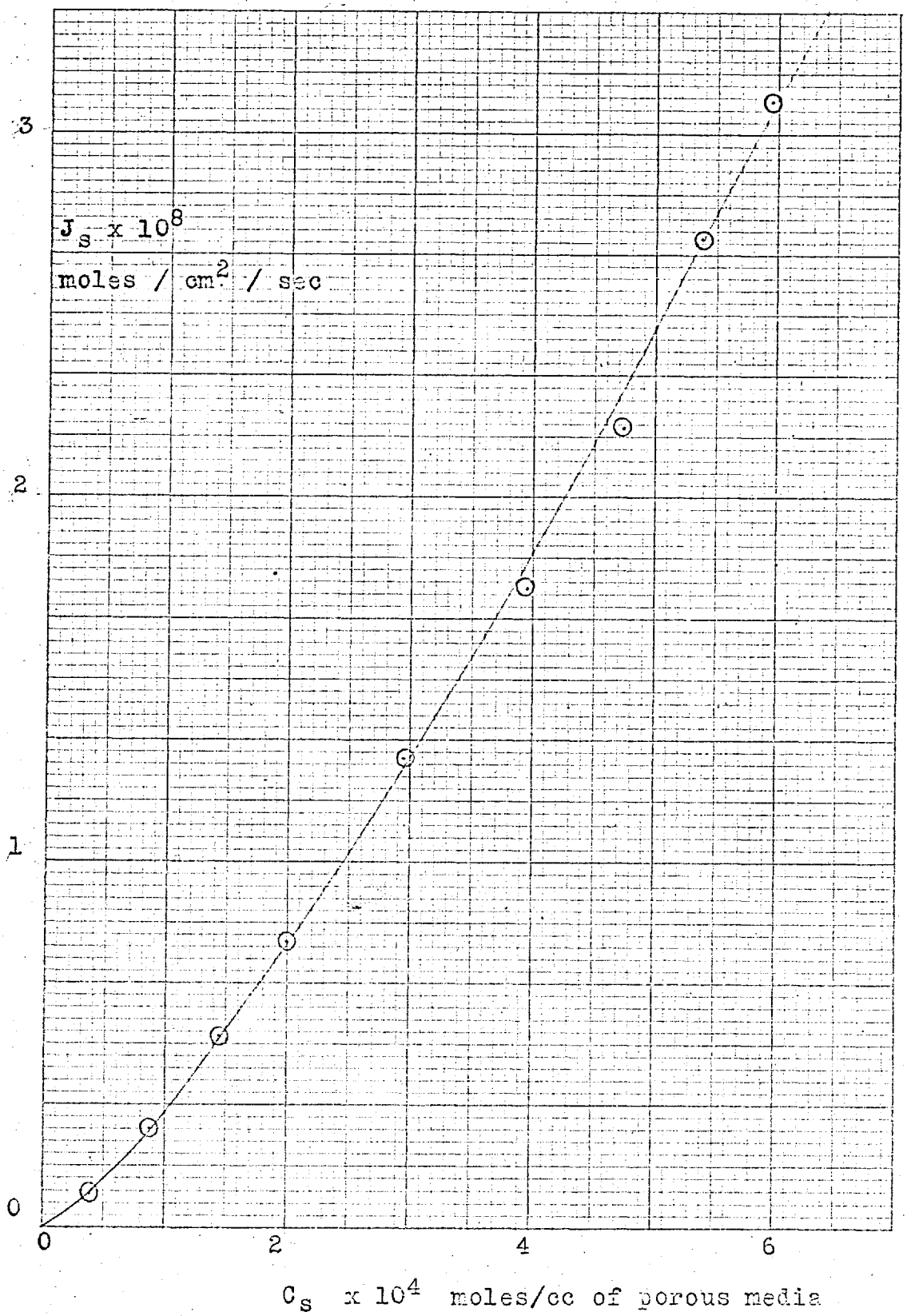

D_{ss} v C_s for Nitrogen through Carbolac I at - 40 °C

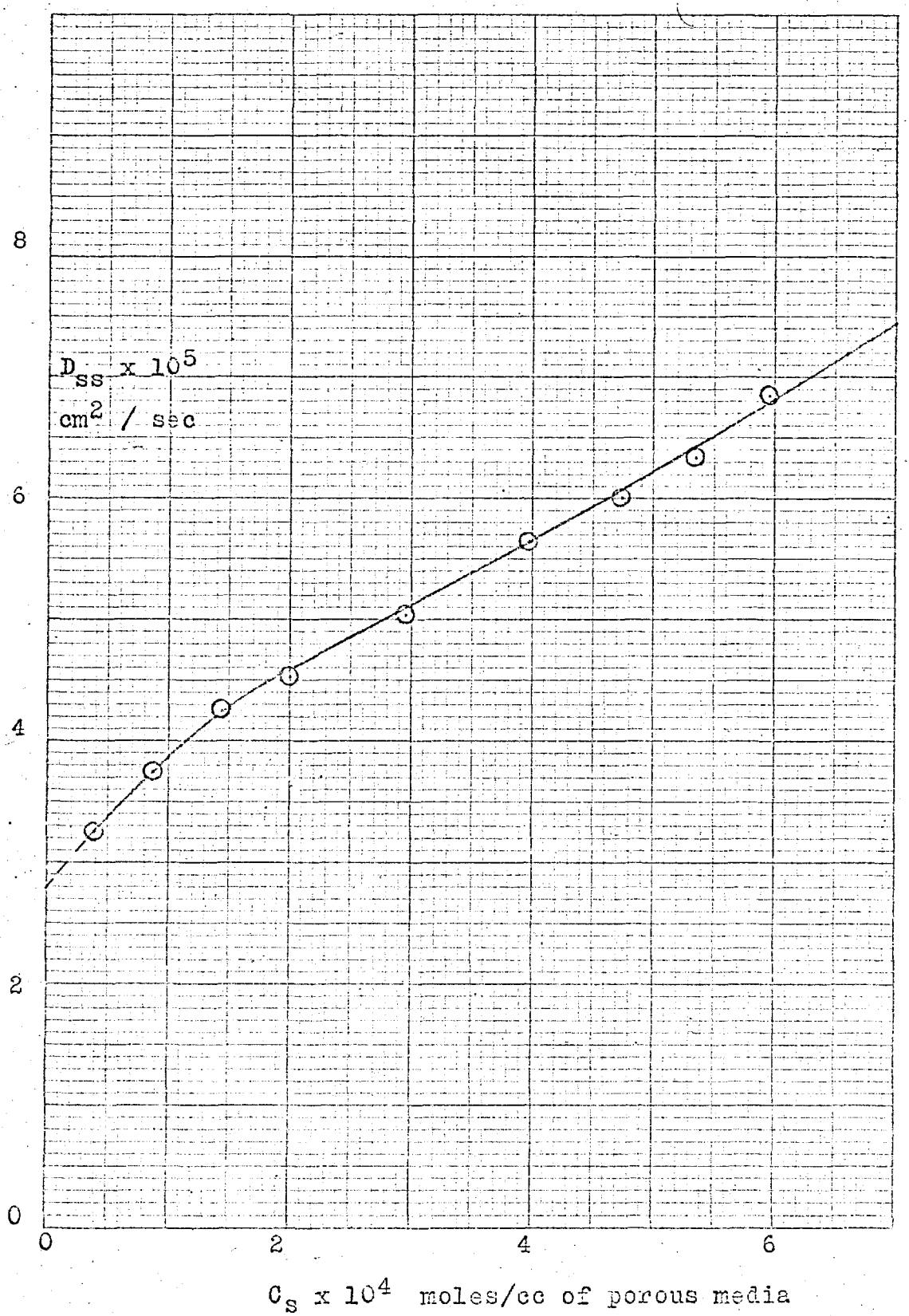

Table 5.11 D_{ss} at zero coverage for H_2, D_2, and N_2 at - 40 °C

Gas	D_{ss} in cm^2/sec	$D_{ss}.M^{1/2}$
H_2	74.0×10^{-5}	1.05×10^{-3}
D_2	55.3×10^{-5}	1.10×10^{-3}
N_2	28.0×10^{-5}	1.48×10^{-3}

coverage and the molecular weight or the temperature. Clint (1966) concluded from his much more extensive data that the surface diffusion coefficient at zero coverage has an 'Arrhenius' relationship with temperature

$$D_{ss\ (C_s \rightarrow o)} = (\text{Const.}).e^{(-E^*/R.T)} \qquad 5.33$$

where E^* is the activation energy for surface migration. This experimental result required no assumptions as to the mechanism of diffusion, the value of E^* and the constant being experimentally evaluated quantities. Experimentally it was also shown that the Henry law constant, k_s, has an exponential form with temperature

$$k_s = (\text{Const.}).e^{("\Delta E"/R.T)} \qquad 5.34$$

"ΔE" being the energy of adsorption in the Henry law region (see section 2.2.2). So for surface flow in the Henry law region of adsorption we may combine equations 2.19, 2.23, 5.33, and 5.34 and express the surface flux as

$$J_s = -\left((\text{Const.}).e^{("\Delta E"-E^*)/R.T}\right).\frac{dC_g}{dx} \qquad 5.35$$

where (Const.) incorporates all the constants whether known or not. We may therefore rewrite the total flux as

$$J = -\left(D_{gs} + (\text{Const.}).e^{("\Delta E"-E^*)/R.T}\right).\frac{dC_g}{dx} \qquad 5.36$$

integrating both sides

$$J.l = \int_0^{C_{g,o}} \left(D_{gs} + (\text{Const.}).e^{("\Delta E"-E^*)/R.T} \right).dC_g \qquad 5.37$$

and differentiating with respect to the concentration at the in-going side

$$\left(\frac{dJ}{dC_g}\right)_{C_{g,o}} .l = \left(D_{gs} + (\text{Const.}).e^{("\Delta E"-E^*)/R.T} \right)_{C_{g,o}} \qquad 5.38$$

When adsorption at the in-going side is in the Henry law region then :

$$K = \frac{J.l}{C^g_{g,o}} = \left(\frac{dJ}{dC_g}\right)_{C_{g,o}} . \frac{l}{\varepsilon} \qquad 5.39$$

If we express D_{gs} in terms of the Knudsen equation (equation 2.4), then we may express the permeability as

$$K = (\text{Konst.}).(T/M)^{\frac{1}{2}} + (\text{Const.}).e^{("\Delta E"-E^*)/R.T} \qquad 5.40$$

where (Konst.) incorporates all the constants of the Knudsen equation. Rearranging equation 5.40 as an expression for the permeability constant $K(M/T)^{\frac{1}{2}}$, then

$$K(M/T)^{\frac{1}{2}} = (\text{Konst.}) + (\text{Const.}).T^{-\frac{1}{2}}.e^{("\Delta E"-E^*)/R.T} \qquad 5.41$$

Equation 5.41 was derived from the experimental results, and it required no adsorption or diffusion model. It is strictly limited to the Henry law region of adsorption. It differs from Hwang and Kammermeyer's theoretically derived equation in the pre-exponential term for temperature (see equation 5.31). This is probably due to incorrect choice of the diffusion model on the part of Hwang and Kammermeyer.
A more satisfactory choice would have been Kruyer's 'random walk' model on a two dimensional lattice, for which the working equation is (Kruyer 1953)

$$D_{ss} = \tfrac{1}{4}.a^{*2}.\nu.e^{(-E^*/R.T)} \qquad 5.42$$

where a* is the mean jump distance associated with a unit diffusion process and ν is the vibration frequency of an adsorbed molecule. This equation has the correct form to be compatible with the results, also using the experimental value for E* and the calculated value of ν from Ross and Olivier (1964), Clint showed that equation 5.42 yielded acceptable values for the mean jump distance a* (Clint 1966).

5.3.4 Single gas flow of Ammonia through Carbolac I

The most unusual feature to emerge from the ammonia flow experiments was the occurrence of a maximum in the plot of total flux versus either the in-going side gas concentration or in-going side total concentration, figures 4.25 and 4.26. To the author's knowledge such maxima have not been previously reported. Comparison of the - 40 and - 50 °C curves in figure 4.26 reveals that the maxima occur at the common total in-going side concentration of 2.1×10^{-2} moles per cc of porous medium. This seems to eliminate the possibility that they are due to an experimental artifact, and it is to be expected that similar maxima would have occurred with the experiments at higher temperatures had it been possible to extend the experiments up and past this value for the total in-going side concentration.

Except in the very low pressure region at the in-going side, we may approximate the total flux as equal to the surface flux. Although the ammonia gas phase flux was calculated from the separate single gas flow helium data to be 10% of the surface flux, the subsequent ammonia/helium mixture experiments indicated that blockage by the adsorbed film reduced the gas phase flux to less than 1% of the total flux as the total flux approached its maximum value. Similarly the surface concentration effectively represented the total

concentration.

When the flow passes through a maximum value with increasing concentration at the in-going side then an anomaly occurs if the flux is defined in terms of the Fick identity

$$J \equiv -D.\frac{dC}{dx} \qquad 2.6$$

The negative sign refers to the concentration gradient down which the material is flowing. The diffusion coefficient was derived from this expression as (see section 2.1.2)

$$[D]_{C_o} = \left(\frac{dJ}{dC_o}\right).L \qquad 2.11$$

The integration involved in the mathematical manipulations to achieve this result required D to be a constant or a function of C only. The sign of the diffusion coefficient, and in turn the term (dJ/dC_o), must always be positive in order to be compatible with the observed and defined direction of flow down the observed and defined negative concentration.gradient. A negative diffusion coefficient, which would automatically occur if equation 2.11 were applied to the experimental results past the point of maximum flux, leads to the absurd situation of either reversal of flow, or flow up a positive concentration gradient. Since this is not the case found in practice then the integration procedure of section 2.1.2 cannot apply to this present situation. The process may still be described by the general identity of Fick's law, equation 2.6, but the diffusion coefficient is no longer a simple function of concentration and may now be an inseparable function of both concentration, C, and distance, x. This may be due to a change in the mechanism of flow, or some external influence.

The nature of flow prior to the point of maximum flux is already unusual. This may be seen from the graphs of the permeability, K, as defined by equation 4.7, plotted against the

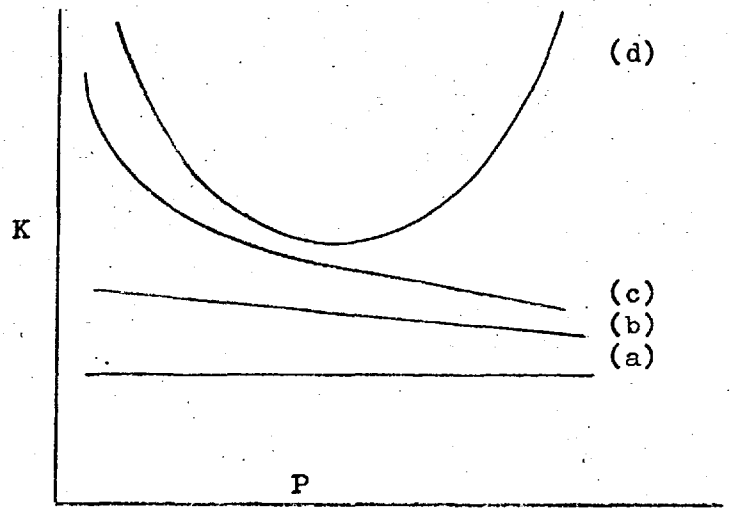

Figure 5.10 K versus P summarised from the results of Gabor (1957), Pope (1961), Clint (1966), Baker (1966).

pressure at the in-going side figure 4.27. This 'conventional' permeability normally varies with temperature and the in-going side pressure in the general pattern shown in figure 5.10. Curve (a) is for a non- or weakly sorbed gas at high temperatures where the permeability is independent of the pressure. As the temperature is lowered the increased adsorption causes the permeability to increase and take on a linear pressure dependence, curve (b). This develops into a pronounced curve for heavier adsorption, curve (c), and as the pressure approaches the saturation vapour pressure the curve forms a minimum, curve (d). In the present work no initial decrease in K was found. At the highest temperature the graph of permeability versus in-going side pressure showed a slight positive slope which became much more pronounced on lowering the temperature. The results are similar to those of the unreported work of Logan for the flow of hydrocarbons through membranes prepared from cracking catalysts.

It was demonstrated in chapter 2 that the variation of the permeability with pressure was a direct result of the functional relationship between J and P, yet this does not

explain the physics of the situation.

The permeability represents a comparative value for the mobility of the permeating fluid. In this case an increased permeability indicates an increased mobility of the adsorbed film. Carman and Malherbe (1950) studied the flow of CF_2Cl_2 at high surface film densities through plugs of Linde Silica II compacted to various porosities. At first sight it appeared that the permeability increased with decreasing porosity. However closer inspection reveals that in lowering the porosity more material per cc of porous medium was compacted into the plug. This increased the surface area per cc of porous medium allowing greater surface flow. In the present work the actual amount of material present is fixed, but it was pointed out in section 5.2.4 that the solid would swell into the void space on adsorbing a gas. This may cause an increase in the surface area and hence mobility of the adsorbed material, but it would also intoduce an x dependency into the flow. Since the membrane was constrained excessive swelling could start to block the pores of the membrane causing a reduction in flux. However, the calculations of section 5.2.4 showed that at the point of maximum flux the degree of swelling was only in the region of 2×10^{-3} cc per cc of porous medium. The calculation did depend on the choice of value for the isothermal compressibility β , and comparison with the results from Flood's adsorption-extension measurements with condensible vapours on a carbon rod (Flood 1957 b) suggests that this value could be in error by a factor of 10. The largest extension observed by Flood was 6.8×10^{-3} cm per cm ($\equiv 2 \times 10^{-2}$ cc per cc) for pentane sorbing at its saturation vapour pressure point. Even so this hardly seems large enough to account for the reduction in flux. As an independent check on the calculations reference may be made to Carman's work on the adsorption of

CF_2Cl_2 on Carbolac I that had been compacted and constrained in a very similar device to the method employed here for the flow experiments. In the compacted and constrained form the Carbolac I would only be able to adsorb up to the limit of the pore space being completely filled with capillary condensate. This limit is very sensitive to the porosity, and hence any marked swelling into the void space would significantly reduce the amount adsorbed. Carman and Raal (1951 b) found that the limiting adsorption values were in fact slightly higher than the calculated values assuming no swelling had occurred. This slight difference was attributed to the adsorbate density being slightly higher than the normal bulk liquid density. So the work did show that even if swelling did occur it would have been very small and of the order calculated in section 5.2.4. The particles themselves may expand into the void space while allowing increased adsorption within the individual particles, in effect causing a reversible redistribution of the void space to occur leaving the total adsorption volume constant, but it is difficult to imagine how this could be demonstrated experimentally. Carman further found that if the plug was not constrained then adsorption would continue past the theoretical limit forming an adsorption isotherm almost identical to that of the free powder. This may be due to the adsorbate forcing the adsorbent particles apart in order to adsorb on all possible surfaces. The porosity of an unrestrained plug changed from 0.63 to 0.65 over the course of an adsorption/desorption and out-gassing cycle. To see if a similar situation occurred for ammonia adsorption a small sample of Carbolac I was compressed to a porosity of 0.5 in a 'single gas' plug holder (this is a diffusion cell similar to those used here but without the side port) and the sample was constrained between retaining plungers. The complete assembly

was placed in a glass envelope and attached to the adsorption apparatus. After out-gassing the system at 200 °C for 72 hours an ammonia adsorption isotherm was measured at - 40 °C. The experiment was prone to large errors due to the very small weight of adsorbent (0.04), a large dead space (23 cc) and long equilibration times (initially 20 hours). It was no doubt due to these errors that the membrane appeared to adsorb to well above the theoretical limit for filling the void space with capillary condensate. This was clearly impossible since the plug was restrained but it does indicate that marked reduction of void space through swelling was absent. Whether or not a redistribution of void space occurred still remains an unanswered question. An unexpected result was that the calculations revealed that the limiting value for filling an unswollen, restrained membrane of porosity 0.5 with ammonia condensate is 2.1×10^{-2} moles per cc of porous medium. This was assuming that the condensate had the normal bulk liquid density of ammonia (0.691 g per cc at - 40 °C, Handbook of Chemistry and Physics, 48th ed., pp E 20). This was the value for the concentration at the in-going side when the flux reached its maximum value. It was also the point at which the adsorption isotherms developed marked hysteresis. Using Ries's value of 11.8 sq Å as the adsorbing area of the ammonia molecule (Ries et al, 1945) this concentration corresponds to a fractional monolayer capacity of $\sim 1.6\,\theta$, and referring back to section 5.2.1 this fractional monolayer capacity will fill all the pores from molecular dimensions up to and including pores of radius 11 Å. This range includes the average pore radius of the membrane, so it is concluded that at the point of maximum flux over half of the pores at the in-going face are filled with capillary condensate. The actual face of the membrane presented to the gas would adsorb in the same manner as

the unrestrained chips but once inside the restrained plug the adsorbate would form a capillary condensate penetrating into the membrane until the concentration had been sufficiently reduced by the gradient to form the normal surface film and gas phase. Thus the overall concentration gradient would take on an unusual function of the length of the porous medium. The formation of capillary condensate so far below the saturation vapour pressure point is due to the exceptionally high uptake of ammonia by a material of high surface area.

Scheidegger (The Physics of Flow through Porous Media, 2nd ed., pp 186) discussed the change in flow mechanism as capillary condensate sets in. The argument was based on Carman's work (1952) who envisaged the flow of capillary condensate as a viscous flow through the pore space under the gradient of capillary pressure maintained between the ends of the filled pore. However, an average pore radius of 11 Å would only allow up to six molecules to fit side by side across the diameter. Under these conditions it is difficult to describe the macroscopic quantity 'capillary pressure'. A more satisfactory approach is via the thermodynamic relationships between the two phases. If the condensate extends a distance x through the membrane, then at the respective gas/liquid boundaries we may say

$$\mu_g = \mu_\lambda \qquad 5.43$$

$$d\mu_g = d\mu_\lambda \qquad 5.44$$

$$V_g . dP_g = V_\lambda . dP_\lambda \qquad 5.45$$

$$dP_\lambda = \frac{V_g}{V_\lambda} . dP_g \qquad 5.46$$

where subscript g and λ refer to the gas phase and liquid phase respectively and the other symbols have their already defined meanings. The derivation has assumed that the phases are in thermodynamic equilibrium with each other. Integrating

for the total pressure drop across the condensate.

$$\int dP_\lambda = \left[P_\lambda\right]_{x=o} - \left[P_\lambda\right]_{x=x} = \Delta P_\lambda = \int_{P_{g,x=x}}^{P_{g,x=o}} \frac{V_g}{V_\lambda} . dP_g \qquad 5.47$$

Since $V_g \gg V_\lambda$ it follows that $\Delta P_\lambda \gg \Delta P_g$ and that the liquid pressure drop between the ends of the condensate is many times larger than that of the gas phase (Scheidegger, 1959 pp 187, Flood referenced by Barrer, 1963 a). Thus we may regard the flow of capillary condensate as viscous flow under the pressure difference ΔP_λ. Under the experimental conditions of the present work the capillary condensate only extends a small distance into the membrane. However, in his experiments Carman (1952) adjusted the out-going side pressure so that capillary condensate flowed through the total length of the membrane. He was thus able to formulate the permeability as

$$K_{c\ (exp)} = \frac{J.l}{\Delta P_\lambda} \qquad 5.48$$

and compared this experimental value with that calculated from the Kozeny equation for viscous flow (Kozeny 1927).

$$K_{c\ (calc)} = \frac{200.\rho_l.\varepsilon^3.b_s}{\eta'.M.A^2.(1-\varepsilon)^2} \qquad 5.49$$

where ρ_l is the bulk liquid density of the adsorbate, η' the bulk liquid viscosity, and b_s degree of pore saturation. The experimental values were 20% below those calculated from equation 5.49. There are many discrepancies with the Kozeny theory (see Scheidegger pp 132) which tend to negate its validity. Carman's own work suggested that the liquid density of an adsorbed film can differ from the normal bulk liquid density. The surface area, A, would include that of the micropores and blind pores, yet these would not contribute to the liquid flow, if this is taken into account then according to section 5.2.1

the effective surface area would only be ~ 250 sq m per g instead of 950 sq m per g. The degree of saturation is a somewhat arbitrary factor in that it depends to a certain extent on the pore size distribution. The viscosity may also vary. Under the normal conditions of viscous flow the viscosity is the coefficient of Newton's equation

$$\tau = \eta' \sigma_r \qquad 5.50$$

τ being shear stress and σ_r rate of shear (Newton 1685). While the viscosity remains constant then the liquid is said to be Newtonian, but there are now many examples of the viscosity being a function of shear stress

$$\eta = f(\tau) \qquad 5.51$$

and the liquid is then said to be non-Newtonian. The viscosity for flow near solid-liquid interfaces is often very much higher than the bulk liquid counter-part, this is now generally attributed to the intermolecular forces at the surface (Criddle 1960). These forces cause an orientation and preferred direction at the surface of an otherwise isotropic liquid, so the viscosity of the fluid may not only be a function of the shear stress but also of the distance from the surface (Oldroyd 1960). Loss of Newtonian properties have been observed for water flowing through beds of powdered quartz. Volkova (1936) showed that the decreasing size of the quartz grains that made up the bed had an immobilizing effect on the water flow. Many similar effects have been observed by other workers and the phenomena was reviewed by Henniker (1952). The marked control of the surface over the flow of liquid through porous media was noted by Weyl and Ormsby (1956) in reporting the work of Martin and Mohiuddin (1953). In the context of the present work where viscous fluid flow is limited to within three molecular diameters from the

surface, with a liquid which has a strong polarity and an adsorbent surface which would tend to form a very strong physical bond with this particular liquid, the surface viscosity would not be expected to be the same as the bulk viscosity. However this does not detract from the basic argument for deriving equation 5.48 and when visualised in this way it may be seen that the surface and capillary fluxes would flow under completely different gradients, the surface flux being along a concentration gradient and the capillary condensate flux via a pressure gradient, the concentration being the fixed liquid density. For each particular capillary the change from one mechanism to another would be abrupt since capillary condensate flow cannot occur until the pore becomes saturated and when this happens the surface flow is automatically precluded. For a porous medium the change over would be gradual due to the spectrum of pore sizes. There is no 'a priori' reason why one mechanism should have greater mobility than the other, and in this particular case the possible immobilising effect of the surface viscosity may reduce the mobility of the condensate. We may therefore represent the total flux through the membrane as being the sum of the fluxes in the gas phase, on the surface, and in the capillary condensate. The variation in the contribution of each particular flux to the total flux with changing concentration at the in-going side is shown diagrammatically in figure 5.11. Initially the gas phase flux makes the sole contribution to the total flux, but as the concentration at the in-going side is increased the total flux is augmented and then dominated by the surface component which blocks off the gas phase. At high concentrations capillary condensate sets in in the smaller pores causing a reduction in the surface flux. Then as further condensation occurs in the

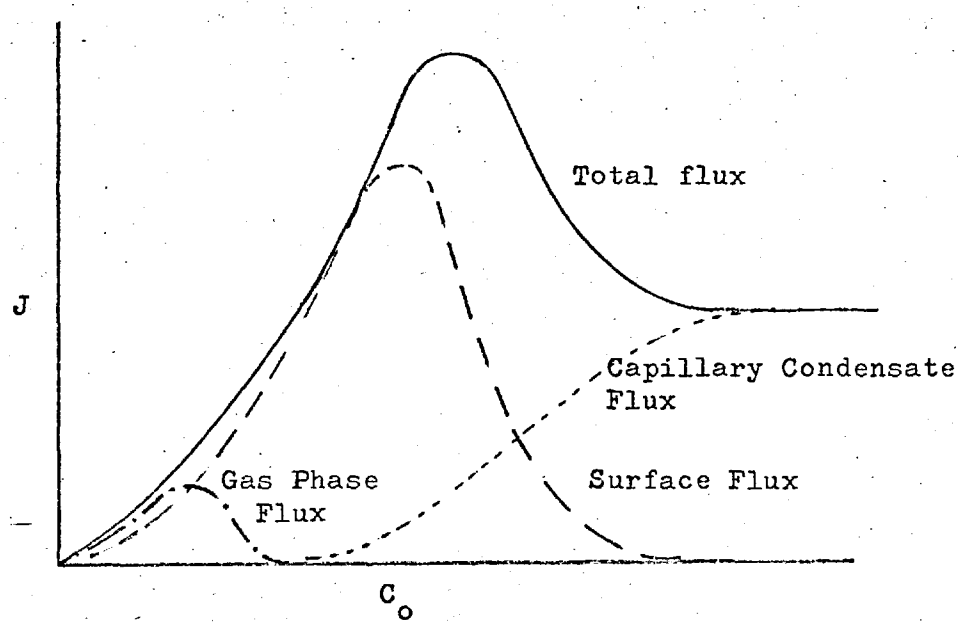

Figure 5.11 Illustrating the contributions of the individual fluxes to the total flux.

the larger pores the flow becomes dominated by the capillary condensate mechanism which because of its reduced mobility in turn reduces the total flux. At - 50 °C the drop in flux (figure 4.25) and permeability (figure 4.27) is remarkably sharp, this does not necessarily mean that the pore size distribution is narrow. Referring back to section 5.2.1 it may be seen that the average pore radius of the medium, $\sim$ 11 Å, lies to one side of a plateau in the plot of θ versus capillary diameter (figure 5.4). This means that at the point of maximum flux a whole range of pores including those of the average pore radius are suddenly filled with capillary condensate and so if the previous argument is correct there will be a sudden cut off in total flux as the mechanism of flow converts from surface flow to capillary condensate flow. At - 40 °C the uptake is less sensitive to the prevailing pressure and so a wider range of pressure is required before

complete saturation is achieved. This is in agreement with figures 4.26 and 4.28 which show that an identical reduction in flux or permeability occurs at a common in-going side concentration irrespective of temperature. Brubaker and Kammermeyer reported a maximum in their permeabilities for ammonia flowing through porous glass. Unfortunately it is not clear if the boundary conditions are the same as in the present work, nor were the fluxes recorded, so the maxima in the permeability may equally well have been due to a point of inflexion in the flux versus pressure graph than a turning point as found here. Apart from the flow of water the only other gases that may show the effect for flow through Carbolac I membranes are hydrogen sulphide and the organic amines. The maximum has not been observed for the flow of 'inert' gases, though Ash, Baker and Barrer (1967) did observe a tailing off of the flux to an almost constant value for the flow of SF_6 through a Graphon membrane. Nor was a maximum found for the flow of acidic gases through Carbolac I (Ash, Barrer and Pope 1963). However, judicious choice of gas and membrane material compacted to very low porosity may reveal other examples of this unusual flow characteristic.

The 'time-lags' were measured for the 0 ^{o}C pilot experiments. Since these proved to be quite long it was decided that the time required for the measurements at the lower temperatures would have interfered with the main program of work so no further transient state measurements were made. What values were obtained are compared in table 5.12 and figure 5.12 with the values calculated according to the method of Ash, Baker and Barrer (1968). Since the data are somewhat meagre no further comment will be made except to say that the positive value for the difference Δ between the calculated and experimental values is in agreement with the

Time-lags for Ammonia through Carbolac I @ 0 °C

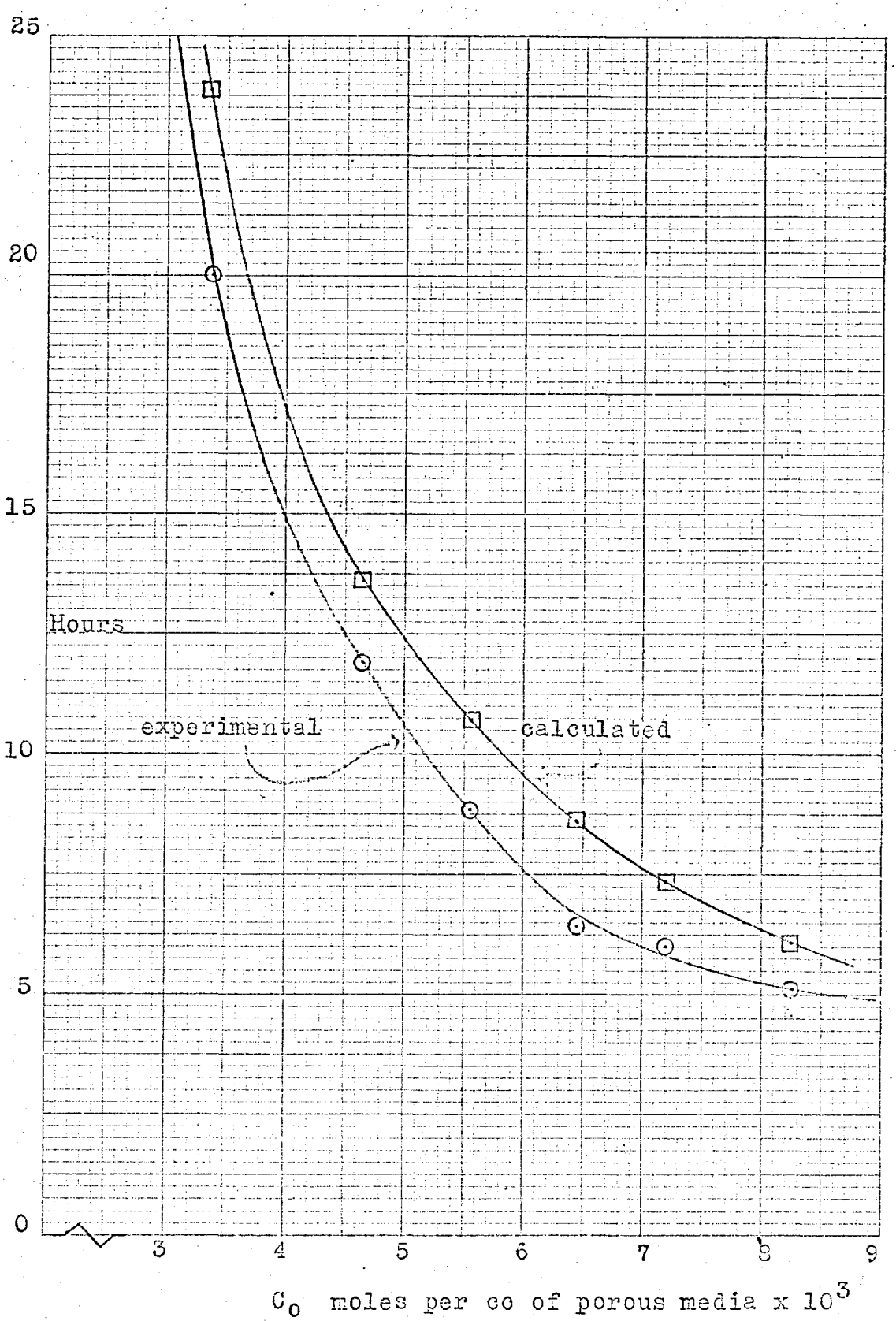

Table 5.12 Time-lags for Ammonia through Carbolac I at 0 °C

L exp. hr	5.10	6.00	6.40	8.87	11.85	20.00
L calc. hr	6.16	7.36	8.65	10.72	13.61	23.82
Δ hr	1.06	1.36	2.25	1.95	1.76	3.82
C_o moles/cc	8.26	7.20	6.46	5.55	4.65	3.39

results found for membranes prepared by several compactions from high area powders. This difference was attributed by Ash, Baker and Barrer to the blind pore character of the membrane.

The surface diffusion coefficients were calculated from the results according to equation 2.52, and are shown as functions of the surface concentration at the in-going side in figure 5.13. At 0 °C the surface flux was calculated from the ammonia/helium mixture runs since these experiments indicated that even at this temperature the sorbed ammonia was beginning to block the gas phase flux. At the lower temperatures the surface flux was approximated to the value of the total flux. The limitations of the integration procedure (D a constant or function of C only) preclude evaluation of the surface diffusion coefficient past the turning point $(dJ/dC_o) = 0$. The graph of D_{ss} versus $C_{o,s}$ is of the correct shape for the surface diffusion coefficient to be proportional to the reciprocal slope of the isotherm, but while the correlation may be correct at the lower coverages, it would be invalid near the maximum in flux due to the onset of viscous flow by capillary condensate in a significant number of the smaller pores near the in-going face of the membrane. Thus the anomalous flow results do not permit a really valid correlation to be made of the type demonstrated by Ash, Baker and Barrer (1967).

Figure 5.13

D_{ss} v C_o for Ammonia through Carbolac I

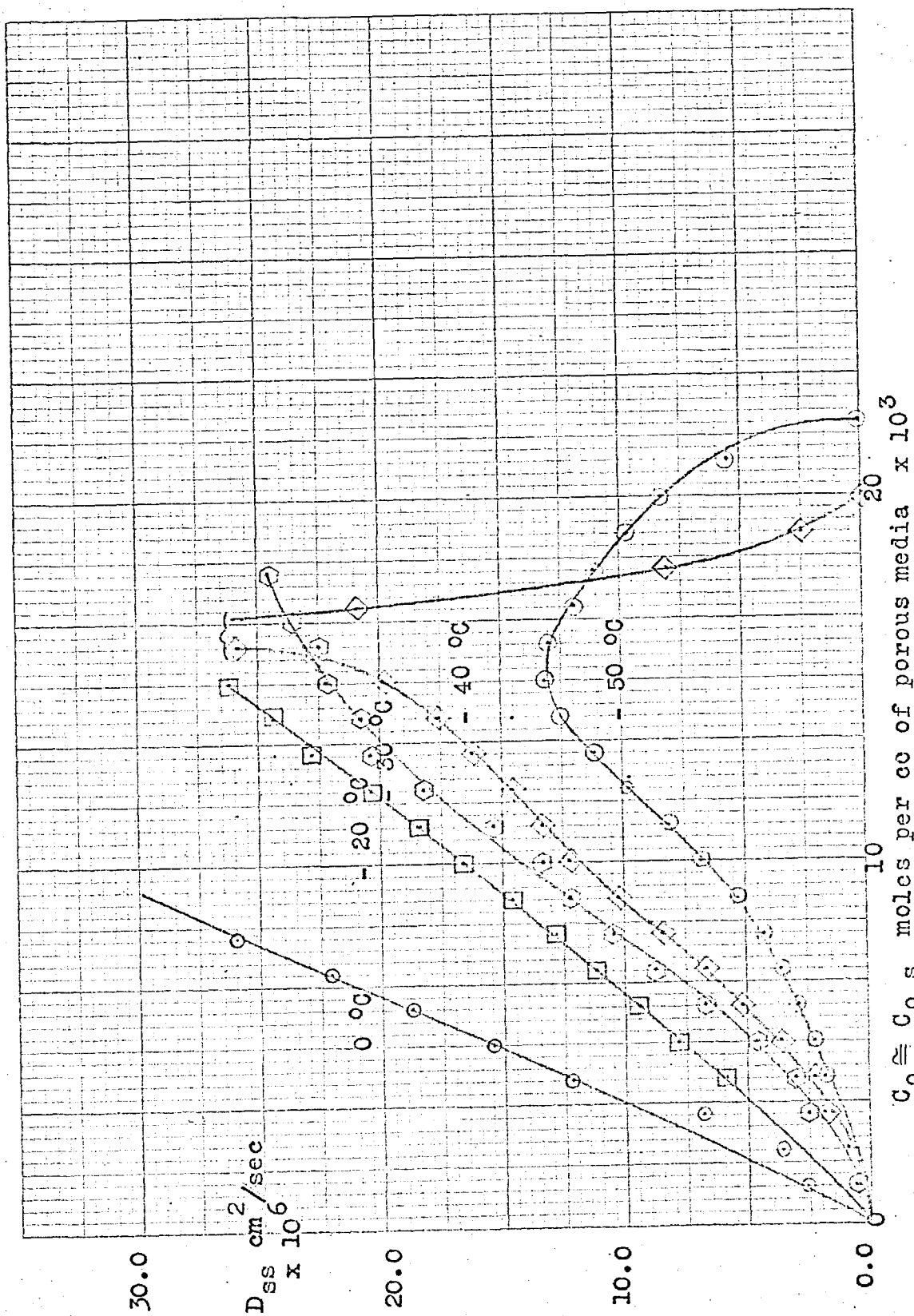

5.4.1 Flow of Ammonia-Helium, Ammonia-Hydrogen and Ammonia-Nitrogen gas mixtures through Carbolac I

The ammonia-helium experiments established two important points. The first the correctness of the method of analysis. Very satisfactory agreement was obtained on comparing the graphs of the ammonia flux versus the ammonia in-going side pressure for the single gas and mixed gas experiments both at 0 and - 40 °C (Figures 4.29 and 4.30). The scatter in figure 4.29 arose from the initial mixture experiments when the author was not fully familiar with the experimental technique. The second point was that the ammonia (i.e. the sorbing component) flowed independently of the helium (i.e. the non-sorbed component). This was demonstrated by set 2. of the 0 °C mixture experiments. In this set the pressure of the ammonia at the in-going side was held constant while the helium pressure was varied from run to run, and it may be seen that within the error of the experiments the ammonia flux remained constant.

The ability of the sorbed ammonia to block off the gas phase is very effectively demonstrated from these helium mixture experiments by plotting the helium permeability constant, $K(M/T)^{\frac{1}{2}}$, as a function of the total ammonia concentration at the in-going side (figure 5.14). The results at the two temperatures form a universal curve which extrapolates to the value of $K(M/T)^{\frac{1}{2}}$ for the pure gas and to the value of C_o for ammonia for a saturated membrane. A similar curve was found by Ash, Barrer and Pope (1963) using a hydrogen-sulphur dioxide mixture flowing through a Carbolac I membrane, however the reported cut-off to hydrogen occurred at 6.5×10^{-3} moles of SO_2 per cc of porous media at the in-going side which was well below the saturation capacity of the membrane of 1.2×10^{-2} moles of SO_2 per cc of porous media.

$K(M/T)^{\frac{1}{2}}$ for Helium / Ammonia mixtures through Carbolac I versus C_o of Ammonia

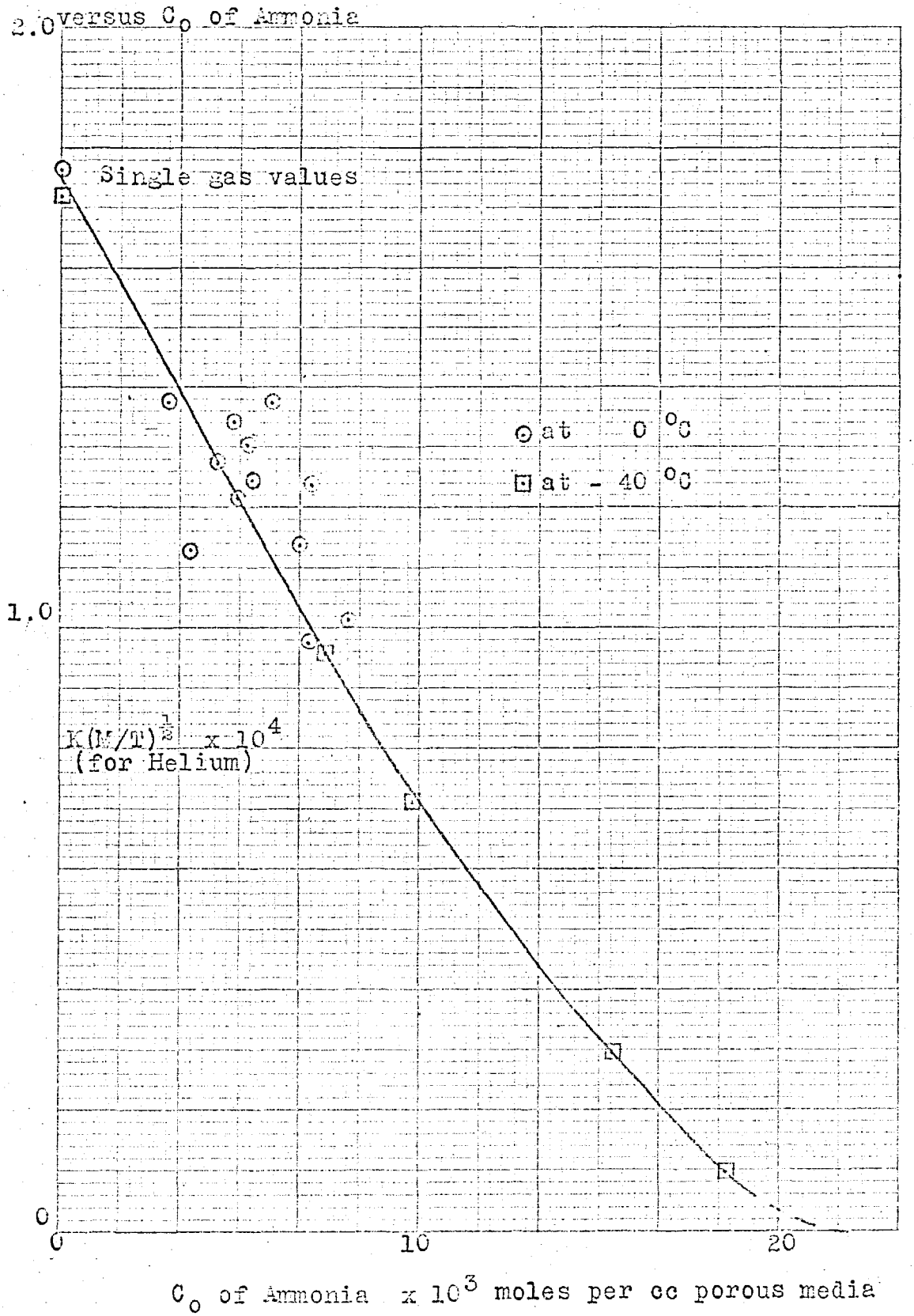

The ammonia-hydrogen and ammonia-nitrogen results were unusual in that the ammonia flux of the gas mixtures diverged from that of the single gas in the vicinity of the saturation concentration at the in-going side (see figure 4.30). The flux from the ammonia-hydrogen mixture monotonically increased with increasing ammonia concentration at the in-going side, but that from the ammonia-nitrogen mixture did reach a maximum value although well above that of the single gas. This may have been due to the experimental method. In the single gas experiments the gas in the vicinity of the in-going side of the membrane was at the membrane temperature. However, in the mixture experiments the gas had to be streamed past the in-going face, and since most of the gas circulation system was at room temperature it is doubtful that the gas mixture was at the temperature of the membrane as it passed the in-going face in spite of the primary and secondary cooling coils. Once the gas had entered the membrane either in the sorbed or gaseous state then the large heat reservoir of the membrane and steel holder would have quickly brought the gas to the equilibrium temperature. In the - 40 ^{o}C temperature region comparison of the ammonia isotherms indicates that the uptake and hence formation of capillary condensate is very sensitive to temperature, so no condensate will be formed at the in-going face if the face is even slightly above the required temperature. Nor will condensate form a small distance inside the membrane even though the membrane is at the correct temperature for the pressure will have dropped below that required for the formation of capillary condensate. With ammonia these temperature and pressure effects will be particularly sensitive at - 40 ^{o}C. The flattening-off of the ammonia flux in the ammonia-nitrogen mixtures at the higher pressures does indicate that condensate will eventually be formed.

An alternative demonstration of blockage of the non- or weakly sorbed components by the ammonia is shown in figure 5.15. Here the ratio of the experimental permeability of the single gas experiments to the experimental permeability in the mixture for helium, hydrogen and nitrogen in their respective ammonia mixtures is plotted as a function of the ammonia concentration at the in-going side. Ideally in the absence of blockage the ratio will be 1 and for complete blockage 0. The curves for each gas will not be co-incident except at their limiting values of none or complete blockage, because of the differing contributions to the single gas permeabilities by the surface flow. The interference of the surface flow by the sorbed ammonia is demonstrated in figure 5.16. The theoretical permeability for the pure gas phase flow of either hydrogen or nitrogen in their respective ammonia mixtures can be calculated from the ammonia-helium results, this permeability is referred to as $K_{(Calc.)}$ and may be compared with the observed permeability in the gas mixture $K_{(Exp.)}$. Figure 5.16 is a plot of the ratio $K_{(Calc.)}/K_{(Exp.)}$ as a function of the ammonia concentration at the in-going side. For pure gas phase flow the ratio is 1 and it may be seen that the sorbed ammonia quickly restricted the hydrogen flow to the gas phase. For nitrogen which had a much larger surface flow contribution in the single gas experiments, the reduction of suface flux is almost on an equal footing with the degree of blockage in the gas phase. The number of points on the graph is somewhat limited because of the small number of helium results. The result at 1.5 moles per cc was recalculated from the hydrogen results assuming that the hydrogen flow was purely in the gas phase at this stage and the value (indicated by the broken square) is in much better agreement with the other nitrogen results. This apparent surface flow of nitrogen above the monolayer

Reduction of permeability, K, of He, N_2 and H_2 in NH_3 mixtures relative to the single gas value versus C_o of NH_3

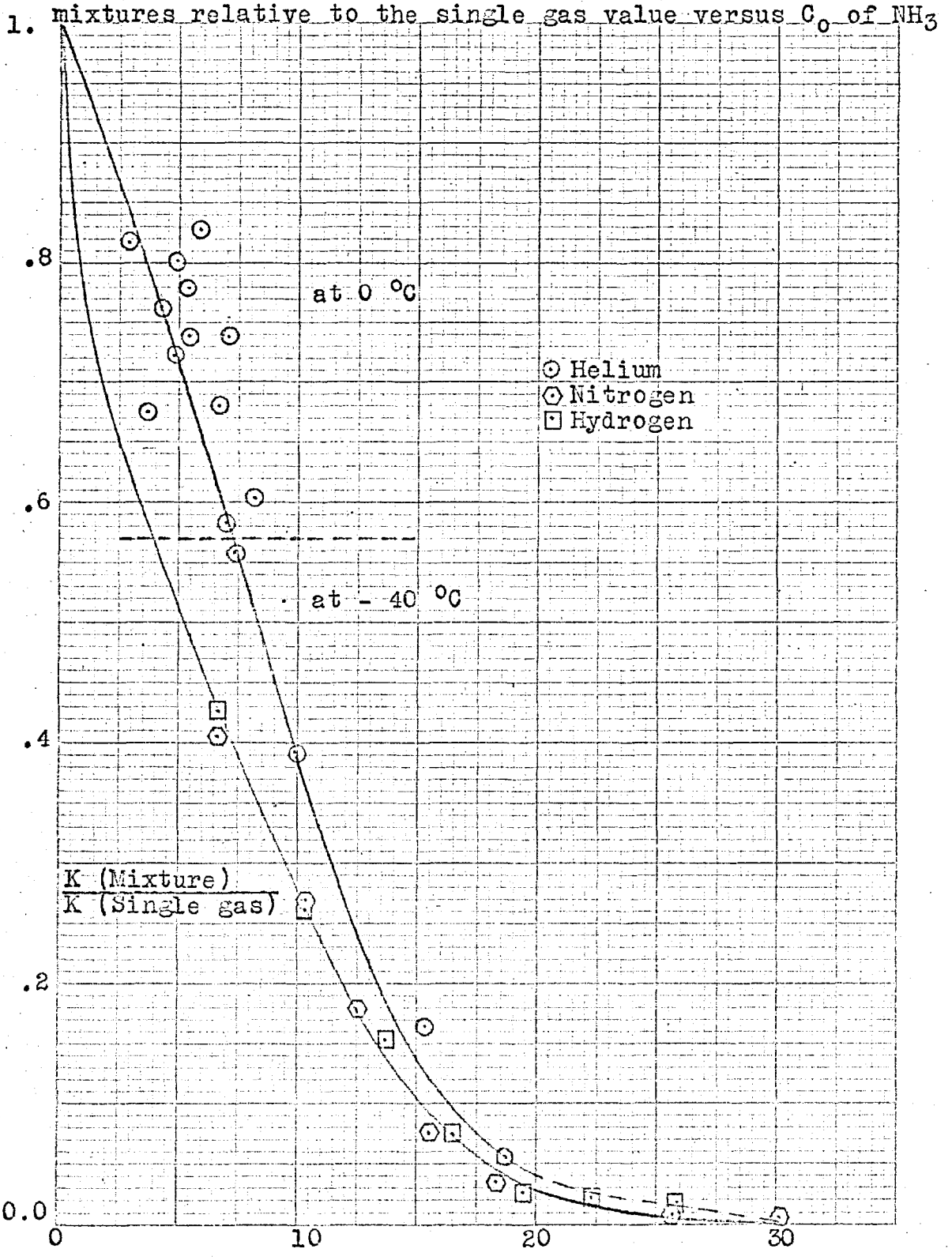

$K_{(Calc.)}/K_{(Exp.)}$ v C_o of NH_3 for H_2 and N_2 in NH_3 mixtures

$K_{(Calc.)}$ determined from He/NH_3 experiments

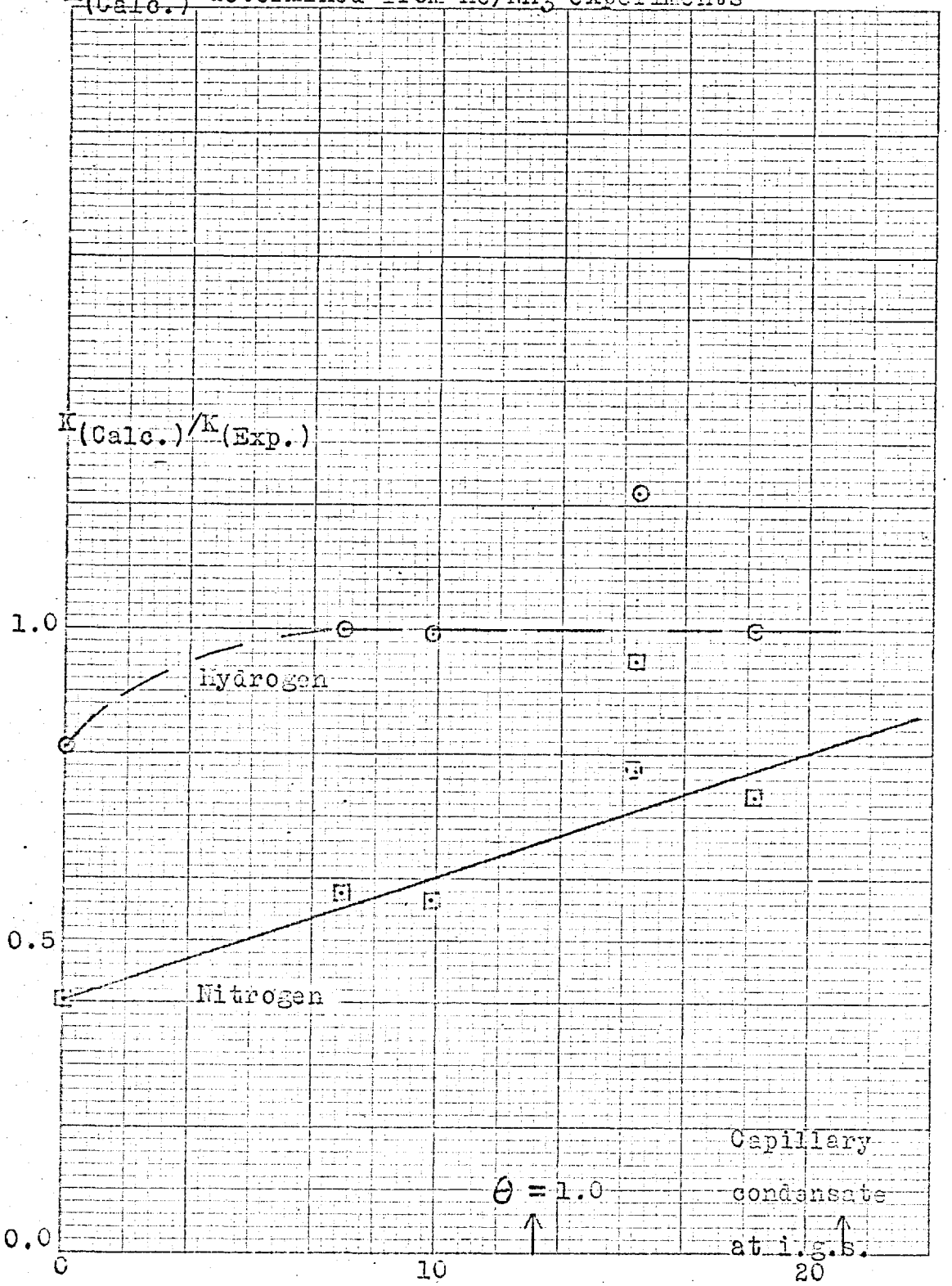

C_o of NH_3 x 10^3 in moles per cc porous media

capacity of sorbed ammonia may be due to the nitrogen dissolving to a small extent in the ammonia film.

Since the experiments show that the helium flux is proportional to its pressure gradient, and that the flow of ammonia is unaffected by the helium flux in the ammonia-helium mixture experiements, then it is possible to make a quantitative estimation of the steady state diffusion coefficient of helium in the blocked membrane following the procedure suggested by Ash, Barrer and Pope (1963). Under these conditions we may calculate from the results of the mixture flow experiments the concentration of helium at the in-going side that would be necessary to maintain a constant flux of helium as the in-going side concentration of ammonia was varied. The corresponding graph of $C_{o,He}$ versus C_{o,NH_3} allows us to evaluate $(dC_{He}/dC_{NH_3})_{J_{He}}$ for constant flux J_{He} of helium. The ammonia surface diffusion coefficient has already been evaluated as a function of the ammonia in-going side concentration in section 5.3.4, and rewriting equation 2.53 allows us to evaluate (dC_{NH_3}/dx),

$$\frac{dC_{NH_3}}{dx} = -\left(\frac{J}{D}\right)_{C_{o,NH_3}} \qquad 5.52$$

Now the flux J_{He} is given by

$$J_{He} = -D_{gs}^{He}\cdot\left(\frac{dC_{He}}{dx}\right)_{J_{He}} \qquad 5.53$$

which rearranges to

$$J_{He} = D_{gs}^{He}\cdot\left(\frac{dC_{He}}{dC_{NH_3}}\right)_{J_{He}}\cdot\left(\frac{J_{NH_3}}{D_{NH_3}}\right)_{C_{o,NH_3}} \qquad 5.54$$

$$\text{or } \left(D_{gs}\right)_{J_{He}} = J_{He}\cdot\left(\frac{D_{NH_3}}{J_{NH_3}}\right)_{C_{o,NH_3}}\cdot\left(\frac{dC_{NH_3}}{dC_{He}}\right)_{J_{He}} \qquad 5.55$$

Log D_{He} and Log D_{H_2} versus C_{o,NH_3}

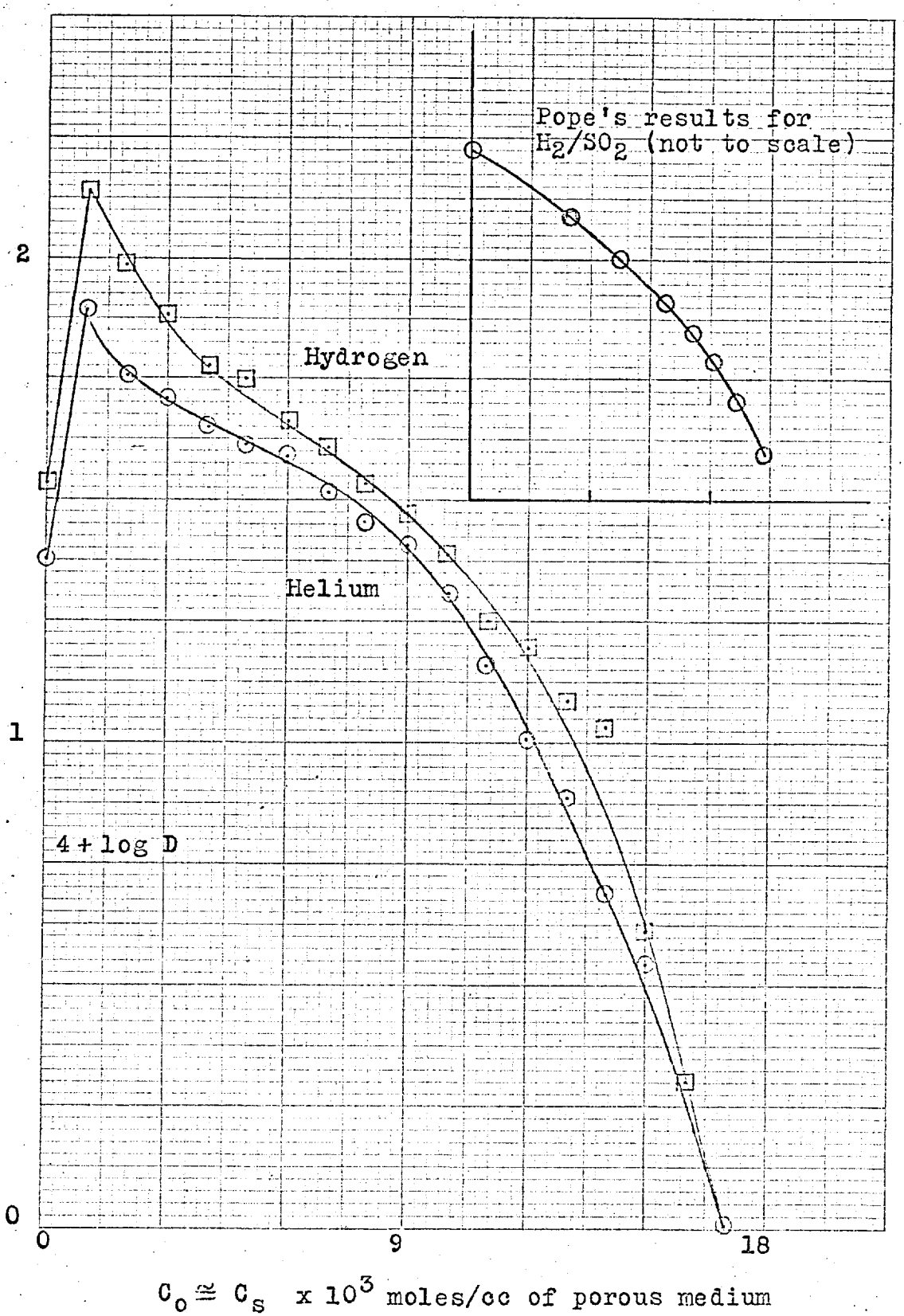

and all the terms on the r.h.s. of the equation may be evaluated. Since figure 5.16 indicates that the hydrogen flux of the ammonia-hydrogen experiments is solely in the gas phase the above analysis may also be applied to these mixture experiments as well.

The scatter of results from the ammonia-helium experiments at 0 °C proved to be too large to allow any worthwhile calculations to be made. The results from the calculations for the - 40 °C ammonia-helium and ammonia-hydrogen mixtures were disappointing. A plot of $\log(D_{gs})_J$ for helium and hydrogen versus C_{o,NH_3} is shown in figure 5.17 together with an inset diagram of the results obtained by Ash, Barrer and Pope (1963) for a hydrogen-sulphur dioxide mixture. The curves should extrapolate to the value for the pure non-sorbed gas as found for the hydrogen-sulphur dioxide case. The discrepancy may be traced back to the value for the ammonia concentration at the in-going side. The discussion in the previous section indicated that C_{o,NH_3} was over-estimated because the adsorption was measured on unrestrained chips. This in turn causes the term $(dC_{NH_3}/dC_{He})_{J_{He}}$ to be too large and hence the value for $(D_{gs})_{J_{He}}$. The argument also applies to the ammonia-hydrogen results, but not to those of Ash, Barrer and Pope (1963) because the sulphur dioxide adsorption isotherm was measured on a restrained membrane.

Another demonstration of progressive blockage is to be found by comparing the ammonia gas phase flux calculated from the pure helium flow runs, J_g, and the ammonia gas phase flux calculated from the ammonia-helium mixture runs, $\mathcal{J}_g$. A plot of $\mathcal{J}_g^{NH_3}$ versus the pressure at the in-going side, $P_{i.g.s.}$, is given in figure 5.18. In the absence of blockage the graph would be linear. Even at 0 °C a slight curve may be

$\mathcal{F}_g$ v $P_{i.g.s.}$ for Ammonia of the ammonia mixtures.

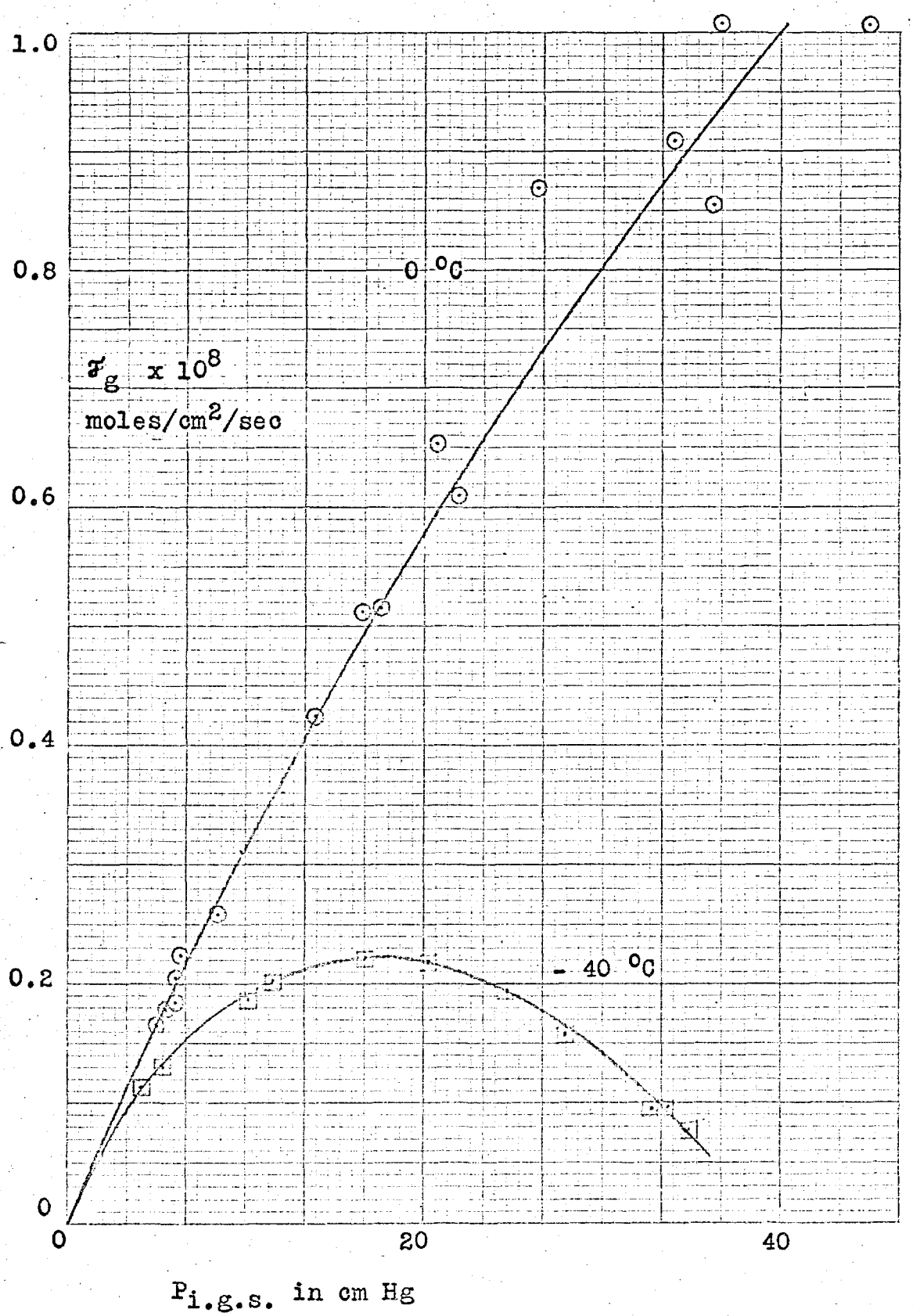

Ammonia concentration profiles for fluxes $\mathcal{F}_g$ and J'_g

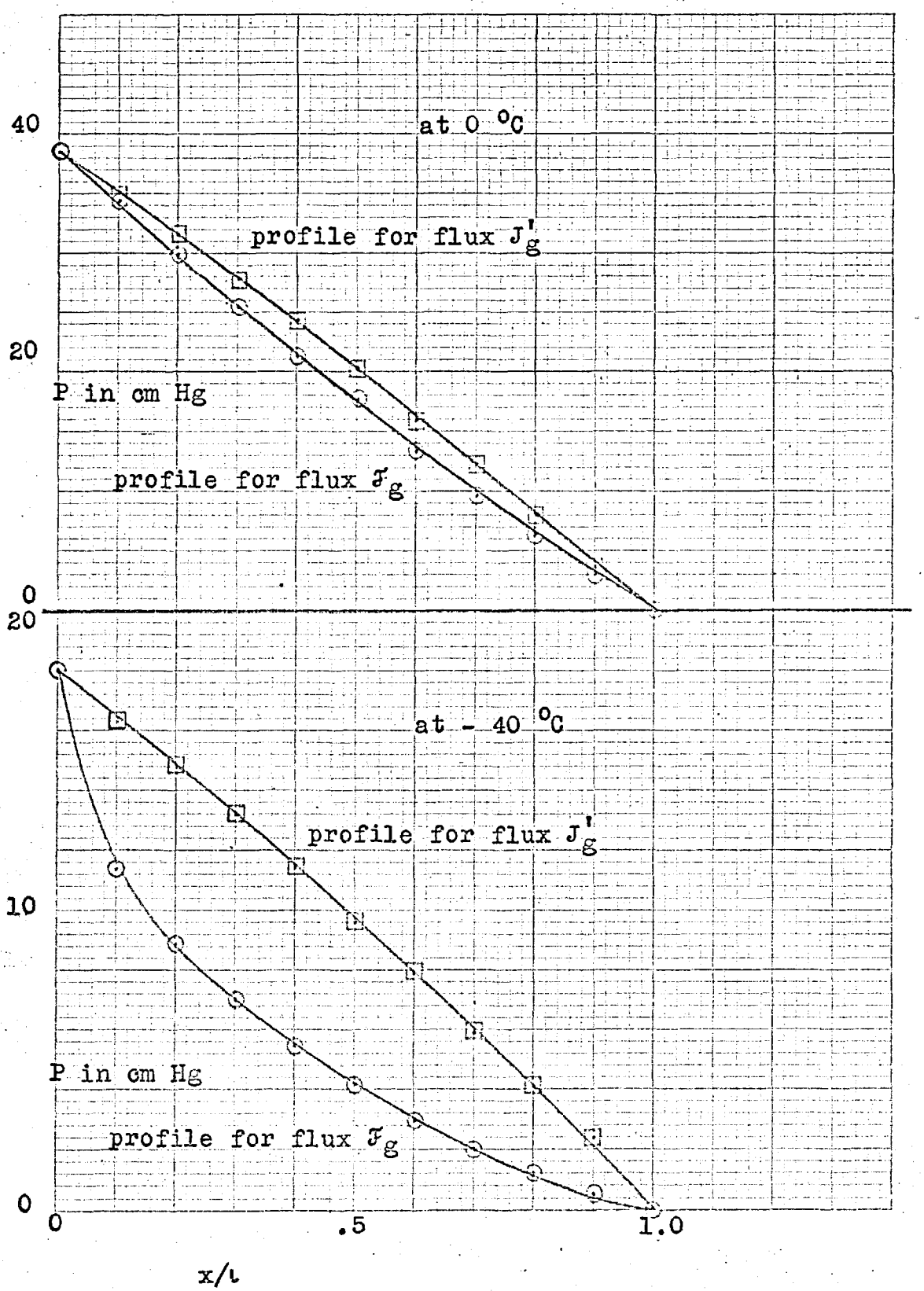

detected indicating a reduction in pore size due to adsorbed material, while at - 40 °C the uptake is so large as to actually reduce the gas phase flux with increasing pressure at the in-going side.

Following the procedure out-lined in sections 2.1.5 and 2.1.7 together with figures 5.17 ($\mathcal{F}_g$ v P), 4.26 ($\sim J_s$ v $\sim C_s$), and 4.12 (the NH_3 adsorption isotherm), it was possible to calculate the gas phase concentration profiles for the fluxes $\mathcal{F}_g$ and J'_g for ammonia. For the 0 °C example the profile was determined for the flux $\mathcal{F}_g = 1.0 \times 10^{-8}$ moles/cm^2/sec, and for the - 40 °C example the profile was for the maximum value of $\mathcal{F}_g$ of 0.222×10^{-8} moles/cm^2/sec. The graph, figure 5.19, demonstrates the difference between the two fluxes and the contribution to the pressure profile arising in the partially blocked medium due to the existence of a mobile adsorbed layer.

An estimate of J'_g may be made from the profiles if it is assumed that at a particular pressure, P, $D_{gs}^{NH_3}$ is the same for both $\mathcal{F}_g$ and J'_g. In this case

$$\frac{\mathcal{F}_g}{J'_g} = \frac{\text{gradient for profile of } \mathcal{F}_g}{\text{gradient for profile of } J'_g} \qquad 5.56$$

Since $\mathcal{F}_g$ is known, J'_g can be found. The assumption regarding $D_{gs}^{NH_3}$ can only be regarded as an approximation, because somewhat different pore geometries may be involved in $\mathcal{F}_g$ and J'_g. The derived values together with the necessary data for the profiles are listed in appendix 7.

Previous studies (Carman 1952, Ash, Barrer and Pope 1963) have attempted to correlate the surface and capillary condensate flow through microporous media with Wyckoff and Botset's (1936) studies of the flow of air-water mixtures through sand beds. The comparison was made by plotting the relative permeabilities K_r against the percentage saturation

of the relevant porous medium. K_r being defined as

$$K_r = \frac{\text{Permeability in unblocked medium}}{\text{Permeability in blocked medium}} \qquad 5.57$$

In this case the ammonia permeability drops on forming a capillary condensate and there is no correlation.

5.4.2 Flow of Nitrogen-Hydrogen gas mixtures through Carbolac I

The nitrogen-hydrogen results indicate that each gas is flowing independently of each other in both the gas phase and on the surface. This suggests that the transport in dilute films takes place by a diffusive mechanism. This is in agreement with the results of Aylmore and Barrer (1966) who studied the flow of krypton-carbon dioxide and krypton-nitrogen mixtures through a Carbolac I compact both in and just above the Henry law region of adsorption. Pope (1967) using an entirely different technique observed that the flow of sulphur dioxide at low surface coverage through a Spheron 6 (2700) compact did not obey the Darken relationship

$$D_{ss} = D^*_{ss} \cdot \left(\frac{\partial \ln a'}{\partial \ln C}\right) \qquad 5.58$$

which relates the surface diffusion coefficient D_{ss} with the surface self-diffusion coefficient D^*_{ss}. This latter coefficient was obtained from counter-current flow of radio-active sulphur dioxide through unlabelled sulphur dioxide there being no total pressure gradient between the faces of the membrane. a' and $\int^{C}_{\lambda}$ represented the activity and concentration of the adsorbed species. Pope attributed the failure of the Darken equation to the surface flow not being fully diffusive. Ash and Barrer (1967) re-examined the validity of the Darken equation from the approach of irreversible thermodynamics, and showed that independent of

the mechanism of flow the correct relationship was

$$D_{A^*} = D_A \left(1 - \frac{C_A L_{A^*A}}{C_{A^*} L_{AA}}\right) \frac{\partial \ln C_A}{\partial \ln a'_A} \qquad 5.59$$

where the L terms are the coefficients of the general thermodynamic relationships for the surface fluxes

$J_A = L_{AA}.X_A + L_{AA^*}.X_{A^*}$ for the unlabelled gas

$J_{A^*} = L_{A^*A^*}.X_{A^*} + L_{A^*A}.X_A$ for the labelled gas

The expression $(C_A L_{A^*A}/C_{A^*} L_{AA})$ accounts for any interaction between the surface flows through the term L_{A^*A} and would be expected to become significant towards higher coverages. However this does not indicate whether or not the flow is diffusive, for in Pope's counter-current experiments where there is no pressure gradient the flow was necessarily diffusive even though there was a measurable value of L_{A^*A}. Hence Pope's method would not establish the mechanism of flow. A possible solution to the problem would be the study over a wide temperature range of a gas pair such as nitrogen and oxygen, or hydrogen and deuterium, which had similar adsorption isotherms. At the higher temperatures in the Henry law region the mechanism would be expected to be diffusive and there would be a separative effect between the flowing components. As the temperature was lowered then the hydrodynamic flow would come to the fore with a corresponding reduction in the separative effect.

5.5 Gas separation

The enrichment factors were calculated according to equation 2.57 and are listed in appendix 7 . For the three ammonia gas pairs there was always enrichment in favour of the ammonia, and in some cases this would be almost to the complete exclusion of the other gases. Figure 5.20 shows a

Enrichment factors for He/NH_3 pair at 0 °C through Carbolac I

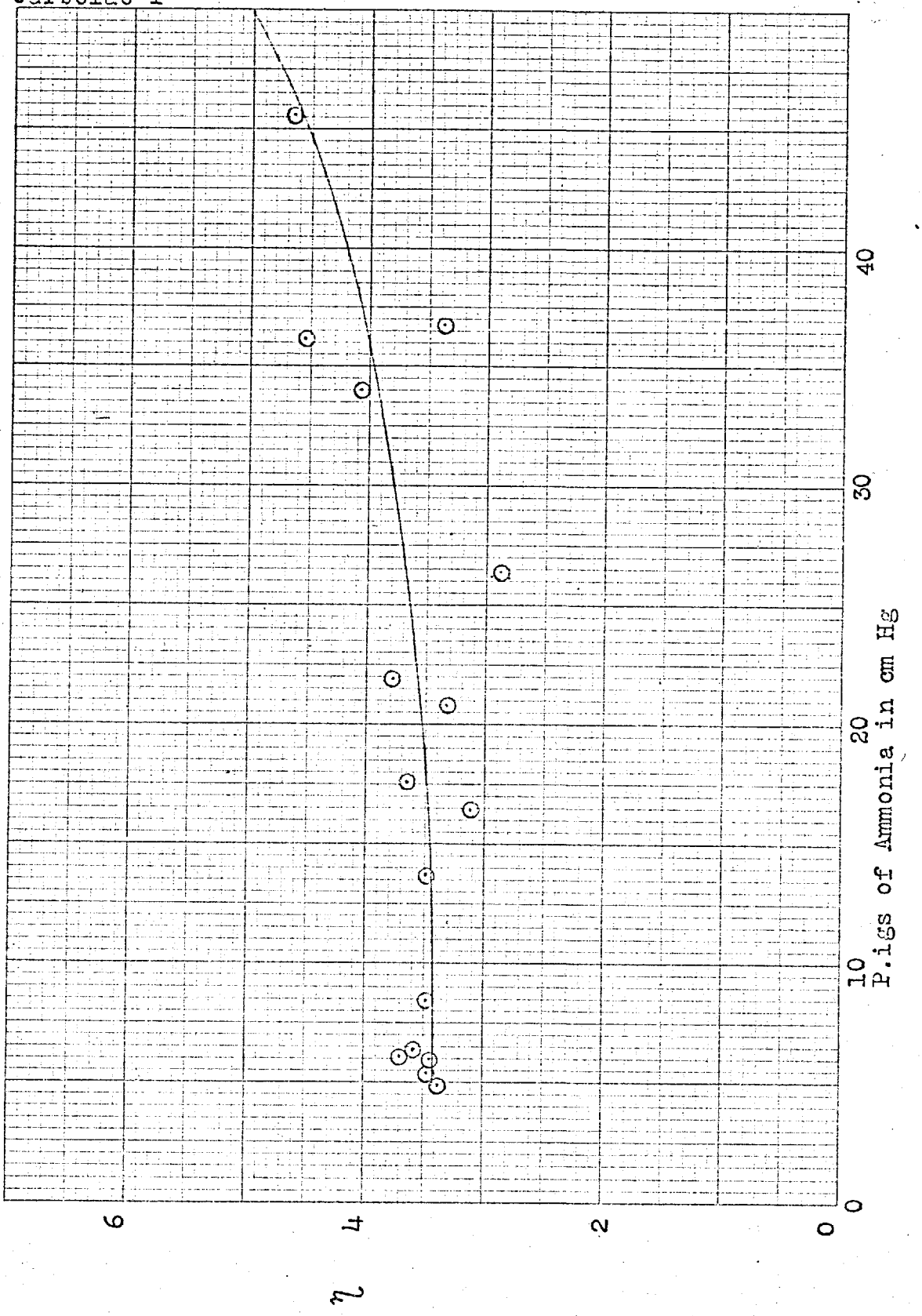

Figure 5.21

Enrichment factors for He/NH_3, H_2/NH_3, N_2/NH_3 pairs through Carbolac I at - 40 °C

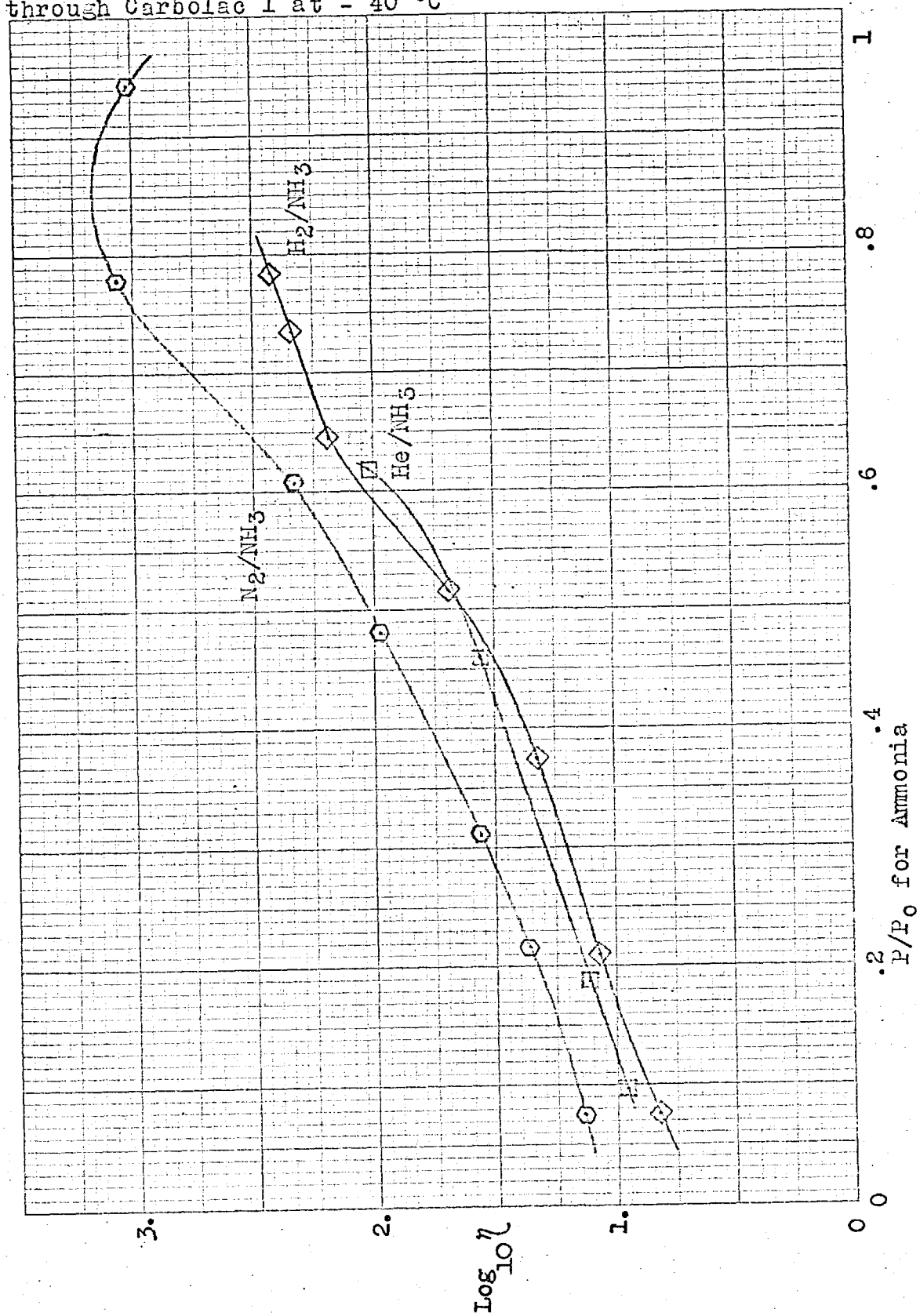

plot of the ammonia enrichment factor for the ammonia-helium experiments at 0 °C as a function of the ammonia pressure at the in-going side; while figure 5.21 is for the ammonia-helium, ammonia-hydrogen and ammonia-nitrogen pairs at - 40 °C. This is shown as a plot of $\log\eta$ versus the ammonia relative pressure P/P_o (NH_3). It may be seen that the sorbed ammonia allows good separations to be obtained at a relative pressure of 0.5, while at 0.8 the membrane has effectively become semi-permeable to ammonia. For the single gas past this point there is a reduction of flow due to the formation of capillary condensate at the in-going face, but the mixture experiments indicate that if the in-going face can be heated to above the temperature for the formation of capillary condensate then even more efficient separations would be obtained. This situation could be used to advantage for certain types of catalytic synthesis in which the reactants are non- or weakly sorbing gases and the products strongly sorbing vapours. The reactor would simply be a membrane capable of sorbing the products up to the limit of capillary condensate, and the in-going face would provide the catalyst surface. The membrane medium may act as the catalyst or be a support material in which case the catalyst would be located on a micro thin section of the membrane at the in-going face. The main body of the membrane would be held at the sorbing temperature of the product, but the in-going face would be heated up to the reaction temperature either by the reactants or by some external heating unit using heat radiation or the 'Piezo' electric effect. The reaction would take place at the in-going face. The products would then flow from the face into the cold membrane with accompanying heavy adsorption so blocking the gas phase flux of the reactants. This immediate separation of products from reactants means that the process

would proceed to 100% conversion. Typical reactions would be the ammonia synthesis, nitrogen fixation, and organic synthesis from basic petroleum materials.

The nitrogen-hydrogen enrichment factor is independent of either gas. In this particular case the nitrogen surface flow is not yet large enough to out-weigh the gas phase separation factor of $(M_{H_2}/M_{N_2})^{\frac{1}{2}}$, and is an example of the surface flow actually reducing the effective separation.

CHAPTER 6

SUMMARY AND RECOMMENDATIONS FOR FUTURE WORK

The flow of four binary gas mixtures (NH_3/He, NH_3/H_2 NH_3/N_2 and N_2/H_2) through a microporous membrane was studied. The membrane was prepared by compressing the carbon black Carbolac I into a steel tube. The gas mixtures were chosen with the view for the possible development of a new technique for the separation of ammonia synthesis gas from its reactants nitrogen and hydrogen. The NH_3/He system was required for determining ammonia gas phase fluxes using the helium as an indicator gas non-sorbed but admixed with the ammonia gas phase. For the three ammonia mixtures the ammonia flowed independently of any of the admixed gases while the admixed gas was greatly reduced by the presence of sorbed ammonia. Excellent separations of ammonia for all the mixtures was obtained, in the limit the membrane becoming semi-permeable to ammonia. This was due to the sorbed ammonia blocking the other gases which were principally in the gas phase.

The individual components of the N_2/H_2 flowed independently of each other both in the gas phase and on the surface.

A study of the flow of ammonia in the region of its saturation vapour pressure revealed the unusual feature of a reduction in flux as capillary condensate set in. In investigating this effect it was revealed that the adsorption data which were measured on unrestrained chips of compressed Carbolac I do not necessarily apply for adsorption isotherms on the constrained membrane. It is recommended that adsorption isotherms of strongly adsorbing gases should be measured on restrained samples compressed to a similar porosity to that of the membrane if the data are to be used for flow experiments.

A critical examination was made for the evidence of helium surface flow through a carbon membrane made from Graphon. It was concluded that within the temperature range 300 to - 200 °C there is no helium surface flow. It was considered that this also applied to the Carbolac I membrane, but the instability of the surface prevented thorough investigation of this point.

A detailed analysis of the Carbolac I material showed it to be principally a very fine particle alkaline carbon. It has a very large surface area which is almost completely covered with an acidic surface oxide. The particles are riddled with micropores which contribute about two thirds of the surface area. Compaction of the powder produced a membrane with a fairly narrow pore distribution, the mean pore diameter being of the order of a few molecular diameters.

Significant differences between the permeability of hydrogen and its isotope deuterium at - 40 °C were found, and could form the basis of a means of separating the isotopes. A marked increase in the adsorption of deuterium over hydrogen was found for adsorption at liquid nitrogen temperatures. Two possible reasons were suggested for this effect. The first was that there is a difference in the zero point energy for the adsorption bond, the second was the different isomer contributions to the rate of adsorption. No conclusion could be drawn as to which explanation was correct.

Several questions have arisen from this project. The first concerns the uniqueness of the ammonia flow results. A number of experiments were suggested in section 5.3.4 to explore this unusual effect. The second concerns the mechanism of surface and capillary condensate flow. For very low uptakes the mechanism is undoubtedly diffusive, but it is still not clear where a change over to a hydrodynamic mechanism occurs. A suitable series of

experiments for identifying this region was suggested in section 5.4.2. The third question was the difference in the hydrogen and deuterium adsorption at low temperatures on Carbolac I which was discussed in section 5.2.3.

The final apparatus proved to be adequate for the purpose. However two improvements are suggested. The first concerns the gas circulation pump. This tended to be temperamental and also produced considerable glass dust. It is recommended that future work incorporates a mercury piston pump of the type shown in figure 6.1 and based on a design by Murphy (1968). The valve system is essentially that used here and by adjusting the pistons to be 180° out of phase to each other there will be no major pressure fluctuations. The success of this type of pump lies in using wide bore cylinders and wide mercury flow lines together with a lazy pumping action.

The second improvement is with the gas analysis gauge. By including a wider bore section in the lower part of the standard and analysing capillaries together with a wide bore vacuum limb the pressure range of the gauge could be much improved. A diagram of the modified gauge is shown in figure 6.2. Analysis of hydrogen-deuterium mixtures may be difficult due to the ortho and para isomers of the isotopes changing through adsorption to the equilibrium concentrations for the temperature of the membrane through which they are diffusing. Particularly at low temperatures this would affect the thermal conductivity of the gas. In this case the soundest method of analysis would be by mass spectrometer. Finally it is recommended that a separate analysis system be included in the in-going side.

Figure 6.1 THE CIRCULATING PUMP

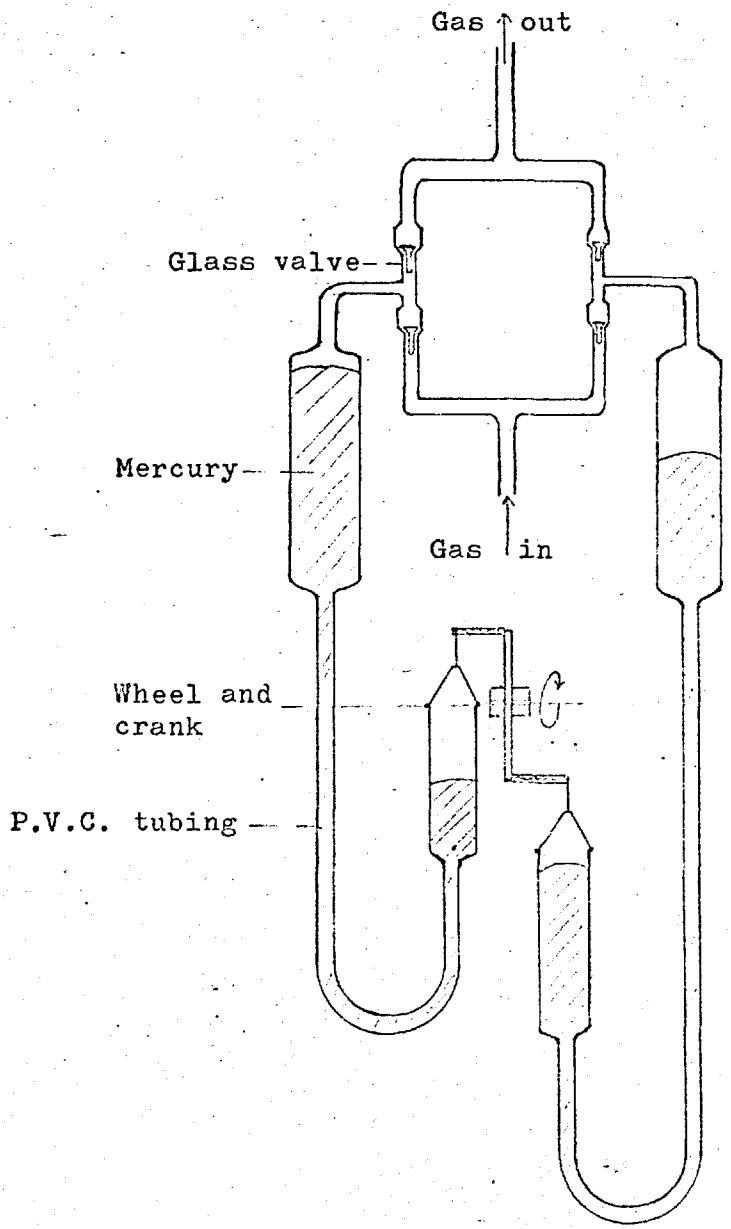

Figure 6.2 MODIFIED GAS ANALYSIS GAUGE

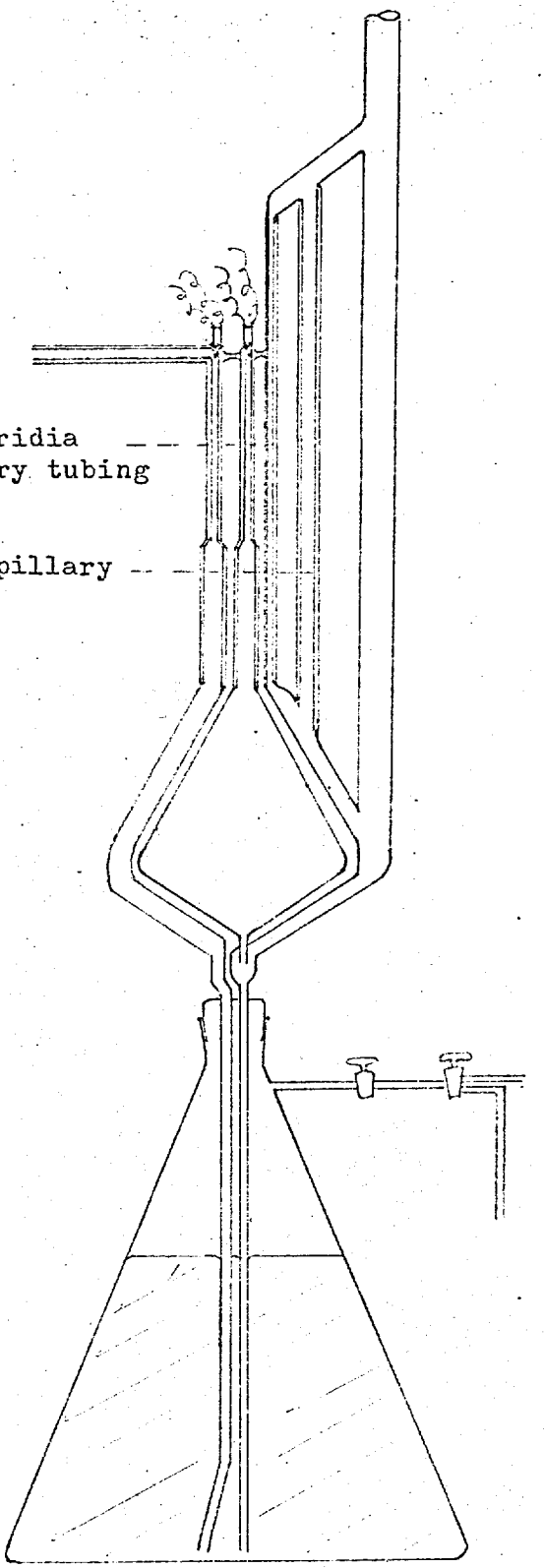

TABLE of SYMBOLS

Symbol		Identifying equation
A	Surface area of solid (cm^3/cm^3 or g of porous medium) calculated from ∞ B.E.T. equation	2.3
	(A_t, A_f, A_w, A_{em}, A_n, A'_n are surface areas in the above units as discussed in section 5.2.1)	
A'	Summation of constants	5.29
A_c	Cross-sectional area of porous medium (cm^2)	2.4
a	Molecular radius (Å) (section 5.2.1)	
a*	Mean jump distance along the surface (Å)	5.42
a'	Activity	5.58
B	Summation of constants	5.29
b_s	Degree of pore saturation in Kozeny equation	5.49
C	Total concentration (moles/cm^3 of porous medium) (Subscripted A, B, or superscripted He, NH_3, etc for concentration of a particular species, superscripted 1, 2, . , n, . , x for a series of experiments)	
C_g	Gas phase concentration (moles/cm^3 of porous medium)	2.16
C_g^g	Gas phase concentration (moles/cm^3 of void space)	2.16
C_s	Surface concentration (moles/cm^3 of porous medium)	2.15
C_s^s	Surface concentration (moles/cm^2 of solid)	2.15
	Prefix Δ for a concentration drop, subscripted o concentration at the in-going side, subscripted ι concentration at the out-going side, subscripted e refers to the equilibrium concentration of equation	5.13
C'	Constant of integration	2.76
c	Velocity of light	
c_t	Concentration of isomer in rate equation after time t	5.12
c_o	Initial concentration of isomer in rate equation	5.12
D'	Spectroscopic dissociation energy (cal/mole)	5.11
D^o	Thermal dissociation energy (cal/mole)	5.11

D	The diffusion coefficient (cm^2/sec) (Discussed in section 2.1.9)	2.6
D_{gs}	The steady state gas phase diffusion coefficient (cm^2/sec)	2.32
D_{ss}	The steady state surface diffusion coefficient (cm^2/sec)	2.23
	The diffusion coefficient is defined by its respective Fick equation and in addition to the above the following were used:- D'_{ss} 2.24, D_e 2.25, D^o_{gs} and D^o_{ss} 2.34, D_a case 2 and D_b case 3 of section 2.1.8, and D^*_{ss} 5.58	
"ΔE"	Energy of Henry law adsorption (cal/mole)	2.71
E^*	Activation energy for surface diffusion (cal/mole).	5.33
ΔE	Energy of frequency shift (cal/mole) (section 5.1.6)	
$E_{v=o}$	Zero point energy (cal/mole)	5.11
f	Fraction of molecules randomly scattered	2.2
G_1, G_2	Kammermeyer's structure factors	5.26
$\Delta\bar{H}$	Partial molar heat of adsorption (cal/mole)	2.59
ΔH	Integral molar heat of adsorption (cal/mole)	2.66
$\Delta\tilde{H}$	Molar heat of adsorption at constant spreading pressure (cal/mole)	2.67
"ΔH"	Heat of Henry law adsorption (cal/mole)	2.70
$\Delta\mathcal{H}$	Molar heat of adsorption at constant chemical potential (cal/mole)	2.74
h	Planck's constant	
J	Flux (moles/cm^2 of membrane/sec)	2.5
	Equation for experimental evaluation	4.3
	The following fluxes were defined for different phases and type of flow:- J_g 2.21, J_s 2.21, J'_g 2.22, J'_s 2.22, J_e 2.25. The experimental fluxes $\mathcal{F}_g$ and $\mathcal{F}_s$ were defined in section 4.4.1 The fluxes were subscripted A, B, or superscripted He, NH_3, etc for a species and superscripted 1, 2, . , n, . , x, for a series	

K	The permeability (cm^2/sec). Defined by equation 2.5, evaluated by equation 4.7 and discussed in detail in section 2.1.8	
	K_K Knudsen permeability for a single capillary	2.1
	K_k Knudsen permeability for porous media	2.4
	$K_B \equiv K$ by Barrer's definition	
	K_c Carman's definition of permeability	
	K_h Knudsen permeability for a repeatedly bent single capillary	
	K_T case 1, K_T^C case 2, K_T^S case 3 of section 2.1.8	
	K_{CC} defined by equation	2.48
	K_{SS} defined by equation	2.49
	K_C an experimental permeability defined by	4.8
	K_r relative permeability defined by	5.57
k	Constant of equation	2.32
k	Force constant	5.10
k	Rate constant	5.12
k_S	Henry law adsorption constant	2.18
L	Time-lag (hours) section 5.1.9 L_1 a calculated time-lag with D a constant or function of C only L_1^1 a calculated time-lag with D a known function of x	
L	The phenomenological coefficient Subscripted for species and cross coefficients	2.7
l	Length of membrane (cm)	2.1
M	Molecular weight. Subscripted A, B, He, NH_3, etc for species, and a for adsorbent	
n_s	Moles of adsorbate	2.61
Q	Kammermeyer's definition of permeability	5.30
q_{st}	Isosteric heat (cal/mole)	2.63
P	Pressure (cm Hg) Subscripted 1, 2, for different temperatures. P^o standard pressure, P' adsorbing pressure section 3.2, P_o saturation vapour pressure	
R	The gas constant per mole	
r	Capillary radius	2.1
r_h	Hydraulic radius	
T	Temperature. Subscripted 1, 2, for different temperatures, d for dead space, b for burette space, r for room temperature, p for membrane temperature	

t	Time (sec)	4.3
t_1	Breakthrough time (see section 4.4.1)	
't'	Thickness of adsorbed layer (Å)	5.2
	t' statistical thickness for filling a particular sized micropore	
V	Volume. $V_{g.s.}^{o}$ volume of the out-going side V_d volume of dead space, V_b volume of burette, V_n and V_n' volume of micropores section 5.2.1	4.3
$\bar{V}_s$	Partial molar volume of adsorbate in solution	2.59
$\tilde{V}_g$	Molar volume of the gas phase	2.59
$\tilde{V}_s$	Molar volume of the adsorbed phase	2.67
ΔV_a	Degree of swelling of adsorbent (cm^3/cm^3 of porous media)	5.24
$\Delta\tilde{V}_a$	Molar degree of swelling of adsorbent	5.18
$\tilde{V}_a^o$	Molar volume of adsorbent prior to swelling	5.15
V'	Molar gas volume	5.23
v	Uptake (cc at N.T.P./g)	4.2
v_m	Monolayer capacity (section 4.2.1)	
v_1, v_2	Absorption band in wave-numbers	
w	Weight (g)	5.24
X	Fractional length of membrane for which the surface flux has joined the gas phase	2.27
X_M	Mole fraction of surface excess	5.19
x	Distance	2.6
x	Mole fraction subscripted A, B, for species	2.57
x_s	Mole fraction of adsorbate in solution	2.59

Greek Symbols

α	Angle subtended (section 5.2.1)	
α'	Coefficient discussed in section 5.1.9	
β	Isothermal compressibility of adsorbent ($atmos^{-1}$)	5.15
γ	Surface tension (dynes cm^{-1})	5.1
δ	Volume elements along a temperature gradient	
Δ'	Kammermeyer quotient	5.28
Δ	Time-lag difference	
Γ	Surface excess ($moles/cm^2$)	2.60
ε	Porosity (cm^3/cm^3)	
η	Separation factor	2.58
η'	Viscosity	5.49
θ	Fractional monolayer capacity	
θ_w	Angle of wetting	5.1
χ	Tortuosity and structure factor	2.4
μ	Chemical Potential	2.7
μ_a	Chemical potential of the adsorbent in the adsorbed state	2.73
μ_a^o	Chemical potential of the adsorbent in the calibrated state	2.73
μ_f	Chemical potential of the surface excess	2.73
ν	Vibrational frequency of an adsorbed molecule (sec^{-1})	5.42
π	Ratio of circumference to diameter of circle	
ρ_λ	Liquid density of adsorbate	5.49
σ	Slope of isotherm	2.34
σ_s	Summation of volume elements	
σ_m	Molecular diameter	
σ_r	Rate of shear	5.50
τ	Shear stress	5.50
ϕ	The two dimensional spreading pressure of the adsorbed phase	2.68
ω	Fundamental vibrational frequency (cm^{-1})	5.10

REFERENCES

Adamson, A.W. (1967) "Physical Chemistry of Surfaces", Interscience.

Adzumi, H. (1937) Bull. Chem. Soc. Japan 12, 285 & 304.

Anderson, R.B. and Emmett, P.H. (1952) J. Phys. Chem. 56, 753.

Arnold, G.M. (1967) Carbon 5, 33.

Ash, R., Baker, R.W. and Barrer, R.M. (1967) Proc. Roy. Soc. 299A, 434.

Ash, R., Baker, R.W. and Barrer, R.M. (1968) Proc. Roy. Soc. 304A, 407.

Ash, R. and Barrer, R.M. (1967) Surface Science 8, 461.

Ash, R., Barrer, R.M. and Nicholson, D. (1963) Z. Phys. Chem. (n.f.) 37, 18.

Ash, R., Barrer, R.M. and Pope, C.G. (1963) Proc. Roy. Soc. 271A, 1 and 19.

Aylmore, L.A.G. and Barrer, R.M. (1966) Proc. Roy. Soc. 290A, 477.

Babbit, J.D. (1950) Canad. J. Research 28A, 449.

Babbit, J.D. (1951 a) Canad. J. Phys. 29, 427

Babbit, J.D. (1951 b) Canad. J. Phys. 29, 437

Babbit, J.D. (1955) J. Chem. Phys. 23, 601.

Babbit, J.D. (1958) Nature 182, 201.

Badger, G.M. (1954) "The Structures and Reactions of Compounds", Cambridge University Press.

Baker, R.W. (1966) Ph.D. thesis, University of London

Bangham, D.H. (1932) Proc. Roy. Soc. 138A, 162.

Bangham, D.H. and Fakhoury, N. (1930) Proc. Roy. Soc. 130A, 81

Bangham, D.H. and Maggs, F.A.P. (1943) Proceedings of Conference on the Ultrafine Structure of Coal and Cokes. June 24, (1943). The British Coal Utilization Research Association. (Distributing Agents, H.K. Lewis and Co. Ltd., London).

Bangham, D.H. and Razouk, R.I. (1938) Proc. Roy. Soc. 166A, 572

Barrer, R.M. (1937) Proc. Roy. Soc. 161A, 476

Barrer, R.M. (1954) Brit. J. appl. Phys. Suppl. No. 3, 41 and 49

Barrer, R.M. (1963 a) Canad. J. Chem. 41, 1763.

Barrer, R.M. (1963 b) Applied Materials Research 2, 129.

Barrer, R.M. (1967) Chap. 19 "The Solid-Gas Interface", Ed. Flood, Arnold.

Barrer, R.M. and Gabor, T. (1959) Proc. Roy. Soc. 251A, 267.

Barrer, R.M. and Gabor, T. (1960) Proc. Roy. Soc. 256A, 267

Barrer, R.M. and Rideal, E.K. (1935) Proc. Roy. Soc. 149A, 231.

Barrer, R.M. and Strachan, E.E. (1955) Proc. Roy. Soc. 231A, 52.

Barrett, E.P., Joyner, L.G. and Halenda, P.P. (1951) J. Am. Chem. Soc. 73, 373.

Bellamy, L.J. (1958) "The Infra-red Spectra of Complex Molecules", Methuen.

Benedict, M, (1947) Trans. Am. Inst. Chem. Engrs. 43, 41.

Bennett, M.J. and Tompkins, F.C. (1957) Trans. Faraday Soc. 53, 185.

Berman, A.S. and Lund, L.M. (1958) Proc. 2nd Geneva Conf. on the "Peaceful Uses of Atomic Energy" 4 359.

Biscoe, J. and Warren, B.E. (1942) J. Appl. Phys. 13, 364.

Boehm, H.P., Diehl, E., Heck, W. and Sappok, R. (1964) Angew. Chem. Internat. Edit. 3, 669.

de Boer, J.H. and Custers, J.F.H. (1934) Z. Phys. Chem. 25, 225.

de Boer, J.H., Linsen, B.G. and Lippens, B.C. (1964 a) J. Catalysis 3, 32.

de Boer, J.H. and Lippens, B.C. (1964 b) J. Catalysis 3, 38 and 44.

de Boer, J.H. and Lippens, B.C. (1965 a) J. Catalysis 4, 319.

de Boer, J.H., Linsen, B.G. and Osinga, Th.J. (1695 b) J. Catalysis 4, 643

de Boer, J.H., Linsen, B.G., van de Plas, Th. and Zondervan, G.J. (1965 c) J. Catalysis 4, 649.

de Boer, J.H., Lippens, B.C., Linsen, B.G., Broekhoff, J.P.C., van de Heuval, A. and Osinga, Th.J. (1966) J. Colloid and Interface Science 21, 405.

Bonhoeffer, K.F. and Harteck, P. (1929) Naturwiss 17, 182.

Breton, E.A. and Massigon, D. (1963) J. Chim. Physique 60, 294.

Brown, J.K. (1955) J. Chem. Soc., 744.

Brubaker, D.W. and Kammermeyer, K. (1953) Proc. Conf. on Nuclear Engineering. Univ. California Berkely Sept. 9 - 11. (1953), F-9-28.

de Bruin, W.J. and van de Plas, Th. (1964) R.G.C. 41, 453.

Brunauer, S., Emmett, P.H. and Teller, E.J. (1938) J. Am. Chem. Soc. 60, 309. For errata see Emmett and de Witt, Industr. Engng. Chem. (anal) 13, 28 (1941).

Brunauer, S., Deming, L.S., Deming, W.E. and Teller, E.J. (1941) J. Am. Chem. Soc. 62, 1723.

Cabot Corporation. Private communication, and the Cabot technical data sheets "Cabot Carbons under the Electron Microscope" and "Cabot Carbon Black Pigments for ink, paint, plastics and paper". Cabot Corporation, 125 High Street, Boston, Mass., U.S.A.

Carman, P.C. (1952) Proc. Roy. Soc. 211A, 526.

Carman, P.C. (1956) "Flow of Gases through Porous Media", Butterworths.

Carman, P.C. and Malherbe, P. le R. (1950) Proc. Roy. Soc. 203A, 165.

Carman, P.C. and Raal, F.A. (1951 a) Proc. Roy. Soc. 209A, 38.

Carman, P.C. and Raal, F.A. (1951 b) Proc. Roy. Soc. 209A, 59.

Clausing, P. (1930) Annalen Physik Leipzig 7, 489.

Clausing, P. (1932) Ann. d. Physik 12, 961.

Clint, J.H. (1966) Ph.D. thesis, University of London.

Colthrup, N.B. (1950) J. Opt. Soc. Amer. 40, 397.

Constabaris, G., Sams, J.R. and Halsey, G.D. (1961) J. Phys. Chem. 65, 367.

Criddle, D.W. (1960) Chap. 11 "Rheology, Theory and Applications", vol 2. ed. F.R. Eirich, Academic Press.

Dacey, J.R. (1961) Advances in Chemistry No. 33, Solid Surfaces and Gas Solid Interfaces. 172.

Damköhler, G.Z. (1935) Z. Phys. Chem. 174A, 222.

D'Arcy, H. (1856) Les Fontaines publique de la Ville de Dijon Damont, Paris.

Dodd, R.E. and Robinson, P.L. (1954) "Experimental Inorganic Chemistry", Amsterdam : Elsevier.

Donnet, J.B. and Bouland, J.C. (1964) R.G.C. 41, 4o7 and 429.

Emmett,P.H. and de Witt, T.W. (1943) J. Am. Chem. Soc. 65, 1253.

Everett, D.H. (1950 a) Trans. Faraday Soc. 46, 453.

Everett, D.H. (1950 b) Trans. Faraday Soc. 46, 942.

Everett, D.H. (1950 c) Trans. Faraday Soc. 46, 957.

Everett, D.H. (1952) Trans. Faraday Soc. 48, 1164.

Farkas, A. (1935) "Light and Heavy Hydrogen", Cambridge.

Fick, A. (1855) Ann. Physick 170, 59.

Field, G.J., Watts, H. and Weller, K.R. (1963) Rev. Appli. Chem. 13, 2.

Fiocchi, R. (1966) Energia Nucleare 13, 24.

Fiocchi, R. (1967) Energia Nucleare 14, 713.

Flood, E.A. and Heyding, R.D. (1954) Canad. J. Chem. 32, 660.

Flood, E.A. and Huber, M. (1955) Canad. J. Chem. 33, 203.

Flood, E.A. (1957 a) Canad. J. Chem. 35, 48.

Flood, E.A. and Lakhanpal, M.L. (1957 b) Proc. 2nd Internat. Cong. of Surface Activity. April 8 - 12 (1957) Butterworths, London. 131.

Flood, E.A. and Lakhanpal, M.L. (1957 c) Canad. J. Chem. 35, 887.

Flood, E.A. and Farhan, F.M. (1963) Canad. J. Chem. 41, 1703.

Fowler, R.H. (1936) Proc. Camb. Phil. Soc. 32, 144.

Freeman, M.P. (1960) J. Phys. Chem. 64, 32.

Fujii, S. (1967) Koggo Kagakn Zasshi 62, 1574.

Fujii, S. and Tsuboi, H. (1966) Fuel 369.

Gabor, T. (1957) Ph.D. thesis, University of London.

Gaede, W. (1913) Ann. d. Physik 41, 289.

Garten, V.A., Weiss, D.E. and Willis, J.B. (1957) Austral. J. Chem. 10, 295.

Gilliland, E.R., Baddour, R.F. and Russell, J.L. (1958) A.I.Ch.E. Journal 4, 90.

Gilliland, E.R., Baddour, R.F. and Engel, H.H.E. (1962) A.I.Ch.E. Journal 8, 530.

Glasstone, S., Laidler, K.J. and Eyring, H. (1941) "Theory of Rate Processes", McGraw-Hill.

Graham, T. (1846) Phil. Trans. Roy. Soc. (London) 136, 573.

Gregg, S.J. and Sing, K.S.W. (1967) "Adsorption, Surface Area and Porosity", Academic Press.

Hair, M.L. (1967) "Infra-red Spectra in Surface Chemistry", Dekker.

Hall, C.E. (1948) J. Applied Physics 19, 271.

Hallum, J.V. and Drushel, H.V. (1958) J. Phys. Chem. 62, 110.

Harkins, W.D. and Jura, G. (1944) J. Am. Chem. Soc. 66, 1356.

Harkins, W.D. and Jura, G. (1946) Colloid Chemistry VI Ed. J. Alexandra. Reinhold. 10.

Harris, M.R. (1967) Chemistry and Industry. 1295

Heckman, F.A. (1964) Rubber Chemistry and Technology 37, 1245.

Henniker, J.C. (1952) J. Colloid Sci. 7, 443.

Henry, D.C. (1922) Phil. Mag. 44, 689.

Herzberg, G. (1950) "Spectra of Diatomic Molecules", D. Van Nostrand.

Hiby, J.W. and Pahl, M.Z. (1956) Naturf. 11A, 80.

Higashi, K., Ito, H. and Oishi, J. (1963) J. At. Energy Soc. Japan (Eng. trans.) 5, 846.

Higashi, K., Ito, H. and Oishi, J. (1964) J. Nuclear Science and Technology 1, 298.

Higashi, K., Ito, H. and Oishi, J. (1966) J. Nuclear Science and Technology 3, 56.

Hill, T. (1949) J. Chem. Phys. 17, 520.

Hill, T. (1950) J. Chem. Phys. 18, 244.

Hill, T. (1952) Adv. in Catalysis 4, 211.

Hill, T. (1956) J. Chem. Phys. 25, 730.

Hill, T. (1960) "An Introduction to Statistical Thermodynamics", Addison-Wesley.

Holmes, J.M. and Beebe, R.A. (1957) Canad. J. Chem. 35, 1542.

Huggill, J.A.W. (1952) Proc. Roy. Soc. 212A, 123.

Hwang, S-T. and Kammermeyer, K. (1966 a) Canad. J. Chem 44, 82.

Hwang, S-T. and Kammermeyer, K. (1966 b) Separation Science 1, 629.

Hwang, S-T. and Kammermeyer, K. (1967) Separation Science 2, 555.

Ishida, K., Shimokawa, J. and Yamamota, Y. (1961) Trans. Faraday Soc. 57, 2018.

Kammermeyer, K. and Rutz, L.O. (1959) Chem. Eng. Prog. Symp. Ser. 55, 163.

Kini, K.A. and Stacy, W.O. (1963) Carbon 1, 17.

Kiselev, A.V. and Poshkus, D.P. (1965) Russian J. Phys. Chem. (Eng. trans.) 39, 204.

Kiselev, A.V., Poshkus, D.P. and Afreimovich, A.Ya. (1965) Russian J. Phys. Chem. (Eng. trans.) 39, 630.

Knudsen, M. (1909) Ann. Physik 28, 75.

Kollensky, W.Y. and Walker, P.L. (1960) Proc. 4th Carbon Conf. Pergamon Press. 423.

Kozeny, J. (1927) S-Ber. Wiener Akad., Abt. IIa 136, 271.

Logan, unreported work from these laboraties.

Lygin, V.I., Kovaleva, N.V., Kavtaradze, N.N. and Kiselev, A.V. (1960) Lolloidnyi Zhurnal (Eng. trans.) 22, 334.

Martin, C.P. and Mohiuddin, S.O. (1953) Science 118, 364.

Mason, E.A., Evans III, R.B. and Watson, G.M. (1961) J. Chem. Phys. 35, 2076.

Mason, E.A., Evans III, R.B. and Watson, G.M. (1962) J. Chem. Phys. 36, 1894.

Mason, E.A., Evans III, R.B. and Watson, G.M. (1963) J. Chem. Phys. 38, 1808.

Mason, E.A. and Malinauskas, A.P. (1964) J. Chem. Phys, 41, 3815.

Mason, E.A., Malinauskas, A.P. and Evans III, R.B. (1967) J. Chem. Phys. 46, 3199.

Meehan, F.T. (1927) Proc. Roy. Soc. 115A, 199.

Mitchell, J.V. (1831) J. Roy. Inst. 2, 101 and 307.

Murphy, V. (1968) Ph.D thesis, University of London.

McBain, J.W., Porter, J.L. and Session, R.F. (1933) J. Am. Chem. Soc. 55, 2294.

McIntosh, J.R. (1966) Ph.D thesis, University of Iowa.

McIntosh, R.L. and Haines, R.S. (1947) J. Chem. Phys. 15, 28.

McIntosh, R.L. and Amberg, C.H. (1952) Canad. J. Chem. 30, 1012.

Newton, Sir I. (1685) "Principia", book 2.

Oldroyd, J.G. (1956) Chap. 16 "Rheology, Theory and Applications", vol. 1 ed. F.R. Eirich, Academic Press.

Pace, E.L. and Siebert, A.R. (1959) J. Phys. Chem. 63, 1398.

Pauling, L. (1960) "Nature of the Chemical Bond", 3rd ed. Cornell University Press.

Pierce, C., Wiley, J.W. and Smith, R.N (1948) J. Phys. and Colloid Chem. 53, 669.

Pollard, W.G. and Present, R.D. (1948) Phys. Rev. 73, 762.

Pope, C.G. (1961) Ph.D. thesis, University of London.

Pope, C.G. (1967) Trans. Faraday Soc. 63, 734.

Present, R. and de Bethune, J. (1949) Phys. Rev. 75, 1050.

Price, W.C. and Tetlow, K.S. (1948) J. Chem. Phys. 16, 1157.

Puri, B.R. and Bansal, R.C. (1964 a) R.G.C. 41, 445.

Puri, B.R. and Bansal, R.C. (1964 b) Carbon 1, 451.

Puri, B.R. and Bansal, R.C. (1964 c) Carbon 1, 457.

Puri, B.R. and Bansal, R.C. (1966 a) Carbon 3, 533.

Puri, B.R. and Bansal, R.C. (1966 b) Carbon 4, 391.

Ries, Jr., H.E., van. Nordstrand, R.A. and Kreger, W.E. (1945) J. Am. Chem. Soc. 69, 35.

Rivin, D. (1962) Proc. 4th Rubber Technology Conf. London.

Ross, S and Olivier, J.P. (1964) "On Physical Adsorption", Interscience.

Rummel, K.W. (1933) Z. f. Physikal Chemie 167A, 221.

Scheidegger, A.E. (1959) "The Physics of Flow through Porous Media", 2nd ed. Univ. Toronto Press.

Smith, S.R. and Garden, A.S (1956) J. Phys. Chem. 60, 759.

Smith, W.R. (1964) "Encyclopedia of Chemical Technology", 2nd ed. vol. 4 pp 243 - 247 and 280 - 281. Interscience.

Smoluchowski, M (1910) Ann. d. Physik. 33, 1559.

Snow, C.W., Wallace, D.R., Lyon, L.L. and Croker, G.R. (1959) Proc. 3rd Carbon Conf. Pergamon Press. 279.

Snow, C.W., Wallace, D.R., Lyon, L.L. and Croker, G.R. (1960) Proc. 4th Carbon Conf. Pergamon Press. 79.

Spencer, W.B., Amberge, C.H. and Beebe, R.A. (1958) J. Phys. Chem. 62, 717.

Steel, W.A. (1956) J. Chem. Phys. 25, 819.

Steel, W.A. and Halsey, Jr., G.D. (1954) J. Chem. Phys. 22, 979.

Steel, W.A. and Halsey, Jr., G.D. (1955) J. ~~Chem.~~ Phys. Chem. ~~Phys.~~ 59, 57.

Studebaker, M.L. (1957) Rubber Chemistry and Technology 30, 1418.

Studebaker, M.L. (1963) Proc. 5th Carbon Conf. Pergamon Press vol. 2, 189.

Studebaker, M.L., Huffman, E.W.D., Wolfs, A.C. and Nabors, L.G. (1956) Ind. Engng. Chem. 48, 162.

Thorp, N., Long, R. and Garner, F.H. (1955) Fuel 534, 1.

Tykodi, R.J. (1954) J. Chem. Phys. 22, 1647.

Volkova, Z.V. (1936) Acta Physicochim. U.R.S.S. 4, 635.

Volmer, M. and Esterman, J. (1921) Z. Physik 7, 13.

Volmer, M. and Adhikari, G. (1925) Z. Physik 35, 170.

Volmer, M. and Adhikari, G. (1926) Z. Phys. Chem. 119, 46.

Vogel, A.L. (1951) "Quantitative Inorganic Analysis" 2nd ed. Longmans.

Vogel, A.L. (1954) "Macro and Semimicro Qualitative Inorganic Analysis", 4th ed. Longmans.

Weber, S. (1954) Konig. Danske Vid. Sels. mat. fys. Med 28, No. 2.

Weyl, W.A. and Ormsby, W.C. (1956) Chap. 7 "Rheology, Theory and Applications", vol 1 ed. F.R. Eirich, Academic Press.

Wicke, E. and Kallenback, R. (1941) Kolloid Z. 97, 135.

Wicke, E. and Voigt, U. (1947) Angew. Chem. 19B, 94.

Wiig, E.O. and Juhola, A.J. (1949) J. Am. Chem. Soc. 71, 561.

Wiegand, W.B. (1937) India Rubber World 96, 43.

Wise, M.E. (1952) Phillips Research Reports 7, 321.

Wyckoff, R.D. and Botset, M.G. (1936) Physica 7, 325.

Yates, D.J.C. (1954) Proc. Roy. Soc. 224A, 526.

Yates, D.J.C. (1956) J. Phys. Chem. 60, 543.

Young, D.M. and Crowell, A.D. (1962) "Physical Adsorption of Gases". Butterworths.

General References

"Elucidation of Structures by Physical and Chemical Methods, part 1. Vol. XI of Techniques of Organic Chemistry". General editor A. Weissberger, Interscience New York, (1963).

"Handbook of Physical Constants". Editor S.P. Clark. The Geological Society of America (1966).

"Handbook of Chemistry and Physics", 48th ed. General editor R.C. West. The Chemical Rubber Co. (1967)

"Chemical Engineers Handbook", 2nd ed. General editor J.H. Perry. McGraw-Hill (1941).

"Physico-Chemical Constants of Pure Organic Compounds", General editor J. Timmerman. Elsevier (1950).

APPENDIXES

Legend to tables

Pressure	In cm Hg, listed as P, P.igs, Av.P.igs
Concentration	In moles per cc of porous medium, listed as C, C_g, C_s, C_o, C_g^g
Uptake	In cc at N.T.P. per g, listed as v
Temperature	In ^oC and ^oK, listed as T
Heat	In Kcals, listed as q_{st}, $\Delta\tilde{H}$
Flux	In moles per cm^2 per sec, listed as J, J_g, J_s, $\mathcal{F}_g$, $\mathcal{F}_s$, J'_g, Flux
Permeability	In cm^2 per sec, listed as K, K_C, Perm., Av.Perm.
Diffusion coefficient	In cm^2 per sec, listed as D_{ss}
Permeability constant	$K(M/T)^{\frac{1}{2}}$, Perm.Const.
Time-lag	In hours, listed as L
Statistical thickness	In $\mathring{A}$, listed as 't'
B.E.T.	See section 4.2.1

P/P_o is the relative saturation vapour pressure, ϕ the spreading pressure, k_s the Henry law constant, η the separation factor and the Pope equivalence factor was 3.312

Nitrogen Isotherm Data

T - 197.8 °C, 77.4 °K (Liquid nitrogen)

adsorption run 1

P	v	P/P_o	BET_3 x 10^3	't'
0.041	97.72	0.005		
0.156	142.62			
0.179	142.90			
0.735	177.51			
0.819	178.84			
2.923	209.30			
3.240	211.90			
3.442	213.39			
3.516	213.96			
3.614	214.49	0.046	0.235	
7.261	235.86	0.097	0.453	3.65
8.593	241.66	0.114	0.534	3.77
9.580	245.28	0.126	0.586	3.89
9.996	246.80	0.131	0.611	3.90
10.414	248.12	0.137	0.637	3.95
13.396	258.83	0.175	0.818	4.19
17.583	267.73	0.229	1.112	4.50
18.235	275.37	0.247	1.191	4.66
19.882	278.23	0.259	1.259	4.75
20.895	281.08	0.273	1.332	4.83
22.635	286.48	0.297	1.476	4.99
28.532	302.48	0.375	1.982	5.48
33.677	313.14	0.442	1.990	6.04

adsorption run 2

0.094	83.70	0.001	0.015	
0.432	158.97	0.006	0.036	
0.525	159.76	0.007	0.044	
5.298	219.00	0.070	0.342	3.42
7.183	228.5	0.095	0.457	3.63
15.490	258.2	0.204	0.991	4.39
19.040	269.8	0.251	1.239	4.69
24.476	285.1	0.322	1.666	5.16
26.882	301.9	0.354	1.813	5.37
33.868	322.1	0.446	2.496	6.06
38.389	336.8	0.505	3.031	6.54
42.060	348.5	0.553	3.556	6.94
45.335	359.3	0.597	4.115	7.33
49.558	379.5	0.652	4.939	7.89

Nitrogen Isotherm Data

T 0.0 °C Ice
273.2 °K

adsorption

P	v
7.440	0.74
14.087	1.53
24.767	2.64
34.329	3.47
44.872	4.37
55.143	5.25

desorption

44.760	4.34
34.304	3.46
24.240	2.53
14.059	1.54
7.451	0.93

T - 40.0 °C
233.2 °K

adsorption

P	v
4.788	1.74
8.292	2.85
13.280	4.20
16.863	5.10
20.090	5.86
22.290	6.36
25.167	7.09
45.135	10.94
74.111	15.40

desorption

55.299	12.67
47.471	11.43
39.238	10.05
30.009	8.21
18.113	5.68
10.406	3.73
6.846	2.72
5.414	2.28
4.201	1.85
1.627	0.92

Isosteric Heats between 0.0 and - 40 °C

v	q_{st}
0.5	5.30
1.0	5.34
1.5	5.44
2.0	5.51
2.5	5.61
3.0	5.62

Computer program for calculating molecular packing in circular micropore capillaries

Control cards

```
C       MØLECULAR PACKING IN CIRCULAR MICRØPØRE CAPILLARIES
        REAL A,L,TØT,C,S,FL,RM,THETA,RD,AA
        INTEGER M,NL,D,NTØT,NA
        DØ 40 NA = 20,50,2
        AA =  NA
        A  =  AA/10.
        WRITE (6,202) A
   202  FØRMAT (1H1,26HFØR MØLECULAR DIAMETER ØF ,F3.1)
        WRITE (6,201)
   201  FØRMAT (1H1,31HDIAMETER   LAYER      MØLECULES,///)
        A  =  3.4
        DØ 30 D  =  4,50
        TØT  =  0.0
        L  =  1.0
        RD  =  D
    10  S  =  RD/2.0-A*(L-1.0)
        IF (S*S-S*A) 11,11,12
    11  M  =  1
        GØ TØ 14
    12  C  =  A/(2.0*SQRT(S*S-S*A))
        M  =  3.142/ATAN (C)
    14  NL =  L
        IF (NL-1) 80,80,81
    80  FL =  M
    81  CØNTINUE
        WRITE (6,203) D,NL,M
   203  FØRMAT (1H ,I2,9X,I2,9X,I3)
        L  =  NL + 1
        RM =  M
        TØT  =  TØT + RM
        THETA  =  TØT/FL
        IF (RD/2.0-A*L) 20,10,10
    20  NTØT  =  TØT
        WRITE (6,204) NTØT,THETA
   204  FØRMAT (1H ,5HTØTAL,3X,I3,6X,5HTHETA,3X,F6.3,///)
    30  CØNTINUE
    40  CØNTINUE
        STØP
        END
```

Computer results for packing 3.4 Å diameter molecules into circular micropore capillaries

Cap. Dia in Å	No. Molecules in layer 1st	2nd	3rd	Total	Theta
4	1	-	-	1	1.0
5	1	-	-	1	1.0
6	1	-	-	1	1.0
7	2	-	-	2	1.0
8	3	-	-	3	1.0
9	4	-	-	4	1.0
10	5	-	-	5	1.0
11	6	1	-	7	1.166
12	7	1	-	8	1.142
13	8	1	-	9	1.123
14	9	2	-	11	1.222
15	10	3	-	13	1.300
16	11	5	-	16	1.455
17	12	6	1	19	1.582
18	13	6	1	20	1.538
19	14	7	1	22	1.571
20	15	8	1	24	1.600
21	16	9	3	28	1.750
22	17	10	4	31	1.824
23	18	11	5	34	1.889
24	18	12	6 & 1	37	2.050

Hyrogen Isotherm Data

T 25.0 °C
298.2 °K

adsorption		desorption	
P	v	P	v
1.124	0.00747	49.277	0.3133
2.854	0.01802	40.140	0.2549
4.357	0.02862	27.173	0.1748
10.025	0.06572	16.119	0.1049
16.579	0.1117	11.918	0.0646
24.707	0.1628	9.479	0.0585
29.872	0.1961	5.216	0.0306
34.279	0.2215	3.094	0.0175
37.893	0.2456	0.600	0.0
40.046	0.2898		
50.090	0.3202		
56.519	0.3622		

T 0.0 °C
273.2 °K

adsorption		desorption	
P	v	P	v
3.089	0.0286	49.531	0.4321
4.988	0.0466	41.395	0.3603
7.397	0.0661	28.068	0.2458
8.656	0.0778	17.115	0.1458
10.441	0.0933	12.014	0.1004
11.971	0.1039	8.703	0.0732
19.609	0.1721	5.975	0.0478
28.206	0.2481	3.646	0.0279
34.486	0.3032		
39.502	0.3433		
41.890	0.3633		
45.677	0.3910		
47.395	0.4113		
49.530	0.4332		
55.618	0.4828		

T - 20.0 °C
253.2 °K

1.711	0.0172	46.918	0.5429
2.699	0.0322	39.803	0.4661
3.889	0.0454	27.708	0.3269
5.491	0.0642	17.209	0.2045
7.189	0.0819	13.530	0.1592
11.526	0.1350	11.122	0.1319
16.362	0.1921	6.605	0.0815
19.367	0.2276	4.070	0.0509
22.823	0.2674	0.982	0.0115
23.317	0.2751		
37.670	0.4417		
53.932	0.6277		
56.111	0.6520		

T - 27.6 °C
245.6 °K

2.443	0.0338	46.485	0.624
3.887	0.0536	41.532	0.551
5.498	0.0762	35.217	0.468
6.400	0.0873	24.861	0.332
7.519	0.1023	15.550	0.214
15.543	0.2118	11.254	0.207
24.865	0.336	11.598	0.161
35.451	0.469	10.166	0.143
41.934	0.555	8.842	0.124
46.004	0.610	6.126	0.0891
49.447	0.652	3.825	0.0629
		0.875	0.0376

T - 40.0 °C
233.2 °K

3.444	0.05407	52.282	0.8489
5.368	0.08874	47.192	0.7714
7.552	0.1233	40.002	0.6545
10.359	0.1685	28.728	0.4717
18.376	0.2998	18.305	0.3023
28.820	0.4686	14.594	0.2424
40.558	0.6499	10.735	0.1777
47.220	0.7634	4.936	0.0799
51.718	0.8367	1.334	0.0197
55.237	0.8854		

T - 183.0 °C (Liquid Oxygen)
90.2 °K

adsorption		desorption	
P	v	P	v
1.077	7.978	45.951	61.206
1.475	9.864	38.433	57.193
3.815	17.494	33.441	53.333
4.874	20.071	24.835	46.675
5.751	22.030	16.787	38.856
6.589	23.649	14.816	36.617
8.457	27.136	12.177	33.135
11.805	32.149	7.231	25.489
14.719	35.937	3.853	18.095
16.457	37.937	2.330	13.535
17.920	39.762		
18.474	40.464		
27.486	48.661		
37.024	55.555		
43.338	59.654		
47.795	62.148		
50.873	63.818		

T - 195.8 °C (Liquid Nitrogen)
77.4 °K

0.201	8.719	49.691	99.122
0.272	9.072	47.170	97.444
0.816	18.069	42.959	94.598
0.937	19.555	37.577	90.469
2.042	28.197	28.607	82.527
2.686	31.850	19.817	72.495
3.738	36.780	17.717	69.668
4.965	41.536	14.944	65.668
5.431	43.181	12.359	61.073
6.719	47.187	9.417	54.973
8.443	52.099	5.511	44.390
9.826	52.001	3.593	37.377
11.266	58.222		
12.366	60.477		
16.684	67.780		
20.926	73.682		
22.692	75.982		
25.110	78.749		
25.726	79.451		
37.860	90.590		
51.952	100.094		
61.013	104.983		

Deuterium Isotherm Data

T 25.0 °C
298.2 °K

adsorption		desorption	
P	v	P	v
2.726	0.0152	51.870	0.3357
4.450	0.0301	42.205	0.2727
6.686	0.0438	28.300	0.1862
8.165	0.0546	16.949	0.1120
10.046	0.0652	12.181	0.0785
11.980	0.0754	8.074	0.0533
20.110	0.1322	5.407	0.0355
29.744	0.1933	3.254	0.0209
36.349	0.2348	0.633	0.0021
42.014	0.2702		
43.825	0.2824		
42.231	0.2753		
52.134	0.3337		
58.357	0.3740		

T 0.0 °C
273.2 °K

adsorption		desorption	
P	v	P	v
1.249	0.0104	50.883	0.4500
2.000	0.0202	30.883	0.2766
2.981	0.0264	22.836	0.1980
4.418	0.0393	19.080	0.1726
5.834	0.0519	15.970	0.1450
9.592	0.0851	10.695	0.0995
13.916	0.1248	6.617	0.0614
16.417	0.1467	1.433	0.0131
20.420	0.1810		
30.745	0.2695		
50.322	0.4426		
73.478	0.6426		

T - 20.0 °C
253.2 °K

2.019	0.024	48.767	0.602
3.222	0.038	42.885	0.535
4.528	0.053	36.350	0.460
6.540	0.077	25.510	0.336
7.684	0.089		
12.350	0.145		
17.786	0.210		
20.759	0.245		
23.217	0.272		
24.279	0.286		
25.307	0.302		
36.386	0.415		
42.996	0.480		
48.611	0.603		
51.788	0.637		

T - 40.0 °C
233.2 °K

2.336	0.038	44.989	0.730
3.674	0.056	42.367	0.689
5.892	0.098	38.505	0.627
6.839	0.112	33.078	0.538
9.830	0.171	23.647	0.387
14.419	0.351	15.053	0.243
21.574	0.360	11.975	0.187
25.000	0.416	8.720	0.138
28.307	0.467	6.402	0.175
29.472	0.488	4.065	0.041
29.768	0.493	1.099	0
41.500	0.682		
47.884	0.783		
54.456	0.887		
56.101	0.914		

T - 183.0 °C (Liquid Oxygen)
90.2 °K

adsorption		desorption	
P	v	P	v
0.562	5.616	46.246	65.779
0.724	7.023	41.320	62.835
0.937	8.305	35.933	59.047
1.988	13.370	26.805	51.781
2.928	16.844	18.100	43.347
3.867	19.845	15.305	40.143
4.872	22.537	13.127	37.215
6.470	26.239	10.597	33.548
7.606	28.480	7.801	28.791
10.226	33.086	5.368	23.645
12.678	36.795	4.195	20.712
15.266	40.202	2.583	15.643
16.640	41.814		
24.112	49.514		
32.291	56.389		
37.467	60.150		
40.452	62.106		
42.820	63.580		
40.993	62.419		
46.132	65.679		
48.608	67.349		

T - 195.8 °C
77.4 °K

0.065	5.050	50.806	108.600
0.300	12.351	48.547	106.580
0.328	12.902	43.796	103.898
0.832	20.195	38.526	99.823
0.841	21.035	29.251	91.275
0.940	21.712	20.591	82.714
4.121	42.737	18.249	77.866
4.872	44.941	13.054	69.679
5.422	47.963	10.030	62.980
5.883	49.730	5.951	51.531
6.954	53.012		
8.641	57.866		
9.976	61.425		
11.174	64.215		
11.935	66.151		
15.804	73.526		
19.328	79.036		
21.058	81.310		
23.326	84.456		
24.228	85.566		
35.622	97.175		
47.712	106.647		
54.375	111.052		

Derived data from Hydrogen and Deuterium isotherms on Carbolac I between - 40 and 25 °C together with data for the range 308 to 378 °K taken from Clint's Ph.D. thesis (1966)

	T °K	$1/T_{10^{-3}}$	$v/P_{10^{-3}}$	$k_{s\,10^{8}}$	$\log_{10}\cdot\frac{v}{P}$	$\log_{10} k_s$
Hydrogen	378.0	2.646	3.105	3.48	$\bar{3}.4921$	$\bar{8}.5416$
	352.9	2.848	3.745	3.92	$\bar{3}.5735$	$\bar{8}.5933$
	333.2	3.005	4.511	4.44	$\bar{3}.6542$	$\bar{8}.6474$
	320.7	3.122	5.113	4.86	$\bar{3}.7084$	$\bar{8}.6866$
	308.2	3.249	5.809	5.31	$\bar{3}.7642$	$\bar{8}.7251$
	298.2	3.358	6.452	5.69	$\bar{3}.8096$	$\bar{8}.7551$
	273.2	3.666	8.701	7.03	$\bar{3}.9395$	$\bar{8}.8472$
	253.2	3.956	11.666	8.74	$\bar{2}.0667$	$\bar{8}.9412$
	245.6	4.092	13.166	9.57	$\bar{2}.1193$	$\bar{8}.9809$
	233.2	4.296	16.191	11.17	$\bar{2}.2101$	$\bar{7}.0480$
Deuterium	298.2	3.358	6.50	5.68	$\bar{3}.8129$	$\bar{8}.7543$
	273.2	3.666	8.83	7.11	$\bar{3}.9460$	$\bar{8}.8521$
	253.2	3.956	11.82	8.92	$\bar{2}.0726$	$\bar{8}.9505$
	233.2	4.296	16.32	11.26	$\bar{2}.2128$	$\bar{7}.0515$

Isosteric heats of adsorption for Hydrogen and Deuterium between 77.4 and 90.2 °K adsorbing on Carbolac I chips

v	q_{st} Kcals Deuterium	q_{st} Kcals Hydrogen	Difference in cals
5	2.22	2.11	100
10	2.06	1.93	130
15	1.92	1.82	100
20	1.79	1.70	90
25	1.69	1.63	60
30	1.61	1.58	30
35	1.60	1.58	20
40	1.58	1.53	50
45	1.57	1.50	70
50	1.55	1.48	70
55	1.51	1.43	80
60	1.49	1.41	80
65	1.49		

25 cc at N.T.P. g^{-1} is about 0.10 of a monolayer

60 cc at N.T.P. g^{-1} is about 0.25 of a monolayer

Ammonia Isotherm Data

T 0.0 °C Run 1
273.2 °K

adsorption		desorption	
P	v	P	v
0.945	18.44	49.606	192.90
0.182	20.53	36.605	169.40
0.416	33.80	35.609	167.52
0.523	34.56	33.417	162.86
0.872	44.24	31.125	158.29
0.817	46.26	27.175	145.73
1.715	54.65	20.205	133.70
2.026	57.82	19.625	131.84
2.788	63.17	17.327	125.79
3.740	68.11	15.098	119.95
4.522	73.68	12.127	110.73
5.471	77.26	11.556	108.83
6.185	81.67	7.628	95.34
7.280	86.88	7.534	94.04
8.832	92.71	5.390	84.65
9.867	96.55	3.860	75.64
10.678	99.76	2.785	70.03
11.969	104.24	2.243	65.48
14.875	113.39	1.648	35.53
17.100	119.33	1.778	35.51
19.646	125.23		
20.982	129.65		
27.038	144.70		
31.804	155.30		
36.201	164.73		
37.276	167.15		
49.718	191.20		
61.014	210.80		

T 0.0 °C Run 6
273.2 °K

adsorption		desorption
P	v	P v
3.007	52.99	not measured
3.950	58.43	
10.185	85.77	
12.348	93.70	
13.946	99.31	
15.825	103.75	
21.464	118.82	
27.796	134.04	
33.056	145.49	
37.446	154.62	
45.534	170.99	
62.511	199.30	

T - 10.0 °C Run 5
263.2 °K

0.248	30.18	45.198	217.60
3.700	73.44	34.622	193.00
4.679	80.10	32.478	187.80
7.152	97.57	29.060	178.97
9.291	105.36	20.360	153.07
9.957	108.43	17.542	144.13
12.087	118.29	12.967	126.99
14.521	127.62	8.749	109.31
16.301	134.23	6.260	96.65
17.921	139.68	4.625	87.30
19.962	147.58	3.532	79.86

T - 20.0 °C Run 4
253.2 °K

0.421	44.10	41.653	267.40
3.101	91.97	39.116	260.80
3.599	97.65	35.372	249.90
7.093	121.29	25.562	216.50
8.009	127.46	24.040	211.20
9.104	133.86	20.329	196.00
13.802	160.61	17.116	182.00
16.072	172.21		
19.024	185.00		
22.391	199.60		
27.005	218.20		

Cont.

adsorption		desorption		adsorption		desorption	
P	v	P	v	P	v	P	v
24.751	162.75			29.243	230.0		
28.036	172.57			32.939	238.5		
30.027	177.40			42.021	266.4		
31.464	182.1			53.781	305.8		
35.414	192.4						
45.479	216.5						
54.339	236.3						
re-adsorption		re-desorption					
4.547	86.47	41.626	208.2				
16.470	133.57	32.509	184.5				
23.213	154.58	29.692	177.4				
25.628	162.14	23.698	159.6				
32.945	184.4	18.983	144.9				
42.770	206.7						
50.492	223.5						
53.013	231.9						

T - 30.0 °C Run 3
243.2 °K

1.200	79.34	45.491	354.10
1.335	81.56	44.267	349.20
2.083	91.84	36.853	319.80
2.376	95.71	30.672	295.10
5.288	137.54	29.164	290.70
5.941	138.06	21.123	252.60
6.832	147.00	15.407	221.90
6.943	146.53	11.825	197.40
7.306	148.79	9.296	178.50
11.277	191.4	7.479	163.37
11.711	186.8	6.137	151.87
13.857	199.9	5.116	141.51
14.119	203.2	4.311	132.80
14.999	208.1	3.665	125.39
15.876	211.4		
18.901	231.6		
20.442	237.6		
23.757	257.2		
25.837	266.1		
30.118	286.5		
36.019	310.3		
39.909	326.3		
43.136	339.2		
46.111	353.1		
55.035	391.6		

T - 40.0 °C Run 2
233.2 °K

0.565	74.3	not measured
1.897	110.3	
2.787	129.7	
3.504	134.7	
8.082	196.7	
8.900	197.6	
11.233	238.4	
14.750	256.5	
15.197	267.2	
19.211	294.7	
25.141	335.5	
29.058	381.2	
33.953	425.7	
39.629	506.3	
40.021	536.1	
43.116	595.3	
44.414	608.8	
46.750	646.0	

T - 50.0 °C Run 7
223.2 °K

adsorption		desorption	
P	v	P	v
0.004	8.71	29.294	827.36
0.019	19.40	27.236	771.25
0.090	28.57	25.243	720.05
0.167	60.55	23.489	671.86
0.525	90.30	22.270	626.36
1.029	117.94	20.862	583.57
1.777	143.62	20.646	541.25
4.431	165.14	18.179	504.19
3.081	181.65	17.798	467.80
3.265	187.37	16.113	434.82
4.159	204.53	15.165	403.89
5.789	234.72	13.537	376.29
6.642	254.70	11.543	353.13
7.992	266.65	10.795	330.99
9.488	295.12	9.353	312.05
11.215	312.24	8.197	295.24
13.274	345.99	7.445	280.03
15.512	370.01	6.502	266.75
17.306	406.54	5.859	254.68
19.271	438.19	5.352	243.76
20.204	469.96	4.998	233.48
22.214	506.76	4.254	224.85
22.540	538.05	4.249	215.97
24.117	579.66		
24.821	598.91		
24.925	645.33		
26.649	656.12		
27.404	706.28		
27.271	719.22		
29.178	769.59		
29.724	828.12		
30.457	882.16		

P	I 0 °C	I - 10 °C	I - 20 °C	I - 30 °C	I - 40 °C	I - 50 °C
1	50.0	103.5	101.6	115.9	141.4	254.0
2	79.9	155.1	155.2	173.3	215.1	349.0
3	100.3	184.6	190.3	212.3	264.7	414.0
4	116.4	205.6	217.9	243.4	303.9	466.0
5	130.0	223.2	241.4	270.6	336.6	513.1
6	141.9	238.9	261.8	295.2	365.2	555.1
7	152.5	253.2	280.0	317.2	391.4	593.4
8	162.3	266.3	296.5	337.5	415.9	628.6
9	171.5	278.4	311.8	356.6	439.3	661.4
10	180.2	289.7	326.2	374.7	461.6	692.1
11	188.4	300.3	339.8	392.1	483.1	721.1
12	196.3	310.3	352.7	408.5	503.6	748.8
13	203.9	319.8	365.0	424.1	523.3	775.4
14	211.1	328.9	376.8	438.9	542.2	801.1
15	218.1	337.7	388.2	453.0	560.2	826.0
16	224.8	346.1	399.1	466.6	577.5	850.1
17	231.2	354.3	409.6	479.6	594.0	873.7
18	236.4	362.3	419.8	492.2	610.0	896.9
19	243.3	370.0	429.7	504.4	625.4	919.9
20	249.1	377.5	439.3	516.4	640.4	942.8
21	254.7	384.8	448.7	528.1	655.0	965.9
22	260.2	391.8	457.8	539.5	669.2	989.1
23	265.6	398.7	466.7	550.7	683.2	1012.6
24	270.8	405.4	475.3	561.6	697.0	1036.3
25	276.0	411.9	483.8	572.3	710.7	1060.3
26	281.1	418.3	492.1	582.7	724.1	1084.8
27	286.1	424.7	500.3	592.8	737.8	1109.8
28	291.0	431.0	508.3	602.8	750.7	1135.1
29	295.8	437.1	516.2	612.5	763.8	1161.2
30	300.5	443.1	524.1	622.0	776.8	1188.5
31	305.1	449.0	531.8	631.4	789.6	1217.7
32	309.6	454.7	539.4	640.7	802.3	
33	314.0	460.3	546.8	649.8	815.0	Limit of isotherm
34	318.4	465.8	553.8	658.9	827.5	
35	322.6	471.2	560.3	667.8	840.0	
36	326.8	476.6	566.3	676.6	852.5	
37	330.9	482.3	571.5	685.2	865.1	
38	335.1	488.3	576.0	693.6	877.8	
39	339.2	494.9	579.8	701.9	890.6	
40	343.4	502.1	583.3	710.1	903.7	
41	347.6	510.1	587.1	718.1	916.9	
42	351.8	519.0	592.3	726.1	930.4	
43	356.1	527.7	600.3	734.0	944.0	
44	360.2	536.3	613.1	741.9	957.8	
45	364.2	543.6	635.1	749.8	971.6	
46	368.0	548.2	663.3	757.5	985.3	
47	371.3	548.4	706.4	765.0	999.1	
48	374.1	542.1	765.0	772.0	1013.2	
49	376.0	527.5	840.4	777.9	1028.3	
50	376.8	503.3	931.6	782.4	1045.7	

Heats of adsorption for Ammonia on Carbolac I between 0 and - 50 °C

v	q_{st} Kcals/mole	ø	$\Delta\tilde{H}$ Kcals/mole
25	18.84	0.5	-
50	11.76	1.0	19.0
75	9.75	1.5	13.7
100	8.48	2.0	9.7
125	7.39	2.5	8.7
150	7.33	3.0	2.3
175	7.14	3.5	2.7
200	6.95	4.0	2.8
225	6.87	4.5	2.9
250	6.81	5.0	2.9
275	6,71	5.5	3.4
300	6.61	6.0	3.2
325	7.26	6.5	3.5
350	7.33	7.0	3.7
375	7.11	7.5	3.9
400	7.03	8.0	3.9
		8.5	3.7
		9.0	3.8
		9.5	4.5
		10.0	4.5
		10.5	4.6
		11.0	4.5
		11.5	5.0
		12.0	5.0
		12.5	5.0
		13.0	5.9
		13.5	5.9
		14.0	6.4
		14.5	6.4
		15.0	6.6

Set/No.	Temp. °C °K	Av.P.igs	Flux x 10^8	Perm. x 10^3	Av.Perm. x 10^3	Perm.Const. x 10^4
1.1	0.0	10.203	1.487	2.409	2.408	2.92
2	273.2	21.632	3.155	2.411		
3		35.025	5.120	2.416		
4		46.773	6.773	2.393		
5		63.058	9.198	2.411		
2.1	25.0	9.835	1.336	2.450	2.544	2.94
2	298.2	21.733	3.053	2.556		
3		35.080	4.885	2.545		
4		46.500	6.529	2.530		
5		63.990	8.890	2.550		
3.1	50.0	6.708	0.857	2.499	2.480	2.76
2	323.2	21.857	2.758	2.467		
3		34.973	4.430	2.477		
4	–	48.757	6.156	2.468		
5		64.244	8.213	2.500		
4.1	74.8	8.563	1.001	2.462	2.471	2.65
2	348.0	23.028	2.711	2.480		
3		37.505	4.389	2.465		
4		50.792	5.949	2.468		
5		63.494	7.469	2.478		
5.1	99.1	9.414	1.062	2.544	2.548	2.64
2	372.3	22.377	2.524	2.544		
3		35.647	4.045	2.559		
4		48.840	5.519	2.549		
5		64.926	7.350	2.553		
6.1	125.0	7.828	0.876	2.698	2.669	2.67
2	398.2	21.029	2.329	2.668		
3		35.117	3.879	2.662		
4		48.474	5.331	2.651		
5		64.357	7.104	2.659		
7.1	150.2	6.614	0.727	2.816	2.819	2.74
2	423.4	20.228	2.218	2.807		
3		36.988	4.053	2.806		
4		50.979	5.468	2.839		
5		63.266	6.833	2.830		
8.1	175.2	7.064	0.775	2.989	2.989	2.82
2	448.4	21.717	2.425	2.990		
3		37.724	4.165	2.990		
4		51.356	5.678	3.000		
5		64.337	7.090	2.990		
9.1	199.8	6.780	0.736	3.110	3.093	2.84
2	473.0	22.693	2.436	3.074		
3		37.027	4.017	3.107		
4		52.716	5.675	3.083		
5		67.135	7.252	3.094		

Set/No.	Temp.	Av.P.igs	Flux	Perm.	Av.Perm.	Perm.Const.
10.1	0.0	6.149	0.887	2.390	2.390	2.89
2	273.2	21.407	3.074	2.380		
3		32.077	4.593	2.370		
4		48.702	7.065	2.400		
5		64.907	9.506	2.420		
11.1	37.5	7.253	0.969	2.439	2.439	2.76
2	310.7	18.533	2.473	2.430		
3		31.385	4.185	2.424		
4		47.664	6.408	2.447		
5		62.667	8.439	2.452		
12.1	62.3	8.908	1.106	2.523	2.517	2.75
2	335.5	20.564	2.555	2.521		
3		33.529	4.139	2.508		
4		49.932	6.157	2.505		
5		67.392	8.392	2.530		
13.1	99.8	5.257	0.611	2.635	2.654	2.75
2	373.0	16.946	1.980	2.636		
3		30.203	3.556	2.658		
4		45.649	5.412	2.680		
5		64.577	7.592	2.653		
14.1	99.8	8.163	0.817	2.262	2.275	2.36
2	373.0	19.240	1.945	2.283		
3		28.366	2.853	2.271		
4		48.083	4.847	2.277		
5		63.797	6.451	2.284		
15.1	99.8	8.008	0.826	2.329	2.323	2.41
2	373.0	17.431	1.792	2.321		
3		30.175	3.091	2.312		
4		48.049	4.946	2.325		
5		64.517	6.661	2.332		
16.1	99.8	9.636	1.161	2.722	2.726	2.82
2	373.0	27.187	3.256	2.704		
3		40.922	4.968	2.741		
4		52.434	6.374	2.745		
5		63.016	7.611	2.728		
17.1	307.1	7.222	0.770	3.747	3.747	3.111
2	580.3	19.158	2.044	3.749		
3		30.640	3.284	3.766		
4		43.061	4.584	3.740		
5		63.827	6.788	3.737		
18.1	274.3	8.150	0.887	3.610	3.631	3.106
2	547.5	19.569	2.139	3.623		
3		35.069	3.867	3.649		
4		48.450	5.332	3.642		
5		62.613	6.858	3.631		

Set/No.	Temp.	Av.P.igs	Flux	Perm.	Av.Perm.	Perm.Const.
19.1	247.9	11.671	1.295	3.501	3.541	3.105
2	521.1	22.505	2.530	3.547		
3		39.512	4.440	3.545		
4		50.957	5.744	3.557		
5		63.357	7.144	3.558		
20.1	222.4	5.918	0.676	3.428	3.455	3.104
2	495.6	17.257	1.981	3.444		
3		30.397	3.515	3.471		
4		43.983	5.066	3.457		
5		63.072	7.307	3.476		
21.1	200.6	6.196	0.722	3.344	3.370	3.098
2	473.8	21.030	2.480	3.379		
3		31.231	3.687	3.383		
4		45.124	5.292	3.361		
5		63.046	7.443	3.384		
22.1	198.4	6.323	0.740	3.340	3.351	3.086
2	471.6	17.491	2.055	3.355		
3		33.413	3.932	3.360		
4		48.121	5.671	3.365		
5		62.234	7.338	3.367		
23.1	168.8	5.237	0.630	3.221	3.229	3.071
2	442.0	15.123	1.823	3.226		
3		31.966	3.864	3.235		
4		44.628	5.384	3.229		
5		62.238	7.522	3.235		
24.1	147.2	4.894	0.604	3.142	3.146	3.067
2	420.4	15.008	1.853	3.142		
3		27.827	3.448	3.154		
4		43.858	5.421	3.147		
5		62.981	7.787	3.147		
25.1	124.0	4.928	0.616	3.005	3.031	3.048
2	397.2	16.417	2.073	3.036		
3		32.511	4.120	3.048		
4		44.983	5.704	3.050		
5		63.382	8.035	3.049		
26.1	100.0	5.060	0.659	2.944	2.952	3.056
2	373.2	22.742	2.971	2.954		
3		33.142	4.330	2.954		
4		44.302	5.772	2.946		
5		62.964	8.260	2.966		
27.1	75.6	4.556	0.614	2.845	2.858	3.060
2	348.8	16.559	2.229	2.843		
3		27.590	3.736	2.860		
4		40.369	5.477	2.865		
5		62.161	8.478	2.880		

Set/No.	Temp.	Av.P.igs	Flux	Perm.	Av.Perm.	Perm.Const.
28.1	50.0	4.444	0.628	2.763	2.743	3.051
2	323.2	18.111	2.551	2.756		
3		30.609	4.250	2.717		
4		44.670	6.251	2.738		
5		62.149	8.713	2.744		
29.1	25.0	4.314	0.622	2.605	2.631	3.047
2	298.2	17.057	2.494	2.640		
3		31.191	4.558	2.639		
4		45.601	6.639	2.629		
5		62.553	9.162	2.645		
30.1	0.0	9.002	0.138	2.540	2.522	3.050
2	273.2	20.560	3.144	2.533		
3		31.564	4.787	2.511		
4		47.487	7.163	2.498		
5		62.478	9.547	2.530		
31.1	- 25.0	3.867	0.613	2.382	2.389	3.033
2	248.2	14.468	2.303	2.392		
3		27.030	4.309	2.395		
4		45.555	7.230	2.385		
5		62.541	9.960	2.393		
32.1	- 50.0	3.860	0.643	2.253	2.266	3.033
2	223.2	17.500	2.920	2.255		
3		33.062	5.571	2.277		
4		48.838	8.199	2.269		
5		62.684	10.575	2.280		
33.1	- 75.0	3.684	0.655	2.134	2.136	3.034
2	198.2	17.689	3.139	2.130		
3		32.468	5.723	2.116		
4		46.082	8.137	2.119		
5		62.796	11.218	2.144		
34.1	- 110.0	3.518	0.685	1.925	1.915	2.998
2	163.2	16.293	3.166	1.920		
3		32.085	6.164	1.898		
4		46.060	8.922	1.914		
5		62.908	14.159	1.916		
35.1	- 183.0	3.211	0.846	1.438	1.434	3.019
2	90.2	18.553	4.835	1.423		
3	(liq.O_2)	30.680	8.011	1.426		
4		47.794	12.592	1.439		
5		62.700	16.596	1.446		

Set/No.	Temp.	Av.P.igs	Flux	Perm.	Av.Perm.	Perm.Const.
36.1	- 195.8	4.699	1.329	1.329	1.327	3.015
2	77.4	17.218	4.877	1.327		
3	(liq.N_2)	28.577	8.122	1.332		
4		45.470	13.056	1.346		
5		63.015	17.523	1.303		
37.1	0.0	12.441	1.897	2.522	2.508	3.034
2	273.2	18.928	2.785	2.513		
3		29.018	4.389	2.502		
4		41.741	6.304	2.498		
5		62.429	9.466	2.508		

Experiments at 0 °C

No.	Av.P.igs	Flux$_8$ x 10^8	Perm$_3$ x 10^3	Av.Perm. x 10^3	Perm.Const. x 10^4	Pope Equiv.
Initial runs						
1.1	9.812	0.873	1.53	1.505	1.85	5.1
2	7.600	0.673	1.475		1.80	4.88
3	15.635	1.41	1.500		1.815	4.97
4	24.295	2.20	1.51		1.83	5.00
After 0 °C Ammonia runs						
2.1	33.220	2.825	1.465		1.775	4.85
2	15.479	1.391	1.469		1.78	4.87
After 0 °C Ammonia-Helium runs						
3.1	16.647	1.39	1.39		1.685	4.61
After - 40 °C Ammonia runs (single and mixtures)						
4.1	4.882	0.412	1.404	1.396	1.69	4.62
2	13.262	1.102	1.382			
3	24.141	2.025	1.395			
4	43.296	3.604	1.383			
5	58.744	4.996	1.414			
After - 40 °C Ammonia mixture runs						
5.1	2.404	0.183	1.265	1.273	1.55	4.21
2	14.031	1.094	1.296			
3	25.153	1.992	1.265			
4	40.877	3.172	1.290			
5	58.303	4.374	1.274			
After - 40 °C Ammonia runs taken to saturation point						
6.1	9.592	0.763	1.323	1.336	1.618	4.424
2	18.899	1.511	1.330			
3	30.445	2.444	1.334			
4	46.075	3.734	1.347			
5	58.717	4.749	1.345			
After - 50 °C Ammonia runs taken to saturation point						
7.1	6.885	0.571	1.380	1.408	1.70	4.65
2	15.059	1.263	1.395			
3	29.214	2.451	1.395			
4	49.993	4.341	1.444			
5.	59.206	5.085	1.428			
Experiments at - 40 °C Performed between sets 3. and 4. at 0 °C						
1.1	6.822	0.638	1.32	1.316	1.72	
2	19.681	1.800	1.30			
3	32.064	3.294	1.34			
4	43.354	3.910	1.29			
5	58.862	5.530	1.33			

No.	Av.P.igs	J x 10^8	J_g x 10^8	J_s x 10^8	K x 10^3
1.1	7.288	1.152	0.946	0.206	2.244
2	7.430	1.213	0.966	0.247	2.317
3	14.149	2.239	1.840	0.399	2.246
4	29.557	4.788	3.840	0.948	2.299
5	40.265	6.455	5.240	1.215	2.275
6	57.987	9.813	7.535	2.278	2.402
2.1	5.088	0.942	0.652	0.290	2.627
2	11.113	2.077	1.448	0.629	2.653
3	17.332	3.200	2.255	0.945	2.620
4	24.485	4.521	3.180	1.341	2.620
5	30.949	5.734	4.025	1.709	2.630
6	42.725	7.848	5.555	2.293	2.607
7	47.243	8.821	6.150	2.671	2.650
8	53.686	9.904	6.980	2.924	2.618
9	58.905	11.077	7.650	3.457	2.669

No.	C_g x 10^6	C_s x 10^6	C x 10^6	K_C x 10^3
1.1	2.646	5.171	7.817	1.438
2	2.698	5.350	8.048	1.477
3	5.140	10.142	15.279	1.428
4	10.73	21.286	31.906	1.462
5	14.62	28.978	43.598	1.445
6	21.05	41.772	62.826	1.520
2.1	1.845	3.675	5.520	1.662
2	4.03	8.040	12.070	1.675
3	6.28	12.530	18.810	1.659
4	8.89	17.698	26.588	1.661
5	11.22	22.35	33.57	1.666
6	15.50	30.85	46.35	1.652
7	17.15	35.15	52.30	1.685
8	19.48	38.80	58.28	1.657
9	21.35	42.52	63.87	1.690

No.	Av.P.igs	J x 10^8	J_g x 10^8	J_s x 10^8	K x 10^3
1. 1	4.911	0.649	0.452	0.197	1.877
2	9.395	1.261	0.864	0.397	1.905
3	15.651	2.111	1.438	0.673	1.914
4	22.307	2.990	2.050	0.940	1.902
5	29.141	3.837	2.680	1.157	1.869
6	35.904	4.717	3.302	1.415	1.865
7	42.336	5.592	3.890	1.702	1.875
8	49.383	6.644	4.580	2.064	1.911
9	53.292	7.145	4.900	2.245	1.902
10	59.425	7.949	5.460	2.489	1.899

No.	C_g x 10^6	C_s x 10^6	C x 10^6	K_C x 10^3
1. 1	1.782	3.575	5.357	1.180
2	3.405	6.820	10.225	1.202
3	5.675	11.40	16.075	1.280
4	8.100	16.22	24.32	1.200
5	10.58	21.21	31.79	1.178
6	13.03	26.10	39.13	1.175
7	15.35	30.80	46.15	1.178
8	17.90	35.90	53.80	1.202
9	19.35	35.80	58.15	1.197
10	21.55	43.20	64.75	1.195

Nitrogen flow through Carbolac I at - 40 °C

No.	Av.P.igs	J x 10^8	J_g x 10^8	J_s x 10^8	K x 10^3
1.1	1.708	0.148	0.058	0.091	1.232
2	5.226	0.451	0.182	0.269	1.224
3	9.668	0.862	0.336	0.526	1.264
4	14.447	1.267	0.488	0.779	1.245
5	23.130	2.072	0.781	1.291	1.270
6	33.899	2.937	1.180	1.757	1.229
7	42.770	3.687	1.490	2.197	1.222
8	50.788	4.489	1.770	2.719	1.253
9	59.559	5.173	2.078	3.095	1.232

No.	C_g x 10^6	C_s x 10^6	C x 10^6	K_C x 10^5	D_{ss} x 10^5
1.1	0.618	37.894	38.514	3.755	3.260
2	1.897	86.934	88.831	4.960	3.735
3	3.510	143.551	147.610	5.69	4.240
4	5.245	200.615	205.860	6.01	4.510
5	8.398	294.235	302.633	6.68	5.025
6	12.308	397.663	409.971	6.98	5.640
7	15.529	473.450	488.979	7.36	6.000
8	18.440	534.972	553.412	7.91	6.325
9	21.625	595.156	616.781	8.18	6.850

No.	Av.P.igs	J x 10^8	J_g x 10^8	J_s x 10^8	K x 10^3
1.1	5.018	1.120	0.216	0.904	3.700
2	11.988	2.717	0.516	2.201	3.771
3	18.828	4.259	0.812	3.447	3.744
4	27.153	5.987	1.170	4.717	3.680
5	34.582	7.851	1.490	6.361	3.789
6	46.076	10.634	1.990	8.644	3.838

	C_g x 10^3	C_s x 10^3	C x 10^3	K_C x 10^5	L
1.1	0.00157	3.391	3.392	0.3222	20.0
2	0.00370	4.652	4.656	0.5682	11.85
3	0.00582	5.547	5.553	0.7490	8.87
4	0.00839	6.457	6.465	0.9030	6.4
5	0.01070	7.196	7.213	1.059	6.0
6	0.01428	8.263	8.277	1.255	5.1

Ammonia flow through Carbolac I at - 20 °C

No.	Av.P.igs	J x 10^8	J_g x 10^8	J_s x 10^8	K x 10^3
1.1	4.050	1.006	0.163	0.849	3.824
2	9.721	2.476	0.391	2.085	3.922
3	14.875	3.810	0.598	3.212	3.945
4	21.305	5.593	0.858	4.735	4.044
5	26.435	7.012	1.064	5.948	4.086
6	30.664	8.160	1.475	6.685	4.099
7	42.589	11.499	1.712	9.787	4.123
8	49.344	13.819	1.985	11.834	4.277
9	56.236	15.865	2.265	13.600	4.315

	C_g x 10^3	C_s x 10^3	C x 10^3	K_C x 10^5
1.1	0.00136	4.457	4.458	0.219
2	0.00326	6.106	6.109	0.396
3	0.00499	7.354	7.359	0.505
4	0.00714	8.691	8.698	0.628
5	0.00886	9.627	9.636	0.710
6	0.01028	10.296	10.306	0.773
7	0.01428	11.967	11.981	0.937
8	0.01654	12.970	12.987	1.039
9	0.01880	13.951	13.969	1.108

No.	Av.P.igs	J x 10^8	J_g x 10^8	J_s x 10^8	K x 10^3
1.1	3.818	1.151	0.157	0.994	4.457
2	7.944	2.471	0.327	2.144	4.601
3	15.288	4.963	0.629	4.346	4.802
4	20.727	6.921	0.854	6.067	4.940
5	26.499	9.034	1.092	8.942	5.042
6	31.670	11.036	1.305	9.731	5.153
7	36.373	13.032	1.496	11.536	5.298
8	44.062	16.224	1.820	14.404	5.445
9	48.400	18.124	1.992	16.132	5.479
10	57.170	22.440	2.358	20.092	5.805

	C_g x 10^3	C_s x 10^3	C x 10^3	K_C x 10^5
1.1	0.00130	5.349	5.351	0.210
2	0.00277	7.087	7.090	0.340
3	0.00533	9.360	9.365	0.517
4	0.00722	10.733	10.740	0.629
5	0.00923	12.034	12.041	0.732
6	0.01104	13.037	13.048	0.826
7	0.01267	13.906	13.919	0.914
8	0.01535	15.333	15.348	1.032
9	0.01704	16.200	16.210	1.091
10	0.01988	17.962	17.980	1.218

Ammonia flow through Carbolac I at - 40 °C

No.	Av.P.igs	J x 10^8	J_g x 10^8	J_s x 10^8	K x 10^3
1.1	5.643	2.855	0.258	2.597	7.177
2	11.081	5.946	0.506	5.440	7.602
3	18.051	10.225	0.825	9.400	8.047
4	23.490	13.828	1.076	12.852	8.350
5	29.553	18.768	1.356	17.418	9.006
6	32.486	21.500	1.486	20.014	9.386
Six months lapsed between set 1. and set 2.					
2.1	34.423	18.45	1.575	16.875	7.607
2	38.911	19.25	1.780	17.470	7.020
3	43.704	15.32	2.000	13.320	4.974
4	49.417	10.83	2.260	8.571	3.111
5	53.739	9.55	2.460	7.090	2.523

No.	C_g x 10^3	C_s x 10^3	C x 10^3	K_C x 10^5
1.1	0.00205	7.62	7.622	0.365
2	0.00402	10.16	10.164	0.570
3	0.00654	12.92	12.927	0.772
4	0.00852	14.88	14.889	0.907
5	0.01072	17.05	17.061	1.071
6	0.01178	18.26	18.272	1.149
2.1	0.01250	19.15	19.163	0.941
2	0.01412	21.85	21.864	0.858
3	0.01585	26.80	26.816	0.551
4	0.01790	30.30	30.318	0.348
5	0.01950	35.62	35.630	0.262

Ammonia flow through Carbolac I at - 50 °C

No.	Av.P.igs	J x 10^8	J_g x 10^8	J_s x 10^8	K x 10^3
1. 1	3.037	1.583	0.131	1.452	7.075
2	5.534	3.000	0.238	2.762	7.357
3	9.461	5.505	0.470	5.035	7.885
4	12.988	8.194	0.558	7.636	8.562
5	16.897	11.389	0.726	11.663	9.148
6	20.767	14.986	0.820	14.166	9.794
7	22.983	14.889	0.938	13.951	8.792
8	25.549	12.048	1.100	10.944	6.400
9	28.701	6.912	1.235	5.677	3.269
10	30.370	6.355	1.305	5.050	2.843

	C_g x 10^3	C_s x 10^3	C x 10^3	K_C x 10^5
1. 1	0.00115	7.933	7.934	0.195
2	0.00210	10.207	10.209	0.287
3	0.00359	12.925	12.928	0.416
4	0.00493	14.931	14.936	0.535
5	0.00642	17.383	17.389	0.639
6	0.00789	21.261	21.269	0.688
7	0.00873	23.810	23.819	0.610
8	0.00970	27.858	27.868	0.422
9	0.01090	33.515	33.526	0.201
10	0.01153	39.313	39.325	0.158

Surface Diffusion Coefficients of Ammonia through Carbolac I

C_s x 10^3	0 °C	- 20 °C	- 30 °C	- 40 °C	- 50 °C
		D_{ss} cm/sec^2 x 10^6			
1	2.67	0.49	0.68	0.81	0.62
2	3.64	0.68	0.90	1.16	0.88
3	6.93	2.51	1.91	1.66	1.30
4	12.28	5.90	3.02	2.39	1.82
5	15.50	7.93	4.68	3.66	2.29
6	18.80	9.45	6.87	5.19	2.92
7	22.05	11.10	8.76	6.69	3.60
8	26.02	12.90	10.47	8.49	4.36
9		14.60	12.20	10.36	5.42
10		16.59	13.30	12.28	6.91
11		18.40	15.43	13.32	8.15
12		20.45	18.29	14.62	9.70
13		22.87	20.41	16.20	11.10
14		24.43	20.82	17.59	14.56
15		26.11	22.22	19.81	13.10
16			22.49	25.85	13.00
17			23.21	20.98	11.90
18			24.53	8.05	11.08
19				2.45	9.66
20				- ve	8.34
21					5.55
22					- ve

Total Gas

No.	P.igs	J x 10^8	C_g x 10^3	C_s x 10^3	C x 10^3	K x 10^3	K_C x 10^5
1.1	24.595	3.840	0.00761	4.745	4.753	2.600	0.788
2	30.064	5.067	0.00929	5.210	5.219	2.810	0.948
3	38.460	6.049	0.01190	5.855	5.867	2.600	1.005
4	53.251	8.652	0.01650	6.990	7.007	2.705	1.205
2.0	14.127	0.546	0.00438	-	0.00438	-	-
1	14.127	1.740	0.00438	3.215	3.219	2.050	0.527
2	18.306	2.141	0.00566	3.145	3.151	1.955	0.663
3	26.338	2.872	0.00816	3.120	3.128	1.815	0.896
4	38.135	3.482	0.01181	3.010	3.022	1.518	1.124
3.0	12.504	0.326	0.00388	-	0.00388	-	-
1	12.504	2.122	0.00388	3.610	3.614	2.835	0.590
2	18.429	3.299	0.00571	4.365	4.371	2.980	0.736
3	26.803	5.064	0.00830	5.349	5.357	3.150	0.922
4	38.688	7.938	0.01142	6.590	6.601	3.575	1.172
5	52.713	10.859	0.01635	8.050	8.066	3.425	1.315
4.0	24.315	1.773	0.00753	-	0.00753	-	-
1	24.315	2.469	0.00753	2.900	2.908	1.692	0.829
2	36.678	5.018	0.01137	4.845	4.856	2.280	1.006
3	55.645	8.950	0.01724	6.800	6.817	2.675	1.280

Helium Gas

No.	P.igs	J x 10^8	J_g x 10^8	$C_g = C$ x 10^3	K x 10^3	K_C x 10^3
1.1	8.200	0.530	0.688	0.00250	1.110	2.080
2	9.308	0.605	0.780	0.00288	1.080	2.042
3	12.056	0.827	1.012	0.00374	1.141	2.162
4	16.537	1.018	1.390	0.00513	1.024	1.938
2.0	7.746	0.564	0.650	0.00240	1.210	2.295
1	7.746	0.440	0.650	0.00240	1.070	2.030
2	12.201	0.751	1.025	0.00378	1.020	1.932
3	20.301	1.422	1.704	0.00630	1.160	2.195
4	32.705	2.222	2.745	0.01013	1.120	2.125
3.0	4.053	0.326	0.340	0.00126	1.336	2.530
1	4.053	0.256	0.340	0.00126	0.938	1.775
2	4.556	0.287	0.382	0.00141	1.055	2.000
3	4.876	0.280	0.410	0.00151	1.026	1.945
4	4.625	0.255	0.388	0.00143	0.841	1.785
5	4.620	0.228	0.388	0.00143	0.836	1.585
4.0	19.360	1.773	0.163	0.00600	1.534	2.905
1	19.360	1.321	0.163	0.00600	1.138	2.155
2	19.082	1.149	0.160	0.00591	1.001	1.895
3	19.415	0.941	0.163	0.00602	0.806	1.525

Ammonia gas

No.	J	J_g (Single gas He)	J_s (Single gas He)	$\mathcal{F}_g$ (Mixture gas He)	$\mathcal{F}_s$ (Mixture gas He)	K	K_C
	x 10^8	x 10^8	x 10^8	x 10^8	x 10^8	x 10^3	x 10^5
1.1	3.310	0.667	2.643	0.514	2.796	3.42	0.680
2	4.463	0.844	3.619	0.653	3.810	3.58	0.653
3	5.222	1.073	4.149	0.870	4.343	3.29	0.879
4	7.634	1.492	6.142	1.095	7.539	3.52	1.063
2.0	-	-	-	-	-	-	-
1	1.30	0.260	1.04	0.225	1.075	3.56	0.395
2	1.39	0.248	1.14	0.183	1.107	3.66	0.431
3	1.45	0.246	1.20	0.205	1.245	3.82	0.453
4	1.26	0.221	1.04	0.179	1.081	3.51	0.408
3.0	-	-	-	-	-	-	-
1	1.866	0.344	1.522	0.259	1.607	3.614	0.503
2	3.012	0.564	2.448	0.424	2.588	3.611	0.673
3	4.784	0.892	3.892	0.610	4.174	3.563	0.869
4	7.683	1.385	6.298	0.910	6.773	3.777	1.135
5	10.631	1.858	8.773	1.093	9.538	3.666	1.287
4.0	-	-	-	-	-	-	-
1	1.148	0.202	0.946	0.164	0.984	3.853	0.386
2	3.869	0.715	3.154	0.514	3.355	3.656	0.778
3	8.009	1.475	6.534	0.854	8.155	3.676	1.147

No.	P.igs	C_g x 10^3	C_s x 10^3	C x 10^3
1.1	16.400	0.00508	4.745	4.750
2	20.756	0.00642	5.210	5.216
3	26.403	0.00816	5.855	5.863
4	36.717	0.01137	6.990	7.001
2.0	6.381	-	-	-
1	6.381	0.00198	3.215	3.217
2	6.105	0.00189	3.145	3.147
3	6.037	0.00187	3.120	3.122
4	5.430	0.00168	3.010	3.012
3.0	8.451	-	-	-
1	8.451	0.00412	3.610	3.614
2	13.873	0.00430	4.365	4.369
3	21.927	0.00680	5.349	5.356
4	34.061	0.01055	6.590	6.601
5	45.623	0.01413	8.050	8.064
4.0	4.955	-	-	-
1	4.955	0.00154	2.900	2.902
2	17.596	0.00545	4.845	4.850
3	36.230	0.01123	6.811	6.822

Total Gas

No.	P.igs	J $\times 10^8$	J_g $\times 10^8$	C_g $\times 10^3$	C $\times 10^3$	K $\times 10^3$	K_C $\times 10^5$
			(Single gas)				
1.0	8.207	0.264	-	0.00298	0.00298	0.458	-
1	8.207	2.635	-	0.00298	7.358	4.555	0.3495
2	13.083	5.176	-	0.00475	9.725	5.620	0.5200
3	27.467	14.216	-	0.00999	15.330	7.345	0.9050
4	35.982	21.526	-	0.01305	18.533	8.500	1.1330
			Helium				$\times 10^3$
1.0	2.982	0.264	0.282	0.00108 = C		1.25	2.380
1	2.982	0.154	0.282	0.00108		0.729	1.380
2	2.982	0.114	0.282	0.00108		0.538	1.020
3	2.835	0.045	0.268	0.00103		0.225	0.426
4	2.807	0.017	0.265	0.00102		0.074	0.141

Ammonia

No.	J	J_g	J_s	$\mathcal{F}_g$	$\mathcal{F}_s$	K	K_C
		(Single gas He)		(Mixture gas He)			
	$\times 10^8$	$\times 10^8$	$\times 10^8$	$\times 10^8$	$\times 10^8$	$\times 10^3$	$\times 10^5$
1.0	-	-	-	-	-	-	-
1	2.481	0.239	2.242	0.130	2.351	6.707	0.3290
2	5.062	0.462	4.600	0.187	4.876	7.084	0.5085
3	14.171	1.132	13.139	0.193	13.979	8.100	0.9020
4	21.509	1.518	19.991	0.098	21.412	9.165	1.1315

No.	P.igs	C_g $\times 10^3$	C_s $\times 10^3$	C $\times 10^3$
1.0	5.221	-	-	-
1	5.221	0.00189	7.355	7.357
2	10.101	0.00367	9.720	9.724
3	24.732	0.00475	15.320	15.325
4	33.175	0.01202	18.520	18.532

Ammonia/Nitrogen mixtures through Carbolac I at - 40 °C

Total Gas

No.	P.igs	J $\times 10^8$	C_g $\times 10^3$	C_s $\times 10^3$	C $\times 10^3$	K $\times 10^3$	K_C $\times 10^5$
1.0	9.778	0.4424	0.00355	0.094	0.097	0.064	-
1	9.778	2.2037	0.00355	6.781	6.784	3.202	0.317
2	17.007	6.1296	0.00616	10.429	10.435	5.13	0.573
3	22.092	9.4525	0.00800	12.577	12.577	6.09	0.733
4	31.006	16.000	0.01125	15.597	15.608	7.33	1.000
5	37.999	21.476	0.01378	18.459	18.472	8.04	1.134
6	46.966	33.623	0.01705	25.716	25.723	10.18	1.275
7	55.709	32.503	0.02021	30.847	30.867	8.29	1.028

Ammonia gas

No.	J x 10^8	J_g x 10^8	J_s x 10^8	$\mathcal{F}_g$ x 10^8	$\mathcal{F}_s$ x 10^8	K x 10^3	K_C x 10^5
1.0	-	-	-	-	-	-	-
1	2.002	0.187	1.815	0.114	1.888	6.965	0.292
2	6.033	0.530	5.503	0.202	5.822	7.390	0.568
3	9.368	0.764	8.604	0.221	9.147	7.968	0.734
4	15.967	1.182	14.785	0.196	15.770	8.777	1.002
5	21.460	1.500	19.96	0.0963	21.364	9.496	1.139
6	33.620	1.900	31.72	-	33.62	11.408	1.280
7	32.500	2.320	30.28	-	32.50	9.114	1.030

Nitrogen gas

1.0	0.442	0.225	0.217	-	-	1.0997	4.52
1	0.202	0.225	?	0.125	0.077	0.501	2.55
2	0.126	0.193	?	0.080	0.046	0.333	1.36
3	0.0845	0.190	?	0.056	0.028	0.221	0.908
4	0.0333	0.185	?	0.0282	0.0051	0.0906	0.365
5	0.0161	0.188	?	0.0119	0.0042	0.0431	0.173
6	0.0035	0.184	?	-	-	0.00961	0.0390
7	0.00312	0.183	?	-	-	0.00863	0.0345

Ammonia gas

No.	P.igs	C_g x 10^3	C_s x 10^3	C x 10^3
1.0	4.075	-	-	-
1	4.075	0.00148	6.687	6.688
2	11.577	0.00420	10.340	10.344
3	16.673	0.00605	12.480	12.486
4	25.798	0.00936	15.510	15.519
5	32.707	0.01186	18.370	18.382
6	41.796	0.01521	25.630	25.645
7	50.578	0.01835	30.760	30.778

Nitrogen gas

1.0	5.705	0.002070	0.0936	0.09569
1	5.705	0.002070	0.0936	0.09569
2	5.430	0.001975	0.0892	0.09117
3	5.419	0.001970	0.0892	0.09070
4	5.208	0.001890	0.0869	0.08879
5	5.292	0.001920	0.0888	0.09072
6	5.170	0.001878	0.0860	0.08787
7	5.131	0.001862	0.0865	0.08836

Total gas

No.	P.igs	J x 10^8	C_g x 10^3	C_s x 10^3	C x 10^3	K x 10^3	K_C x 10^5
1.0	10.683	0.952	0.00388	0.0047	0.0086	1.266	-
1	10.683	2.652	0.00388	6.695	6.699	3.530	0.386
2	17.803	6.783	0.00646	10.255	10.261	5.405	0.644
3	26.325	12.353	0.00956	13.734	13.744	6.670	0.877
4	33.903	18.782	0.01230	16.494	16.506	7.860	1.108
5	40.832	25.599	0.01481	19.394	19.409	8.905	1.288
6	45.409	32.613	0.01647	22.294	22.310	10.220	1.425
7	48.094	37.210	0.01748	25.864	25.881	10.990	1.400

Ammonia gas

No.	J x 10^8	J_g x 10^8	J_s x 10^8	$\mathcal{F}_g$ x 10^8	$\mathcal{F}_s$ x 10^8	K x 10^3	K_C x 10^5
1.0	-	-	-	-	-	-	-
.1	2.13	0.185	1.94	0.113	2.02	7.51	0.2765
2	6.47	0.518	5.95	0.199	6.27	8.13	0.6155
3	12.18	0.927	11.25	0.219	11.96	8.56	0.8650
4	18.70	1.275	17.42	0.157	18.54	9.54	1.105
5	25.57	1.592	24.48	0.0795	25.49	10.85	1.285
6	32.59	1.805	30.78	-	32.59	11.75	1.423
7	37.19	1.930	35.26	-	37.19	12.75	1.400

No.	P.igs	C_g x 10^3	C_s x 10^3	C x 10^3
1.0	4.034	-	-	-
1	4.034	0.001463	6.69	6.691
2	11.300	0.00411	10.25	10.254
3	20.212	0.00735	13.73	13.737
4	27.812	0.01010	16.49	16.500
5	34.732	0.01260	19.39	19.403
6	39.358	0.01435	22.29	22.304
7	42.041	0.01527	25.86	25.875

Hydrogen gas

No.	J x 10^8	J_g x 10^8	J_s x 10^8	$\mathcal{F}_g$ x 10^8	$\mathcal{F}_s$ x 10^8	K x 10^3	K_C x 10^3
1.0	0.9515	-	-	-	-	2.03	1.285
1	0.5216	0.888	?	0.5455	?	1.113	0.705
2	0.3131	0.870	?	0.3345	?	0.683	0.436
3	0.1726	0.815	?	0.1925	?	0.401	0.258
4	0.0821	0.820	?	0.1000	?	0.191	0.123
5	0.0294	0.825	?	0.0407	?	0.0684	0.0439
6	0.0225	0.807	?	-	-	0.0527	0.0337
7	0.0197	0.808	?	-	-	0.0464	0.0295

Hydrogen cont.

No.	P.igs	C_g x 10^3	C_s x 10^3	C x 10^3
1.0	6.651	0.00252	0.00470	0.00722
1	6.651	0.00252	0.00470	0.00722
2	6.503	0.00236	0.00465	0.00701
3	6.113	0.00222	0.00432	0.00654
4	6.091	0.00221	0.00432	0.00653
5	6.100	0.00222	0.00432	0.00654
6	6.051	0.00220	0.00432	0.00652
7	6.053	0.00220	0.00432	0.00652

Nitrogen/Hydrogen mixtures through Carbolac I at - 40 °C

No.	P.igs	C_g x 10^6	C_s x 10^6	C x 10^6	J x 10^8	K x 10^3	K_C x 10^4
1. 1	9.648	3.50	115.351	118.851	0.8685	1.275	0.7145
2	16.073	5.84	102.380	108.220	2.338	2.065	2.012
3	27.750	10.07	133.450	143.520	4.307	2.203	2.930
4	34.294	12.45	147.500	159.950	5.726	2.370	3.495
5	44.210	16.05	176.080	192.130	7.288	2.340	3.695
6	52.270	18.98	173.220	202.200	8.711	2.365	4.205
7	59.111	21.45	162.600	184.050	10.070	2.417	5.300
8	13.037	4.74	95.501	100.241	1.798	1.958	1.750
9	19.021	6.91	175.551	182.461	2.354	1.756	1.257
10	28.596	10.37	286.795	297.165	3.201	1.589	1.052
11	37.941	13.75	380.185	393.935	4.037	1.510	1.001
12	47.000	17.05	461.450	478.500	4.837	1.461	0.986
13	50.434	18.30	488.600	506.900	5.114	1.439	0.985
14	59.092	21.45	550.745	572.395	5.842	1.403	0.994

Nitrogen/Hydrogen mixtures through CarbolacI at - 40 °C

Nitrogen gas

No.	P.igs	C_g x 10^6	C_s x 10^6	C x 10^6	J x 10^8	K x 10^3	K_C x 10^5
1. 1	7.226	2.635	113.6	116.233	0.4275	0.837	3.595
2	5.866	2.125	95.0	97.125	0.5867	1.419	5.890
3	7.881	2.860	119.1	121.960	0.6902	1.243	5.520
4	9.397	3.405	139.5	142.905	0.7703	1.164	5.260
5	10.301	3.740	151.5	155.240	0.8122	1.119	5.101
6	9.618	3.490	142.6	146.090	0.7815	1.153	5.215
7	8.216	2.985	125.8	128.785	0.7802	1.209	5.720
8	5.541	2.010	90.1	92.11	0.516	1.322	5.460
9	11.888	4.31	170.4	174.71	0.992	1.184	5.540
10	21.961	7.97	282.0	289.97	1.911	1.235	6.445
11	31.453	11.42	375.5	386.92	2.732	1.233	6.890
12	40.843	14.82	457.0	471.82	3.537	1.229	7.300
13	44.079	16.02	484.0	500.02	3.966	1.277	7.740
14	52.533	19.07	546.0	565.70	4.688	1.267	8.060

Hydrogen gas

							x 10^4
1. 1	2.422	0.88	1.751	2.631	0.4275	2.522	1.586
2	10.206	3.74	7.380	11.120	1.752	2.436	1.536
3	19.869	7.21	14.35	21.56	3.617	2.583	1.635
4	24.898	9.04	18.00	27.04	4.955	2.825	1.790
5	33.909	12.30	24.58	36.88	6.476	2.710	1.715
6	42.652	15.49	30.62	45.11	7.929	2.639	1.710
7	50.895	18.45	36.80	54.25	9.368	2.613	1.682
8	7.496	2.72	5.401	8.121	1.338	2.535	1.608
9	7.133	2.585	5.151	7.736	1.362	2.709	1.722
10	6.634	2.405	4.795	7.200	1.290	2.760	1.750
11	6.488	2.355	4.685	7.040	1.304	2.854	1.820
12	6.157	2.235	4.450	6.685	1.300	2.998	1.900
13	6.355	2.305	4.600	6.905	1.148	2.564	1.622
14	6.559	2.385	4.745	7.130	1.154	2.498	1.580

	$C_o^{NH_3}$ x 10^3	K x 10^3	$K(M/T)^{1/2}$ x 10^4	$K_{(M)}/K_{(S)}$
NH_3/He at 0 °C	4.750	1.110	1.340	0.800
	5.216	1.080	1.304	0.777
K of single gas is	5.863	1.140	1.375	0.826
1.39 x 10^{-3}	7.001	1.024	1.238	0.738
	3.614	0.938	1.132	0.675
	4.369	1.055	1.272	0.760
	5.356	1.026	1.242	0.738
	6.601	0.941	1.139	0.677
	8.064	0.836	1.010	0.602
	2.902	1.138	1.378	0.818
	4.850	1.001	1.212	0.721
	6.811	0.806	0.976	0.580
NH_3/He at - 40 °C	7.357	0.729	0.954	0.554
	9.724	0.538	0.705	0.387
K of single gas is	15.325	0.225	0.295	0.162
1.32 x 10^{-3}	18.532	0.074	0.097	0.053
NH_3/N_2 at - 40 °C	6.688	0.501		0.403
	10.340	0.333		0.268
K of single gas is	12.486	0.221		0.178
1.24 x 10^{-3}	15.519	0.0906		0.073
	18.382	0.0431		0.031
	25.645	0.0096		0.0069
	30.778	0.0086		0.0062
NH_3/H_2 at - 40 °C	6.691	1.113		0.424
	10.254	0.683		0.260
K of single gas is	13.737	0.401		0.152
2.63 x 10^{-3}	16.500	0.191		0.0725
	19.403	0.0684		0.0260
	22.304	0.0527		0.0200
	25.875	0.0464		0.0176

K is the permeability of the non- or weakly sorbed gas in the gas mixture.

$K_{(M)}$ is the same.

$K_{(S)}$ permeability of single gas.

Data for figure 5.16 $K_{(Calc)}/K_{(Exp)}$ versus $C_o^{NH_3}$ where $K_{(Calc)}$ was calculated from the helium data of the NH_3/He results and the formula $K^{He}(M_{He}/M)^{1/2}$.

$K_{(Exp)}$ was interpolated from the graph of K versus $C_o^{NH_3}$ from the respective mixture experiments.

Hydrogen

$C_o^{NH_3}$ x 10^3	K_{He} x 10^3	$K_{(Calc)}$ x 10^3	$K_{(Exp)}$ x 10^3	$K_{(C)}/K_{(E)}$
Pure gas $C_o^{NH_3}=0$	1.31	1.852	2.27	0.816
Initial flow	1.25	1.767	2.00	0.884
7.357	0.728	1.030	1.03	1.0
9.724	0.538	0.760	0.77	0.988
15.325	0.225	0.318	0.26	1.221 ?
18.532	0.074	0.105	0.105	1.0

Nitrogen

Pure gas $C_o^{NH_3}=0$	1.31	0.497	1.24	0.401
Initial flow	1.25	0.474	1.10	0.431
7.357	0.728	0.276	0.48	0.575
9.724	0.538	0.204	0.360	0.566
15.325	0.225	0.085	0.090	0.947
18.532	0.074	0.028	0.038	0.739
15.325	calculated from the hydrogen result			0.775

Data for Ammonia pressure profiles of fluxes $\mathcal{F}_g$ and J'_g

	0 °C			- 40 °C		
x/l	$P_{\mathcal{F}_g}$	$P_{J'_g}$	J'_g x 10^8	$P_{\mathcal{F}_g}$	$P_{J'_g}$	J'_g x 10^8
0.0	38.6	38.6	8.125	18.0	18.0	0.0125
.1	34.3	35.0	7.64	11.35	16.3	0.110
.2	29.9	31.5	7.25	8.85	14.8	0.161
.3	25.5	27.8	8.64	7.02	13.2	0.220
.4	21.2	24.2	9.35	5.55	11.4	0.254
.5	17.1	20.1	10.28	4.20	9.6	0.295
.6	13.2	16.0	10.88	2.90	7.9	0.385
.7	9.8	12.2	11.43	2.00	5.9	0.498
.8	6.2	8.0	12.05	1.20	4.1	0.625
.9	3.0	3.6	12.75	0.55	2.4	0.755
1.0	0	0	14.42	0	0	1.122
$\mathcal{F}_g$	1.0 x 10^{-8} moles/cm^2/sec			$\mathcal{F}_g$	0.22 x 10^{-8} moles/cm^2/sec	
$\mathcal{F}_s$	8.05 x 10^{-8} "			$\mathcal{F}_s$	9.05 x 10^{-8} "	
C_s	7.03 x 10^{-3} moles/cc PM			C_s	12.92 x 10^{-3} moles/cc PM	
P	38.6 cm Hg			P	18.0 cm Hg	

Ammonia mixtures $\eta = \frac{P_A}{P_{NH_3}}\left(\frac{J_{NH_3}}{J_A}\right)$ enriching to ammonia

No.	P.igs of NH_3	
NH_3/He at 0 °C		
1.1	3.12	16.400
.2	3.31	20.756
.3	2.88	26.403
.4	3.38	36.717
2.1	3.58	6.381
.2	3.70	6.105
.3	3.44	6.037
.4	3.48	5.430
3.1	3.49	8.451
.2	3.49	13.873
.3	3.78	21.927
.4	4.08	34.061
.5	4.67	45.623
4.1	3.39	4.955
.2	3.66	17.596
.3	4.56	36.230

No.	P/P_o of NH_3	
NH_3/He at - 40 °C		
1.1	9.21	0.097
.2	13.10	0.188
.3	36.05	0.460
.4	107.2	0.617
NH_3/N_2 at - 40 °C		
1.1	14.10	0.076
.2	22.50	0.218
.3	36.05	0.311
.4	97.00	0.480
.5	215.50	0.608
.6	1190.0	0.778
.7	1058.0	0.943
NH_3/H_2 at - 40 °C		
1.1	6.75	0.075
.2	11.90	0.211
.3	21.30	0.377
.4	49.70	0.518
.5	152.30	0.646
.6	222.50	0.733
.7	271.50	0.783

Hydrogen-Nitrogen mixtures $\eta = \left(\frac{P_{H_2}}{P_{N_2}}\right)\cdot\left(\frac{J_{N_2}}{J_{H_2}}\right)$

No.		No.	
1.1	0.336	.8	0.523
.2	0.583	.9	0.437
.3	0.482	.10	0.448
.4	0.411	.11	0.431
.5	0.413	.12	0.409
.6	0.434	.13	0.499
.7	0.383	.14	0.469

Computer program for binary gas diffusion experiments

This program was written for calculating the in-going side total, nitrogen, and hydrogen pressures from the manometer limb readings and the percentage composition; and the out-going side total, nitrogen and hydrogen pressures from the McLeod gauge limb readings and the percentage composition.

Data to be read in. All data in floating point.

1st card:
- EVEL Top of McLeod closed limb
- VØGS Volume of out-going side in cc
- TR Room temperature ^{o}K
- TP Plug temperature ^{o}K
- APERH Hydrogen percentage in-going side composition

Format by statement 15 and 25

2nd to (J)th card: For (J) readings
- T(J) Time in seconds
- AML(J) Manometer limb
- AMR(J) "
- CL(J) Vacuum limb of McLeod
- CR(J) Closed limb of McLeod
- PERH(J) Hydrogen percentage out-going side composition

McLeod constants to be inserted in statement 200

Flux constants (see equation 4.3) to be inserted in statements 301, 302, 303

Permeability constants (see equation 4.4) to be inserted in statements 401, 402, 403

The slope ($\Delta P/\Delta t$) was calculated by least squares statements 51, 52, 53

Computer control cards

```
C       NITRØGEN-HYDRØGEN MIXTURES
        DIMENSIØN T(10), AML(10), AMR(10), CL(10), CR(10), PIGS(10),
       1 PØGS(10), PERH(10), PØGSH(10), PØGSN(10)
        DØ 99 I = 1,13
```

```
      READ (5,15) EVEL, VØGS, TR, TP, APERH
   15 FØRMAT (5F10.5)
      DØ 1 J = 1,10
    1 READ (5,25) T(J), AML(J), AMR(J), CL(J), CR(J), PERH(J)
   25 FØRMAT (6F10.5)
      AVPIGS = 0.
      X = 0.
      XX = 0.
      XY = 0.
      Y  = 0.
      XYH = 0.
      YH  = 0.
      XYN = 0.
      YN  = 0.
      DØ 2 J = 1,10
      PIGS(J) = AML(J) - AMR(J)
  200 PØGS(J) = 0.03139*(CL(J) - CR(J)*(EVEL - CR(J))
     1 /(274.41 - 0.03139*(EVEL - CR(J)))
      AVPIGS = AVPIGS + PIGS(J)
      PØGSH(J) = PØGS(J)*PERH(J)/100.
      PØGSN(J) = PØGS(J) - PØGSH(J)
      X = X + T(J)
      XX = XX + T(J)*T(J)
      Y = Y + PØGS(J)
      XY = XY + T(J)*PØGS(J)
      YH = YH + PØGSH(J)
      YN = YN + PØGSN(J)
      XYH = XYH + T(J)*PØGSH(J)
      XYN = XYN + T(J)*PØGSN(J)
    2 CØNTINUE
      AVPIGS = 0.1*AVPIGS
      APIH = AVPIGS*APERH/100.
      APIN = AVPIGS - APIH
   51 S = (Y*X - 10.*XY)/(X*X - 10.*XX)
   52 SH = (YH*X - 10.*XYH)/(X*X - 10.*XX)
   53 SN = (YN*X - 10.*XYN)/(X*X - 10.*XX)
  301 FLUX J = S *VØGS/(443.9266*TR)
  302 FLUXHJ = SH*VØGS/(443.9266*TR)
  303 FLUXNJ = SN*VØGS/(443.9266*TR)
  401 PERM K = 0.976 *S *VØGS*TP/(0.07119*TR*AVPIGS)
  402 PERMHK = 0.976 *SH*VØGS*TP/(0.07119*TR*APIH)
  403 PERMNK = 0.976 *SH*VØGS*TP/(0.07119*TR*APIN)
      WRITE (6,40)
   40 FØRMAT (1H1,4TIME,11X,4HPIGS,11X,4HPØGS,11x,
     1 28HPØGS HYDRØGEN  PØGS NITRØGEN,///)
      DØ 41 J = 1,10
   41 WRITE (6,42) T(J), PIGS(J), PØGS(J), PØGSH(J), PØGSN(J)
   42 FØRMAT (1H ,F6.1,9X,F6.3,9X,F10.8,5X,F10.8,5X,F10.8)
```

```
      WRITE (6,43)
   43 FØRMAT (1HO,10X,6HAVPIGS,9X,5HSLØPE,10X,4HFLUX,11X,
     1 12PERMEABILITY)
      WRITE (6,44) AVPIGS,S,FLUXJ,PERMK
   44 FØRMAT (1HO,5HTØTAL,5X,F6.3,9X,E10.4,5X,E10.4,5X,E10.4)
      WRITE (6,45) APIH, SH, FLUXHJ, PERMHK
   45 FØRMAT (1HO,8HHYDRØGEN,2X,F6.3,9X,E10.4,5X,E10.4,5X,E10.4)
      WRITE (6,46) APIN, SN, FLUXNJ, PERMNK
   46 FØRMAT (1HO,8HNITRØGEN,2X,F6.3,9x,E10.4,5x,E10.4,5X,E10.4)
   99 CØNTINUE
      STØP
      END
```